Impact of degradation and aging on properties of PFSA membranes for fuel cells

Mylène Robert

École Doctorale SIMPPÉ : Sciences et Ingénierie des Molécules, des Produits, des Procédés et de l'Énergie

THÈSE

En vue de l'obtention du titre de

DOCTEUR DE L'UNIVERSITÉ DE LORRAINE

Mention « Énergie et Mécanique »

Impact of degradation and aging on properties of PFSA membranes for fuel cells

Impact des dégradations et du vieillissement sur les propriétés des membranes PFSA pour piles à combustible

---

Présentée par

Mylène Robert

Soutenue publiquement le 12 Janvier 2021

Composition du jury :

Rapporteurs :	M. Vito Di Noto	Professeur, Université de Padoue, ChemTech, Padoue (Italie)
	Mme Cristina Iojoiu	Directrice de recherche, CNRS, LEPMI, Grenoble
Examinateurs :	Mme Corine Bas	Professeur, Université Savoie Mont-Blanc, LMOPS, Le Bourget du lac
	M. Bruno Ameduri	Directeur de recherche, CNRS, ICGM, Montpellier
	Mme Assma El Kaddouri (co-encadrante de thèse)	Maître de conférences, Université de Lorraine, LEMTA, Nancy
Encadrants :	M. Olivier Lottin (directeur de thèse)	Professeur, Université de Lorraine, LEMTA, Nancy
	M. Jean-Christophe Perrin (co-directeur de thèse)	Maître de conférences, Université de Lorraine, LEMTA, Nancy
Invité :	M. Stéphane André	Professeur, Université de Lorraine, LEMTA, Nancy

---

Laboratoire Énergies & Mécanique Théorique et Appliquée (LEMTA) – UMR CNRS 7563
2 Avenue de la Forêt de Haye, 54500 Vandœuvre-lès-Nancy

« Success is not the key to happiness. Happiness is the key to success. If you like what you are doing, you will be successful. »

Albert Schweitzer

Merci à vous

Me voilà arrivée au bout de cette aventure unique. Bien sûr tout n'a pas toujours été tout beau tout rose mais ce sont justement ces épreuves et leur franchissement qui font la richesse, la complexité et l'authenticité de ce travail de thèse. Beaucoup de personnes ont contribué à son aboutissement, mais également à me faire évoluer tant d'un point de vue professionnel que personnel, et je me dois donc de leur exprimer toute ma gratitude avant de clore ce manuscrit.

Je tiens tout d'abord à remercier les membres du jury pour avoir accepté d'évaluer mon travail. Merci aux rapporteurs, Vito Di Noto et Cristina Iojoiu, pour leurs commentaires très intéressants sur mon manuscrit, et à Bruno Ameduri pour son analyse fine et approfondie du manuscrit ainsi que pour sa gestion, en qualité de président du jury, d'une soutenance malheureusement organisée en visioconférence en ces temps difficiles. Merci à vous trois mais également à Corine Bas et Stéphane André pour les discussions enrichissantes, et ouvrant de nombreuses nouvelles pistes de réflexion sur ce travail de thèse, à l'issue de ma soutenance.

Tout ceci a été permis grâce à trois personnes fantastiques, trois encadrants de haut niveau se complétant à la perfection pour ce travail de thèse, qui ont su me guider et me donner envie de donner le meilleur de moi-même. Assma, Olivier et Jean-Christophe, il est difficile de trouver les mots justes pour vous exprimer une gratitude à la hauteur de tout ce que vous m'avez apporté pendant ces dernières années. Vous m'avez donné l'opportunité dès mon master de découvrir un domaine de recherche plus que passionnant, mais également de découvrir un laboratoire et une équipe au top offrant un cadre professionnel convivial et chaleureux dans lequel on ne peut que réussir. Je vous remercie tous les trois pour vos conseils, votre disponibilité, votre dévouement et votre ténacité au travail, votre aptitude à transmettre vos connaissances et vos savoir-faire avec pédagogie, sans oublier votre bonne humeur constante et votre bonne entente. On ne peut pas rêver mieux pour un encadrement de thèse :-)

Merci Assma pour ta force indéfectible, tes multiples conseils et tout le temps que tu as consacré pendant ces nombreuses discussions que l'on a pu avoir toutes les deux pour comprendre mes résultats. Ton dynamisme, ta patience et ta ténacité ont été pour moi une source d'inspiration pour traverser les diverses péripéties qu'apporte le travail de thèse.

Jean-Christophe, merci pour ton dynamisme, ta gentillesse et ta rigueur scientifique, pour les nombreux échanges que l'on a pu avoir. Bien évidemment, je te rendrai la pareille en te

transmettant ma capacité à organiser et classer les échantillons de membranes sans se mélanger les pinceaux ;-)

Merci à Olivier de m'avoir fait partager un peu de ta grande culture scientifique, d'avoir cru en moi pour mener à bien ce travail de thèse, d'avoir été disponible pour répondre à mes nombreuses interrogations et d'avoir scruté la moindre faute dans les différentes publications et dans mon manuscrit.

Merci à Pascal Boulet et tout le personnel administratif et technique qui travaillent durs pour assurer les très bonnes conditions de travail qui sont celles du LEMTA. Merci aux secrétaires pour leur travail irréprochable et les discussions matinales autour d'un bon thé chaud, merci à Franck pour son aide si précieuse à la gestion du labo de chimie, merci à Alain pour sa bienveillance et les petites discussions de couloir, merci à Hadrien pour m'avoir si gentiment accordé un accès si régulier aux spectros IR.

J'exprime également ma reconnaissance envers Fabrice Lemoine, directeur du laboratoire à ce moment-là, pour m'avoir donné la chance d'effectuer cette thèse au sein du LEMTA. Je remercie l'ensemble de l'équipe HSE (ou pile pour les intimes) pour les échanges et les discussions à droite et à gauche dans le dédale des couloirs du LEMTA ou lors de la pause-déjeuner : Julia et son leadership, Sophie et sa bonne humeur, Nicolas et ses petits-mots toujours gentil en passant devant le bureau, Feina et ses précieuses connaissances sur les membranes et les techniques de caractérisation, Gaël et son sourire constant, Jérôme et sa maîtrise inégalable des bancs d'essai, Sébastien et son aide inestimable quand il s'agit de résoudre un problème avec les spectros RMN. Un merci tout particulier à Kévin pour son implication dans mon travail de thèse, pour ses connaissances et sa méthodologie ; tu m'as été d'une aide et d'un soutien réels pour la réalisation de mes expériences et de mes mesures. Enfin, je souhaite le meilleur à la relève de l'équipe pile : Zarina, Feryal, Meriem, William, Rémi, Christine.

Un grand merci au bureau 016V, que ce soit avec les anciens occupants ou les nouveaux, la bonne ambiance, les fous-rires et les discussions à n'en plus finir sur des sujets divers et variés sont toujours de rigueur : merci Saïd pour avoir accueilli la petite nouvelle doctorante que j'étais, Milad pour m'avoir fait découvrir un petit bout de ta culture et Salah pour les nombreuses discussions que l'on a pu avoir ensemble. Toi et tes petites entourloupes pour avoir toujours plus de gâteaux fait maison, grrrr ! ^^ Tu es une belle personne et je n'ai aucun doute que tu vas réussir à clore ta thèse en beauté. Julian, mon cher co-bureau adoré ! Merci pour ton aide et ton oreille attentive, tu as toujours été là, que ce soit pour me remonter le moral lors de

mes coups de stress ou pour rigoler et passer de bons moments au bureau. Merci également à Meriem, la petite dernière arrivée, qui a très vite adopté l'attitude du bureau et avec qui il est toujours très plaisant de discuter et d'échanger à propos de tout.

Merci à tous les potos de promo du LEMTA pour les nombreuses discussions sur notre situation de doctorant, pour les déjeuner partagés ensemble au quatrième étage, au RDC ou dehors, pour les formations DCCE qui nous ont permis de nous découvrir : Romain et Mehdi (je me suis si souvent arrêté dans votre bureau pour refaire le monde !), Lucas, Axel, Anas (t'as vu finalement t'en a pas cassé tant que ça des pointes d'AFM !), Arthur, Alexandre, Shririn.

Merci également à tous les collègues du LEMTA avec qui j'ai aimé partager une bonne bière (ou autre breuvage) : Giuseppe, ou plutôt Peeeppe!, dont le large sourire n'a d'égal que sa générosité et sa joie de vivre, Mathilde, avec qui j'ai apprécié partager le labo de chimie mais également de bons petits gâteaux pour le goûter, Juan David, toujours le sourire et le petit mot pour faire rire, Ahmad, le savoureux mélange des culture française et libanaise, Arthur, dont le sourire éclatant et toujours plus grand ainsi que le rire bien caractéristique resteront gravé au LEMTA, Justine, ami RMNiste au caractère bien trempé qui la conduira loin dans les sciences, sans oublier Solange, ma petite pompière adoré dont le naturel avenant, généreux et optimiste en fait une personne merveilleuse et une amie inestimable.

Et puisque l'on termine toujours par le meilleur, j'exprime ma profonde gratitude à ma famille, à mes amis et plus particulièrement à mes parents. Je vous remercie tous les deux de nous avoir inculqué – à Pierre, Vincent et moi – de belles valeurs, de nous avoir élevé dans un environnement où partage, entraide, générosité et famille sont les maîtres-mots. Merci pour vos sacrifices, votre soutien inépuisable, votre présence dans les moments de joie comme dans la difficulté, qui ont largement contribué à faire de moi la personne que je suis aujourd'hui. On n'a pas l'habitude de le dire ou de le montrer dans la famille Robert mais je vous aime tant.

D'innombrables mercis également à mon cher et tendre Dr Olivier Carrivain, que j'ai eu la chance de rencontrer entre deux spectros IR en salle Carnot au LEMTA, et dont les précieux conseils et mots-doux font de moi une femme épanouie, heureuse et un petit peu moins anxieuse. Merci d'être là pour moi au quotidien, que ce soit pour partager les bonnes nouvelles ou pour m'aider à gérer mes multiples crises d'angoisse/remises en question, tu me pousses toujours à me dépasser, donner le meilleur de moi et je t'en suis extrêmement reconnaissante.

Table of contents

Résumé élargi

Contexte de l’étude

« La transition énergétique est une course contre la montre du changement climatique qui nous menace.»

Il y a trois ans, Nicolas Hulot, alors ministre de la Transition écologique et solidaire, promulguait ces mots pour présenter son "plan climat" visant à accélérer la transition énergétique et climatique de la France, mais aussi à assurer le respect des objectifs de la France fixés lors de la COP21. Plus particulièrement, deux des principaux objectifs de ce plan climat sont de porter la part des énergies renouvelables dans le mix énergétique à 32 % d'ici 2030 et d'atteindre une neutralité carbone d'ici 2050. Ces deux objectifs nécessiteront le bouleversement de notre société moderne et l'introduction de mesures drastiques pour réduire considérablement nos émissions de gaz à effet de serre (GES) d'origine anthropique.

Au cours des dernières décennies, la concentration de CO_2 a atteint des valeurs sans précédents depuis des centaines de millénaires. Selon l'Agence internationale de l'énergie (AIE), les émissions anthropiques de GES ont été multipliées par 145 en moins de 200 ans, entraînant une augmentation de la température mondiale moyenne d'environ 0,85 °C. Les effets du réchauffement climatique ne peuvent plus être ignorés puisqu’ils nous entourent au quotidien : multiplication des catastrophes naturelles et des vagues de chaleur, fonte des calottes glaciaires, élévation du niveau des mers, etc. Dans le contexte du réchauffement climatique actuel qui s'accélère un peu plus chaque année, la place de l'hydrogène comme vecteur énergétique dans le mix énergétique vert de demain ne fait plus aucun doute. Par exemple, le stockage et la distribution de l'hydrogène produit par l'électrolyse de l'eau seraient bénéfiques pour augmenter la part des énergies renouvelables dans le mix énergétique en compensant l'intermittence des ressources naturelles telles que l'énergie solaire ou éolienne. En France, le gouvernement a lancé – en septembre 2020 – son plan hydrogène vert avec un investissement de 7,2 milliards d'euros pour la prochaine décennie, visant à promouvoir le développement de l'électrolyse de l'eau et des véhicules à pile à combustible à hydrogène (bus, poids lourds, trains).

Le développement de la filière hydrogène et des énergies vertes repose en partie sur celui des piles à combustible à membrane échangeuse de protons (PEMFC en anglais), source d'énergie prometteuse et non polluante qui convertit directement une énergie chimique en une énergie électrique. La réaction électrochimique se produisant au cœur de la pile repose sur l'oxydation du dihydrogène à l'anode, générant des électrons et des protons transportés jusqu'à la cathode afin de permettre la réduction du dioxygène (Figure 1). Les électrons transitent par un circuit externe afin de générer la puissance électrique de la pile tandis que les protons sont transportées par une membrane polyélectrolyte ionomère, *i.e.* un copolymère thermoplastique possédant une faible proportion de groupements ioniques (≈ 1–10 % de motifs de répétition). D'un point de vue pratique, la pile à combustible est constituée de divers matériaux, ayant chacun un rôle bien spécifique dans le bon fonctionnement de la pile, qui sont empilés en série afin d'obtenir une puissance totale pouvant aller de quelques watts à plusieurs mégawatts.

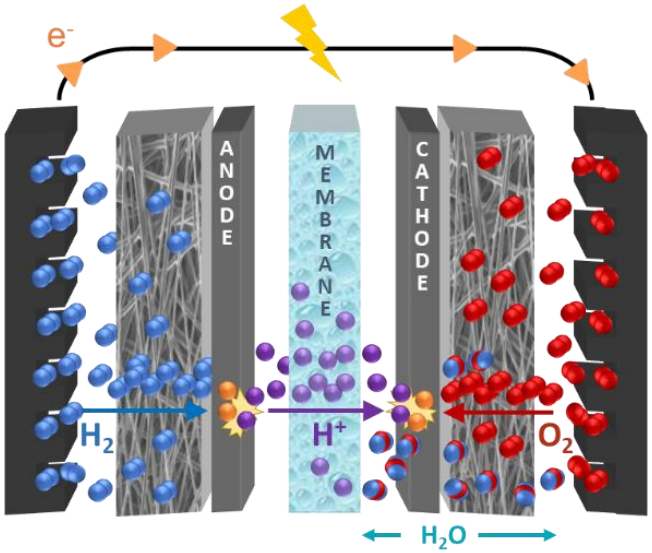

Figure 1 – Représentation schématique du fonctionnement d'une pile à combustible (Adapté de la référence [1] avec la permission de l'auteure).

Les PEMFC présentent des avantages intéressants car elles offrent une alternative attrayante et efficace aux combustibles fossiles avec un large éventail d'applications possibles dans les domaines stationnaire, portable et des transports. Cependant, malgré les nombreux progrès technologiques réalisés au cours de ces dernières décennies, la commercialisation à grande échelle des PEMFC est encore limitée par des coûts de fabrication trop élevés ainsi que par des

1. El Kaddouri A. 2014 Mise en évidence de la dégradation du liant ionomère dans les électrodes de pile à combustible. Grenoble. See http://www.theses.fr/2014GRENI014.

problèmes de durabilité et de performance. De nombreuses études ont été menées ces dernières années afin de mieux comprendre les phénomènes de vieillissement et ceux-ci ont permis d'identifier la dégradation de la membrane polyélectrolyte comme l'un des principaux facteurs limitant la durée de vie des PEMFC [2–4]. Dans ces études, il a été clairement démontré que la membrane est exposée à des conditions difficiles lors du fonctionnement, impliquant d'importantes contraintes chimiques et mécaniques qui peuvent conduire à de graves dégradations de la structure et des propriétés de la membrane et, dans le pire des cas, à l'arrêt de la pile à combustible en raison de la défaillance de la membrane.

Par ailleurs, le bon fonctionnement de la pile repose en partie sur la capacité de la membrane à acheminer les protons de l'anode vers la cathode. La conductivité protonique de la membrane dépend de la mobilité de l'eau dans sa structure, elle-même fortement liée à sa capacité de sorption d'eau. La gestion de l'eau dans la membrane est donc un paramètre essentiel pour optimiser les performances des piles à combustible et améliorer leur durabilité. Pour cette raison, il est nécessaire d'avoir de fortes connaissances sur les effets des dégradations mécaniques et chimiques sur la capacité de sorption et le transport de l'eau dans la membrane. De nos jours, les membranes d'acide perfluorosulfonique (PFSA en anglais) sont les matériaux les plus couramment utilisés dans les systèmes PEMFC, grâce à leur remarquable conductivité protonique et à leur stabilité chimico-mécanique, mais souffrent encore d'un taux de dégradation élevé pendant le fonctionnement de la pile [5]. Bien qu'il soit communément admis que les contraintes chimiques et mécaniques rencontrées lors du fonctionnement en pile interagissent les unes avec les autres, induisant une accélation de la dégradation globale des membranes, seules quelques recherches ont été consacrées à l'effet des contraintes combinées sur les membranes PFSA parmi d'innombrables études menées indépendamment sur chacune de ces contraintes. En conséquence, il est nécessaire de comprendre cette interaction synergique entre les dégradations mécaniques et chimiques ainsi que son impact sur la structure et les propriétés des membranes PFSA. Par ailleurs, malgré les différentes stratégies développées pour prolonger la durée de vie des membranes PFSA, telles que l'introduction d'un renfort

2. Borup R et al. 2007 Scientific aspects of polymer electrolyte fuel cell durability and degradation. Chem. Rev. 107, 3904–3951. (doi:10.1021/cr050182l)
3. Dubau L et al. 2014 A review of PEM fuel cell durability: materials degradation, local heterogeneities of aging and possible mitigation strategies. Wiley Interdiscip. Rev. Energy Environ. 3, 540–560. (doi:10.1002/wene.113)
4. Zhao J, Li X. 2019 A review of polymer electrolyte membrane fuel cell durability for vehicular applications: Degradation modes and experimental techniques. Energy Conversion and Management 199, 112022. (doi:10.1016/j.enconman.2019.112022)
5. Zatoń M, Rozière J, Jones DJ. 2017 Current understanding of chemical degradation mechanisms of perfluorosulfonic acid membranes and their mitigation strategies: a review. Sustainable Energy Fuels 1, 409–438. (doi:10.1039/C7SE00038C)

mécanique ou de stabilisants chimiques, les membranes composites actuelles sont encore insuffisamment durables pour un fonctionnement à long terme des piles à combustible [6,7].

Synthèse des résultats de l'étude

Les objectifs de ce travail de thèse sont d'apporter, grâce à des protocoles de vieillissement *ex-situ*, de nouvelles connaissances sur l'effet de la combinaison des contraintes chimiques et mécaniques sur la dégradation de la membrane PFSA – qu'elle soit renforcée ou non – ainsi qu'à caractériser et comprendre son impact sur les propriétés de la membrane et les performances en pile. Les mécanismes complexes de vieillissement associant les contraintes chimiques et mécaniques doivent donc être traités dans le cadre d'une approche multidisciplinaire. À cet égard, et grâce à une caractérisation multi-techniques, l'analyse de la structure chimique et des propriétés fonctionnelles des membranes PFSA avant et après les tests de vieillissement ont permis de corréler certaines propriétés physico-chimiques de la membrane à ses caractéristiques structurelles et ainsi de mettre en évidence plusieurs indicateurs de dégradation chimique.

Dans un premier temps, avant d'envisager une contrainte chimique et mécanique conjointe, il est nécessaire d'étudier l'impact d'une dégradation chimique pure *ex-situ* sur une membrane PFSA renforcée par rapport à une membrane non renforcée. La réaction de Fenton est un protocole de vieillissement *ex-situ* accéléré largement utilisé dans la littérature pour étudier la dégradation chimique des membranes PFSA qui permet de reproduire l'environnement fortement oxydant observé pendant le fonctionnement des piles à combustible. Il consiste ainsi à faire réagir du peroxyde d'hydrogène H_2O_2 avec des ions ferreux Fe^{2+} afin de générer les radicaux hydroxyle $HO^{\bullet}$ et hydroperoxyle $HOO^{\bullet}$. Cependant, un large éventail de combinaisons de concentrations en réactifs de Fenton peut être trouvé dans la littérature et semble avoir des effets différents sur les membranes PFSA, ce qui rend difficile la détermination de conditions – en terme de concentration en réactifs – de vieillissement *ex-situ* adéquat. À cet égard, une étude a été menée afin de clarifier l'influence des concentrations en réactifs de Fenton sur la dégradation chimique des membranes Nafion™ XL (renforcée) et NR211 (non renforcée).

6. De Moor G, Bas C, Charvin N, Dillet J, Maranzana G, Lottin O, Caque N, Rossinot E, Flandin L. 2016 Perfluorosulfonic acid membrane degradation in the hydrogen inlet region: A macroscopic approach. *Int. J. Hydrog. Energy* **41**, 483–496. (doi:10.1016/j.ijhydene.2015.10.066)
7. Robert M, El Kaddouri A, Perrin J-C, Leclerc S, Lottin O. 2018 Towards a NMR-Based Method for Characterizing the Degradation of Nafion XL Membranes for PEMFC. *J. Electrochem. Soc.* **165**, F3209–F3216. (doi:10.1149/2.0231806jes)

Nos résultats ont mis en évidence une forte dépendance de la dégradation des membranes aux concentrations de réactifs de Fenton, tant du point de vue chimique que morphologique. En effet, des concentrations élevées en H_2O_2 peuvent induirent des évolutions de la morphologie des membranes PFSA – formation de cloques/bulles – qui n'ont jamais été rencontrés lors du fonctionnement en pile. Cette étude préliminaire a ainsi permis d'établir les conditions les plus appropriées requises pour induire une dégradation chimique efficace sans induire de changements morphologiques sévères.

Un suivi plus approfondi de la dégradation chimique *ex-situ* a ensuite été effectué afin d'étudier son impact sur la structure chimique et les propriétés de transport et de sorption de l'eau des membranes Nafion™ composite et conventionnelle : les membranes XL et NR211, respectivement.

Nos résultats ont démontré que les membranes XL et NR211 sont toutes deux chimiquement dégradées de manière significative par l'exposition à un environnement radicalaire puisque d'importantes pertes de poids et des concentrations élevées en ions fluorures ont été mesurées. Plus particulièrement, la RMN du fluor à l'état liquide a permis de mettre en évidence des émissions élevées de diacide perfluoro(3-oxapentane)-1-sulfonique-4-carboxylique – nommé ici Produit A pour plus de simplicité –, un composé fluoré dérivé de la chaîne latérale du PFSA qui a déjà été identifié dans la littérature comme l'un des principaux produits de dégradation du PFSA [8]. Toutefois, aucune évolution de la structure chimique ni aucun changement de la capacité d'échange ionique (CEI) n'ont été observés, ce qui implique que la dégradation des chaînes principales et latérales du PFSA se produit en proportions égales. Ce résultat indique que la décomposition du polymère se fait probablement par une réaction dite de « *unzipping* », entraînant ainsi la perte des chaînes latérales et la formation du produit A. De plus, la caractérisation des propriétés d'auto-diffusion et de sorption d'eau des membranes PFSA après 96 heures d'exposition aux réactifs de Fenton a mis en évidence que la dégradation chimique ne modifie pas ces propriétés de manière significative. Ces comportements sont très différents de ceux détectés dans une précédente étude après un fonctionnement de longue durée des piles à combustible, pour lesquelles une réduction de la capacité de sorption et de la mobilité de l'eau ont été observés [7]. Néamoins, des hétérogénéités de dégradation de la membrane, et plus généralement de l'assemblage membrane-électrodes, après un fonctionnement en pile ont déjà

8. Healy J, Hayden C, Xie T, Olson K, Waldo R, Brundage A, Gasteiger H, Abbott J. 2005 Aspects of the chemical degradation of PFSA ionomers used in PEM fuel cells. *Fuel Cells* **5**, 302–308. (doi:10.1002/fuce.200400050)

été reportés dans la littérature [6,9]. Plus particulièrement, notre précédente étude a porté sur une région spécifique – d'entrée/sortie des gaz réactifs –, connue pour être soumise à de sévères conditions de fonctionnement (forte perméation à l'hydrogène, faible humidité des gaz) et par conséquent propice à d'importantes dégradations [7]. Ainsi, la différence observée dans ce travail de thèse pourrait suggérer que nos conditions ne sont pas suffisamment représentative de la dégradation sévère rencontrée dans la région d'entrée/sortie des gaz et que d'autres régions sujettes à une dégradation moins sévère pourraient avoir des comportements plus semblables. Par ailleurs, bien que la réaction de Fenton vise à accélérer la dégradation chimique des membranes PFSA, il ne peut être écarté que la durée du processus de dégradation (c'est-à-dire 96 heures contre plus de 12000 heures) ne soit pas assez longue pour observer les effets de la dégradation sur les propriétés fonctionnelles des membranes PFSA.

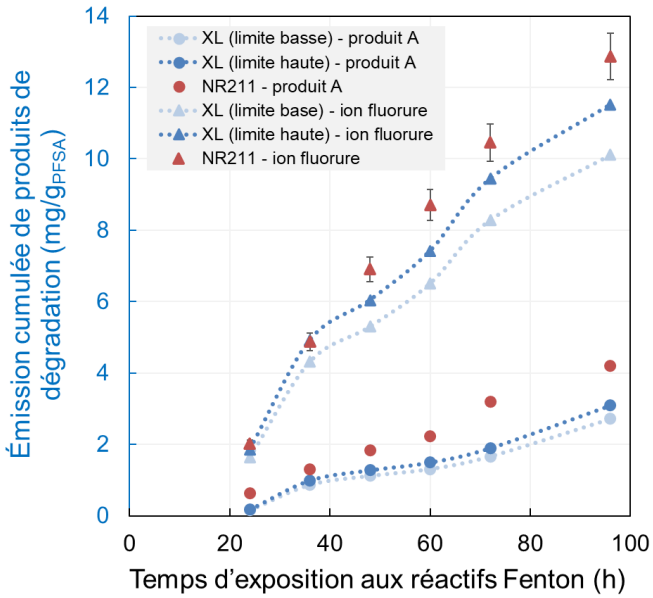

Figure 2 – Comparaison de l'évolution de la quantité de produit de dégradation entre une membrane Nafion™ XL renforcée et une membrane Nafion™ NR211 conventionnelle. Les courbes en traits pointillés se réfèrent à la quantité de produits de dégradation émis lorsque la part du renfort de PTFE de la XL n'est pas prise en compte afin d'étudier la dégradation du PFSA seul.

La particularité de ce travail réside dans l'étude de la stabilité chimique de la membrane composite Nafion™ XL. À ce jour, les publications récentes ne se sont concentrées que sur la contribution de la couche de renfort ou sur l'impact de la dégradation chimique sur la durabilité mécaniques des membranes Nafion™ XL, mais aucune d'entre elles n'a étudié sa stabilité chimique. Nos résultats ont démontré que la dégradation chimique de la membrane XL est

9. Durst J *et al.* 2013 Degradation heterogeneities induced by repetitive start/stop events in proton exchange membrane fuel cell: Inlet vs. outlet and channel vs. land. *Appl. Catal. B-Environ.* **138**, 416–426.(doi:10.1016/j.apcatb.2013.03.021)

inférieure à celle de la NR211 non renforcée, ce qui peut s'expliquer par la présence d'un renfort supplémentaire riche en PTFE, qui maintient l'intégrité mécanique de la membrane et évite ainsi une décomposition chimique supplémentaire, et/ou par la présence de piégeurs de radicaux à base de cérium qui peuvent atténuer les attaques radicalaires sur les chaînes de polymères (Figure 2).

Enfin, les effets de la contrainte mécanique et chimique combinée sur les membranes PFSA ont été étudiés, toujours par une approche *ex-situ*, avec un dispositif sur mesure (Figure 3). L'objectif de ce dispositif était de reproduire des conditions de vieillissement proches de celles rencontrées par la membrane lors du fonctionnement de la pile à combustible. De nombreux tests de vieillissement ont été réalisés afin de mieux comprendre l'influence des contraintes mécaniques, qu'elles soient statiques ou cycliques avec un niveau de pression négligeable ou élevé, sur la dégradation chimique des membranes Nafion™, et son impact sur leur structure chimique et leurs propriétés fonctionnelles.

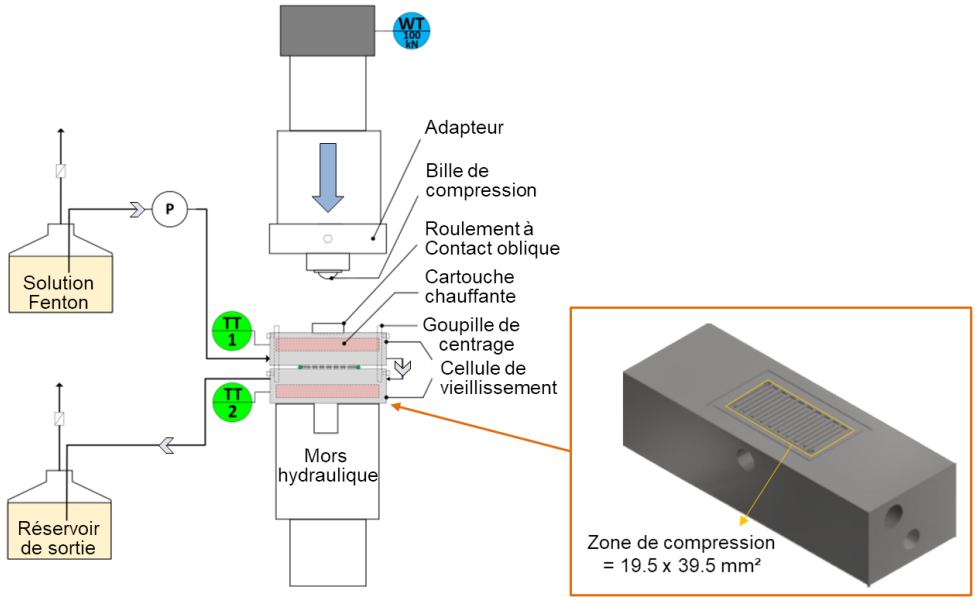

Figure 3 – Représentations schématiques du dispositif de vieillissement couplant contraintes mécanique et chimique et de la cellule de vieillissement.

Les résultats ont démontré que l'application d'une contrainte mécanique ne modifie pas les mécanismes de dégradation chimique puisque des produits de dégradation identiques à ceux identifiés dans le cas d'une contrainte chimique seule ont été détectés. Cependant, le comportement de la membrane XL face à la contrainte chimique semble légèrement différent puisque la combinaison d'une contrainte mécanique a conduit à l'apparition de bulles et de cloques près de la surface de la membrane. Par ailleurs, des taux d'émission de fluorure plus élevés ainsi que des courants de perméation d'hydrogène plus importants ont été obtenus avec

la NR211 plutôt qu'avec la XL dans la plupart des cas, ce qui pourrait s'expliquer par la meilleure résistance mécanique fournie par la couche de renfort supplémentaire présente dans la membrane XL. Cependant, cet avantage semble disparaître lorsque le niveau de pression est considérablement augmenté – de 5 à 10 MPa – puisque des taux de dégradation similaires ont été mesurés pour les membranes XL renforcée et NR211 non renforcée. De plus, bien qu'une décomposition significative du polymère ait été observée après des tests de contraintes combinées, ni les propriétés fonctionnelles telles que la capacité de sorption et d'auto-diffusion de l'eau, ni les performances de la membrane n'ont été significativement affectées. Comme dans le cas de la dégradation chimique seule, ces résultats peuvent également suggérer que la durée de dégradation mise en œuvre dans notre étude n'était pas assez longue pour induire des effets significatifs sur les propriétés fonctionnelles des membranes. Toutefois, il est important de noter que nos résultats se réfèrent à la dégradation globale de la membrane alors que les contraintes sont certainenement éprouvées différemment par la membrane sous les dents ou dans le canal. Il serait donc intéressant d'étudier de manière plus locale ces différentes zones.

D'autre part, les tests de vieillissement effectués avec des couches de diffusion des gaz (GDL en anglais) introduites entre la membrane et les plaques d'écoulement de la solution ont conduit à une diminution des émissions d'ions fluorures, suggérant que la GDL protège la membrane de cette dégradation conjointe. Néanmoins, il est possible que la présence de GDL entrave une bonne distribution et un renouvellement efficace de la solution à la surface de la membrane, ce qui aurait pour conséquence une dégradation moins importante. De plus, les nombreux dépôts de fibre de carbone observés à la surface des membranes ainsi que la chute de la tension en circuit ouvert et la hausse du courant de perméation mesurées tendent à montrer que l'utilisation de GDL dans les conditions de notre étude a un impact négatif et que sa dégradation sous l'effet de la compression pourrait conduire à de graves dommages irréversibles (*i.e.* perforations dues aux fibres de carbone cassées) de la membrane [10]. Il est donc difficile de conclure avec certitude sur l'effet protecteur de la GDL sur la dégradation conjointe des membranes PFSA.

Le développement de notre dispositif sur mesure et les tests de vieillissement accéléré associés constituent les éléments de base d'une meilleure compréhension des phénomènes de dégradation chimique et mécanique des membranes PFSA et ouvrent ainsi une grande variété de perspectives possibles.

10. Yi P, Peng L, Lai X, Ni J. 2011 A Numerical Model for Predicting Gas Diffusion Layer Failure in Proton Exchange Membrane Fuel Cells. *J. Fuel Cell Sci. Technol* **8**. (doi:10.1115/1.4002312)

Preamble

« La transition énergétique est une course contre la montre du changement climatique qui nous menace. »

Three years ago, Nicolas Hulot, minister of Ecological and Solidarity Transition at that time, promulgated these words to introduce its "climate plan" aiming to accelerate the energy and climate transition of France, but also to ensure compliance with France's objectives set at COP21. More especially, two of the main goals of this climate plan are to increase the part of renewables energies in the energy mix to 32 % by 2030 and to reach a carbon neutrality by 2050. These two objectives will require the disruption of our modern society and the introduction of drastic measures to considerably reduce our anthropogenic greenhouse gas (GHG) emissions.

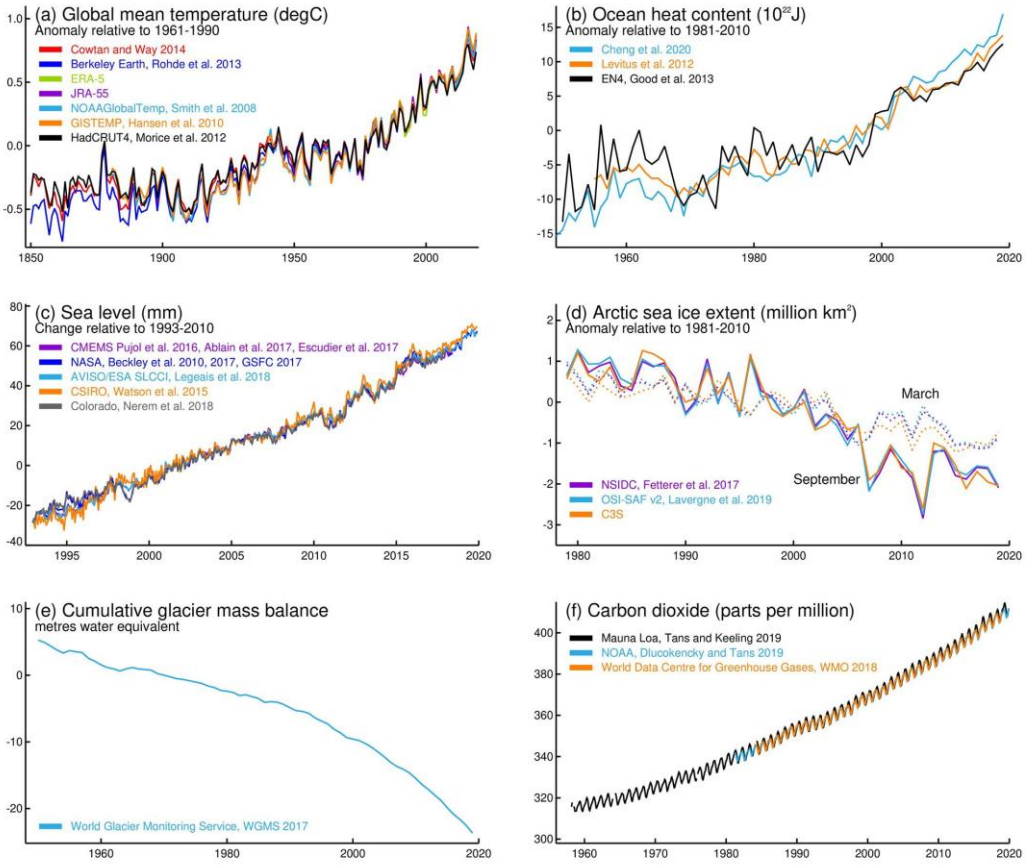

Figure 4 – Evolution of some key indicators of the climate change for the last decades [1].

1. Kennedy JJ, Kendon M, Killick RE, Dunn RJH, Allan RJ, Rayner NA, McCarthy M. 2020 Global and regional climate in 2019. *Weather* **75**, 264–271. (doi:10.1002/wea.3822)

In recent decades, the concentration of CO_2 indeed attained values that have never been seen for hundreds of millennia. According to the International Energy Agency (IEA), anthropogenic GHG emissions were multiplied by 145 in less than 200 years, causing an increase of global average temperature of about 0.85 °C. The effects of global warming cannot be ignored anymore as they surround us on a daily basis: multiplication of natural disasters and heat waves, melting of the ice caps, rising sea levels, and so on…(Figure 4). In the context of today's global warming accelerating a little more every year, the place of hydrogen as an energy vector in the green energy mix of tomorrow is no longer in doubt. For instance, the storage and distribution of hydrogen produced by the electrolysis of water would be valuable to increase the part of renewable energies into the energy mix by compensating the intermittency of natural resources such as solar or wind power. The French government launched in September 2020 its green hydrogen plan with an investment of 7.2 billion euros for the next decade aiming to promote the development of water electrolysis and of hydrogen fuel cell vehicles (buses, heavy-duty trucks, trains).

The development of the hydrogen industry and of green energies partly relies on that of Proton-Exchange Membrane Fuel Cells (PEMFC), promising zero-emission power sources which directly converts a chemical energy into an electrical energy. PEMFC bring interesting benefits since they offer an attractive and efficient alternative to fossil fuel with a wide range of possible applications in stationary, portable and transportation domains. However, in spite of numerous technological advances over these past decades, the large-scale commercialization of PEMFC is still impeded by too high manufacturing cost as well as durability and performance issues.

In recent years, countless studies have been carried out to provide a better understanding of aging phenomena. They identified the degradation of polyelectrolyte membrane as one of the main factor limiting the PEMFC lifetime. In these studies, it was clearly demonstrated that the membrane is exposed to harsh conditions entailing important chemical and mechanical stresses that may lead to severe degradations of membranes chemical structure and functional properties and, in worst cases, to the fuel cell shutdown due to the membrane failure. Moreover, the proton conductivity of the membrane depends on the water mobility into the membrane structure which is itself strongly related to the water sorption capacity. Water management within the membrane is thus a critical parameter to optimize fuel cell performances and improve their durability. For this reason, deep understandings of the effects of the mechanical and chemical degradations on the water transport and sorption properties of membranes are required. Nowadays,

perfluorosulfonic acid (PFSA) membranes are the most-commonly used materials in PEMFC systems, thanks to their remarkable proton conductivity and their chemical-mechanical stability, but they still suffer from high degradation rate during fuel cell operation. Although it is commonly admitted that chemical and mechanical stresses occurring during fuel cell operation interact with each other to accelerate the global membrane degradation, this assertion may not be clearly evidenced so far and, in any case, a clear understanding of these interactions and their impact on the structure and the properties of PFSA membranes is required.

In this context, this thesis work has the double ambition to:

- Bring some key understandings on – simultaneous – chemical and mechanical degradation mechanisms of PFSA membranes during fuel cell operation,
- Characterize and understand the impact of these chemical and mechanical degradations on the water sorption and transport properties of PFSA membranes as well as on their fuel cell performances.

At the end of this thesis work, new insights will be provided on the coupling of mechanical and chemical stresses as well as the evolution of chemical structure, functional properties and cell performances of the PFSA membranes.

Chapter I

State of the art of proton-exchange membrane fuel cell (PEMFC) systems

Table of contents

This first chapter aims at providing an overview of the literature on PEMFC systems and more particularly on the electrolyte perfluorosulfonic acid (PFSA) membranes, key elements of PEM fuel cells, in order to define the context of this thesis work. A good knowledge of the place and role of PFSA membranes in the operation of PEMFC as well as of their morphology and functional properties are thus required to better understand the membrane degradation mechanisms occurring during fuel cell operation.

In that purpose, this literature review will be divided into three main parts:

- First section is dedicated to a brief description of PEMFC operating principle and a deeper description of PEMFC components,
- Second section is focused on the main functional properties of Nafion™ membranes in relation with the morphology of the polymer,
- Finally, the last section will describe the principle degradation mechanisms of membranes-electrode assemblies (MEA) with an emphasis on those of PFSA membranes.

1. Overview of PEMFC

1.1.Operating principle of PEMFC

PEMFC (for Proton Exchange Membrane Fuel Cells or Polymer Electrolyte Membrane Fuel Cells) are electrochemical devices that allow the direct conversion of chemical energy into electrical power. They are composed of a solid polyelectrolyte, an ionomer membrane, sandwiched between two porous electrodes where electrochemical reactions take place. The operating principle of PEMFC and the associated electrochemical reactions are illustrated on Figure 1.1. A gaseous flux of hydrogen is supplied to the anode side while the cathode side is fed with air or pure oxygen. At the anode side, the hydrogen is decomposed into protons and electrons according to the following half-reaction (*hydrogen oxidation reaction*, HOR):

$$\mathrm{H_{2\,(g)}} \rightarrow 2\mathrm{H^+} + 2\mathrm{e^-} \qquad \mathrm{E^0_{H^+/H_2}} = 0\ \mathrm{V_{SHE}} \qquad \textbf{Eq. 1.1}$$

where E is the standard cell voltage by reference to the SHE (Standard Hydrogen Electrode).

Protons are carried to the cathode through the membrane while the electrons are collected by an external circuit, generating an electrical current. The electrons recombine with protons at the cathode side to reduce the oxygen and produce water according to the following half-reaction (*oxygen reduction reaction*, ORR):

$$O_{2\,(g)} + 4H^+ + 4e^- \rightarrow 2H_2O_{(l)} \qquad E^0_{O_2/H_2O} = 1.23\ V_{SHE} \qquad \textbf{Eq. 1.2}$$

The global reaction of the fuel cell between hydrogen and oxygen generates heat and electrical energy with liquid water as the only by-product:

$$2H_{2\,(g)} + O_{2\,(g)} \rightarrow 2H_2O_{(l)} + W_{elect} + Q \qquad \textbf{Eq. 1.3}$$

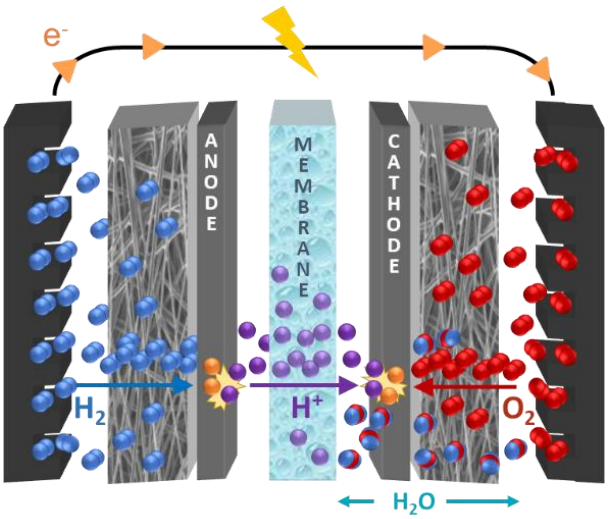

Figure 1.1 - Schematic representation of the PEMFC operating principle (Adapted with permission from ref. [1])

At the equilibrium and under normal conditions of temperature and pressure, the ideal fuel cell voltage is given by the Nernst equation:

$$E = E^0 - \frac{RT}{2F} ln \left[\frac{a_{H_2O}}{a_{H_2} \times \left(a_{O_2}\right)^{\frac{1}{2}}} \right] = E^0 - \frac{RT}{2F} ln \left[\frac{1}{P_{H_2} \times \left(P_{O_2}\right)^{\frac{1}{2}}} \right] \qquad \textbf{Eq. 1.4}$$

where E^0 is the standard cell voltage, R is the gas constant, T the temperature, F the Faraday constant equal to 96,845 C.mol^{-1} and a_i the activity of each species. As the operating temperature of a PEMFC is generally below 100 °C, the water activity is usually assumed equal to 1 because liquid and vapor phases are at equilibrium. H_2 and O_2 are generally considered as ideal gases so that their activity can be expressed as a function of their partial pressure P_i.

The Nernst equation describes the difference between the electrode potential of the O_2/H_2O redox couple at the cathode and the electrode potential of the H^+/H_2 redox couple at the anode and gives an ideal fuel cell voltage of 1.23 Volts at room temperature.

The fuel cell theoretical efficiency, which corresponds to the ratio between the effective electrical power and the total energy released by the reaction, is about 83 % based on the higher heating value (HHV) of hydrogen and about 95 % by considering the hydrogen's lower heating value (LHV). The difference between the higher and the lower heating values corresponds to the heat of water vaporization. The fuel cell efficiency is therefore different if the produced water is in the liquid form (HHV) or in the vapor form (LHV). Nevertheless, during operation the fuel cell efficiency is much lower because of several losses and the actual voltage deviates from the ideal voltage due to various polarization phenomena:

- Activation polarizations (η_{act}), concerning the charge transfer at the membrane-electrode interface,
- Ohmic polarizations (η_{ohm}), resulting from the electrical resistivity of fuel cell components and mainly that of the membrane, as well as the interface resistances between these components.
- Concentration polarizations (η_{conc}), depending on the electrolyte concentration around the electrodes.

Fuel cells are primarily characterized by their polarization curve, *i.e.* voltage *vs.* current density (in A/cm²) or current (in A) curve. The Figure 1.2 represents a typical polarization curve and shows that these polarization phenomena entail a significant decrease of the fuel cell voltage.

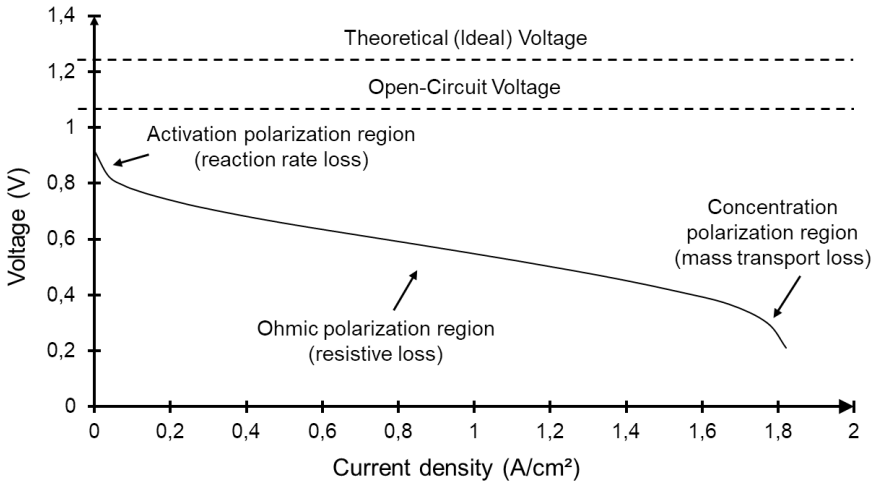

Figure 1.2 - Typical fuel cell polarization curve.

The activation polarization η_{act} is due to the activation energy of the electrochemical reactions taking place at the electrodes. Indeed, an activation energy is required to initiate the reactions and overcome the energy barrier. The kinetics of the HOR (Eq. 1.1) being slower than that of the ORR (Eq. 1.2), this voltage loss is mainly governed by the ORR.

In the intermediate range of current density, the ohmic loss η_{ohm} is due to the electrical resistivity of the components and more particularly the protonic resistance of the membrane. The voltage drop is linearly dependent on the current density and can be determined using Ohm's law:

$$\eta_{ohm} = R \times i \qquad \textbf{Eq. 1.5}$$

where i is the current density and R the total ohmic resistance of the components. However, it must be kept in mind that the total resistance of the cell can be strongly dependent on the operating conditions. In all cases, resistive losses can be minimized by reducing the thickness of the membrane or by improving its transport properties (ionic conductivity).

In the region of high current densities, the fuel cell voltage rapidly decreases since the transfer rate of reactant gases increases more slowly than the reaction rate. The reactant gases are progressively consumed when diffusing through the electrode and a concentration gradient is thus observed from one electrode to the other. This transport process depends on several parameters such as pressure, temperature, reactant concentration, electrode porosity, etc. The transport losses are mainly due to convective or diffusive phenomena and conduct to the decrease of the fuel cell voltage and reaction rate. The voltage variation induced by the concentration gradient is called concentration polarization η_{conc} and can be established from the Nernst equation to describe the voltage loss, and by the Butler-Volmer equation to describe the reaction rate reduction. In both cases, the general equation can be expressed as follows:

$$\eta_{conc} = \frac{RT}{2F} \ln\left(1 - \frac{i}{i_l}\right) \qquad \textbf{Eq. 1.6}$$

with i_l the limiting current density. Furthermore, the oxygen contribution is predominant for voltage losses induced by concentration gradient since it diffuses more slowly than hydrogen. The concentration polarization can be minimized by optimizing the reactants distribution at the surface of the electrodes or the properties of the electrode (porosity, structure) in addition to the optimization of the operating conditions (P, T).

Consequently, the actual voltage of the fuel cell is calculated by subtracting the contribution of each polarization phenomenon to the theoretical value given by the Nernst equation (Eq. 1.4):

$$E = E^0 - (\eta_{act} - \eta_{ohm} - \eta_{conc}) \qquad \textbf{Eq. 1.7}$$

In practice, the theoretical open-circuit voltage is not reachable, due to parasitic reactions as well as the low gas permeability of the membrane, and the actual open-circuit voltage of a PEMFC is approximately 1.0 V. For instance, the oxidation of platinum (Pt) particles, contained in the electrodes, occurs at a voltage above 0.75 V and significantly limits the open-circuit voltage.

1.2.Fuel cell components

The power generated by the PEMFC covers the range from ~1 watt to several megawatts, depending on the active surface and the number of elementary cells that can be stacked together. The actual elementary cell voltage being in the range from 0.6 V to 0.95 V, the elementary cells are connected in series to obtain the desired voltage. Each of them consists in two bipolar plates between which are comprised two gas diffusion layers (GDL) coated on the electrode side with a microporous layer (MPL), the electrodes and the membrane. The so-called membrane-electrode assembly (MEA) stands in general for the membrane and the two electrodes, as well as the two GDL with MPL. Each component has a specific role to play in the mechanical stability of the stack, the gas distribution or the electrical (ionic and/or electronic) conduction.

1.2.1. Bipolar plates (BPP)

The bipolar plates (BPP) have to fulfill various functions to ensure the optimum operation of the fuel cell. They are engraved with channels (around 0.5 to 1 mm in width and height) to provide the homogeneous distribution of the reactant gases on the whole active surface of the electrodes and to facilitate the management of water and heat produced during the reaction as well as the evacuation of excess gases. Moreover, BPP ensure the separation of individual cells and a good mechanical strength in the stack [2].

Over the past decades, many different materials have been investigated for manufacturing the bipolar plates. They can be divided into three groups: graphite, metallic and composite bipolar plates [2–4]. Graphite BPP present good chemical resistance and electrical conductivity but a poor mechanical strength and a high cost while metallic BPP have a great mechanical strength and good thermal and electrical conductivities, but poor chemical stability. However, fuel cell systems require great mechanical strength but also good chemical stability since corrosion issues can be generated by the acidic environment (pH = 2-3) and the temperature (80 °C) of the fuel cell [5]. Carbon-polymer composite BPP were developed to that purpose. However, their mechanical strength can be limited and they suffer from a low electrical conductivity [2].

Bipolar plates are also characterized by different flow-field configurations, elaborated for the optimization of the fuel cell operation [4,6]. Among these configurations, the most commonly used are parallel, interdigitated, and serpentine flow-field designs (Figure 1.3). More particularly, serpentine flow-field design have long been considered as giving the best performances [7,8].

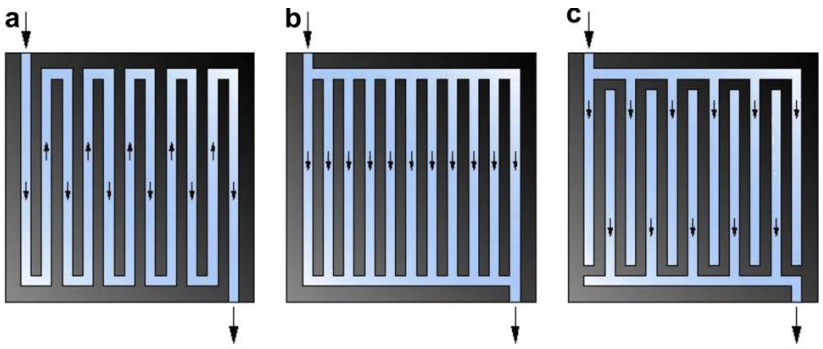

Figure 1.3 - Example of flow-field design: (a) single serpentine channels, (b) parallel channels and (c) interdigitated channels [9].

1.2.2. Gas diffusion layers (GDL)

Gas diffusion layers (GDL) are composed of a porous carbon mesh, with a thickness of 100 to 300 µm at the top of which is deposited a hydrophobic agent (typically based on polytetrafluoroethylene or PTFE)) in order to facilitate water management and thus avoid electrode flooding during operation [10]. They have multiple functions and properties [11,12]:

- Gas permeability, to supply reactant gases from the flow-field channels of bipolar plates to the electrodes,
- Water permeability, to evacuate the water produced during the reaction at the electrodes to the flow-field channels,
- Electrical and thermal conductivity, to evacuate electrons and heat to the flow-field channels,
- Mechanical strength, to provide mechanical support to the MEA.

Two kinds of porous supports based on carbon fibers have been used to manufacture GDL: carbon papers or carbon cloths (Figure 1.4) [13]. The porosity of such materials is high (around 80 %) and the pore size can vary from 10 to 30 µm within one GDL. This porous nature ensures a homogeneous distribution of reactant gases to the electrodes and facilitates water management.

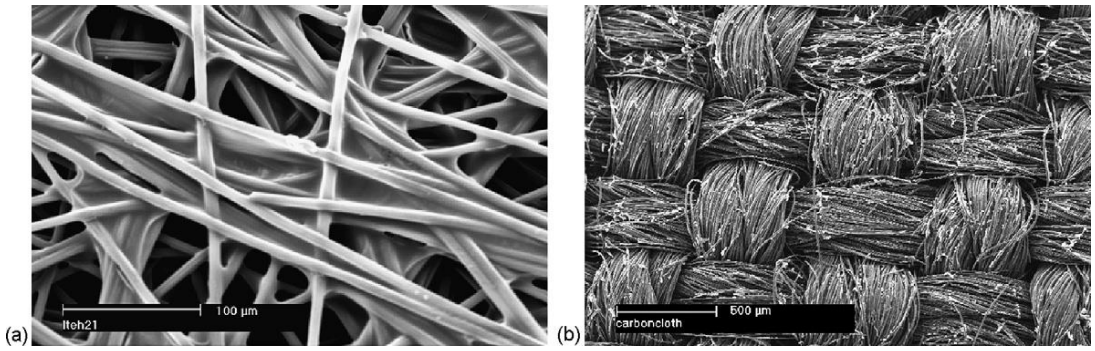

Figure 1.4 - Micrographs from Scanning Electron Microscope (SEM) of (a) carbon paper and (b) carbon cloth [13].

Furthermore, the high tortuosity of carbon paper induces important mass transport limitations under wet conditions but also permits to retain a more significant quantity of water, thus improving the membrane hydration, under dry conditions [13]. Consequently, the carbon paper is still an interesting alternative thanks to its low cost and because the deposit of the MPL at its surface is facilitated [14].

As mentioned earlier, water and reactant gases management of GDL is facilitated by the addition of a hydrophobic agent. More precisely carbon fibers are impregnated with PTFE (5 to 35 wt.%). It has been demonstrated that better performances were obtained at high and low current densities for an optimal PTFE loading of about 20 wt.% [15–17]. However, this optimal rate probably depends on the operating conditions. If the loading is too high, the PTFE will fill the pores of the GDLs and thus isolate the carbon fibers from each other, leading to an alteration of the GDL properties and, more particularly, to an increase of ohmic and water transport resistances [10,16–18].

In addition to this hydrophobic treatment, a thin microporous layer, less than 50 µm thick, is deposited on the surface of the GDL at the electrode side in order to improve the cell performances [19–21]. The MPLs are composed of carbon black and PTFE with a pore size smaller than that of GDL (0.01 to 15 µm *vs.* 10 to 30 µm). MPLs differ from the GDLs in their more dense and granular structure (Figure 1.5) [14]. They improve water and gases management by creating a porosity gradient and enhance the electrical contact between the GDL and the electrodes [22–24].

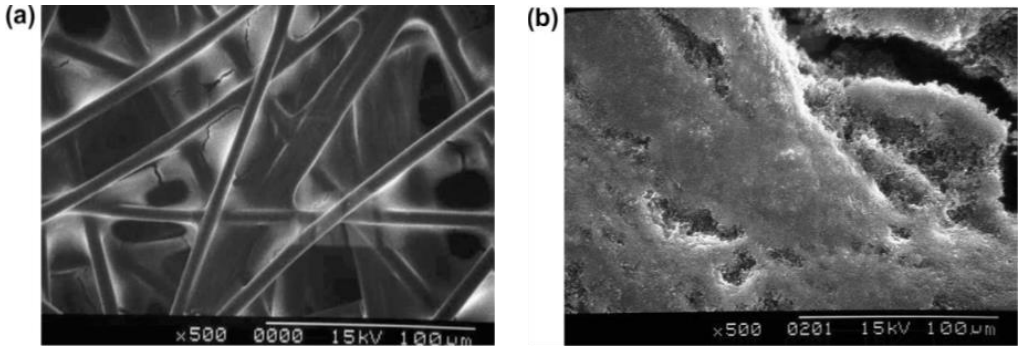

Figure 1.5 - SEM micrographs of GDL (a) with MPL and (b) without MPL [14].

In the case of MPL, an optimal PTFE loading of 20-35 wt.% enhances fuel cell performances, mainly for high current densities (> 0.5 A.cm^{-2}) [14,16,25]. If the PTFE loading is too high, or if the MPL is too thick (> 90 µm [14]), the gas permeability and the electron conductivity decrease, which limits the fuel cell voltage [14,16,25].

1.2.3. Electrodes or catalyst layers (CL)

The electrodes or catalyst layers are thin materials (8 to 15 µm) placed between the gas-diffusion layers and the membrane where the electrochemical reactions occur: oxidation on the anode side and reduction on the cathode side. For optimal fuel cell operation, the electrodes must meet several criteria: be porous to ensure the gas distribution to the reaction sites, facilitate the evacuation of excess reactants gases as well as by-products, have good electronic and proton conductivities but also support the deposited catalyst.

They are porous composite materials with a wide diversity of composition and manufacturing process [26]. They are made from a carbon-based support with dispersed catalyst particles to which is added a ionomer solution as a binder and an ionic conductor medium, with the same chemical composition than the membrane.

Despite a large variety of electrodes, two main categories can be distinguished: PTFE-bound [27,28] and thin-film electrodes [29,30]. The PTFE-bound electrode consists in creating a suspension by mixing together a Pt/C powder and a PTFE emulsion which is deposited on the GDL. Once the electrode is dry, GDLs are impregnated with a Nafion™ solution by brushing or spraying. The thin-film electrode is made from an ink that is based on an ionomer solution (the most commonly used is the Nafion™) in which Pt/C powder is added. This manufacturing process is nowadays the most commonly used since it leads to a more uniform distribution of polymer in the electrode and thus increases the electrode active area [28–31].

The most common catalyst is platinum (Pt) thanks to its low activation energy. The electrodes are generally composed of Pt nanoparticles dispersed on a carbon support to maximize its specific surface area. In order to increase the catalyst efficiency and thus decrease the loading, various carbon-based supports [32,33] and manufacturing processes (spraying, impregnation, etc.) [34–36] were investigated. For instance, the elaboration of supports from carbon aerogels [36] or the impregnation of carbon nanofibers with platinum aggregates by plasma spraying were studied [37,38]. On the other hand, the carbon black powder is extensively used for commercial MEAs manufacturing and for numerous investigations since it has the benefit of being widely available and cheap as well as having a high electronic conductivity. Although it is the most commonly used support, some of its main drawbacks, such as the presence of a micro-porosity in the carbon aggregates which can lead to Pt particles or Nafion™ capture [32,39], conduct to the research of new alternatives. Progress have been made to develop new carbon-based supports from mesoporous carbon. They demonstrate better mass transport properties thanks to a controlled porosity and a high specific surface area but they are also more prone to the corrosion [40]. Carbon nanotubes, carbon nanofibers and graphene, which present an enhanced durability and a higher specific surface area, have also been investigated but they remain expensive alternatives for an industrial use [41]. Furthermore, non-carbonaceous materials, such as metal oxide nanostructures based on titanium, indium, silica, or tungsten as well as conducting polymers, have been widely investigated to deal with the carbon corrosion issue (see § 3.2.2) [32].

Furthermore, the electrochemical reactions occur in a specific area named "triple phase boundary" where the electronic conductor (*i.e.* the carbon-based support), the catalyst (*i.e.* the Pt particles) and the protonic conductor (*i.e.* the ionomer binder) are simultaneously present (Figure 1.6). The exact mechanisms occurring at the triple phase boundary are not yet fully understood and its characterization is still difficult to implement [42]. However, it is important to note that this specific area is a useful but not realistic representation of reaction mechanisms since it would entail in practice the presence of infinite gaseous flux whereas its surface is necessarily zero.

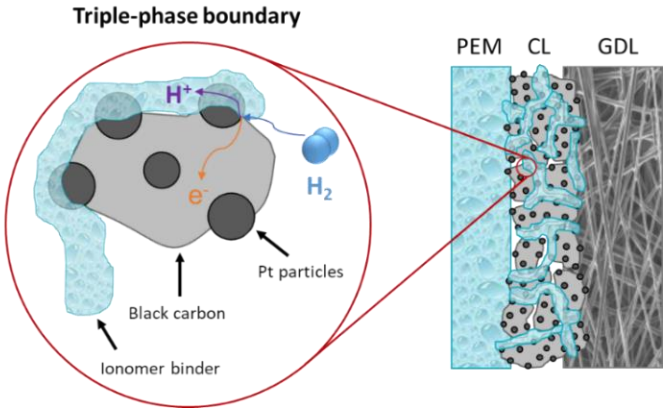

Figure 1.6 - Schematic representation of the triple phase boundary at the anode side. PEM = proton exchange membrane, CL = catalyst layer, GDL = gas diffusion layer PEMFC (Adapted with permission from ref. [1]).

In the case of PEMFC, the strong sensitivity of platinum to carbon monoxide contaminant (100 ppm at 80 °C) is a critical issue when hydrogen is obtained by steam reforming of hydrocarbons [43]. To overcome this issue, two methods have been developed. In the one hand, the CO content can be decreased below to 10 ppm after fuel reforming [44,45] thanks to a process called selective oxidation while, on the other hand, binary alloys (Pt/Co, Pt/Ru, Pt/Ni, Pt/Mn) or tertiary alloys (Pt/Ru/Mo, Pt/Ru/Co, Pt/Ru/Cr) can be used instead [46–48]. Nevertheless, these alloys still suffer from a lack of stability during fuel cell operation, causing the disappearance of one of the elements and the formation of hollow particles [49].

The ionomer present in the electrodes is a thermoplastic co-polymer characterized by its low concentration of ionic groups (< 15 mol.% of the repeating units). Its roles are to bind the catalyst to the membrane and to facilitate the proton transport through the electrodes (from the anode side to the membrane and from the membrane to the cathode side). The addition of an ionomer phase increases the dispersion of the catalyst and provides better mechanical strength to the electrode. The most commonly used ionomer in the PEMFC are long side chain (LSC) perfluorosulfonic acid (PFSA), commercialized under the name Nafion™ [46]. Moreover, other ionomers based on PFSA have been developed in order to improve cell performances; for example, Solvay Solexis S.A. elaborated PFSA with short side chains named Aquivion® [50,51]. This kind of ionomer provides better performances than LSC-PFSA for high current densities (> 1 $A.cm^{-2}$) in high-humidity conditions and low temperature (60-80 °C). This enhancement is even better for low current densities (< 0.5 $A.cm^{-2}$) when the fuel cell operates at high temperature (90-110 °C) in low-humidity conditions. Alternatives to PFSA-based ionomers such as sulfonated polyetheretherketone (s-PEEK) [52–54], sulfonated hydrocarbons [55] and other sulfonated polymers [32] are also currently studied.

In addition to the ionomer, a hydrophobic agent based on PTFE can be added [15,46]. It has been demonstrated that the presence of PTFE improves the cell performances and the power density, regardless of the humidity level [56,57]. Nevertheless, the presence of PTFE is not essential since good performances can be obtained with PTFE-free electrodes thanks to the presence of the MPL (see § 1.2.2).

Finally, a high ionomer loading can negatively affect the cell performances by decreasing the gas permeability, the proton (effective or apparent) conductivity and the access of reactants to the catalyst by clogging the pores of the electrode [58,59]. Some studies were performed to determine the optimal loading and it is now established that the best cell performances are obtained for a loading of about 25 to 35 wt.% [60–62].

1.2.4. Membrane

Likewise the ionomer binder comprised in the electrodes, the membrane is a thermoplastic ionomer with hydrophilic ionic groups. It is present in the form of a thin film and it must fulfill several essential functions for the correct operation of the fuel cell:

- Proton conductor: high proton conductivity (~100 $mS.cm^{-1}$) guarantees the proton migration from the anode to the cathode while limiting thermal losses.
- Electrical insulator: the membrane isolates the cathode from the anode to avoid short circuits.
- Gas impermeability: good barrier properties limit yield losses due to the diffusion of reactant gases and prevent gas crossover, a factor that leads to thermal and chemical degradations.
- Mechanical and chemical stability: the membrane must resist mechanical stress, caused by the operating conditions of the fuel cell, and chemical attacks from the formation of reactive oxygen species (ROS).

Nowadays, PFSA ionomers are the most commonly used membrane materials in PEMFC systems. They are composed of a hydrophobic PTFE backbone and perfluorinated side chains ended by hydrophilic sulfonic groups ($-SO_3^-H^+$). The microstructure is organized in two phases: the first is rich in polymer chains and confers to the membrane its mechanical strength and its relatively good chemical inertness to prevent chemical degradation in the oxidizing environment of the PEMFC. The second phase is rich in ionic sites, which promotes the sorption of water and the presence of continuous conduction path to enable the efficient transport of the

protons though the membrane. A deeper description of the chemical nature and properties of PFSA membranes will be developed in § 2.

Ionomer membranes are usually classified by their thickness (15 to 250 µm) and their equivalent weight (EW). The EW corresponds to the mass of dry polymer needed to neutralize an equivalent of base. It is directly linked to the ion exchange capacity (IEC) expressed in milliequivalents per gram of dry polymer by the following relation:

$$EW\ (g.eq^{-1}) = \frac{1000}{IEC} \qquad \textbf{Eq. 1.8}$$

Over the past decades, multitudinous researches have been carried out on PFSA membranes in order to improve their mechanical strength, increase their conductivity, lengthen their lifetime while reducing their cost and thus extend their large-scale commercialization. In that respect, plenty of commercial PFSA membranes have been developed in the industry for the use in PEMFC and can be henceforth distinguished into several categories [63], among which:

- Non-reinforced long side chain (LSC) or short side chain (SSC) PFSA membranes [64,65].
- Reinforced PFSA membranes with a microporous support based on PTFE [64,65].
- Multi-Acid Side Chain (MASC) membranes based on Perfluoro Imide Acid (PFIA) or modified-PFIA [66–68].
- Copolymer membranes based on vinylidene fluoride (VDF) and hexafluoropropene (HFP) [69,70].
- Chemically cross-linked membranes [71].
- Organic-inorganic nanocomposite membranes, which are modified-PFSA membranes containing nanoparticles of inorganic materials, metals or metal oxides such as SiO_2, TiO_2, ZrO_2, SnO_2 [72–74].

However, the upper conductivity limit of current PFSA membranes being practically reached, it is now necessary to develop new perfluorinated materials with innovative structural attributes while maintaining the good properties of traditional PFSA membranes [72]. However, the upper conductivity limit of current PFSA membranes being practically reached, it is now necessary to develop new perfluorinated materials with innovative structural attributes while maintaining the good properties of traditional PFSA membranes [75]. In that respect, PFIA membranes seem to be promising candidates despite their chemical stability issue. Moreover, the glass transition temperature of PFSA membranes being around 90 to 125 °C [76,77], their

utilization for high temperature fuel cells (> 90 °C) are not suitable and many research works are nowadays focused on the synthesis of new non-fluorinated polymers and thus the elaboration of alternative membranes. Among these, sulfonated aromatic polymers seem to be encouraging possibilities since they possess great mechanical and thermal properties as well as a high glass transition temperature. For instance, thermostable membranes have been synthesized from polystyrene (PS), polyphenylene (PPBP), polyetheretherketone (PEEK), polyimide (PI) or polybenzimidazole (PBI) [78].

Despite the fact that a wide variety of perfluorosulfonated membranes exist, LSC-PFSA membranes and especially Nafion™ membranes whether reinforced or not are still, these days, the most commonly used materials in PEMFC.

Non-reinforced PFSA membranes

The synthesis of perfluorosulfonated membranes consists in the copolymerization of tetrafluoroethylene (TFE) with a perfluorovinylether, the perfluoro-(4-methyl-3,6-dioxa-7-octene-1-sulfonyl fluoride) (PFSVE) [79]. The various commercially available PFSA membranes have similar chemical structures but differ from the length of their side chain: Nafion™ (DuPont de Nemours), Flemion® (Asahi Glass) and Aciplex® (Asahi Kasei) are categorized as long-side chain (LSC) PFSA membranes, Aquivion® (Solvay Specialty Polymers) is referred as a short-side chain (SSC) PFSA membranes while the 3M company developed intermediate side chain (MSC) PFSA membranes [80]. Their respective chemical structures are illustrated on Figure 1.7:

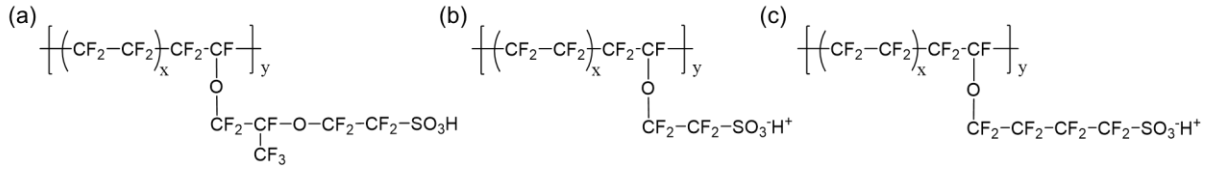

Figure 1.7 - Chemical structure of (a) long-side chain, (b) short-side chain and (c) intermediate side chain PFSA membranes.

The development of Nafion™ membranes started in the 1970s with the elaboration of Nafion™ N117 membrane and numerous other generations have been elaborated over the past decades in order to improve their chemical and/or mechanical stability and reduce their thickness. Nafion™ membranes are named according to a combination of their equivalent weight (EW) and their thickness: the first generation N117 membrane have an EW of 11*100 $g.eq^{-1}$ and a thickness of 7 milli-inches (i.e. 177.8 µm). Thinner membranes were then

developed to enhance the water permeability of the membrane and thus improve fuel cell performances: N115 (127 µm) and N112 (50.8 µm) membranes have emerged. First generation of Nafion™ membranes (N117, N115, N112) were manufactured by a melt extrusion process. They are slightly anisotropic because the polymer chains are oriented in the machine direction during the manufacturing process, which impacts the swelling and the mechanical properties of the membrane. In order to manufacture thin films with suitable mechanical resistance, DuPont de Nemours utilized the solution casting process. This new process permitted to produce isotropic membranes by controlling the thickness and the uniformity of the materials and gave birth to a second generation of Nafion™ membranes: NR211 (25.4 µm) and NR212 (50.8 µm) membranes. Furthermore, the Nafion™ NR21x membranes were also chemically stabilized to prevent membrane degradation and thus increase their lifetime: since the PFSA degradation process was believed to occur *via* radical attack of weak H-containing endgroups (i.e. –COOH) of the fluorinated chains (see § 3.3.2.4), an additional step consisting in the fluorination of reactive end groups was introduced [81,82]. This process indeed demonstrated its ability to reduce the number of reactive end groups [83,84]. Over the last decades, another improvement has been made on the membrane's mechanical stability by the introduction of a microporous support based on PTFE.

SSC-PFSA membranes were developed in the 1980s by the Dow Chemical company and presented greater properties and better fuel cell performances than Nafion™ membranes [85,86]. However, due to a high production cost in comparison with its competitor, Dow Chemical never extended the SSC-PFSA membranes commercialization to a large-scale. Thereafter, Solvay Solexis developed a new and cheaper synthesis process than that initially elaborated by Dow Chemical for SSC-PFSA membranes and commercialized its products under the tradename of Aquivion® (Figure 1.7) [64].

Reinforced PFSA membranes

Over the past decades, efforts have been made to reduce the ionic resistivity of the membrane without compromising its mechanical robustness and its protonic conductivity. In that respect, the incorporation of a microporous support inside the membrane permitted to elaborate thinner film (up to 15 µm) while maintaining good mechanical properties and chemical stability.

For instance, the manufacturer W.L. Gore & Associates developed a PFSA membrane reinforced with a microporous expanded-PTFE (e-PTFE) matrix: The Gore-SELECT® membrane [87]. To ensure a continuous transport network in the membrane thickness,

perfluorinated ionomer are both dispersed on the surface and poured into the pores of e-PTFE reinforced layer. The addition of the reinforcement provides better dimensional and mechanical stability of the membrane during fuel cell operation [88,89]. It is nevertheless important to notice that e-PTFE constitutes a nonconductive layer which lead to a decrease of membrane conductivity [90]. Fortunately, this conductivity loss can be compensated by the use of thinner membranes.

Another example is the Nafion™ XL membrane manufactured by DuPont de Nemours™ (Figure 1.8). This reinforced membrane is composed of an additional microporous layer of PTFE impregnated on both sides with PFSA ionomer. Similarly to the e-PTFE matrix of the Gore-SELECT™ membrane, this reinforced layer provides an improved mechanical stability to the membrane and enhances its durability in comparison with their unreinforced analogue [91]. On another note, Nafion™ XL membranes also contain radical scavengers able to mitigate PFSA chemical decomposition [92–95]. More details on radical scavenging properties will be provided in § 3.3.2.5.

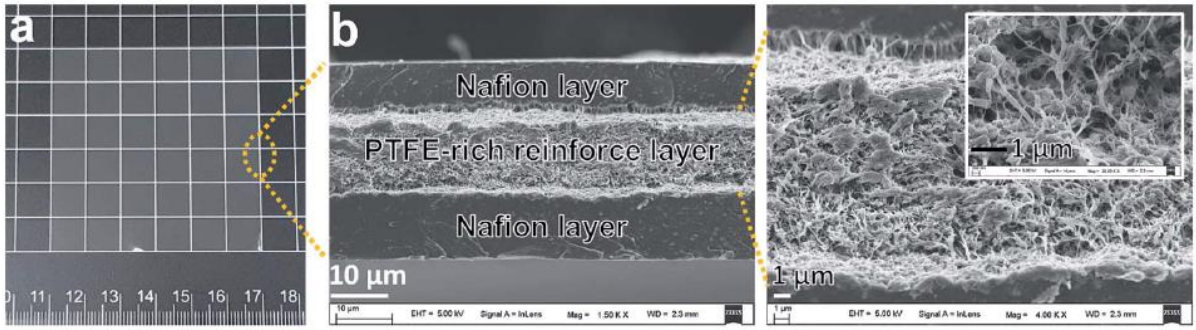

Figure 1.8 - (a) photograph and (b) cross-section SEM micrographs with different magnification of the Nafion™ XL morphology [91].

In 2016, Shi *et al.* [96] studied the structure and properties of Nafion™ XL membrane and more particularly the impact of reinforcement on its properties. They demonstrated that the presence of an additional reinforcement significantly reduced the in-plane swelling of the membrane, which corresponds to the reinforcement direction, while it enhances the swelling in the thickness direction. In this way, the total water uptake remains similar to that of a non-reinforced membrane. Moreover, the analysis of the transport properties showed that the ionic conductivity was still very high in spite of the addition of a non-conductive PTFE layer.

Alternatives to PFSA membranes

Since the beginning of the development of Nafion™ membranes in the 1960s, many improvements have been made in terms of manufacturing process, as well as chemical and mechanical stability for an extended lifetime. However, they still suffer from a few disadvantages, especially their high cost and their limited operating temperature (between 0 and 90 °C) The development of alternative membranes has therefore become essential.

To this end, new ionomer membranes with a proton conductivity similar to that of Nafion™ have been developed to overcome the problems of production cost and thermal stability. As mentioned earlier, the sulfonated aromatic polymers are cheaper and some of them possess also better mechanical and/or chemical stability which facilitates the fuel cell operation at higher temperature with a suitable proton conductivity even at low hydration levels. Moreover, Kraystberg and Ein-Eli published a complete review about these alternative membranes and their benefits in comparison with Nafion™ membranes [78].

2. Generalities on PFSA membranes

To ensure optimal fuel cell operation, membranes have to strike a balance between several crucial properties: proton conductivity, chemical stability, and mechanical endurance. These properties are strongly related to the microstructure and the morphology of the membrane. A good knowledge of the membrane morphology and microstructure is thus necessary to understand their degradation mechanisms. Recently, Kusoglu and Weber published an outstanding review summarizing all the current knowledge on PFSA membrane structure, morphology, physico-chemical and mechanical properties, and other key topics [77]. The description provided here is partly inspired by this review.

2.1.Chemical structure and morphology

Many analytical methods have been used to characterize the structural properties of Nafion™ membranes. Among them, the use of Nuclear Magnetic Resonance (NMR) spectroscopy permitted to characterize the molecular structure of Nafion™ membranes since the beginning of their development [97–100]. NMR spectroscopy is a powerful technique allowing to determine the structure of molecules (from simple molecules to complex macromolecules) thanks to the chemical environment of each constituting atom. In the case of Nafion™, the molecular formula and structure was assumed based on those of the initial monomers (PSFVE and TFE) used for synthesis.

As described in § 1.2.4, the Nafion™ membrane microstructure is composed of two phases: a hydrophilic phase constituted by the sulfonic groups and a hydrophobic phase constituted by the PTFE backbone. The two-phase structure of Nafion™ has been widely investigated over the past decades thanks to numerous sophisticated techniques, such as small- and wide-angle scattering with X-ray or neutrons (SAXS, WAXS and SANS), as well as transmission electronic (TEM) or atomic force microscopies (AFM). Several models have also been proposed to describe the multi-scale structure of Nafion™ membrane. Among them, three were widely used: the cluster-network model, the rod-like elongated polymeric aggregates model and the locally-flat interconnected domains model [77].

The first investigation was carried out by Gierke *et al.* [101,102] in the 80s with the use of SAXS and WAXS. The authors proposed the cluster-network model (Figure 1.9) which is based on the aggregation of ionic groups in the form of spherical clusters dispersed in a hydrophobic PTFE matrix. The spherical clusters might be linked to an inverted micellar structure. According to this model, water is adsorbed and accumulated within the ionic clusters which conducts to their growth when the hydration level increases. At high hydration, the ionic clusters are interconnected by nanochannels to ensure the proton conductivity of the membrane.

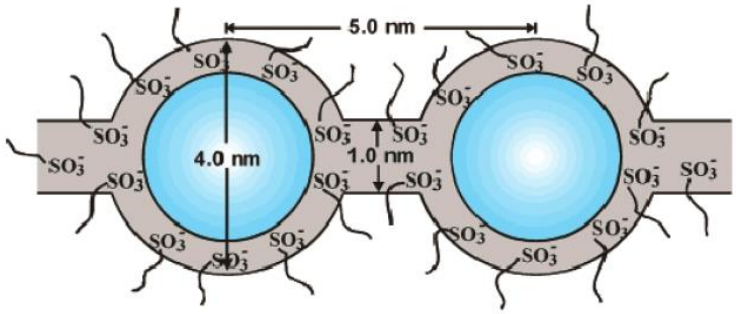

Figure 1.9 - "Cluster-network" model from Gierke *et al.* (Adapted from ref. [101]).

Another structural model based on the formation of elongated polymer aggregates surrounded by hydrophilic domains was suggested by Gebel *et al.* [103]. The authors monitored the morphological changes of the polymer from dry to fully hydrated state by SAXS and revealed an inversion of the polymer structure for a water volume fraction around 0.5: the reorganization of the hydrophobic matrix leads to a change from water within clusters surrounded by polymer to polymer surrounded by water (Figure 1.10). Their investigation highlighted that the structure of dry membranes consists in interconnected ionic clusters embedded in a polymer matrix which expand with the hydration level, as described by Gierke

et al.. On the other hand, the structure of fully hydrated membranes corresponds to a network of elongated polymeric aggregates in a cylindrical shape surrounded by water domains.

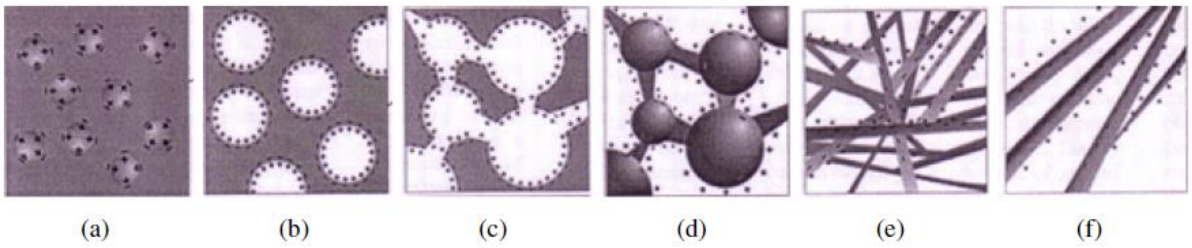

Figure 1.10 - Schematic representation of the Nafion™ structural evolution: (a) dry membrane , (b) swollen membrane, (c) percolation, (d) structure inversion, (e) connected network of polymer rods, (f) colloidal dispersion of rod-like particles (Adapted from ref. [103]).

Thereafter, Rubatat [104–106] performed a deeper investigation of Nafion™ structure from nanoscale to microscale and revised the model already proposed by Gebel. These studies permitted to demonstrate that the elongated polymeric aggregates were more likely present in the form of ribbon than cylinder but also that these aggregates were present in Nafion™ membrane even for weak water volume fraction. According to the model proposed by Rubatat *et al.*, the fluorocarbon chains aggregates at the nanoscale in the form of ribbon, ionic groups being located at the surface of the aggregates (Figure 1.11). At the micron scale, the elongated polymeric aggregates collapse to form relatively ordered bundles which are themselves randomly distributed and separated by amorphous domains. Furthermore, the membrane swelling does not include a structure inversion but corresponds to a continuous process of polymeric dilution when the water content increases.

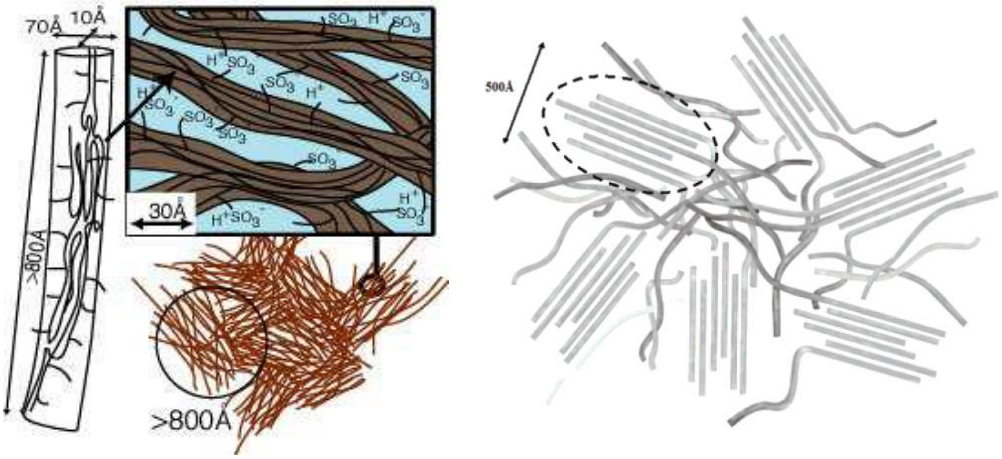

Figure 1.11 - Model of cylindrical polymeric aggregates proposed by Rubatat *et al.* [105,106].

In 2007, Schmidt-Rohr and Chen [107] proposed a new model by reinterpreting the SAXS measurements from the literature and described a network of parallel water channels surrounded

by partially hydrophilic side chains (Figure 1.12a). Contrary to the model proposed by Rubatat in which water circulates between the polymeric aggregates, water circulates inside the parallel water channels organized in the form of inverted-micelle cylinders, with a diameter comprised between 1.8 and 3.5 nm at high water content (20 vol.%). However, the authors do not contradict the ribbon-like structure but believed that the water volume fraction significantly influenced their presence.

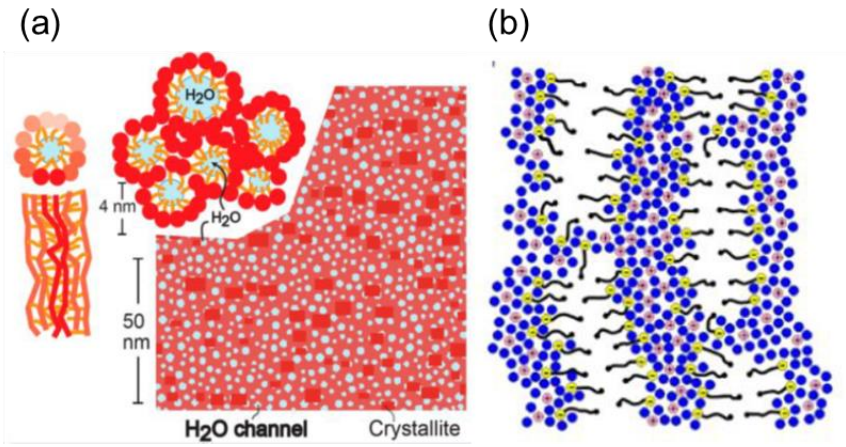

Figure 1.12 - (a) Parallel water-channel model proposed by Schmidt-Rohr & Chen [107] and (b) locally-flat interconnected domains model proposed by Kreuer & Portale [108].

This latter model was recently criticized by Kreuer and Portale [108] because of the misinterpretation of SAXS spectra evolution which can originate from a significant underestimation of the experimental water volume fraction (40 % for Kreuer and Portale *vs.* 20 % initially determined by Schmidt-Rohr and Chen). Consequently, they proposed a locally-flat morphology with a semi-lamellar organization of the PTFE backbone (Figure 1.12b). In this model, the authors suggested the formation of thin water films having a stabilizing effect on the polymer morphology and facilitating the balance of the electrostatic interactions.

2.2.Sorption and transport of water and protons

The proton conductivity of the membrane is directly related to its hydration level and is strongly dependent on external conditions such as temperature and relative humidity (RH) [109,110]. During fuel cell operation, a low humidity rate exposes the membrane to mechanical degradations while an excessive humidity rate leads to cell flooding and, possibly, to chemical degradations [111]. Water management within the membrane is thus a crucial parameter to keep the fuel cell performances and increase its durability.

2.2.1. Water sorption

The water sorption capacity of the membrane is ensured by the presence of the hydrophilic sulfonic groups. These -SO_3H functions are easily ionized and dissociate into protons H^+ and sulfonate groups -SO_3^- in the presence of polar molecules such as water. Moreover, the high acidity level of the sulfonic groups, with a pKa comprised between -1 and -5.1 [112], allows the membrane to adsorb water molecules even for very low water activity. This phenomenon explains the difficulty to totally dehydrate the membrane and thus to access its dry weight.

When the membrane is exposed to a humid gas flow, the membrane adsorbs a certain amount of water, depending on the relative humidity of the gas. Its water content is defined by the parameter λ, which corresponds to the number of water molecules per mole of sulfonic groups, expressed in mol.g^{-1}, and is related to the water-mass uptake for a given EW by the following relation:

$$\lambda = \frac{n(H_2O)}{n(SO_3^-)} = \frac{EW}{M_{water}} \times \frac{\Delta m}{m_p} \qquad \textbf{Eq. 1.9}$$

where M_{water} is the molar mass of water (18 g.mol^{-1}), m_p is the dry mass of the polymer and Δm is the mass variation between the hydrated and the dry states of the membrane.

The measurement of water sorption of a polymer is generally performed thanks to a gravimetric analysis. The method consists in monitoring the weight variations of a membrane exposed to a controlled water activity at a given temperature. The plot of the equilibrium mass, or of the parameter λ, as a function of the water activity a_w at constant temperature generates a sorption isotherm (Figure 1.13). The shape of the sorption isotherm is generally associated to three distinct sorption mechanisms:

- At very low water activity ($a_w < 0.15$), the water uptake increases steeply due to the dissociation of the highly hydrophilic sulfonic groups,
- For intermediate water activity ($0.15 < a_w < 0.70$), the water uptake increases linearly with the water activity,
- At high activity ($a_w > 0.70$), the water uptake rapidly increases again due to the aggregation of water molecules.

Furthermore, water sorption causes a macroscopic swelling of the membrane which can reach 15 % in thickness and 50 % in volume [113,114]. Such high swelling can be explained by the growth of water domains between the hydrophobic domains, separating the polymeric chains away from each other.

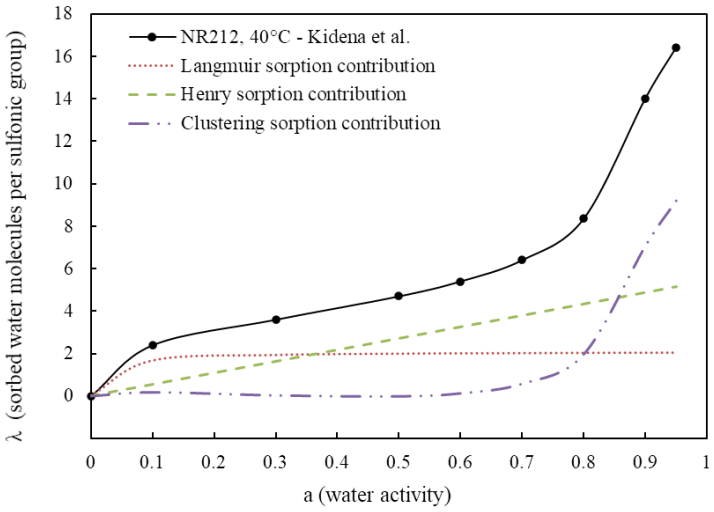

Figure 1.13 - Sorption isotherm of Nafion™ NR212 membrane at 40°C with the contribution of the different sorption mechanisms (Adapted from Ref. [115]).

Several models have been proposed to describe the sigmoidal shape and the different mechanisms of the sorption isotherm. According to the equation established by Park [116], the sorption isotherm can be divided into three contributions as graphically illustrated in Figure 1.13:

- The Langmuir contribution characterizes the formation of the first hydration shell in which sulfonic groups form strong hydrogen bonds with water molecules. This sorption mechanism occurs only at low water activity because it corresponds to a solvation process $SO_3^-H^+ + H_2O \rightarrow SO_3^- + H_3O^+$ [117].
- For a water activity comprised between 0.15 et 0.70, the adsorption of tightly bond water on the initial hydration shell is governed by Henry's law. The water uptake increases linearly with the water activity and the slope of the line characterizes the solubility of the water in the polymer.
- At high water activities, the weakly bond water molecules aggregate and adopted a bulk water behavior. This contribution can be described by the Flory-Huggins theory.

Although a sigmoidal shape of the sorption isotherm is always found in the literature, λ values can vary according to the experiments and the observed differences can be explained in two ways: first, the water uptake depends on several parameters such as the EW, the thickness or the temperature as well as the pretreatment [112,118,119]. On the other hand, the initial drying of the samples and thus the reference dry state differ according to the authors. As explained earlier, the complete dehydration of the polymer is quite difficult and numerous FTIR studies [120–124] have shown that a residual amount of water subsists in the membrane even

for intense drying processes. For instance, Korzeniewski *et al.* [123] estimated at $\lambda = 3$ the amount of residual water per sulfonic group after 24 hours of drying at 110 °C whereas according to Ludvigsson *et al.* [124], λ is still equal to 1.5 after vacuum-drying at room temperature. Moreover, Maldonado *et al.* [125] utilized the NMR spectroscopy to determine the amount of residual water in N115 membrane samples. The authors estimated this latter to $\lambda = 1.5 \pm 0.5$ when the membrane samples are heated in an oven during 24h at a moderate temperature ($60°C < T_{dry} < 100°C$). These various studies have thus proved that the establishment of water sorption isotherm is based on an initial value of λ highly dependent upon the drying conditions and frequently different from zero. More recently, several authors proposed alternative protocols to carefully dry conventional and hybrid nanocomposite Nafion™ membranes to eliminate all the water molecules and thus study the membranes in their dry state [74,126,127].

Furthermore, it has been demonstrated that the number of water molecules in a membrane exposed to a saturated environment ($a_w = 1$) is different depending on the way the equilibrium takes place: several authors reported a higher water uptake in Nafion™ exposed to liquid water than in the membrane exposed to saturated water vapor ($\lambda_{liq} \sim 22$ *vs.* $\lambda_{vap} \sim 14$), even though both states are thermodynamically stable and the activity of water is equal to one in both cases [118,119,128,129]. This difference has been called "Schroeder's paradox" in reference to the work of Schroeder [130]. Although the origin and the cause of this phenomenon has been extensively investigated, it has not been yet satisfactorily explained and is still open to debate. The phenomenon has been attributed for instance to the effect of pre-treatments on the polymer morphology, differences in the experimental protocols between authors or to kinetics effects. New studies are now rather focusing on the membrane interface or the thermal history experienced by the membrane.

2.2.2. Water diffusion

The transport of water through the membrane and its management represent key phenomena for the correct operation of the fuel cell. The membrane has to be adequately hydrated to facilitate proton migration from anode to cathode but the fuel cell should not contain an excess of liquid water which would have a detrimental effect on its performances. Indeed, the presence of water at the membrane-catalyst layer interface, as in the pores of the GDL (see § 3.1), restricts the access to the active sites and leads to a performance loss and an increase of the MEA degradation rate.

Under operation, several water transport mechanisms of different nature coexist in the membrane:

- electro-osmosis: the water molecules are dragged by the protons during their migration from the anode to the cathode.
- back-diffusion: this process corresponds to the transport of water molecules *via* a concentration gradient through the membrane (from cathode to anode).
- thermo-osmosis: this process occurs under the effect of a temperature gradient and causes the migration of water molecules from the hottest side to the coldest one.
- hydraulic permeation: this process corresponds to the motion of water molecules caused by a pressure gradient in the membrane.

All these mechanisms are interrelated and described by parameters linked to the water content.

The water diffusion can be assessed by several techniques such as steady-state permeation measurements, dynamic gravimetric water uptake, time-resolved FTIR or Pulsed Field Gradient NMR (PFG-NMR). These techniques can be divided into two groups according to the information of interest: PFG-NMR provides information about the water mobility at the micrometric scale by measuring the water self-diffusion coefficient (D_s) while the other techniques only provide global information about the average diffusion though the membrane at larger scale.

Water self-diffusion coefficient D_s describes the motion of water molecules under the influence of Brownian motion in the absence of a concentration gradient. If a lot of water molecules are observed over a long time, the mean square displacement $< r^2 >$ is different from zero and is given by the Einstein-Schmoluchowski equation as:

$$< r^2 > = 6D_s t \qquad \textbf{Eq. 1.10}$$

Figure 1.14 displays the typical evolution of the water self-diffusion coefficient, measured by PFG-NMR, as a function of λ in a Nafion™ membrane.

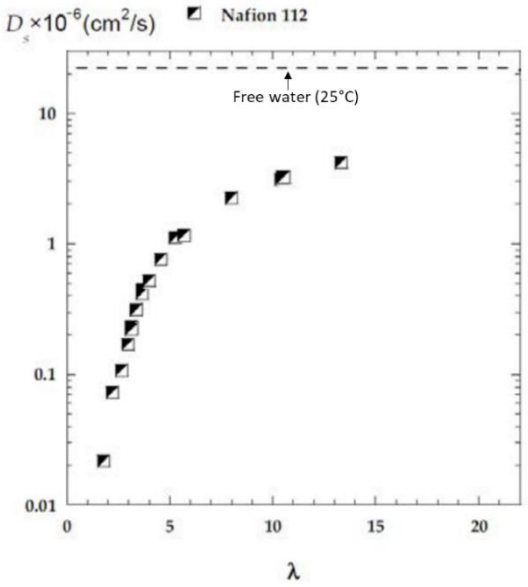

Figure 1.14 - Evolution of the water self-diffusion coefficient in Nafion™ N112 membrane at 25°C (Adapted from ref. [131]).

It can be noticed here that D_s increases rapidly with the water content at low hydration level ($\lambda < 5$) but slowly at higher hydration level ($\lambda > 5$). Furthermore, the maximum value obtained for the fully hydrated membrane (at $\lambda \sim 13$) approximates that of free water measured at a similar temperature ($D_s = 2..3.10^{-5}\ cm^2.s^{-1}$) since only a factor of five is observed between them. This result demonstrates that the polymer matrix is relatively unobtrusive for the water diffusion and that the tortuosity of the porous environment is weak at a fully hydrated state.

Monitoring the evolution of the water self-diffusion coefficient in the membrane when it is submitted to various stresses (mechanical and/or chemical) is an efficient method to correlate structural changes and water diffusion evolution as well as to provide some understanding about the proton conductivity of Nafion™ membranes.

2.2.3. Proton transport

Overall proton transport mechanisms are strongly related to the water transport and involve first the dissociation of the sulfonic groups. As mentioned in § 1.2.4, Nafion™ membranes have a significant acid strength which facilitates the -SO_3H dissociation and solvation into protons and sulfonate ions (Figure 1.15). It has been shown by Paddison and Paul [132] that this process requires the presence of at least two or three water molecules per sulfonic group. The solvation of sulfonic groups gradually conducts to the formation of hydronium ions H_3O^+ at low hydration and then bigger complex ions (Zundel-ions $H_5O_2^+$ or Eigen-ions $H_9O_4^+$, Figure 1.15) at high hydration, which enhances the mobility of protons in the water domains when the water content

increases. Indeed, with the addition of supplementary water molecules, the hydrophilic domains grow and interconnect with each other, leading to the formation of a percolated network and to the increase of the proton conductivity.

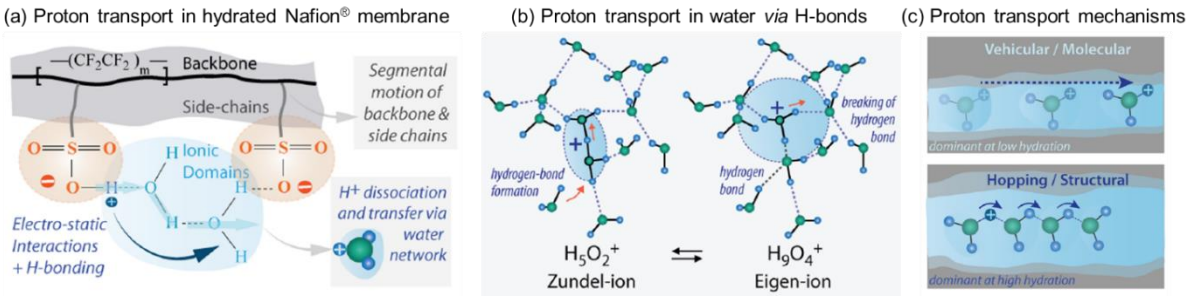

Figure 1.15 - Representation of the proton transport in hydrated Nafion™ membranes as illustrated by Kusoglu *et al.* [77]: (a) Nafion™ chemical structure and -SO_3H dissociation mechanism leading to the proton transport, (b) role of Zundel- and Eigen-ions in the proton transfer via H-bonds and (c) illustration of vehicular and hopping transport mechanisms.

The proton conductivity in the Nafion™ membranes has been widely assessed, discussed and modeled in the literature [109,133,134]. It is generally admitted that the proton transport is governed by two mechanisms: the Grotthuss hopping mechanism (structural diffusion) and the vehicular mechanism (mass diffusion), as illustrated in Figure 1.15. The Grotthuss hopping mechanism was first described by Agmon [135] as the transfer of a proton through a H-bond network between water molecules. It occurs mainly at high hydration level because it implies the fast breaking and forming of H-bonds as well as the reorientation of water molecules. At low hydration level, the hydrophilic domains are small and the ions resulting from the -SO_3H dissociation are poorly solvated, which limits the migration of the protons and the ionic rearrangements [136]. At this stage, the structural diffusion is slower and becomes vehicular, *i.e.* the proton is transferred *via* the ion-charge carrier H_3O^+ and thus depends on water diffusion: the result is in a very low proton conductivity [137].

This description of proton transport in the membrane has ben complemented by Choi *et al.* [137] with the introduction of a third transport mechanism: the surface diffusion taking place near the pore surface in the solvation shell of sulfonic groups. Several authors have studied the transport of water and protons in the membrane pores [109,136–138] and demonstrated that two kinds of water can be distinguished: water with a bulk-like behavior in the center of the hydrophilic domains, in which the proton transport is ensured *via* the Grotthuss hopping mechanism, and a surface water strongly bonded to the sulfonate ions. For this surface water, the proton migration is restricted by electrostatic interactions between -SO_3^- and H_3O^+ and the protons diffuses along the pores surface of the membrane by hopping from one sulfonate group

to the adjacent one. At low hydration level, most of water is bound and the major contribution to proton conduction is the surface diffusion which permits the interpretation of conductivity drop by the slow motion of protons at the interface of sulfonate ions. The conductivity drop can be osbserved in Figure 1.16 illustrating the evolution of the proton conductivity as a function of water activity in Nafion™ membrane at a fuel cell operating temperature of 80 °C [125].

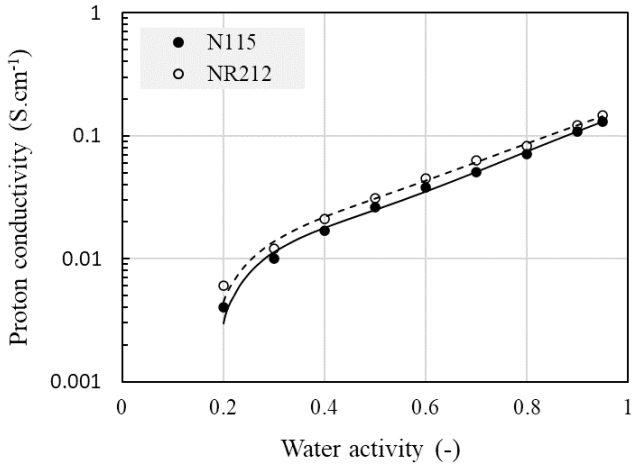

Figure 1.16 - Proton conductivity *vs.* water activity at 80°C for N115 and NR212 Nafion™ membranes (Adapted from ref. [125]).

Indeed, two regions can be distinguished on the curve in Figure 1.16: for a low water activity ($0.2 < a_w < 0.3$), the proton conductivity increases at first rapidly with the hydration, and then much more gradually. The proton conductivity is commonly measured over the relative humidity/water activity of the membrane *via* the electrochemical impedance spectroscopy (EIS) and its typical value for a fully hydrated Nafion™ membrane is about 0.15 S.cm^{-1} at 80 °C.

Since proton conductivity involves multiple phenomena as a function of the hydration level and since some morphological orientation can result from the manufacturing process of the ionomer film, a perfect isotropy of the conductivity cannot be guaranteed. For instance, it has been shown that the conductivity in the plane of the membrane is higher than that through the plane (cell assembly direction) in composite membranes such as Nafion™ XL since a preferential orientation can be induced at various length scales [96]. On the other hand, several studies demonstrated that the membrane pretreatment modifies the water-uptake capacity and thus the proton conductivity: both parameters decrease in the case of predrying and increase in the case of preboiling [125,139,140].

2.3.Mechanical properties

As mentioned in § 1.2.4, the PTFE backbone governs the mechanical properties of the membrane and thus confers to the membrane its mechanical endurance . During transient fuel cell operation, the succession of swelling/shrinkage events caused by changes in water uptake and temperature creates high stresses and can lead to the membrane failure by formation of cracks or pinholes, as well as to the delamination of the membrane-electrode interface.

A lot of studies were carried out to characterize the mechanical stability of PFSA membranes by analyzing various parameters such as the dynamic mechanical response and thermal transitions, the stress-strain behavior and plastic deformation, the time-dependent behavior and the visco-elastic/plastic response as well as the fracture behavior [88,141–144]. In general, the uniaxial tensile test is the most commonly used technique since the analysis of stress-strain curves can provide multiple key parameters such as the Young modulus (E), the proportional limit stress (PLS) or the yield strength (YS) and the break strain. Figure 1.17 illustrates typical stress-strain curves measured on a Nafion™ membrane exposed to various humidity and temperature conditions.

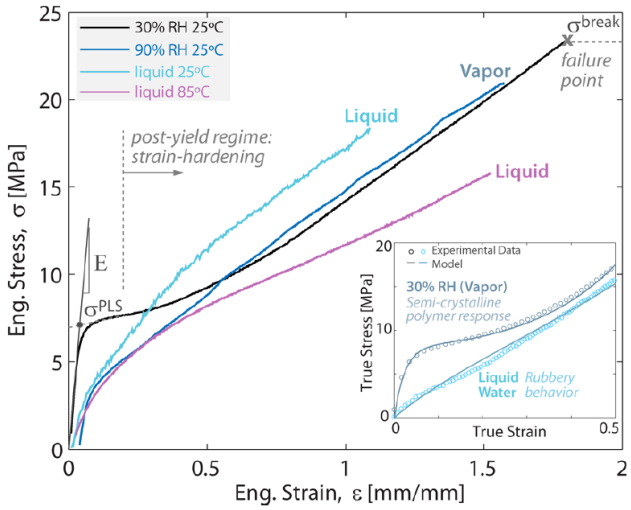

Figure 1.17 - Stress-strain response of a Nafion™ membrane under various environmental conditions. The inset illustrates the mechanical behavior of the membrane as a function of the nature of the sorbed water [77].

The stress-strain curve can be divided into two parts: an elastic behavior of the membrane which follows the Hook's law and a plastic behavior associated to non-recoverable changes. As seen on Figure 1.17, this behavior is strongly dependent on the temperature and humidity conditions because of the two-phase separated morphology of the polymer. At low hydration level, the mechanical response of PFSA membranes is similar to that of semi-crystalline polymeric material whereas a rubbery behavior can be observed at high hydration levels (as shown by the inset of the Figure 1.17).

Several other studies have also demonstrated the dependence of the mechanical properties to the pretreatment conditions (RH and T) and manufacturing processes since they can induce structural changes and thus different deformation responses [114,141,145–149]. For example, Kusoglu and his co-workers [114,145,146] highlighted that extruded membranes exhibit greater mechanical properties in the machine direction in comparison with the transversal direction while the mechanical properties of cast membranes present less anisotropy in the plane. Lu *et al.* [147] studied the influence of relative humidity (RH) and temperature (T) on the in-plane swelling and the mechanical properties of a Nafion™ NR211 (Figure 1.18). The authors demonstrated that the change from ambient conditions (25 °C, 30 % RH) to fuel cell operating conditions (80 °C, 100 % RH) induced a 15 % increase of the membrane length and a drastic decrease of its mechanical strength. For example, the Young modulus and the proportional limit stress are respectively reduced from 350 to 30 MPa and from 14 to 3 MPa, showing a dramatic loss of material stiffness.

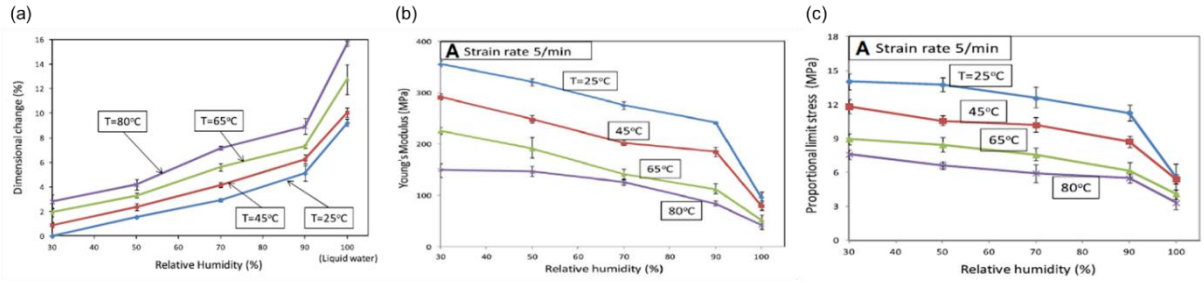

Figure 1.18 - Evolution of (a) in-plane swelling, (b) Young's modulus, (c) proportional limit stress of Nafion™ NR211 membrane as a function of relative humidity for various temperature [147].

More recently, Kusoglu *et al.* [145] also studied the effect of compression on PFSA membrane mechanical properties. Indeed, most of the studies have been focused on the mechanical response of PFSA membranes submitted to tensile force whereas membranes operating in fuel cell systems are most probably exposed to compressive stress in a global way and only locally exposed to tensile stress. Thanks to SAXS analysis, they demonstrated that the application of a compressive stress on the membrane leads to an anisotropy of its nanostructure related to swelling. The authors showed that the slight conductivity reduction induced by compression in high humidity conditions is consistent with the water-uptake and morphology changes.

Furthermore, composite PFSA membranes with a PTFE-based reinforcement reveals enhanced mechanical properties [88,150–152]. For example, Tang *et al.* [88] demonstrated that reinforced Gore-select™ membrane, containing an e-PTFE matrix, exhibited higher mechanical

strength than the unreinforced Nafion™ N112 membrane with a Young modulus more than two times greater at ambient conditions (25 °C, 30 % RH).

3. Degradation mechanisms of membrane-electrode assemblies (MEA)

Over the past decades, a lot of studies considered aging and reliability of the MEA and provided some understandings on their degradation mechanisms, with the overall objectives to improve their durability and reduce their cost [49,153–155].

This section summarizes the main degradation mechanisms of MEA components, with an emphasis on the membrane in § 3.3. Although interest of this thesis work is focused on PFSA membrane, the two following sections aim at providing an overview of the gas diffusion media and catalyst layers degradation, which are components as much important as membrane in the efficient operation of PEMFC. Nevertheless, these sections are not indispensable for the understanding of subsequent chapters of the manuscript. On another note, it is important to keep in mind that the other cell components (i.e. bipolar plates and gaskets) are also likely to deteriorate during fuel cell operation, although their degradation mechanism will not be fully described in this memoire. In short, gaskets made from silicon are prone to degrade and pollute the membrane and the electrodes [156] while metallic bipolar plates can release cationic impurities into the MEA [157].

3.1. Gas diffusion media

Gas diffusion layer (GDL) and microporous layer (MPL) aim at facilitating reactant gases transport as well as to evacuate the water produced by the electrochemical reaction. Some studies have demonstrated that these materials degrade during fuel cell operation, leading to a hydrophobicity loss and a mass reduction [158–160]. Moreover, MPL are found to be vulnerable to chemical oxidation by water, entailing the formation of surface carbon oxides (CO and CO_2) [161,162]. This carbon loss by chemical oxidation diminishes MPL hydrophobicity with, as a result, the accumulation of more water in the pores, thus inducing a restricted access of gases to the actives sites. Several investigations [163–167] have highlighted the relation between microstructure changes and mass transport properties, showing that a decrease of GDL and MPL hydrophobicity and a modification of pore size can significantly impact the mass transport.

3.2. Catalyst layers

The catalyst layers are composed of three elements: carbon-based support, Pt or Pt-alloy catalyst and ionomer binder. Each of them can be the subject of various degradation processes during fuel cell operation leading to a loss of electrochemical active surface area (ECSA) and thus to the decrease of fuel cell performances.

3.2.1. Degradation mechanisms of the catalyst

Mechanisms of Pt catalyst degradation during fuel cell operation have been intensively investigated during the past decades. It is well established that the decrease of ECSA is far more severe at the cathode side than at the anode side due to higher local potentials in regular operation as well as during transients [168,169].

First of all, Pt particles are sensitive to their environment and may be contaminated by impurities coming from the gases (hydrogen or air), the fuel cell or its auxiliaries (metallic components or other chemicals) [170]. The presence of contaminants in the fuel cell system can generate reversible or irreversible performance losses [171,172]. Indeed, Pt particles are sensitive to ionic impurities, such as Cl^-, F^- or HSO_4^- [154,170]. Schmidt *et al.* [173] especially highlighted a reduction of ORR activity due to the presence of ClO_4^-, HSO_4^- and Cl^-. Contamination of the fuel cell by carbon oxide (CO), hydrogen sulfide (H_2S) or ammonia (NH_3) species have also been extensively examined in the literature [170,174,175]. Indeed, they can be absorbed at the Pt surface blocking the access of the catalytic sites to H_2 or O_2. The ECSA losses can originate from multiple catalyst degradation mechanisms [154,176–178]. They are generally divided into four categories:

- Particles dissolution and redeposition,
- Electrochemical Ostwald ripening,
- Particles migration and coalescence/agglomeration,
- Particles detachment.

A summary of these degradation mechanisms is illustrated in the Figure 1.19.

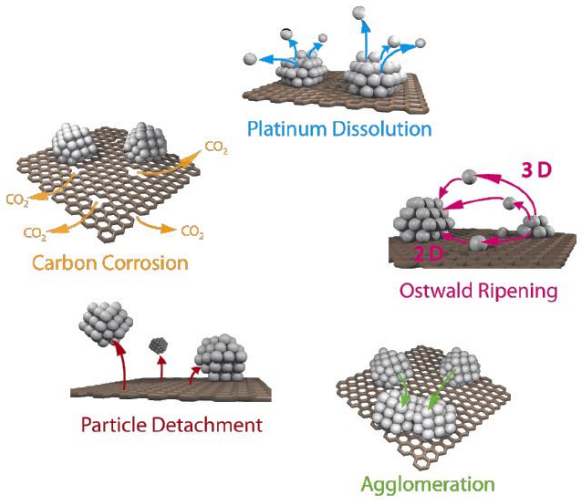

Figure 1.19 - Schematic representation of degradation mechanisms for Pt particles and carbon-based support in PEMFC catalyst layers proposed by Meier *et al.* [179].

The dissolution-redeposition process corresponds to the dissolution of Pt^0 particles into Pt^{n+} ions which will then migrate through the ionomer, both in the catalyst layers and the membrane, over long distances. As the Pt catalyst is unstable in acidic environment and at high voltage, the dissolution into Pt^{n+} ions on the cathode side can occur:

$$Pt \rightarrow Pt^{2+} + 2e^- \qquad E^0 = 1.12 + 0.03\log[Pt^{2+}] \qquad \textbf{Eq. 1.11}$$

The dissolved Pt species will migrate and may then precipitate in the membrane by reacting with the hydrogen coming from the anode side (by hydrogen crossover):

$$Pt^{2+} + H_2 \rightarrow Pt^0 + 2H^+ \qquad \textbf{Eq. 1.12}$$

The predominant mechanism or pathway for the dissolution-redeposition of Pt particles is still under discussion: it is difficult to determine whether fuel cell operating conditions lead to a dissolution by direct oxidation of Pt^0 or *via* the formation of intermediate Pt oxides [180,181]:

$$Pt^0 + H_2O \rightarrow PtO + 2H^+ + 2e^- \qquad E^0 = 0.98 - 0.06\text{pH} \qquad \textbf{Eq. 1.13}$$

$$PtO + 2H^+ \rightarrow Pt^{2+} + H_2O \qquad \textbf{Eq. 1.14}$$

$$PtO + H_2O \rightarrow PtO_2 + 2H^+ + 2e^- \qquad E^0 = 1.05 - 0.06\text{pH} \qquad \textbf{Eq. 1.15}$$

$$PtO_2 + 4H^+ + 2e^- \rightarrow Pt^{2+} + 2H_2O \qquad E^0 = 0.84 - 0.12\text{pH} - 0.03\log[Pt^{2+}] \qquad \textbf{Eq. 1.16}$$

At high operating voltage (> 0.85 V_{SHE}), the passivation of Pt particles has been observed and generates the formation of PtO and/or PtO_2 at the surface of particles, which in turn decreases the availability of catalytic active sites [155]. The presence of such oxides has been detected both at the anode and the cathode sides by X-ray photoelectron spectroscopy (XPS) [168].

The electrochemical Ostwald ripening also implies the dissolution of Pt particles into the ionomer phase. Contrary to the dissolution-redeposition process detailed earlier, the migration occurs only over short distances, leading to the redeposition of Pt^{n+} ions in catalyst layer on preexisting particles and consequently to the formation of larger Pt particles. This mechanism is believed to be more severe for smaller Pt particles since their surface energy is greater, so that they dissolve at lower potentials.

The migration and coalescence process consists in the migration of Pt particles on carbon support surface which will collide to give rise to a larger particle. This phenomenon permits to reach a lower surface/volume ratio and thus diminishing the surface energy of Pt particles.

The Pt particle detachment from the carbon-based support directly results from carbon corrosion (see § 3.2.2) and causes a loss of ECSA. Once separated from the support, Pt particles can either remain isolated or agglomerate with other Pt particles.

This agglomeration phenomenon has been highlighted by Nikkuni *et al.* [182] thanks to identical-location transmission electron spectroscopy (ILTEM) measurements. This technique permitted to carry out particles aging tests on a TEM grid and thus obtain micrographs of an identical area before and after aging (as illustrated on Figure 1.20).

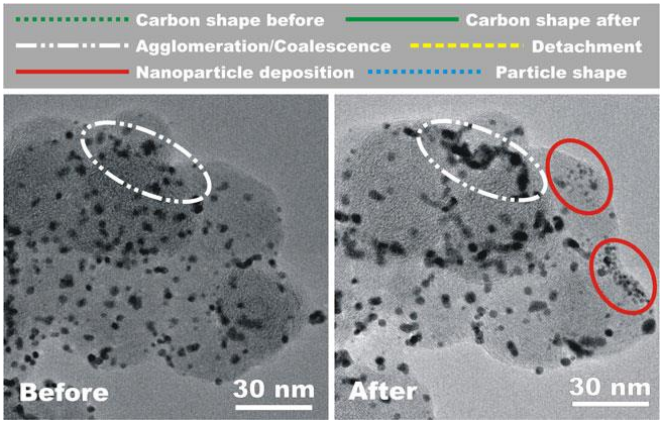

Figure 1.20 - Micrographs of a specific area obtained by the ILTEM technique highlighting different catalyst degradation mechanisms [182].

Pt particles have a diameter size in the range of nanometer (2-3 mm) to attain a higher specific area. Particles dissolution is partially dependent on the electrode potentials as well as on potential variations (steady state or transient FC operation) [176,183,184]. Indeed, potential cycling between the oxidation and reduction regions of the catalyst accelerates the Pt particles dissolution process while holding the potential at a high level, *i.e.* in the oxide formation region, decreases the Pt particle dissolution thanks to the formation of protective oxide film at the

particle surface [184]. Furthermore, humidity is also an important factor for catalyst degradation: Xie *et al.* [185] have demonstrated for instance that catalyst particles agglomeration and growth worsened significantly when the gas inlet relative humidity was increased from 20 % to 70 %.

Numerous studies demonstrated the formation of a Pt band into the membrane, as a result of the dissolution-redeposition of Pt particles, after fuel cell operation [153,177,178,186–189]. More particularly, Péron *et al.* [189] demonstrated that Pt band can already be seen after only 50 hours of Open-Circuit Voltage (OCV) hold (Figure 1.21).

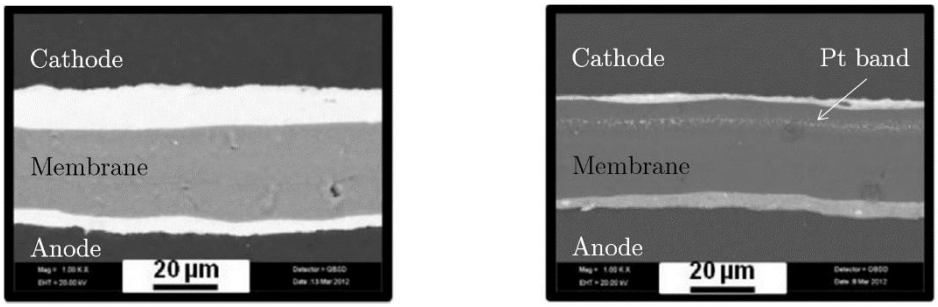

Figure 1.21 - cross-section SEM images (magnification x1,000) of (a) pristine MEA and (b) aged MEA after 136 startup and shutdown cycles [190].

The location of the Pt band depends on gases crossover, *i.e.* on the respective fluxes of oxygen and hydrogen through the membrane [191,192]. Kim *et al.* [193] studied the location of the Pt band in a reinforced membrane submitted to various fuel cell operating conditions and reported different distribution patterns of Pt particles deposition (Figure 1.22). They observed the formation of a Pt band at 1-10 µm of the cathode-membrane interface when the cell is fed with air, that moves towards the anode when the pure oxygen is employed due to an increase of crossover oxygen and a decrease of crossover hydrogen. On the other hand, they also reported a higher Pt deposition rate under OCV than under constant current operation.

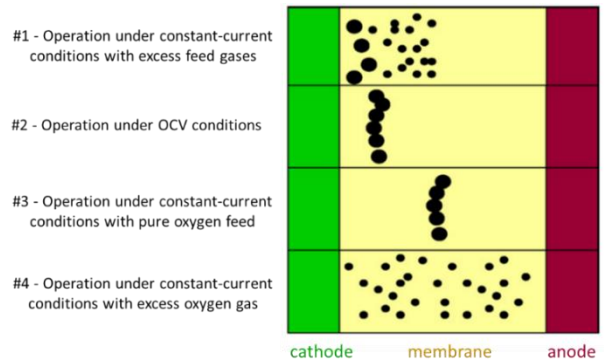

Figure 1.22 - Distribution patterns of Pt band in the membrane under various operating conditions (Adapted from ref. [193]).

The presence of Pt species in the membrane, whether it is under the form of Pt^{n+} ions or Pt band, can impact its chemical degradation mechanisms. However, their influence is not yet completely understood since both an acceleration of the membrane chemical degradation and an improvement of the membrane stability have been demonstrated [194,195]. The influence of Pt band and Pt^{n+} ions on the membrane degradation will be discussed in § 3.3.2.2.

3.2.2. Degradation mechanisms of the carbon-based support

The degradation of the carbon-based support is another important issue which limits the catalyst layers durability [161,196–198]. The carbon-based support is thermodynamically unstable in the operating conditions of the PEMFC and is particularly prone to oxidation during FC startup and shutdown, or other fuel starvation events [199,200]. The reaction of carbon with water entails the formation of CO and CO_2:

$$C + H_2O \rightarrow CO + 2H^+ + 2e^- \qquad E^0 = 0.207\ V_{SHE} \qquad \textbf{Eq. 1.17}$$

$$C + 2H_2O \rightarrow CO_2 + 4H^+ + 4e^- \qquad E^0 = 0.518\ V_{SHE} \qquad \textbf{Eq. 1.18}$$

CO_2 formation reaction prevails on CO formation, following a two-step process involving surface oxides and their oxidation by O-abstraction from water:

$$C + 2H_2O \rightarrow CO_{ad} + 2H^+ + 2e^- \qquad \textbf{Eq. 1.19}$$

$$CO_{ad} + H_2O \rightarrow CO_2 + 4H^+ + 4e^- \qquad \textbf{Eq. 1.20}$$

And one can easily understand from these equations that a high relative humidity of gases as well as water accumulation within the cell will increase the carbon corrosion rate [196,201]. In addition, high temperatures also increase the kinetic of carbon corrosion.

In addition to the temperature and the humidity level, other factors greatly affect the carbon-based support degradation during the fuel cell operation such as the potential and consequently the operating conditions of the PEMFC (OCV or repeated startup and shutdown conditions, for example), the nature of the catalyst as well as the chemical state of carbon. In the list below is detailed the impact of these various factors on the carbon corrosion rate.

Potential

The kinetic of carbon oxidation being slow in regular FC operating conditions, it is generally accepted that carbon corrosion becomes significant only above 1 V. Maass *et al.* [196] observed an important increase of the carbon corrosion rate beyond this threshold, with a doubling of the corrosion rate between 1.0 and 1.2 V. Moreover, during startups and shutdowns, or when the

cell is let in Open-Circuit, high cathode potential accelerates carbon corrosion [197], which can lead to a gradual thinning of the catalyst layers and modify their porous structure.

Nature of the catalyst

The nature of anode and cathode catalyst is also a factor that can accelerate the carbon corrosion. For instance, Roen *et al.* [201] demonstrated that CO_2 emission rate were significantly higher with Pt/C or PtRu/C catalyst layers than with free-catalyst layers.

Chemical state of carbon

Castanheira *et al.* [202] observed by XPS and Raman spectroscopies the formation of oxygen species for potential lower than 1 V. Indeed, commercial MEA are based on graphitized carbon and present some amorphous areas with crystal defects which are prone to be oxidize even at low potentials. The hydrophobic properties of the carbon are thus altered causing a loss of gas transport efficiency and a mismanagement of the water. Among the mitigation strategies developed in the last few years, the used of more graphitized carbon-based support comprising less crystal defect prone to the oxidation seems promising to limit the carbon corrosion. Although carbon corrosion is more likely to happen at high voltage, this phenomenon has also been reported for a voltage below 0.2 V and was attributed to chemical oxidation by hydrogen peroxide [196].

To conclude, carbon corrosion entails several consequences: it leads to an electrode thinning [169,203,204] as well as it weakens the interaction between the carbon and the Pt particles, promoting the Pt detachment and agglomeration (by coalescence and/or Ostwald ripening), causes an ECSA reduction and thus a loss of performances [205].

3.2.3. Degradation mechanisms of the ionomer binder

Despite numerous publications focusing on membrane degradation mechanisms, only a few were conducted on the degradation of the ionomer binder in the electrodes. Indeed, its low amount in catalyst layers as well as the difficulty to extract properly the ionomer from the other components (Pt particles and carbon-based support) impede the observation of structural changes with traditional characterization techniques (SEM, TEM, Raman, IR).

Danérol *et al.* [203] have shown by X-ray diffraction (XRD) that the structure of the electrode was modified after 1397 hours of fuel cell operation at 60°C. The X-ray analysis was carried out on pristine and aged MEA. On the X-ray diffractogram presented in Figure 1.23, two new elements appeared at 14° and 18° which are assigned to structural modification of the

ionomer binder. Indeed, these two peaks are characteristic of ionomer chain reorganization and more precisely to an increase of crystallinity. This structural change can be explained by a possible decrease of side chains as a result of chemical degradation or by the formation of shorter ionomer chains due to unzipping reaction of main chains. El Kaddouri [1] studied this further thanks to X-ray diffractometer by analyzing directly electrodes that were mechanically extracted from aged MEA, thus permitting to study separately anode and cathode sides. They also conclude that the chain organization of ionomer binder changes after fuel cell operation. On the cathode side, they observed an increased ionomer binder crystallinity while on the anode side it tends to slightly decrease. The ionomer binder degrades differently at the anode and cathode, which could be understand by the fact that operating conditions are very different in both electrodes.

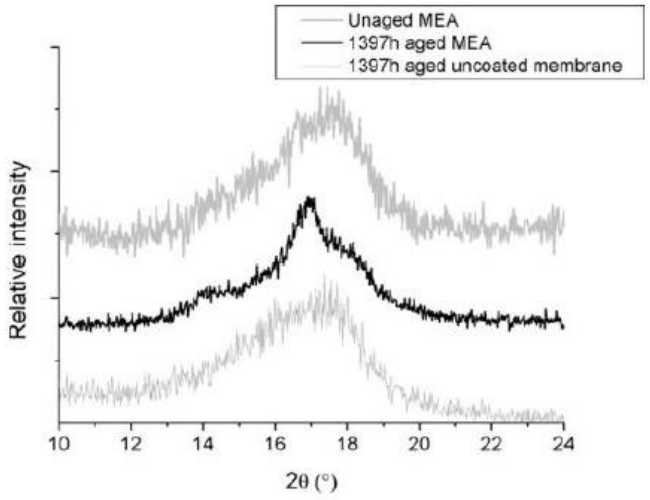

Figure 1.23 - X-ray diffractogram of pristine MEA and 1397h aged MEA before and after removing electrodes [203].

Accelerated stress tests in single cells highlighted structural modification and material loss after aging [206–208]. Parry *et al.* [207] analyzed electrodes after voltage cycling under pure hydrogen and under hydrogen with 5 ppm of CO at the anode: XPS analyses revealed a decrease of CF_2 – and CF_3 – bonds corresponding to a ionomer loss around 13.2 % after 550 h of voltage cycling with pure hydrogen and around 10.6 % after 630 h of voltage cycling with pure hydrogen polluted with 5 ppm of CO. Zhang *et al.* [206] confirmed a ionomer loss with a decrease of fluorine content from 50 % to 39 % after 300 h of voltage cycling.

Aoki *et al.* [209] performed *ex-situ* experiments to study the ionomer binder decomposition caused with the gas crossover by measuring the fluoride ion emissions characteristic of PFSA chemical degradation. In the absence of ionomer membrane, Gas Diffusion Electrode (GDE)

were submitted to a mixed gas of H_2 and air with various relative humidity: hydrogen containing 10 % of air (H_2-rich conditions) at the anode side and air containing 2 % of hydrogen (O_2-rich conditions) at the cathode side has been employed to simulate gas crossover during fuel cell operation. The authors highlighted a significant degradation of ionomer binder dependent on the nature and relative humidity of gases (Figure 1.24).

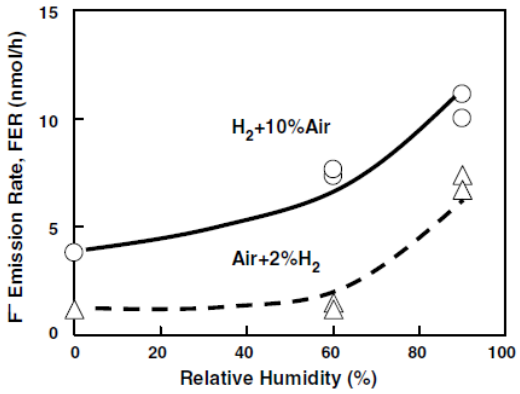

Figure 1.24 - Dependencies of FER on the relative humidity in H_2/air mixed gas at 80°C in the absence of membrane between GDEs [209].

Morawietz *et al.* [210] have measured the thickness of ionomer film in anode and cathode catalyst layers from pristine and aged MEAs thanks to the atomic force microscopy (AFM). Aged commercial and experimental MEAs were characterized after 235 h of steady state operation in a single cell. For the aged commercial MEA, the authors reported an important thinning (33 %) of the ionomer film in the anode catalyst layer whereas no significant thickness variation was observed on the cathode side. On the contrary, the ionomer layer thickness of the aged experimental MEA significantly decrease on both sides (42 % at the anode side and 33 % at the cathode side).

More recently, El Kaddouri *et al.* [204] investigated the degradation of PFSA ionomer binder in catalyst layers extracted from MEAs after several thousand hours of operation. They identified, thanks to liquid ^{19}F Nuclear Magnetic Resonance (NMR) spectroscopy and after water Soxhlet extraction, a dominant degradation product: 1,1,2,2-tetrafluoro-2-(1,2,2,2-tetrafluoroethoxy)ethanesulfonic acid (*H-CF(CF₃)-O-CF₂-CF₂-SO₃H*). The chemical structure of this degradation product is clearly related to the PFSA side-chain and is specific to the degradation of ionomer binder in catalyst layer since it has been detected only after Soxhlet extraction performed on electrodes and not on membrane with the same batch of aged MEA. Moreover, this degradation product has been observed both at the anode and cathode sides. Furthermore, El Kaddouri *et al.* [1] also highlighted two others degradation products from

dimethylacetamide extracts of aged electrodes. Indeed, they detected trifluoroacetic acid – known as decomposition by-product of PFSA unzipping degradation [185,211,212] – and triflic acid which have similar chemical structure as the end of side chain. In addition, Takasaki *et al.* [213] also investigated the degradation of PFSA ionomer binder in catalyst layers after accelerated stress (OCV-hold and load cycling) tests by analyzing PFSA polymer residues of catalyst layers thanks to ^{19}F NMR spectroscopy. In that purpose, the authors carefully peeled off the catalyst layers from the MEAs and elaborated a specific extraction protocol to isolate the eventual degradation products. They revealed the presence of six degradation products (Figure 1.25), including that identify by El Kaddouri *et al.*, which seems to originate from radical attacks of PFSA side-chains. Moreover, they observed similar degradation rates between anode and cathode sides either for the OCV-hold test or the load cycling test and also a significant variation between these two tests, the amount of degradation products being four times higher for the OCV-hold test than for the load-cycling test (Figure 1.25).

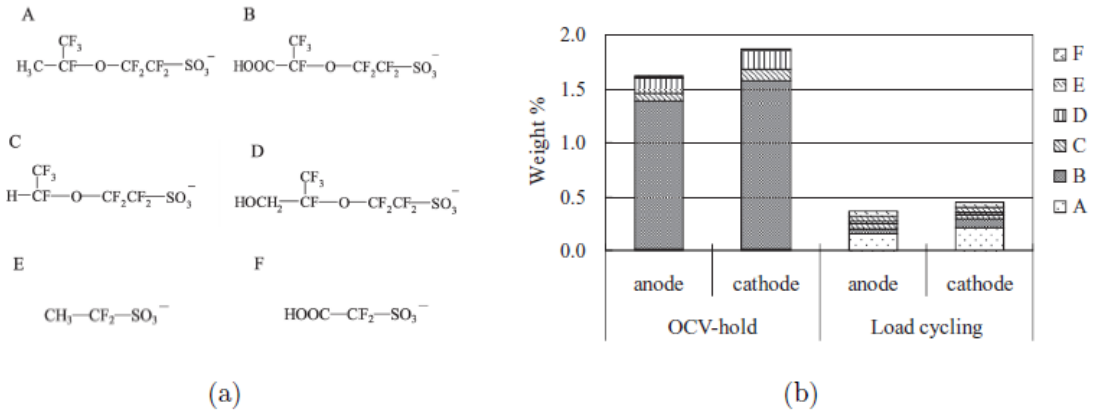

Figure 1.25 - (a) chemical structure and (b) abundance of side-chain fragments identified in extracts from catalyst layers after accelerated aging protocols [213].

In conclusion, likewise the carbon-based support and the Pt particles, the ionomer binder in the catalyst layers is also subject to degradation. Nevertheless, the ionomer binder degradation has been less studied than that of Pt particles or carbon-based support because of its low-level presence in the catalyst layers and the difficulty to dissociate the ionomer membrane degradation from that of the ionomer binder after fuel cell operation.

3.3.PFSA membranes

The degradation of PFSA membranes remains one of the main factor limiting PEM fuel cells lifetime as membranes are exposed to harsh conditions during fuel cell operation, among which aggressive chemical environment and mechanical fatigue prevail. Through the years,

innumerable studies have been carried out to provide key understandings on degradation mechanisms as well as their impact on the structure and properties of PFSA membranes [77,154,155,214,215].

Multitude of stressors affects the membrane stability during fuel cell operation and leads to the polymer chemical decomposition, the membrane thinning, the loss of mechanical integrity as well as the formation and growth of creeps, cracks, pinholes. Figure 1.26 illustrates the relations between the operating conditions, the main degradation mechanisms and the measurable effects as initially proposed by Bruijn *et al.* [155].

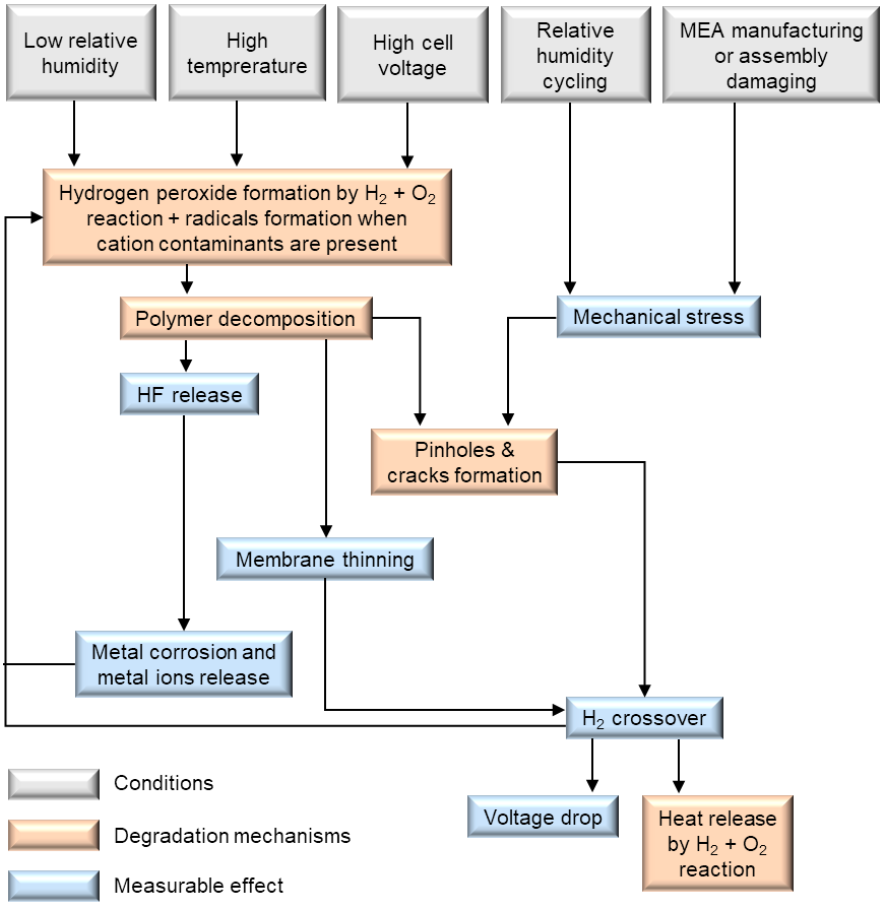

Figure 1.26 - Degradation effects, conditions, and mechanisms for PFSA membranes (Adapted from ref. [155]).

Although the membrane degradation is believed to occur due to complex and interrelated chemical and mechanical mechanisms [216–219], these stressors are most often studied alone and more rarely considered together. In that respect, each degradation mode (mechanical or chemical) will be first detailed separately in order to introduce the different degradation mechanisms proposes in literature and then the conjoint effect of these two will be considered to describe the overall membrane degradation.

3.3.1. Mechanical degradation

Mechanical fatigue is typically considered as the main source of early-life failure for thin membranes (< 50 µm) and manifests itself through the appearance and growth of cracks, pinholes, creeps and tears into the membrane or by delamination at the membrane/electrode interface (Figure 1.27). However, it is important to note that delamination between the membrane and the electrodes is not necessarily a consequence of the mechanical fatigue occurring during fuel cell operation but can also originates from polymer decomposition at the membrane/electrodes interface or from the degradation of the carbon-based support in the electrodes, for example. These defects can be originally introduced by the MEA manufacturing process, due to the presence of foreign particles which can perforate the membrane or due to a mismanagement of mechanical stresses at the reactant inlets and close to the edge of MEA frame. It is also important to note that, despite the presence of gas diffusion layers on both sides of the membrane-electrodes assembly (MEA), the distribution of constraints remains non-uniform due to the complex shape of the flow field plates [220].

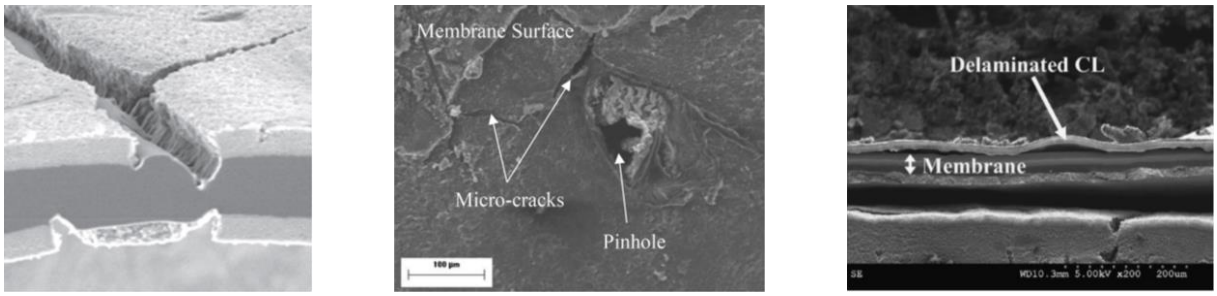

Figure 1.27 – Consequence of the membrane mechanical degradation: crack formation (*left*) [221] – pinhole formation (*middle*) [218] – delamination at the membrane/electrodes interface (*right*) [222].

During fuel cell operation, PFSA membranes are exposed to humidity cycling which generates large variations of the membrane water-uptake. When repeated many times, these swelling/shrinkage cycles weaken the mechanical integrity of the membrane, alter its structure by causing irreversible plastic deformations and may subsequently lead to the formation and growth of cracks and pinholes [221,223–225]. More particularly, the channel/land transition area – where the membrane is constrained under the land and free to move under the channel – has been shown as a high-constraint area in which residual tensile stress in the plane of the membrane can reach up to 10 MPa and can accelerate the membrane degradation as a consequence of membrane swelling/shrinkage cycles [226–228]. In addition, inadequate humidification of reactant gases, and thus of the membrane, accelerates the membrane degradation since it becomes more brittle and prone to plastic deformation under low humidity

conditions [229,230]. Water management during fuel cell operation and membrane hydration are thus crucial parameters affecting its mechanical and thermal properties.

Mechanical endurance of PFSA membranes is usually investigated with uniaxial tensile tests in order to assess the Young modulus (E), proportional limit stress (PLS) or yield strength (YS), and break strain. However, these do not completely represent all mechanical stress that membrane undergoes during fuel cell operation since some failure are due to crack initiation and propagation. This is why other *ex-situ* investigations as essential work of fracture (EWF) tests were proposed as a complement to tensile tests in order to represent initiation and propagation of cracks. Indeed, Moukheiber *et al.* demonstrated that crack propagation was favored in the direction of polymer chains, indicating that the membrane durability can be extend by positioning the membrane in order to orientate polymer chains perpendicular to gas channels. Furthermore, they also highlighted that reinforced Nafion™ XL membrane show a better resistance to crack initiation and propagation than unreinforced membranes [231]. On another note, Jia *et al.* demonstrated that the presence of cationic contaminants into the membrane has a detrimental effect on its fracture resistance and especially at the membrane/electrodes interfaces [232].

The principle mitigation strategy developed in order to increase the membrane resistance to crack initiation and propagation is the introduction of reinforced structure into the membrane. The reinforcement layer permits to reduce the swelling in the plane of the membrane, and thus stresses generating plastic deformation [233,234], as well as to reduce the fatigue crack initiation and propagation [225,231,235]. In addition, it is possible to optimize the operating conditions, such as the speeds of startup and shutdown, humidification level of reactant gases or the cell temperature, in order to ensure a good water management in the membrane to reduce the swelling/shrinking cycles.

More details can be found in the comprehensive review of Qiu *et al.* which aims at describing the various mechanisms of membrane mechanical failure, their impact on fuel cell performances and the mitigation strategies developed for improved membrane mechanical durability [236].

3.3.2. Chemical degradation

Through the years, chemical decomposition of PFSA membranes have been clearly identified during fuel cell operation [214,215,237]. It results from the formation of hydrogen peroxide and its decomposition into reactive oxygen species (ROS): the hydroxyl (HO•),

hydroperoxyl ($HOO^{\bullet}$) and hydrogen ($H^{\bullet}$) radicals (see § 3.3.2.1) [237–239]. These reactive oxygen species attack the most vulnerable bonds of the PFSA structure, located both in the fluorocarbon backbone and the perfluorinated side chains, leading to the polymer decomposition. A lot of studies have been carried out to provide understandings on chemical degradation mechanisms following different approaches: fuel cell aging in real operating conditions as well as *in-situ* and *ex-situ* aging protocols.

In the case of fuel cell systems that have operated in the field in real conditions, the different operating conditions (RH, temperature, cell voltage, stoichiometry, start/stop cycles, etc.) are not controlled and the overall degradation could thus result from multiple degradation mechanisms. Hence different accelerated stress tests (AST) have been developed with both *in-situ* and *ex-situ* approaches in order to accelerate failure modes of field-operated fuel cell systems and study membrane degradation after hundreds hours of operation instead of several thousands.

In-situ aging tests consist in performing tests with instrumented, and sometimes segmented, single-cells or stacks during which one or several specific operating conditions are controlled. The use of instrumented and segmented single-cells permits to analyze the effect of one or more controlled parameters locally and precisely on MEA degradation. The most commonly-used *in-situ* AST mimicking the chemical membrane degradation is the fuel cell operation at open-circuit voltage (OCV). On the other hand, e*x-situ* aging tests are based on the reproduction of one specific fuel cell condition/environment to investigate its impact on the membrane decay. With the aim of replicating the aggressive radical environment of the fuel cell, membrane exposure to hydrogen peroxide (H_2O_2) solution is the most widely employed *ex-situ* aging tests.

3.3.2.1.Formation of hydrogen peroxide and reactive oxygen species (ROS)

The formation of hydrogen peroxide during fuel cell operation have been observed into the membrane [240,241] as well as in exhaust water from anode and cathode sides [242,243]. More especially, Liu *et al.* [240] estimated H_2O_2 concentration between 0.1 and 1.1 $mmol.L^{-1}$, depending on the membrane thickness and operating conditions. Two distinct mechanisms of H_2O_2 formation have been proposed in the literature: the first has been suggested by Pozio *et al.* [157] and consists in the incomplete reduction of oxygen on the platinum surface at the cathode side:

$$O_2 + 2H^+ + 2e^- = H_2O_2 \qquad E^0_{O_2/H_2O_2} = 0.67\ V_{SHE} \qquad \textbf{Eq. 1.21}$$

This parasitic 2-electron reduction reaction (Eq. 1.21) is encouraged when cell voltage is below to 0.67 V at the expense of the ORR (Eq. 1.2). Furthermore, PFSA membrane not being perfectly impermeable to gases, oxygen crossover can diffuse towards the anode side and promote the formation of H_2O_2 since anode cell voltage is lower than cathode one [238,243]. LaConti *et al.* [238] proposed another mechanism based on the gas crossover through the membrane and their combination on the platinum surface to form H_2O_2 according to the following three-step process:

$$H_2 \rightarrow 2H^{\bullet} \text{ (}via\text{ Pt catalyst)} \quad \textbf{Eq. 1.22}$$

$$H^{\bullet} + O_2 \text{ (crossover)} \rightarrow HOO^{\bullet} \quad \textbf{Eq. 1.23}$$

$$HOO^{\bullet} + H^{\bullet} \rightarrow H_2O_2 \text{ (which can diffuse into the membrane)} \quad \textbf{Eq. 1.24}$$

The gas crossover and the presence of platinum catalyst are prerequisite conditions to entail H_2O_2 formation during fuel cell operation, which confirm that H_2O_2 can be observed both to the anode and the cathode sides or even within the membrane. However, H_2O_2 itself is not harmful for the polymer structure but its decomposition into free radicals expose the membrane to chemical degradation [244].

Formation of ROS occurs through the homolysis of O–O bond in H_2O_2 which is catalyzed by metal cations like Fe^{2+}, Cu^{2+} or Ti^{3+} [185,238,239]:

$$H_2O_2 + M^{z+} \rightarrow M^{(z+1)+} + HO^{\bullet} + HO^{-} \quad \textbf{Eq. 1.25}$$

$$H_2O_2 + HO^{\bullet} \rightarrow HOO^{\bullet} + H_2O \quad \textbf{Eq. 1.26}$$

Metal ions in MEA can originated from the corrosion of stack and/or cell components as well as impurities in air steams, coolants or humidifiers [157]. Pozio *et al.* [157] studied the influence of end plate composition on the membrane degradation and highlighted a correlation between fluoride release and metal ion contamination. On another note, sulfonic acid groups have a higher affinity for metal ionsthan protons, except for Li^{+}, which leads to detrimental loss of conductivity, less water-uptake and thus reduced cell performances [214,245]. Moreover, it has also been suggested that contaminant ions accelerate the membrane degradation by catalyzing H_2O_2 decomposition and consequently ROS formation [238].

Another mechanism that does not involve neither H_2O_2 formation nor metal contaminants has been proposed for radical formation and relies on the crossover of reactant gases [246,247]. Indeed, ROS can be directly generated *via* the chemical reaction of oxygen and hydrogen on the platinum surface according to the following equations:

$$H_2 + O_2 \rightarrow 2HO^{\bullet} \text{ (}via\text{ Pt catalyst)} \quad \textbf{Eq. 1.27}$$

$$HO^{\bullet} + H_2 \rightarrow H_2O + H^{\bullet} \quad \textbf{Eq. 1.28}$$

$$O_2 + H^{\bullet} \rightarrow HOO^{\bullet} \quad \textbf{Eq. 1.29}$$

The formation of hydroxyl ($HO^{\bullet}$), hydroperoxyl ($HOO^{\bullet}$) and hydrogen ($H^{\bullet}$) radicals during fuel cell operation have been detected by spin trapping electron paramagnetic resonance (EPR) spectroscopy [248,249].

3.3.2.2.Chemical changes observed after *in-situ* experiments

Analysis of PEMFC collecting water during fuel cell operation permitted to highlight the membrane chemical decomposition thanks to the detection of various degradation products. The best-known degradation product is fluoride ion, resulting from the production of hydrofluoric (HF) during PFSA decomposition [185,209,212,229,243,247]. In addition to fluoride ions, sulfate ions have been revealed thanks to ion chromatography analysis [185,212] while the use of ^{19}F NMR spectroscopy permits to identify several perfluorinated carboxylic acids [213,229]. The main degradation products identified in the literature are summarized in Table 1.1.

Fluoride ion emission rate (FER) measured in fuel cell water exhaust or solution extracts of aged MEA provides an accurate indication of chemical degradation level of the PFSA membrane during or after fuel cell operation. It has been highlighted that FER depends upon chemical nature and relative humidity of reactant gases [209,243,250], the current density of the cell [250], temperature [251] as well as the membrane thickness [247,252]. Indeed, Zhao *et al.* [252] recently demonstrated the importance of membrane thickness on fluoride emissions and thus polymer chemical decomposition which are directly correlated to hydrogen permeation (Figure 1.28). On another note, the counter-ion nature of sulfonic groups also plays a crucial role on membrane degradation. It has been shown that FER was higher in the case of membranes in proton form in comparison to membranes which are polluted with alkaline or alkaline earth metal ions [247,253]. However, Kinumoto *et al.* [253] also demonstrated that the presence of Fe^{2+} or Cu^{2+} ions strongly increases the polymer decomposition.

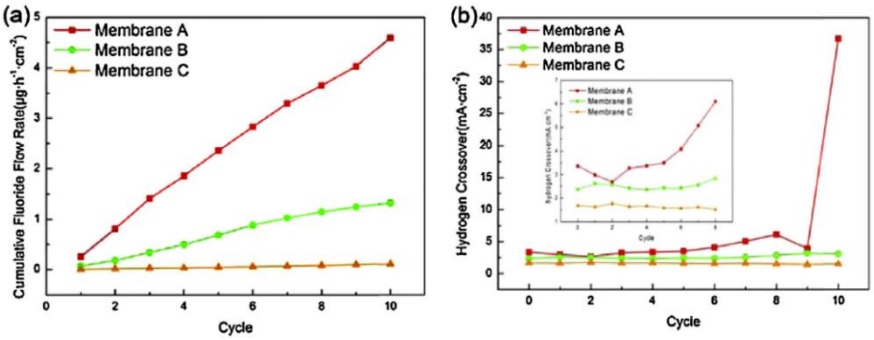

Figure 1.28 – (a) Cumulative fluoride release rate of cathode water exhaust and (b) hydrogen permeation during OCV tests [252].

Analysis of degraded PFSA membranes by FTIR and Raman spectroscopies are useful to detect the formation of carboxylic acid groups or PFSA chemical structure evolution after fuel cell operation. For instance, Holber *et al.* [254] reported significant intensity decrease of C-S, S-O and C-O-C vibration bands with respect to that of backbone CF_2 groups on Raman spectra, indicating the entire side chain loss due to radical attacks on ether linkages. This assumption is supported by the study of Bas *et al.* [255] who demonstrated by ^{19}F NMR spectroscopy that the integral ratio between side chain -CF groups and backbone -CF_2 groups decreased after fuel cell operation. However, the authors also detected no IEC variation, indicating that degradation could not occur *via* side chain scission but *via* radical attack on -CF groups. Change in IEC value after aging tests is not clearly established since some authors underlined an IEC decrease after fuel cell operation [212,256] while others observed any IEC variation in spite of significant membrane thinning [255]. To go even further, Endoh *et al.* [257] carried out FTIR and electron probe microanalyses to measure the concentration of carboxylic groups in the cross-section of MEA degraded under OCV conditions at 90 °C during 200 h. Their results highlighted an inhomogeneous distribution of -COOH groups in the membrane thickness and more particularly a higher -COOH concentration at the anode side (Figure 1.29).

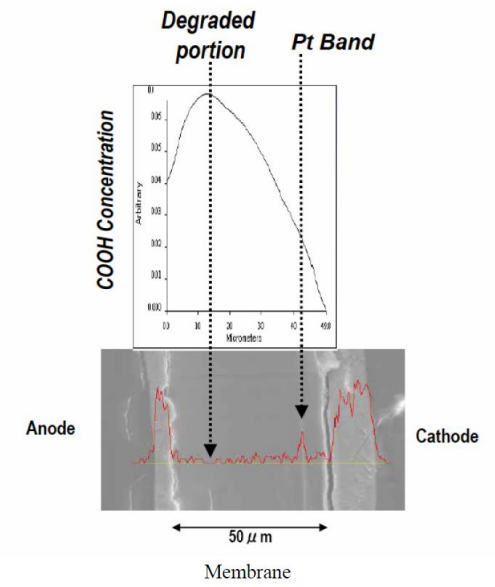

Figure 1.29 – COOH concentration profile in the cross-section of membrane degraded under OCV conditions thanks to electron probe microanalyzer (EPMA) and FTIR analyses [257].

This behavior has been confirmed by Danilczuk *et al.* [258] who highlighted the appearance of C-H and C=O groups near to the membrane/anode interface thanks to micro FTIR analysis of degraded MEA (OCV conditions, 90 °C, 30 % RH, 180 h) cross-section. Additionally, the authors suggested that the degradation location was presumably linked to the location of Pt band formation into the membrane (see § 3.2.1).

Several authors observed an increased membrane degradation as a consequence of Pt band formation into the membrane. For example, Ohma *et al.* [259] reported a significant membrane degradation in the area surrounding the Pt band and demonstrated that the amount of fluoride emissions in fuel cell water exhaust is consistent with the Pt band location. Likewise, Zhao *et al.* [260] evaluated membrane durability with both *in-situ* and *ex-situ* experiments and revealed that the presence of Pt into the membrane accelerates its degradation through the increase of H_2O_2 and ROS formation. On the contrary, other authors demonstrated that Pt particles into the membrane enhance its stability by scavenging H_2O_2 or free radicals [195,209]. For instance, Macauley *et al.* [195] demonstrated that field-operated MEA containing a Pt band into the membrane have longer lifetime than pristine MEA since OCV decay and fluoride emission rate were significantly lower after 13 AST cycles (Figure 1.30). Similarly, Endoh *et al.* [257] showed that fluoride emission rate were considerably diminished when membranes contain dispersed Pt particles and concluded that Pt particles deposited in the membrane do not participate in membrane degradation (see Figure 1.29). These discrepancies with regard to the effect of Pt species on membrane degradation can be attributed to particle size/shape/loading

[261,262] or can result from the coexistence of the different species (Pt^0, Pt^{2+} and Pt^{4+}) in the membrane [263]. Hence the protective or destructive effect of Pt particles into the membrane on its decomposition is still controversial.

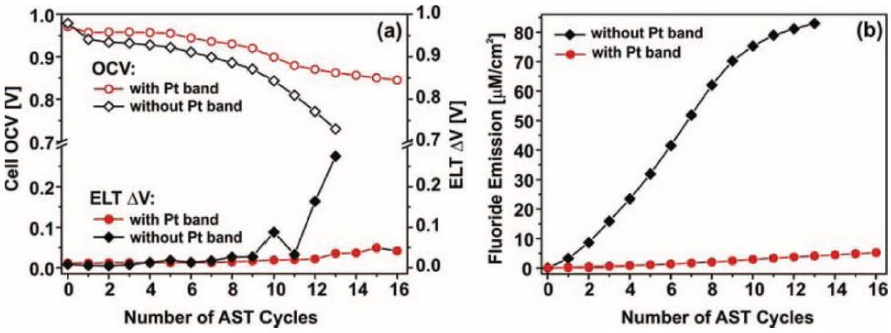

Figure 1.30 – Influence of the presence of Pt band in the membrane on (a) fuel cell performances and (b) fluoride emission during *in-situ* AST [195].

Whether degradation is studied at single-cell or stack scale and in accelerated or standard conditions, the various observations mentioned above underlines the multiplicity of degradation mechanisms and therefore the difficulty to clearly conclude on PFSA membrane degradation – behavior and mechanism – during fuel cell operation.

3.3.2.3.PFSA membrane degradation through *ex-situ* aging protocols

Membrane exposure to hydrogen peroxide (H_2O_2) solution are commonly-used as *ex-situ* aging tests in order to investigate the impact of chemical stress without considering the other stresses that could affect the membrane durability during *in-situ* aging tests. This approach enables to mimic the aggressive chemical environment, and especially the formation of free radicals encountered during fuel cell operation, while accelerating the overall membrane degradation. As previously described, H_2O_2 decomposition into free radicals can be catalyzed by metal ions (eq. 1.25) and more particularly the reaction between H_2O_2 and ferrous ions Fe^{2+}, known as Fenton's reaction, constitutes the most widely-used accelerated *ex-situ* aging test. However, ROS generation does not necessarily require the presence of metal ions. Few authors have indeed initiated the formation of highly reactive radicals thanks to UV irradiation [264], gamma-ray irradiation [265] or electron-beam irradiation [266], but these approaches remain very minority at this time. Alternatively, aging method based on gas-phase H_2O_2 exposure have been developed in order to better replicate fuel cell operating conditions [216,254,257,267–269]. Hommura *et al.* [267] indeed suggested that this accelerated aging method is more suitable for membrane degradation studying since no contamination is endured by the membrane during the test. It has been nevertheless suggested that gas-phase H_2O_2 exposure induces more severe

degradation than Fenton's reagents exposure [268] but also that degradation mechanism were distinct from that occurring in aqueous conditions [269].

Investigations on membrane exposure to H_2O_2 or Fenton's reagents, regardless of the aging method used, highlighted the release of several degradation products such as fluoride ions, sulfate or hydrogen sulfate ions as well as various fluorinated carboxylic acids (Table 1.1). FTIR and/or NMR analyses of H_2O_2 or Fenton's solution after the chemical degradation process permitted to detect several decomposed fragments coming from PFSA side chains. The appearance of -C=O, -S=O and -CF stretching bands on IR spectra [270,271] as well as the detection of $-CF_x$ (x = 0–3) and -C=O resonance peaks by ^{13}C-NMR spectroscopy [270] reveals the presence of $-SO_3^-$, -COOH and -CF- groups in solution. More particularly, Healy *et al.* [229] investigated the degradation of Nafion™ membranes through *in-situ* (fuel cell operation) and *ex-situ* (Fenton's reaction) experiments and demonstrated by ^{19}F-NMR and mass spectroscopies that a similar fluorocarboned molecule directly deriving from the PFSA side-chain were released in both cases: the perfluoro(4-methyl-3-oxa)pentane-1-sulfonic-5-carboxylic diacid, $HOOC–CF(CF_3)–O–CF_2–CF_2–SO_3H$.

Table 1.1 – Main degradation products of PFSA membranes identified during *in-situ* and *ex-situ* aging tests [1].

Moiety or molecule compounds	*In-situ* aging protocol	*Ex-situ* aging protocol
F^-	[185,209,212,229,243,247]	[83,84,253,267,270–276]
SO_4^{2-}	[185,212]	[253,275,277]
HSO_4^-	Undetected	[268]
CF_3-COO^-	[213]	[213,268]
$HOOC-CF_2-SO_3^-$	[213]	[268]
$HOOC-CF_2-CF_2-COO^-$	Undetected	[268]
$HOOC-CF(CF_3)-O-CF_2-CF_2-SO_3^-$	[213,229]	[213,229,268,276]

On the other hand, monitoring of PFSA structure evolution after chemical degradation by Fourier-transform infrared (FTIR) spectroscopy highlighted a decrease of the typical vibration bands of PFSA structure [270–273]. It is important to notice that this trend is not systematically observed; indeed others studies did not detect significant IR spectra evolution even though other marker show membrane degradation [253,274,278]. Some authors also highlighted the appearance of new vibration bands around 2900 cm^{-1}, 1690 cm^{-1}, 1440 cm^{-1} and 870 cm^{-1} on IR spectra, which can be attributed to -CH [272], -C=O [269,275], -S=O [253,275,277] and Fe-O-Fe or O-O bonds [275], respectively. The presence of -S=O bond in the membrane can suggest S-O-S cross-linking between sulfonic groups or the formation of $-SO_2F$ bonds

[253,277] while the presence of -C=O bond is characteristic of -COOH groups introduction into the degraded membranes.

Recently, Luo *et al.* [279] studied the effect of chemical degradation on water transport properties of PFSA membranes and reported higher proton mobility and larger hydrophilic volume fraction after Fenton's reagents exposure. The authors attributed these changes to the appearance of important physical defects into the membrane which induce a significant increase of the water uptake. The appearance of defects into the membrane and especially the evolution of microbubbles into pinholes have already been observed [270,271,273,274,278,280,281]. For instance, Mu *et al.* [273] compared the impact of H_2O_2 and H_2O_2/Fe^{2+} (*i.e.* Fenton's reagents) exposure on membrane degradation and demonstrated that the presence of ferrous ions strongly affected membrane morphology. The authors indeed observed the appearance of many micro-cracks and microbubbles when membranes are exposed to Fenton's reagents (Figure 1.31) while H_2O_2 exposure only induced small bumps appearance. Such morphological changes have never been observed in the case of fuel cell systems operating in real conditions and could raise doubts about the relevance of chemical degradation induced by Fenton's reaction. However, it should be considered that the appearance of such defects after *ex-situ* chemical degradation is not systematic and these morphological changes seem to be related to the operating conditions and especially the concentration of Fenton's reagents. This understanding will be investigated in the first chapter of this thesis work.

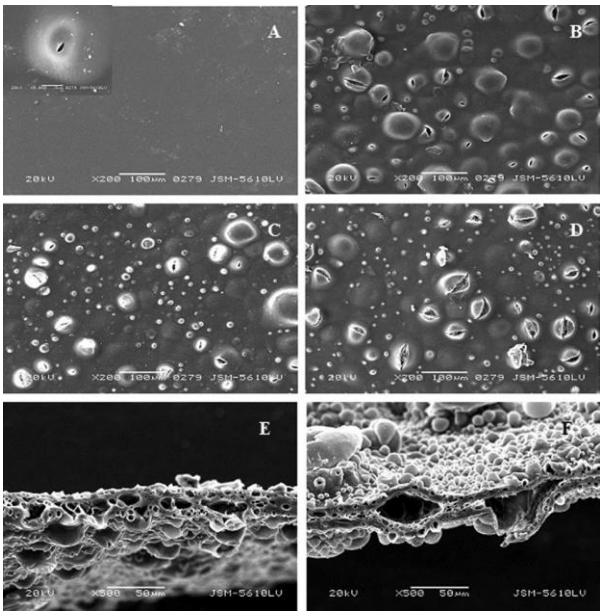

Figure 1.31 – SEM images of Nafion™ membrane surface (A-D) and cross-section (E, F) after various time of exposure to Fenton's reagents [273].

More recently, Shi and his coworkers investigated the impact of chemical degradation induced by Fenton's reaction on the mechanical properties of Nafion™ NR212 membranes [281]. The authors observed a decrease of the Young's modulus, the proportional limit stress as well as the break strain with increasing Fenton's reagents exposure, implying a reduction of membrane fracture toughness. On the other hand, they observed an increase of the strain-hardening modulus, indicating the change from ductile to brittle fracture behavior of the membrane. Furthermore, by comparing the fatigue crack propagation behavior of composite Nafion™ XL membrane with un-reinforced NR212 one after chemical degradation, they demonstrated that fatigue crack propagation rate is larger for NR212 than XL which can be ascribed to the reinforcement layer [225]. Fatigue crack propagation is accelerated according to two distinct mechanisms in the case of unreinforced NR212 membranes: bubbles coalescence at the membrane surface and interconnection of pores in the membrane cross-section. In the case of reinforced XL membrane, the two fatigue crack propagation mechanisms are delamination at the interface between reinforcement layer and outer ionomer layer as well as crack growth in outer ionomer layers and only the latter mechanism is accelerated by the chemical degradation.

The numerous results, and more particularly the identification of various degradation products in both *ex-situ* and *in-situ* experiments, thus permits to better understand the chemical degradation of PFSA membranes and propose several chemical degradation mechanisms.

3.3.2.4.Chemical degradation mechanisms

Numerous degradation mechanisms have been proposed in the literature over the past decades. One of the most commonly accepted degradation mechanisms is the "unzipping" reaction and consists in the $HO^{\bullet}$ radical attack on H-containing end groups [83,211]. These H-containing end groups, such as -COOH or -CF_2H, are believed to be introduced during the manufacturing process [238] and are the most vulnerable sites since C-H bonds have lower stability than C-F bonds [282]. As described in Eq. 1.30 – 1.32, degradation begins with the hydrogen abstraction by $HO^{\bullet}$ radical, generating CO_2 and HF, and the perfluorocarbon radical can then further react to reform a carboxylic end group [83].

$$R_f - CF_2COOH + HO^{\bullet} \rightarrow R_f - CF_2^{\bullet} + CO_2 + H_2O \quad \textbf{Eq. 1.30}$$

$$R_f - CF_2^{\bullet} + HO^{\bullet} \rightarrow R_f - CF_2OH \rightarrow R_f - COF + HF \quad \textbf{Eq. 1.31}$$

$$R_f - COF + H_2O \rightarrow R_f - COOH + HF \quad \textbf{Eq. 1.32}$$

Once initiated, unzipping reaction propagates along the polymer backbone and can lead to the entire side chain loss and the formation of perfluoro(4-methyl-3-oxa)pentane-1-sulfonic-5-carboxylic diacid, HOOC–CF(CF_3)–O–CF_2–CF_2–SO_3H, by reaching a junction with a side chain [211,212]. This specie can then diffuse out of the membrane or further decompose *via* unzipping reaction, as –COOH end group is still present (Figure 1.32).

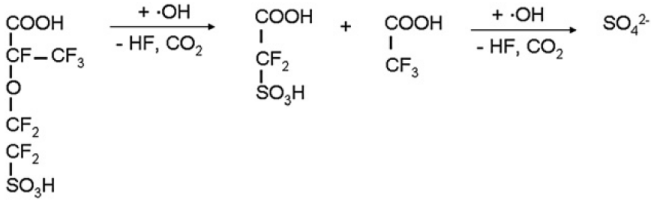

Figure 1.32 – Product A degradation *via* unzipping reaction [211].

As mentioned in § 1.2.4, it has been shown that introducing an additional step of post-fluorination in Nafion™ membrane synthesis permitted to considerably reduce by 61 % the number of carboxylic end groups and to decrease by 56 % the fluoride ion emission in comparison with untreated one [83]. Although post-fluorination of carboxylic end groups in PFSA membranes enhances their stability against chemical degradation, chemically stabilized membranes are nevertheless not completely rid of vulnerable sites. Indeed, several authors reported that observed fluoride release is not directly proportional to the concentration of –COOH end groups in PFSA membranes and suggest that other degradation mechanisms occur [276,283].

In addition to the unzipping degradation mechanisms, several authors [246,247,283,284] suggested that C–S bonds of PFSA side chain also represent vulnerable sites to radical attacks. Ghassemzadeh *et al.* [246] proposed a side chain degradation mechanism (Figure 1.33) based on HO• radical attack on C–S bond and further unzipping of side chain fragments up to reach the junction with the main chain.

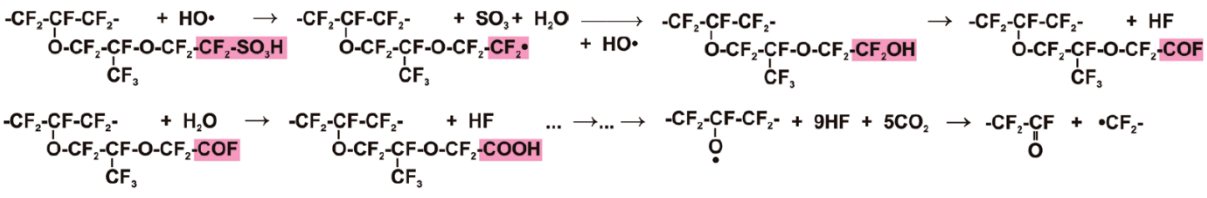

Figure 1.33 – Side chain degradation mechanism by unzipping the side chain *via* radical attack to the C–S bond proposed by Ghassemzadeh *et al.* [246].

This mechanism is supported by the presence of side chain fragments in exhaust water [246] after *in-situ* degradation experiments as well as the detection of –O–CF_2–CF_2–SO_3• and –O–

CF_2–$CF_2^{\bullet}$ radicals by EPR spectroscopy after *ex-situ* degradation experiments [285]. Moreover, these observations agree with initial assumptions of Xie *et al.* and Hommura *et al.* stating that side chain cleavage occurs and can then cause main chain cleavage by unzipping reaction, leading to the introduction of new –COOH end groups in the main chain structure [211,267].

A third degradation mechanism based on the attack of $HO^{\bullet}$ radical on the C–O–C bond close to the sulfonic group has been suggested in the literature [239,266,286,287]. This mechanism (Figure 1.34) is supported by the detection of $^{\bullet}OCF_2R$ radicals by spin trapping EPR analysis [239] and confirms the greater stability of PFSA SSC ionomers compared to Nafion™ ionomer since this latter contains a supplementary ether linkage [288]. Ghassemzadeh *et al.* shown that C–O–C bond close to the sulfonic group is primarily attacked rather than that near to the junction between main and side chains. However, they were unable to conclude whether **C–O**-C bond or C-**O–C** bond is cleaved during radical attack [266,287].

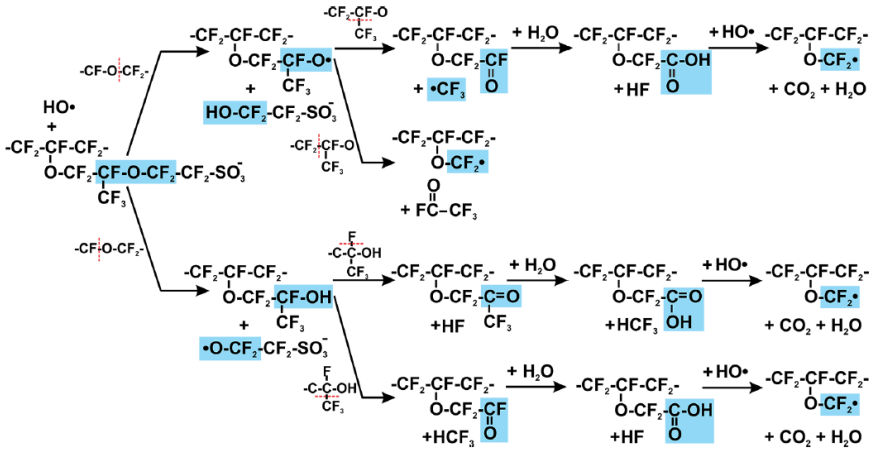

Figure 1.34 – Mechanism of $HO^{\bullet}$ radical attack on ether linkage proposed by Ghassemzadeh *et al.* [266].

As mentioned earlier, hydrogen ($H^{\bullet}$) radical is also formed during fuel cell operation and its presence has been recently confirmed by EPR spectroscopy [249]. Based on the presence of this radical, Ghassemzadeh *et al.* [266] as well as Danilczuk *et al.* [258] proposed another membrane degradation mechanism consisting in $H^{\bullet}$ radical attack on tertiary C–F bonds of both main chain and side chain. Radical attack on CF bond in the side chain results in side chain cleavage and further decomposition up to the junction with main chain while radical attack on CF bond in the main chain directly conducts to the entire side chain loss (Figure 1.35).

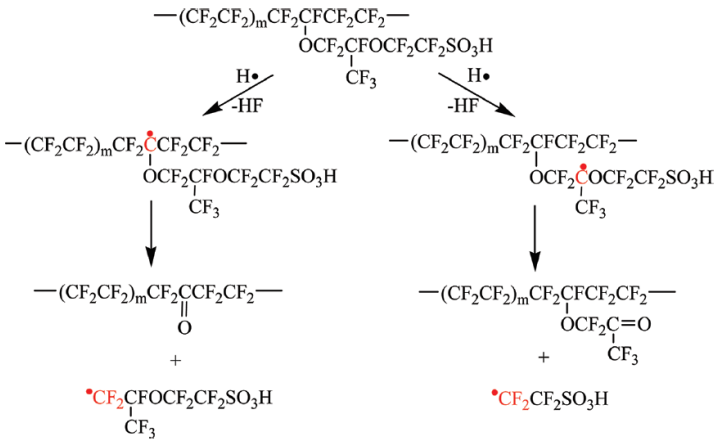

Figure 1.35 – Mechanism of H• radical attack on Nafion™ main chain and side chain suggested by Danilczuk *et al.* [258].

Although HOO• radical has been observed during fuel cell operation, no degradation mechanism by HOO• radical attack on polymer structure has been described in the literature whereas plenty of degradation pathways based on the attack of HO• radical, and more recently on H• radical, have been proposed. This can be explained by the ranking of oxidative strength of oxygen species: HO• > H• > HOO• > H_2O_2 [289].

In conclusion, thanks to the innumerable studies investigating chemical structure evolution of degraded PFSA membranes, it is possible to summarize the various vulnerable sites of both main and side chains attacked by HO• and H• radical as illustrated by Figure 1.36:

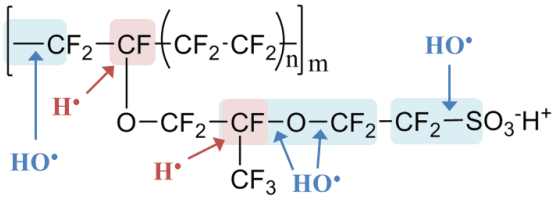

Figure 1.36 – Summary of chemical degradation mechanisms by radical attacks on PFSA polymer structure.

To this day, it cannot be properly concluded on the dominance of one of these mechanisms since the different mechanisms probably all play a specific role in the PFSA membrane degradation during fuel cell operation.

3.3.2.5.Mitigation strategies

Although PFSA membranes have been chemically stabilized to extend their lifetime (see § 1.2.4), these improvements did not fully overcome polymer decomposition issues. In that respect, different strategies have been proposed to minimize the effect of chemical degradation on PFSA membranes and more particularly to prevent the formation of H_2O_2 and free radicals.

An efficient strategy to mitigate chemical decomposition of the membrane is the introduction of radical scavengers that can deactivate harmful free radicals before they react with polymer chains. In that respect, several inorganic compounds have been proposed: metal oxides like TiO_2, ZrO_2, SnO_2, MnO_2 or CeO_2 as well as metal particles such as Ce, Mn, Pd, Pt, Ag or Au [237]. Among them, cerium (Ce) and manganese (Mn) derivatives species (ionic forms [290,291], metal oxides [94,292–295], metal nanoparticles [93] or immobilized onto silica support [296]) are the most commonly used in PEMFC membrane electrode assemblies. The scavenging ability of Ce^{3+} and Mn^{2+} ions is ensured by three main characteristics:

- their self-generative property, the two oxidation states of Ce or Mn permitting to easily decompose ROS and H_2O_2 thanks to their complementary roles,
- their stability, Ce^{3+} and Mn^{2+} reacting with $HO^{\bullet}$ *via* one-electron redox reaction to produce water and the corresponding cation,
- their chemical kinetics, the reaction rate constant being two orders of magnitude faster with $HO^{\bullet}$ than with polymer chains.

Numerous studies have demonstrated the high efficacy of Ce and Mn species to reduce fluoride emission rate and thus extend PEMFC lifetime [297]. Moreover, only small quantities are required to efficiently diminish chemical degradation and do not affect the membrane conductivity. However, it has been shown that small amounts of Ce or Mn ions are released by the membrane during fuel cell operation and can be leached in water exhaust [95] or can migrate into catalyst layers, thanks to their high mobility, and thus alter fuel cell performances [92,94,95,298].

On the other hand, investigations have been carried out on the introduction of metal oxides instead of metal cations to mitigate radical attack membrane degradation [93,292–294]. These various studies shown that the incorporation of CeO_2 particles into the membranes is also highly effective to enhance membrane durability. Nevertheless, Prabhakaran *et al.* observed a decay of scavenging efficiency with time [93]. In order to improve the regenerative activity of CeO_2/MnO_2 radical scavengers, several authors have attempted to dope them with other metal cations or to immobilize them onto inert supports such as silica nanoparticles [295,299–301]. For instance, Trogadas *et al.* investigated the effect of platinum particles on the scavenging efficiency of ceria and demonstrated that Nafion™/Pt/CeO_2 membranes are slight more resistant against radical attacks than Nafion™/CeO_2 membranes [302]. This result can be explained by the ability of Pt to catalyze H_2O_2 decomposition whereas Ce^{3+} can only deactivate $HO^{\bullet}$.

Furthermore, D'Urso *et al.* investigated the durability of reinforced Aquivion® membranes including cerium-based radical scavenger supported on sulfonated silica particles in comparison with Ce^{3+}-exchanged reinforced Aquivion® membranes [296]. Their work demonstrated that silica support provides lower MEA resistance and thus longer fuel cell lifetime thanks to its better dispersion and stabilization of Ce-based radical scavengers (Figure 1.37). It is important to note that silica is a commonly-used inorganic filler in PEMFC that improves membrane properties such as its proton conductivity, its water retention capacity and its mechanical strength.

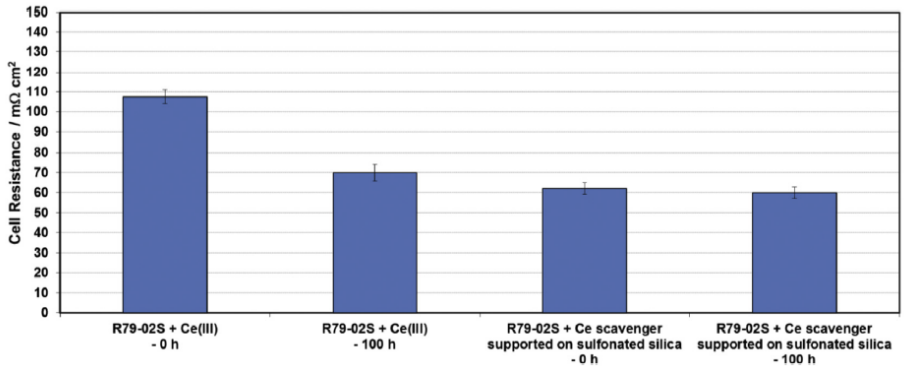

Figure 1.37 – Comparison of the cell resistance for MEA containing reinforced Aquivion® PFSA membrane + Ce(III) ions or Ce scavenger supported on sulfonated silica at various operating time [296].

3.3.3. Conjoint chemical and mechanical degradations

Until now, degradation mechanisms have been principally considered separately, distinguishing between chemical degradation on the one hand and mechanical degradation on the other hand. Nevertheless, it has been highlighted that membrane decomposition results from the synergistic interaction between mechanical stress and chemical degradation [216,217,303,304].

As summarized by Kusoglu and Weber in their review of the literature [305], the combination of chemical and mechanical stressors, that interact synergistically during fuel cell operation, leads to an acceleration of the overall membrane degradation. As seen earlier, PFSA chemical degradation by radical attacks alters the structure and the mechanical integrity of the membrane, leading to its thinning and the appearance of defects. These structure changes conduct to the growth of defects into cracks and/or pinholes and to increased gas crossover of hydrogen and oxygen to their respective opposite electrodes [154,215,221]. Crossover gases can then react on the catalyst surface, either to the anode side or to the cathode side, thus polarizing the cell and leading to a voltage drop. Moreover, the combustion reaction between

O_2 and H_2 being highly exothermic, local hot spots are created and engender the softening or the melting of the membrane, allowing the further membrane degradation. In addition, changes in membrane water-uptake imposed by the humidity cycling during fuel cell operation induce additional swelling stress, the membrane being constrained by the fuel cell geometry, which can generate the growth of pinholes and therefore the increase of gas crossover. Furthermore, it has been shown that defect size and distribution are strongly related to the chemical degradation level [306]. Consequently, a destructive cycle (Figure 1.38) takes place, increasing gas crossover as well as radical generation and thus accelerating the overall PFSA membrane degradation up to the final breakdown.

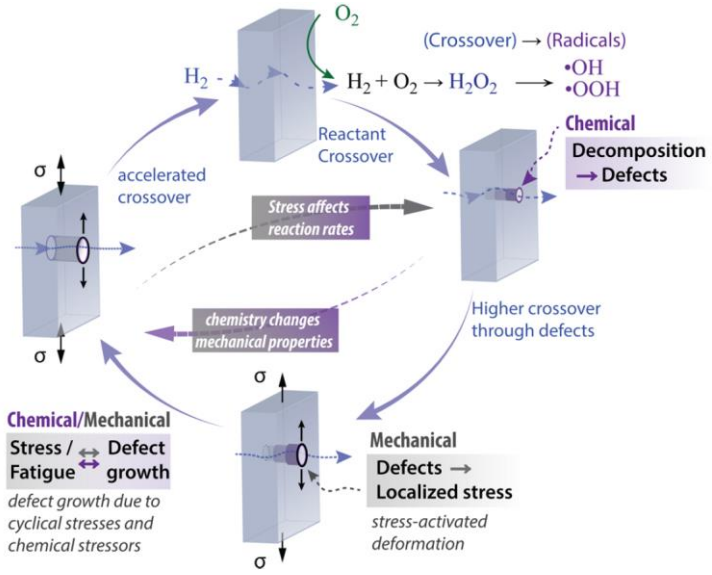

Figure 1.38 – Schematic representation of membrane degradation mechanisms [305].

Specific accelerated stress tests (AST) were recently developed to study the impact of coupled mechanical and chemical stressors on PFSA membranes during fuel cell operation [218,219,303,307]. For instance, Lim *et al.* evaluated the *in-situ* degradation of PFSA membranes during conjoint mechanical and chemical membrane accelerated stress tests [218]. They demonstrated that the combination of steady-state Open Circuit Voltage (OCV) phases and periodic wet/dry cycles led to a consistent and fast degradation with significant fluorine losses and uniform membrane thinning. Additionally, the authors observed a drop of the fracture strain and an increase of the elastic modulus during fuel cell operation, indicating increased stiffness and brittleness of the membrane structure and thus larger vulnerability to pinhole formation. Moreover, they highlighted the acceleration of the overall degradation since membrane failure occurred after only 160 hours of operation. Using an *ex-situ* approach, few authors highlighted the acceleration of PFSA chemical decomposition under tensile stress [216]

and under compressive stress [217]. Indeed, Kusoglu *et al.* recently developed a specific compression apparatus in order to study the effect of a normal stress on Nafion™ membranes exposed to radical attacks [217]. The authors showed that coupling mechanical static stressor to chemical stressor exhibit higher fluoride release compared to membrane undergoing just chemical stressor (Figure 1.39). They showed that applying a static compression to a membrane exchanged with ferrous ions and immersed in hydrogen peroxide solution affects its microstructure and accelerates the chemical decomposition of the polymer chains (Figure 1.39).

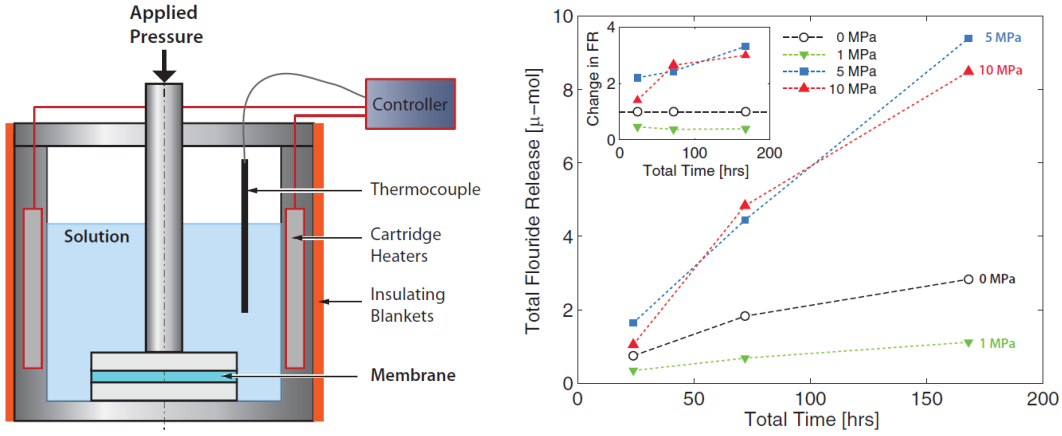

Figure 1.39 – Schematic of the compression apparatus developed by Kusoglu *et al.* (*left*) and fluoride emission measured as a function of time for various compressive stress (*right*) [217].

More recently, Ehlinger *et al.* [304] developed a comprehensive model to study the synergistic nature of chemical and mechanical stressors and its impact on PEMFC performance and durability. Their model includes three main characteristics: 1) transport properties and performance of the fuel cell, 2) mechanical stress induced by the membrane swelling and the formation and growth of pinholes, 3) membrane chemical degradation through the formation and transport of hydrogen peroxide and fluoride ions. Their fully-coupled models demonstrated the importance of considering both mechanical and chemical degradations as well as their conjoint effect on transport properties to understand the membrane decomposition occurring during fuel cell operation.

4. Objectives of the thesis work

As highlighted through this bibliographical study, the MEA and more particularly the PFSA membranes are key elements of fuel cell systems but they still suffer from severe damages during fuel cell operation. Membrane degradation, as a consequence of the synergistic interaction between chemical and mechanical stresses, remains one of the main detrimental

factor limiting PEMFC lifetime. However, despite innumerable studies focusing independently on chemical or mechanical degradations these past decades, only a few have been focused on the effect of combined stresses on PFSA membranes. Consequently, there is still a need to understand this synergistic interaction between mechanical and chemical degradations and its impact on the structure and the properties of PFSA membranes. Furthermore, in spite the various mitigation strategies developed to extend their lifetime, current composite membranes are still insufficiently durable for long-time fuel cell operation.

To this end, this thesis work aims at providing, through ex-situ aging protocols, new insights on the effect of conjoint chemical and mechanical stress on the degradation of PFSA membrane, whether it is reinforced or not, as well as characterizing and understanding its impact on membrane properties and fuel cell performances. The complex aging mechanisms associating the chemical and mechanical stresses have to be therefore dealt with a multidisciplinary approach. In that respect, and thanks to a multi-techniques characterization, the analysis of the chemical structure and functional properties of PFSA membranes before and after aging tests permitted to correlate physico-chemical properties of the membrane to its structural characteristics and to highlight several indicators of chemical degradation. **Chapter II** is dedicated to the description of the various experimental techniques used in this thesis work.

As a first step, before considering conjoint chemical and mechanical stress, it has been necessary to understand the impact of pure *ex-situ* chemical degradation on PFSA membrane. More particularly, **Chapter III** was focused on the study of the effects of Fenton's reagent concentrations on the membrane degradation.

A deeper time-resolved monitoring of ex-situ chemical degradation has been then performed in **Chapter IV** to study its impact on the chemical structure and the water transport and sorption properties of composite and conventional Nafion™ membranes. This study also permitted to provide some clarifications on the contribution of the reinforcement layer and the radical scavengers against PFSA membrane chemical degradation.

Finally, the effects of combined mechanical and chemical stress on PFSA membranes have been studied, always through an *ex-situ* approach, with a custom-made device. **Chapter V** was dedicated to the development of this specific device and the different *ex-situ* conjoint mechanical and chemical stress tests allowing to investigate the impact of coupled stresses on the chemical structure, functional properties and fuel cell performances of PFSA membranes.

References

1. El Kaddouri A. 2014 Mise en évidence de la dégradation du liant ionomère dans les électrodes de pile à combustible. Grenoble. See http://www.theses.fr/2014GRENI014.

2. Song Y, Zhang C, Ling C-Y, Han M, Yong R-Y, Sun D, Chen J. 2019 Review on current research of materials, fabrication and application for bipolar plate in proton exchange membrane fuel cell. *Int. J. Hydrog. Energy* (doi:10.1016/j.ijhydene.2019.07.231)

3. Taherian R. 2014 A review of composite and metallic bipolar plates in proton exchange membrane fuel cell: Materials, fabrication, and material selection. *J. Power Sources* **265**, 370–390. (doi:10.1016/j.jpowsour.2014.04.081)

4. Leng Y, Ming P, Yang D, Zhang C. 2020 Stainless steel bipolar plates for proton exchange membrane fuel cells: Materials, flow channel design and forming processes. *J. Power Sources* **451**, 227783. (doi:10.1016/j.jpowsour.2020.227783)

5. Antunes RA, Oliveira MCL, Ett G, Ett V. 2010 Corrosion of metal bipolar plates for PEM fuel cells: A review. *Int. J. Hydrog. Energy* **35**, 3632–3647. (doi:10.1016/j.ijhydene.2010.01.059)

6. Kahraman H, Orhan MF. 2017 Flow field bipolar plates in a proton exchange membrane fuel cell: Analysis & modeling. *Energy Convers. Manag.* **133**, 363–384. (doi:10.1016/j.enconman.2016.10.053)

7. Mason TJ, Millichamp J, Neville TP, El-kharouf A, Pollet BG, Brett DJL. 2012 Effect of clamping pressure on ohmic resistance and compression of gas diffusion layers for polymer electrolyte fuel cells. *J. Power Sources* **219**, 52–59. (doi:10.1016/j.jpowsour.2012.07.021)

8. Jeon DH, Greenway S, Shimpalee S, Van Zee JW. 2008 The effect of serpentine flow-field designs on PEM fuel cell performance. *Int. J. Hydrog. Energy* **33**, 1052–1066. (doi:10.1016/j.ijhydene.2007.11.015)

9. Manso AP, Marzo FF, Barranco J, Garikano X, Garmendia Mujika M. 2012 Influence of geometric parameters of the flow fields on the performance of a PEM fuel cell. A review. *Int. J. Hydrog. Energy* **37**, 15256–15287. (doi:10.1016/j.ijhydene.2012.07.076)

10. Dai W, Wang H, Yuan X-Z, Martin JJ, Yang D, Qiao J, Ma J. 2009 A review on water balance in the membrane electrode assembly of proton exchange membrane fuel cells. *Int. J. Hydrog. Energy* **34**, 9461–9478. (doi:10.1016/j.ijhydene.2009.09.017)

11. Park S, Lee J-W, Popov BN. 2012 A review of gas diffusion layer in PEM fuel cells: Materials and designs. *Int. J. Hydrog. Energy* **37**, 5850–5865. (doi:10.1016/j.ijhydene.2011.12.148)

12. Mathias MF, Roth J, Fleming J, Lehnert W. 2010 Diffusion media materials and characterisation. In *Handbook of Fuel Cells*, American Cancer Society. (doi:10.1002/9780470974001.f303046)

13. Wang Y, Wang C-Y, Chen KS. 2007 Elucidating differences between carbon paper and carbon cloth in polymer electrolyte fuel cells. *Electrochimica Acta* **52**, 3965–3975. (doi:10.1016/j.electacta.2006.11.012)

14. Tseng C-J, Lo S-K. 2010 Effects of microstructure characteristics of gas diffusion layer and microporous layer on the performance of PEMFC. *Energy Convers. Manag.* **51**, 677–684. (doi:10.1016/j.enconman.2009.11.011)

15. Antolini E. 2004 Review in Applied Electrochemistry. Number 54 Recent Developments in Polymer Electrolyte Fuel Cell Electrodes. *J. Appl. Electrochem.* **34**, 563–576. (doi:10.1023/B:JACH.0000021923.67264.bb)

16. Velayutham G, Kaushik J, Rajalakshmi N, Dhathathreyan KS. 2007 Effect of PTFE Content in Gas Diffusion Media and Microlayer on the Performance of PEMFC Tested under Ambient Pressure. *Fuel Cells* **7**, 314–318. (doi:10.1002/fuce.200600032)

17. Lufrano F, Passalacqua E, Squadrito G, Patti A, Giorgi L. 1999 Improvement in the diffusion characteristics of low Pt-loaded electrodes for PEFCs. *J. Appl. Electrochem.* **29**, 445–448. (doi:10.1023/A:1026419102310)

18. Bevers D, Rogers R, von Bradke M. 1996 Examination of the influence of PTFE coating on the properties of carbon paper in polymer electrolyte fuel cells. *J. Power Sources* **63**, 193–201. (doi:10.1016/S0378-7753(96)02465-2)

19. Qi Z, Kaufman A. 2002 Improvement of water management by a microporous sublayer for PEM fuel cells. *J. Power Sources* **109**, 38–46. (doi:10.1016/S0378-7753(02)00058-7)

20. Atiyeh HK, Karan K, Peppley B, Phoenix A, Halliop E, Pharoah J. 2007 Experimental investigation of the role of a microporous layer on the water transport and performance of a PEM fuel cell. *J. Power Sources* **170**, 111–121. (doi:10.1016/j.jpowsour.2007.04.016)

21. Lee H-K, Park J-H, Kim D-Y, Lee T-H. 2004 A study on the characteristics of the diffusion layer thickness and porosity of the PEMFC. *J. Power Sources* **131**, 200–206. (doi:10.1016/j.jpowsour.2003.12.039)

22. Nam JH, Lee K-J, Hwang G-S, Kim C-J, Kaviany M. 2009 Microporous layer for water morphology control in PEMFC. *Int. J. Heat Mass Transf.* **52**, 2779–2791. (doi:10.1016/j.ijheatmasstransfer.2009.01.002)

23. Chen J, Xu H, Zhang H, Yi B. 2008 Facilitating mass transport in gas diffusion layer of PEMFC by fabricating micro-porous layer with dry layer preparation. *J. Power Sources* **182**, 531–539. (doi:10.1016/j.jpowsour.2008.04.031)

24. Ramasamy RP, Kumbur EC, Mench MM, Liu W, Moore D, Murthy M. 2008 Investigation of macro- and micro-porous layer interaction in polymer electrolyte fuel cells. *Int. J. Hydrog. Energy* **33**, 3351–3367. (doi:10.1016/j.ijhydene.2008.03.053)

25. Velayutham G. 2011 Effect of micro-layer PTFE on the performance of PEM fuel cell electrodes. *Int. J. Hydrog. Energy* **36**, 14845–14850. (doi:10.1016/j.ijhydene.2011.03.037)

26. Majlan EH, Rohendi D, Daud WRW, Husaini T, Haque MA. 2018 Electrode for proton exchange membrane fuel cells: A review. *Renew. Sustain. Energy Rev.* **89**, 117–134. (doi:10.1016/j.rser.2018.03.007)

27. Uchida M, Aoyama Y, Eda N, Ohta A. 1995 New Preparation Method for Polymer-Electrolyte Fuel Cells. *J. Electrochem. Soc.* **142**, 463. (doi:10.1149/1.2044068)

28. Wilson MS, Valerio JA, Gottesfeld S. 1995 Low platinum loading electrodes for polymer electrolyte fuel cells fabricated using thermoplastic ionomers. *Electrochimica Acta* **40**, 355–363. (doi:10.1016/0013-4686(94)00272-3)

29. Cheng X, Yi B, Han M, Zhang J, Qiao Y, Yu J. 1999 Investigation of platinum utilization and morphology in catalyst layer of polymer electrolyte fuel cells. *J. Power Sources* **79**, 75–81. (doi:10.1016/S0378-7753(99)00046-4)

30. Chun Y-G, Kim C-S, Peck D-H, Shin D-R. 1998 Performance of a polymer electrolyte membrane fuel cell with thin film catalyst electrodes. *J. Power Sources* **71**, 174–178. (doi:10.1016/S0378-7753(97)02792-4)

31. Litster S, McLean G. 2004 PEM fuel cell electrodes. *J. Power Sources* **130**, 61–76. (doi:10.1016/j.jpowsour.2003.12.055)

32. Sharma S, Pollet BG. 2012 Support materials for PEMFC and DMFC electrocatalysts—A review. *J. Power Sources* **208**, 96–119. (doi:10.1016/j.jpowsour.2012.02.011)

33. Ma S, Chen Q, Jøgensen FH, Stein PC, Skou EM. 2007 19F NMR studies of Nafion^{TM} ionomer adsorption on PEMFC catalysts and supporting carbons. *Solid State Ion.* **178**, 1568–1575. (doi:10.1016/j.ssi.2007.10.007)

34. Rajalakshmi N, Dhathathreyan KS. 2007 Catalyst layer in PEMFC electrodes—Fabrication, characterisation and analysis. *Chem. Eng. J.* **129**, 31–40. (doi:10.1016/j.cej.2006.10.035)

35. Abaoud HA, Ghouse M, Lovell KV, Al-Motairy GN. 2005 A hybrid technique for fabricating PEMFC's low platinum loading electrodes. *Int. J. Hydrog. Energy* **30**, 385–391. (doi:10.1016/j.ijhydene.2004.07.003)

36. Smirnova A, Dong X, Hara H, Vasiliev A, Sammes N. 2005 Novel carbon aerogel-supported catalysts for PEM fuel cell application. *Int. J. Hydrog. Energy* **30**, 149–158. (doi:10.1016/j.ijhydene.2004.04.014)

37. Kadjo AJ-J, Brault P, Caillard A, Coutanceau C, Garnier J-P, Martemianov S. 2007 Improvement of proton exchange membrane fuel cell electrical performance by optimization of operating parameters and electrodes preparation. *J. Power Sources* **172**, 613–622. (doi:10.1016/j.jpowsour.2007.05.019)

38. Marie J, Berthon-Fabry S, Achard P, Chatenet M, Pradourat A, Chainet E. 2004 Highly dispersed platinum on carbon aerogels as supported catalysts for PEM fuel cell-electrodes: comparison of two different synthesis paths. *J. Non-Cryst. Solids* **350**, 88–96. (doi:10.1016/j.jnoncrysol.2004.06.038)

39. Eikerling M. 2006 Water Management in Cathode Catalyst Layers of PEM Fuel Cells: A Structure-Based Model. *J. Electrochem. Soc.* **153**, E58. (doi:10.1149/1.2160435)

40. Ding J, Chan K-Y, Ren J, Xiao F. 2005 Platinum and platinum–ruthenium nanoparticles supported on ordered mesoporous carbon and their electrocatalytic performance for fuel cell reactions. *Electrochimica Acta* **50**, 3131–3141. (doi:10.1016/j.electacta.2004.11.064)

41. Carmo M, Paganin VA, Rosolen JM, Gonzalez ER. 2005 Alternative supports for the preparation of catalysts for low-temperature fuel cells: the use of carbon nanotubes. *J. Power Sources* **142**, 169–176. (doi:10.1016/j.jpowsour.2004.10.023)

42. O'Hayre R, Prinz FB. 2004 The Air/Platinum/Nafion Triple-Phase Boundary: Characteristics, Scaling, and Implications for Fuel Cells. *J. Electrochem. Soc.* **151**, A756. (doi:10.1149/1.1701868)

43. Oetjen H-F, Schmidt VM, Stimming U, Trila F. 1996 Performance Data of a Proton Exchange Membrane Fuel Cell Using H 2 / CO as Fuel Gas. *J. Electrochem. Soc.* **143**, 3838. (doi:10.1149/1.1837305)

44. Chung C-C, Chen C-H, Weng D-Z. 2009 Development of an air bleeding technique and specific duration to improve the CO tolerance of proton-exchange membrane fuel cells. *Appl. Therm. Eng.* **29**, 2518–2526. (doi:10.1016/j.applthermaleng.2008.12.021)

45. Tjønnås J, Zenith F, Halvorsen IJ, Klages M, Scholta J. 2016 Control of Reversible Degradation Mechanisms in Fuel Cells: Mitigation of CO contamination. *IFAC-Pap.* **49**, 302–307. (doi:10.1016/j.ifacol.2016.07.309)

46. Mehta V, Cooper JS. 2003 Review and analysis of PEM fuel cell design and manufacturing. *J. Power Sources* **114**, 32–53. (doi:10.1016/S0378-7753(02)00542-6)

47. Paulus UA, Wokaun A, Scherer GG, Schmidt TJ, Stamenkovic V, Radmilovic V, Markovic NM, Ross PN. 2002 Oxygen Reduction on Carbon-Supported Pt−Ni and Pt−Co Alloy Catalysts. *J. Phys. Chem. B* **106**, 4181–4191. (doi:10.1021/jp013442l)

48. Antolini E, Salgado JRC, Gonzalez ER. 2006 The stability of Pt–M (M=first row transition metal) alloy catalysts and its effect on the activity in low temperature fuel cells: A literature review and tests on a Pt–Co catalyst. *J. Power Sources* **160**, 957–968. (doi:10.1016/j.jpowsour.2006.03.006)

49. Dubau L *et al.* 2014 A review of PEM fuel cell durability: materials degradation, local heterogeneities of aging and possible mitigation strategies. *Wiley Interdiscip. Rev.-Energy Environ.* **3**, 540–560. (doi:10.1002/wene.113)

50. Peron J, Edwards D, Haldane M, Luo X, Zhang Y, Holdcroft S, Shi Z. 2011 Fuel cell catalyst layers containing short-side-chain perfluorosulfonic acid ionomers. *J. Power Sources* **196**, 179–181. (doi:10.1016/j.jpowsour.2010.06.050)

51. Park Y-C, Kakinuma K, Uchida H, Watanabe M, Uchida M. 2015 Effects of short-side-chain perfluorosulfonic acid ionomers as binders on the performance of low Pt loading fuel cell cathodes. *J. Power Sources* **275**, 384–391. (doi:10.1016/j.jpowsour.2014.10.149)

52. Kim W-K, Sung KA, Oh K-H, Choo M-J, Cho KY, Cho K-Y, Park J-K. 2009 A new catalyst layer based on in situ pore generation of sulfonated poly(ether ether ketone) for PEMFC. *Electrochem. Commun.* **11**, 1714–1716. (doi:10.1016/j.elecom.2009.07.003)

53. Lee JK, Li W, Manthiram A. 2008 Sulfonated poly(ether ether ketone) as an ionomer for direct methanol fuel cell electrodes. *J. Power Sources* **180**, 56–62. (doi:10.1016/j.jpowsour.2008.02.015)

54. Sung KA, Kim W-K, Oh K-H, Park J-K. 2009 The catalyst layer containing sulfonated poly(ether ether ketone) as the electrode ionomer for polymer electrolyte fuel cells. *Electrochimica Acta* **54**, 3446–3452. (doi:10.1016/j.electacta.2009.01.024)

55. Yoon YJ, Kim T-H, Yu DM, Park J-Y, Hong YT. 2012 Modification of hydrocarbon structure for polymer electrolyte membrane fuel cell binder application. *Int. J. Hydrog. Energy* **37**, 13452–13461. (doi:10.1016/j.ijhydene.2012.05.136)

56. Ünlü M, Zhou J, Anestis-Richard I, Kim H, Kohl PA. 2011 Improved gas diffusion electrodes for hybrid polymer electrolyte fuel cells. *Electrochimica Acta* **56**, 4439–4444. (doi:10.1016/j.electacta.2011.02.017)

57. Song W, Yu H, Hao L, Miao Z, Yi B, Shao Z. 2010 A new hydrophobic thin film catalyst layer for PEMFC. *Solid State Ion.* **181**, 453–458. (doi:10.1016/j.ssi.2010.01.022)

58. Passalacqua E, Lufrano F, Squadrito G, Patti A, Giorgi L. 2001 Nafion content in the catalyst layer of polymer electrolyte fuel cells: effects on structure and performance. *Electrochimica Acta* **46**, 799–805. (doi:10.1016/S0013-4686(00)00679-4)

59. Passalacqua E, Lufrano F, Squadrito G, Patti A, Giorgi L. 1998 Influence of the structure in low-Pt loading electrodes for polymer electrolyte fuel cells. *Electrochimica Acta* **43**, 3665–3673. (doi:10.1016/S0013-4686(98)00124-8)

60. Xie J, Xu F, Wood DL, More KL, Zawodzinski TA, Smith WH. 2010 Influence of ionomer content on the structure and performance of PEFC membrane electrode assemblies. *Electrochimica Acta* **55**, 7404–7412. (doi:10.1016/j.electacta.2010.06.067)

61. Mu S, Tian M. 2012 Optimization of perfluorosulfonic acid ionomer loadings in catalyst layers of proton exchange membrane fuel cells. *Electrochimica Acta* **60**, 437–442. (doi:10.1016/j.electacta.2011.11.108)

62. Yu H, Roller JM, Mustain WE, Maric R. 2015 Influence of the ionomer/carbon ratio for low-Pt loading catalyst layer prepared by reactive spray deposition technology. *J. Power Sources* **283**, 84–94. (doi:10.1016/j.jpowsour.2015.02.101)

63. Di Noto V, Zawodzinski TA, Herring AM, Giffin GA, Negro E, Lavina S. 2012 Polymer electrolytes for a hydrogen economy. *Int. J. Hydrog. Energy* **37**, 6120–6131. (doi:10.1016/j.ijhydene.2012.01.080)

64. Arcella V, Merlo L, Ghielmi A. 2011 15 - Proton exchange membranes for fuel cells. In *Advanced Membrane Science and Technology for Sustainable Energy and Environmental Applications* (eds A Basile, SP Nunes), pp. 465–495. Woodhead Publishing. (doi:10.1533/9780857093790.4.465)

65. de Bruijn FA, Makkus RC, Mallant RKAM, Janssen GJM. 2007 Chapter Five - Materials for State-of-the-Art PEM Fuel Cells, and Their Suitability for Operation Above 100°C. In *Advances in Fuel Cells* (eds TS Zhao, K-D Kreuer, T Van Nguyen), pp. 235–336. Elsevier Science. (doi:10.1016/S1752-301X(07)80010-X)

66. Schaberg MS, Abulu JE, Haugen GM, Emery MA, O'conner SJ, Xiong PN, Hamrock SJ. 2010 New multi acid side-chain ionomers for proton exchange membrane fuel cells. *ECS Trans 2010* , 627–633.

67. Yandrasits M, Lindell M, Schaberg M, Kurkowski M. 2017 Increasing Fuel Cell Efficiency by Using Ultra-Low Equivalent Weight Ionomers. *Electrochem. Soc. Interface* **26**, 49. (doi:10.1149/2.F05171if)

68. Kusoglu A *et al.* 2020 Transport and Morphology of a Proton Exchange Membrane Based on a Doubly Functionalized Perfluorosulfonic Imide Side Chain Perflourinated Polymer. *Chem. Mater.* **32**, 38–59. (doi:10.1021/acs.chemmater.8b05012)

69. Prakash O, Jana KK, Jain R, Shah P, Manohar M, Shahi VK, Maiti P. 2018 Functionalized poly(vinylidene fluoride-co-hexafluoro propylene) membrane for fuel cell. *Polymer* **151**, 261–268. (doi:10.1016/j.polymer.2018.07.086)

70. Seck S, Magana S, Prébé A, Buvat P, Bigarré J, Chauveau J, Améduri B, Gérard J-F, Bounor-Legaré V. 2020 New fluorinated polymer- based nanocomposites via combination of sol -gel chemistry and reactive extrusion for polymer electrolyte membranes fuel cells (PEMFCs). *Mater. Chem. Phys.* **252**, 123004. (doi:10.1016/j.matchemphys.2020.123004)

71. Ghassemi H, Zawodzinski T, Schiraldi D, Hamrock S. 2012 Cross-Linked Low EW PFSA for High Temperature Fuel Cell. In *Polymers for Energy Storage and Delivery: Polyelectrolytes for Batteries and Fuel Cells*, pp. 201–220. American Chemical Society. (doi:10.1021/bk-2012-1096.ch012)

72. Di Noto V, Bettiol M, Bassetto F, Boaretto N, Negro E, Lavina S, Bertasi F. 2012 Hybrid inorganic-organic nanocomposite polymer electrolytes based on Nafion and fluorinated TiO2 for PEMFCs. *Int. J. Hydrog. Energy* **37**, 6169–6181. (doi:10.1016/j.ijhydene.2011.07.131)

73. Kim DJ, Jo MJ, Nam SY. 2015 A review of polymer–nanocomposite electrolyte membranes for fuel cell application. *J. Ind. Eng. Chem.* **21**, 36–52. (doi:10.1016/j.jiec.2014.04.030)

74. Noto VD, Piga M, Negro E, Giffin GA, Polizzi S, Zawodzinski TA. 2013 New nanocomposite proton conducting membranes based on a core–shell nanofiller for low relative humidity fuel cells. *RSC Adv.* **3**, 18960–18969. (doi:10.1039/C3RA40305J)

75. Yandrasits MA, Lindell MJ, Hamrock SJ. 2019 New directions in perfluoroalkyl sulfonic acid–based proton-exchange membranes. *Curr. Opin. Electrochem.* **18**, 90–98. (doi:10.1016/j.coelec.2019.10.012)

76. Jung H-Y, Kim JW. 2012 Role of the glass transition temperature of Nafion 117 membrane in the preparation of the membrane electrode assembly in a direct methanol

fuel cell (DMFC). *Int. J. Hydrog. Energy* **37**, 12580–12585. (doi:10.1016/j.ijhydene.2012.05.121)

77. Kusoglu A, Weber AZ. 2017 New Insights into Perfluorinated Sulfonic-Acid Ionomers. *Chem. Rev.* **117**, 987–1104. (doi:10.1021/acs.chemrev.6b00159)

78. Kraytsberg A, Ein-Eli Y. 2014 Review of Advanced Materials for Proton Exchange Membrane Fuel Cells. *Energy Fuels* **28**, 7303–7330. (doi:10.1021/ef501977k)

79. Grot WG. 1994 Perfluorinated ion exchange polymers and their use in research and industry. *Macromol. Symp.* **82**, 161–172. (doi:10.1002/masy.19940820117)

80. Guerra MA. 2003 Preparation of perfluorinated vinyl ethers having a sulfonyl fluoride end-group.

81. Imbalzano JF, Kerbow DL. 1988 Stable tetrafluoroethylene copolymers.

82. Morgan RA, Sloan WH. 1986 Extrusion finishing of perfluorinated copolymers.

83. Curtin DE, Lousenberg RD, Henry TJ, Tangeman PC, Tisack ME. 2004 Advanced materials for improved PEMFC performance and life. *J. Power Sources* **131**, 41–48. (doi:10.1016/j.jpowsour.2004.01.023)

84. Merlo L, Ghielmi A, Cirillo L, Gebert M, Arcella V. 2007 Resistance to peroxide degradation of Hyflon® Ion membranes. *J. Power Sources* **171**, 140–147. (doi:10.1016/j.jpowsour.2006.11.012)

85. Eisman GA. 1990 The application of Dow Chemical's perfluorinated membranes in proton-exchange membrane fuel cells. *J. Power Sources* **29**, 389–398. (doi:10.1016/0378-7753(90)85012-2)

86. Ghielmi A, Vaccarono P, Troglia C, Arcella V. 2005 Proton exchange membranes based on the short-side-chain perfluorinated ionomer. *J. Power Sources* **145**, 108–115. (doi:10.1016/j.jpowsour.2004.12.068)

87. Liu W, Ruth K, Rusch G. 2001 Membrane durability in PEM fuel cells. *J. New Mater. Electrochem. Syst.* **4**, 227–232.

88. Tang Y, Kusoglu A, Karlsson AM, Santare MH, Cleghorn S, Johnson WB. 2008 Mechanical properties of a reinforced composite polymer electrolyte membrane and its simulated performance in PEM fuel cells. *J. Power Sources* **175**, 817–825. (doi:10.1016/j.jpowsour.2007.09.093)

89. Roelofs MG, Choudhury B, Siddiqui JA, Banerjee S. 2012 Improved composite polymer electrolyte membrane.

90. Jao T-C, Jung G-B, Kuo S-C, Tzeng W-J, Su A. 2012 Degradation mechanism study of PTFE/Nafion membrane in MEA utilizing an accelerated degradation technique. *Int. J. Hydrog. Energy* **37**, 13623–13630. (doi:10.1016/j.ijhydene.2012.02.035)

91. Yu L, Lin F, Xu L, Xi J. 2017 Structure–property relationship study of Nafion XL membrane for high-rate, long-lifespan, and all-climate vanadium flow batteries. *RSC Adv.* **7**, 31164–31172. (doi:10.1039/C7RA04996J)

92. Baker AM, Mukundan R, Spernjak D, Judge EJ, Advani SG, Prasad AK, Borup RL. 2016 Cerium Migration during PEM Fuel Cell Accelerated Stress Testing. *J. Electrochem. Soc.* **163**, F1023–F1031. (doi:10.1149/2.0181609jes)

93. Prabhakaran V, Arges CG, Ramani V. 2012 Investigation of polymer electrolyte membrane chemical degradation and degradation mitigation using in situ fluorescence spectroscopy. *Proc. Natl. Acad. Sci. U. S. A.* **109**, 1029–1034. (doi:10.1073/pnas.1114672109)

94. Stewart SM, Spernjak D, Borup R, Datye A, Garzon F. 2014 Cerium Migration through Hydrogen Fuel Cells during Accelerated Stress Testing. *Ecs Electrochem. Lett.* **3**, F19–F22. (doi:10.1149/2.008404eel)

95. Zatoń M, Prélot B, Donzel N, Rozière J, Jones DJ. 2018 Migration of Ce and Mn Ions in PEMFC and Its Impact on PFSA Membrane Degradation. *J. Electrochem. Soc.* **165**, F3281–F3289. (doi:10.1149/2.0311806jes)

96. Shi S, Weber AZ, Kusoglu A. 2016 Structure/property relationship of Nafion XL composite membranes. *J. Membr. Sci.* **516**, 123–134. (doi:10.1016/j.memsci.2016.06.004)

97. Boyle NG, McBrierty VJ, Eisenberg A. 1983 NMR investigation of molecular motion in Nafion membranes. *Macromolecules* **16**, 80–84. (doi:10.1021/ma00235a016)

98. Schlick S, Gebel G, Pineri M, Volino F. 1991 Fluorine-19 NMR spectroscopy of acid Nafion membranes and solutions. *Macromolecules* **24**, 3517–3521. (doi:10.1021/ma00012a008)

99. Chen Q, Schmidt-Rohr K. 2004 F-19 and C-13 NMR signal assignment and analysis in a perfluorinated ionomer (Nafion) by two-dimensional solid-state NMR. *Macromolecules* **37**, 5995–6003. (doi:10.1021/ma049759b)

100. Chen Q, Schmidt-Rohr K. 2007 Backbone Dynamics of the Nafion Ionomer Studied by 19F-13C Solid-State NMR. *Macromol. Chem. Phys.* **208**, 2189–2203. (doi:10.1002/macp.200700200)

101. Gierke TD, Munn GE, Wilson FC. 1981 The morphology in nafion perfluorinated membrane products, as determined by wide- and small-angle x-ray studies. *J. Polym. Sci. Polym. Phys. Ed.* **19**, 1687–1704. (doi:10.1002/pol.1981.180191103)

102. Hsu WY, Gierke TD. 1983 Ion transport and clustering in nafion perfluorinated membranes. *J. Membr. Sci.* **13**, 307–326. (doi:10.1016/S0376-7388(00)81563-X)

103. Gebel G. 2000 Structural evolution of water swollen perfluorosulfonated ionomers from dry membrane to solution. *Polymer* **41**, 5829–5838. (doi:10.1016/S0032-3861(99)00770-3)

104. Rubatat L. 2003 Nouveau modèle structural des membranes Nafion ®, polymère de référence pour l'application pile à combustible basse température. thesis, Grenoble 1. See http://www.theses.fr/2003GRE10142.

105. Rubatat L, Gebel G, Diat O. 2004 Fibrillar structure of Nafion: Matching Fourier and real space studies of corresponding films and solutions. *Macromolecules* **37**, 7772–7783. (doi:10.1021/ma049683j)

106. Rubatat L, Rollet AL, Gebel G, Diat O. 2002 Evidence of Elongated Polymeric Aggregates in Nafion. *Macromolecules* **35**, 4050–4055. (doi:10.1021/ma011578b)

107. Schmidt-Rohr K, Chen Q. 2008 Parallel cylindrical water nanochannels in Nafion fuel-cell membranes. *Nat. Mater.* **7**, 75–83. (doi:10.1038/nmat2074)

108. Kreuer K-D, Portale G. 2013 A Critical Revision of the Nano-Morphology of Proton Conducting Ionomers and Polyelectrolytes for Fuel Cell Applications. *Adv. Funct. Mater.* **23**, 5390–5397. (doi:10.1002/adfm.201300376)

109. Kreuer K-D, Paddison SJ, Spohr E, Schuster M. 2004 Transport in Proton Conductors for Fuel-Cell Applications: Simulations, Elementary Reactions, and Phenomenology. *Chem. Rev.* **104**, 4637–4678. (doi:10.1021/cr020715f)

110. Zawodzinski TA, Springer TE, Uribe F, Gottesfeld S. 1993 Characterization of polymer electrolytes for fuel cell applications. *Solid State Ion.* **60**, 199–211. (doi:10.1016/0167-2738(93)90295-E)

111. Williams MV, Kunz HR, Fenton JM. 2004 Operation of Nafion((R))-based PEM fuel cells with no external humidification: influence of operating conditions and gas diffusion layers. *J. Power Sources* **135**, 122–134. (doi:10.1016/j.jpowsour.2004.04.010)

112. Choi P, Jalani NH, Datta R. 2005 Thermodynamics and Proton Transport in Nafion: I. Membrane Swelling, Sorption, and Ion-Exchange Equilibrium. *J. Electrochem. Soc.* **152**, E84. (doi:10.1149/1.1855872)

113. Gebel G, Aldebert P, Pineri M. 1993 Swelling Study of Perfluorosulphonated Ionomer Membranes. *Polymer* **34**, 333–339. (doi:10.1016/0032-3861(93)90086-P)

114. Tang Y, Karlsson AM, Santare MH, Gilbert M, Cleghorn S, Johnson WB. 2006 An experimental investigation of humidity and temperature effects on the mechanical properties of perfluorosulfonic acid membrane. *Mater. Sci. Eng. A* **425**, 297–304. (doi:10.1016/j.msea.2006.03.055)

115. Kidena K, Ohkubo T, Takimoto N, Ohira A. 2010 PFG-NMR approach to determining the water transport mechanism in polymer electrolyte membranes conditioned at different temperatures. *Eur. Polym. J.* **46**, 450–455. (doi:10.1016/j.eurpolymj.2009.12.012)

116. Park GS. 1986 Transport Principles—Solution, Diffusion and Permeation in Polymer Membranes. In *Synthetic Membranes: Science, Engineering and Applications* (eds PM Bungay, HK Lonsdale, MN de Pinho), pp. 57–107. Dordrecht: Springer Netherlands. (doi:10.1007/978-94-009-4712-2_3)

117. Rivin D, Kendrick CE, Gibson PW, Schneider NS. 2001 Solubility and transport behavior of water and alcohols in Nafion™. *Polymer* **42**, 623–635. (doi:10.1016/S0032-3861(00)00350-5)

118. Zawodzinski TA, Derouin C, Radzinski S, Sherman RJ, Smith VT, Springer TE, Gottesfeld S. 1993 Water Uptake by and Transport Through Nafion® 117 Membranes. *J. Electrochem. Soc.* **140**, 1041. (doi:10.1149/1.2056194)

119. Majsztrik PW, Satterfield MB, Bocarsly AB, Benziger JB. 2007 Water sorption, desorption and transport in Nafion membranes. *J. Membr. Sci.* **301**, 93–106. (doi:10.1016/j.memsci.2007.06.022)

120. Blanchard RM, Nuzzo RG. 2000 An infrared study of the effects of hydration on cation-loaded nafion thin films. *J. Polym. Sci. Part B Polym. Phys.* **38**, 1512–1520. (doi:10.1002/(SICI)1099-0488(20000601)38:11<1512::AID-POLB110>3.0.CO;2-2)

121. Laporta M, Pegoraro M, Zanderighi L. 1999 Perfluorosulfonated membrane (Nafion): FT-IR study of the state of water with increasing humidity. *Phys. Chem. Chem. Phys.* **1**, 4619–4628. (doi:10.1039/A904460D)

122. Ostrowska J, Narebska A. 1983 Infrared study of hydration and association of functional groups in a perfluorinated Nafion membrane, Part 1. *Colloid Polym. Sci.* **261**, 93–98. (doi:10.1007/BF01410686)

123. Korzeniewski C, Snow DE, Basnayake R. 2006 Transmission infrared spectroscopy as a probe of Nafion film structure: analysis of spectral regions fundamental to understanding hydration effects. *Appl. Spectrosc.* **60**, 599–604. (doi:10.1366/000370206777670620)

124. Ludvigsson M, Lindgren J, Tegenfeldt J. 2000 FTIR study of water in cast Nafion films. *Electrochimica Acta* **45**, 2267–2271. (doi:10.1016/S0013-4686(99)00438-7)

125. Maldonado L, Perrin J-C, Dillet J, Lottin O. 2012 Characterization of polymer electrolyte Nafion membranes: Influence of temperature, heat treatment and drying protocol on sorption and transport properties. *J. Membr. Sci.* **389**, 43–56. (doi:10.1016/j.memsci.2011.10.014)

126. Negro E, Vittadello M, Vezzù K, Paddison SJ, Di Noto V. 2013 The influence of the cationic form and degree of hydration on the structure of Nafion™. *Solid State Ion.* **252**, 84–92. (doi:10.1016/j.ssi.2013.09.017)

127. Vittadello M, Negro E, Lavina S, Pace G, Safari A, Noto VD. 2008 Vibrational Studies and Properties of Hybrid Inorganic−Organic Proton Conducting Membranes Based on Nafion and Hafnium Oxide Nanoparticles. *J. Phys. Chem. B* **112**, 16590–16600. (doi:10.1021/jp804117w)

128. Bass M, Freger V. 2008 Hydration of Nafion and Dowex in liquid and vapor environment: Schroeder's paradox and microstructure. *Polymer* **49**, 497–506. (doi:10.1016/j.polymer.2007.11.054)

129. Choi P, Datta R. 2003 Sorption in Proton-Exchange Membranes: An Explanation of Schroeder's Paradox. *J. Electrochem. Soc.* **150**, E601. (doi:10.1149/1.1623495)

130. Schroeder P von. 1903 Über Erstarrungs- und Quellugserscheinungen von Gelatine. *Z. Für Phys. Chem.* **45U**. (doi:10.1515/zpch-1903-4503)

131. Perrin J-C. 2006 Etude expérimentale multi-échelles de la dynamique de l'eau dans les membranes ionomères utilisées en pile à combustible. thesis, Grenoble 1. See http://www.theses.fr/2006GRE10175.

132. Paddison SJ, Paul R. 2002 The nature of proton transport in fully hydrated Nafion®. *Phys. Chem. Chem. Phys.* **4**, 1158–1163. (doi:10.1039/B109792J)

133. Hwang GS, Kaviany M, Gostick JT, Kientiz B, Weber AZ, Kim MH. 2011 Role of water states on water uptake and proton transport in Nafion using molecular simulations and bimodal network. *Polymer* **52**, 2584–2593. (doi:10.1016/j.polymer.2011.03.056)

134. Eikerling M, Kornyshev AA, Spohr E. 2008 Proton-Conducting Polymer Electrolyte Membranes: Water and Structure in Charge. In *Fuel Cells I* (ed GG Scherer), pp. 15–54. Berlin, Heidelberg: Springer. (doi:10.1007/12_2008_132)

135. Agmon N. 1995 The Grotthuss mechanism. *Chem. Phys. Lett.* **244**, 456–462. (doi:10.1016/0009-2614(95)00905-J)

136. Paul R, Paddison SJ. 2001 A statistical mechanical model for the calculation of the permittivity of water in hydrated polymer electrolyte membrane pores. *J. Chem. Phys.* **115**, 7762–7771. (doi:10.1063/1.1405851)

137. Choi P, Jalani NH, Datta R. 2005 Thermodynamics and Proton Transport in Nafion: II. Proton Diffusion Mechanisms and Conductivity. *J. Electrochem. Soc.* **152**, E123. (doi:10.1149/1.1859814)

138. Eikerling M, Kornyshev AA. 2001 Proton transfer in a single pore of a polymer electrolyte membrane. *J. Electroanal. Chem.* **502**, 1–14. (doi:10.1016/S0022-0728(00)00368-5)

139. Sone Y, Ekdunge P, Simonsson D. 1996 Proton Conductivity of Nafion 117 as Measured by a Four-Electrode AC Impedance Method. *J. Electrochem. Soc.* **143**, 1254. (doi:10.1149/1.1836625)

140. Lee K, Ishihara A, Mitsushima S, Kamiya N, Ota K. 2004 Effect of Recast Temperature on Diffusion and Dissolution of Oxygen and Morphological Properties in Recast Nafion. *J. Electrochem. Soc.* **151**, A639. (doi:10.1149/1.1652052)

141. Khattra NS, Karlsson AM, Santare MH, Walsh P, Busby FC. 2012 Effect of time-dependent material properties on the mechanical behavior of PFSA membranes subjected to humidity cycling. *J. Power Sources* **214**, 365–376. (doi:10.1016/j.jpowsour.2012.04.065)

142. Kawano Y, Wang Y, Palmer RA, Aubuchon SR. 2002 Stress-Strain Curves of Nafion Membranes in Acid and Salt Forms. *Polímeros* **12**, 96–101. (doi:10.1590/S0104-14282002000200008)

143. Bauer F, Denneler S, Willert-Porada M. 2005 Influence of temperature and humidity on the mechanical properties of Nafion® 117 polymer electrolyte membrane. *J. Polym. Sci. Part B Polym. Phys.* **43**, 786–795. (doi:10.1002/polb.20367)

144. Lin Q, Liu Z, Wang L, Chen X, Shi S. 2018 Fracture property of Nafion XL composite membrane determined by R-curve method. *J. Power Sources* **398**, 34–41. (doi:10.1016/j.jpowsour.2018.07.052)

145. Kusoglu A, Hexemer A, Jiang R, Gittleman CS, Weber AZ. 2012 Effect of compression on PFSA-ionomer morphology and predicted conductivity changes. *J. Membr. Sci.* **421–422**, 283–291. (doi:10.1016/j.memsci.2012.07.027)

146. Kusoglu A, Tang Y, Santare MH, Karlsson AM, Cleghorn S, Johnson WB. 2009 Stress-Strain Behavior of Perfluorosulfonic Acid Membranes at Various Temperatures and Humidities: Experiments and Phenomenological Modeling. *J. Fuel Cell Sci. Technol.* **6**, 011012. (doi:10.1115/1.2971069)

147. Lu Z, Lugo M, Santare MH, Karlsson AM, Busby FC, Walsh P. 2012 An experimental investigation of strain rate, temperature and humidity effects on the mechanical behavior of a perfluorosulfonic acid membrane. *J. Power Sources* **214**, 130–136. (doi:10.1016/j.jpowsour.2012.04.094)

148. Solasi R, Huang X, Reifsnider K. 2010 Creep and stress-rupture of Nafion® membranes under controlled environment. *Mech. Mater.* **42**, 678–685. (doi:10.1016/j.mechmat.2010.04.005)

149. Huang X, Rodgers M, Yoon W, Li B, Mohajeri N. 2008 Mechanical Degradation Behavior of Recast Composite PFSA Membrane and Nafion® N-112 Membrane under OCV Condition. *ECS Trans.* **16**, 1573–1579. (doi:10.1149/1.2981997)

150. Ballengee JB, Pintauro PN. 2011 Composite Fuel Cell Membranes from Dual-Nanofiber Electrospun Mats. *Macromolecules* **44**, 7307–7314. (doi:10.1021/ma201684j)

151. Cleghorn S, Kolde J, Liu W. 2010 Catalyst coated composite membranes. In *Handbook of Fuel Cells*, Hoboken, NJ (USA): John Wiley & Sons, Ltd. (doi:10.1002/9780470974001.f303049)

152. Satterfield MB, Majsztrik PW, Ota H, Benziger JB, Bocarsly AB. 2006 Mechanical properties of Nafion and titania/Nafion composite membranes for polymer electrolyte membrane fuel cells. *J. Polym. Sci. Part B Polym. Phys.* **44**, 2327–2345. (doi:10.1002/polb.20857)

153. Wu J, Yuan XZ, Martin JJ, Wang H, Zhang J, Shen J, Wu S, Merida W. 2008 A review of PEM fuel cell durability: Degradation mechanisms and mitigation strategies. *J. Power Sources* **184**, 104–119. (doi:10.1016/j.jpowsour.2008.06.006)

154. Borup R *et al.* 2007 Scientific aspects of polymer electrolyte fuel cell durability and degradation. *Chem. Rev.* **107**, 3904–3951. (doi:10.1021/cr050182l)

155. Bruijn FA de, Dam V a. T, Janssen GJM. 2008 Review: Durability and Degradation Issues of PEM Fuel Cell Components. *Fuel Cells* **8**, 3–22. (doi:10.1002/fuce.200700053)

156. Schulze M, Knori T, Schneider A, Gulzow E. 2004 Degradation of sealings for PEFC test cells during fuel cell operation. *J. Power Sources* **127**, 222–229. (doi:10.1016/j.jpowsour.2003.09.017)

157. Pozio A, Silva RF, De Francesco M, Giorgi L. 2003 Nafion degradation in PEFCs from end plate iron contamination. *Electrochimica Acta* **48**, 1543–1549. (doi:10.1016/S0013-4686(03)00026-4)

158. St-Pierre J, Jia NY. 2002 Successful demonstration of Ballard PEMFCS for space shuttle applications. *J. New Mater. Electrochem. Syst.* **5**, 263–271.

159. Oszcipok M, Riemann D, Kronenwett U, Kreideweis M, Zedda M. 2005 Statistic analysis of operational influences on the cold start behaviour of PEM fuel cells. *J. Power Sources* **145**, 407–415. (doi:10.1016/j.jpowsour.2005.02.058)

160. Frisk JW, Hicks MT, Atanasoski RT, Boand WM, Schmoeckel AK, Kurkowski MJ. 2004 MEA Component Durability.

161. Stevens DA, Dahn JR. 2005 Thermal degradation of the support in carbon-supported platinum electrocatalysts for PEM fuel cells. *Carbon* **43**, 179–188. (doi:10.1016/j.carbon.2004.09.004)

162. Cai M, Ruthkosky MS, Merzougui B, Swathirajan S, Balogh MP, Oh SH. 2006 Investigation of thermal and electrochemical degradation of fuel cell catalysts. *J. Power Sources* **160**, 977–986. (doi:10.1016/j.jpowsour.2006.03.033)

163. Jordan LR, Shukla AK, Behrsing T, Avery NR, Muddle BC, Forsyth M. 2000 Diffusion layer parameters influencing optimal fuel cell performance. *J. Power Sources* **86**, 250–254. (doi:10.1016/S0378-7753(99)00489-9)

164. Williams MV, Begg E, Bonville L, Kunz HR, Fenton JM. 2004 Characterization of Gas Diffusion Layers for PEMFC. *J. Electrochem. Soc.* **151**, A1173. (doi:10.1149/1.1764779)

165. Pasaogullari U, Wang C-Y, Chen KS. 2005 Two-Phase Transport in Polymer Electrolyte Fuel Cells with Bilayer Cathode Gas Diffusion Media. *J. Electrochem. Soc.* **152**, A1574. (doi:10.1149/1.1938067)

166. Pasaogullari U, Wang C-Y. 2004 Two-phase transport and the role of micro-porous layer in polymer electrolyte fuel cells. *Electrochimica Acta* **49**, 4359–4369. (doi:10.1016/j.electacta.2004.04.027)

167. Weber AZ, Darling RM, Newman J. 2004 Modeling Two-Phase Behavior in PEFCs. *J. Electrochem. Soc.* **151**, A1715. (doi:10.1149/1.1792891)

168. Wang Z-B, Zuo P-J, Chu Y-Y, Shao Y-Y, Yin G-P. 2009 Durability studies on performance degradation of Pt/C catalysts of proton exchange membrane fuel cell. *Int. J. Hydrog. Energy* **34**, 4387–4394. (doi:10.1016/j.ijhydene.2009.03.045)

169. Iojoiu C, Guilminot E, Maillard F, Chatenet M, Sanchez J-Y, Claude E, Rossinot E. 2007 Membrane and Active Layer Degradation Following PEMFC Steady-State Operation. *J. Electrochem. Soc.* **154**, B1115. (doi:10.1149/1.2775282)

170. Cheng X, Shi Z, Glass N, Zhang L, Zhang J, Song D, Liu Z-S, Wang H, Shen J. 2007 A review of PEM hydrogen fuel cell contamination: Impacts, mechanisms, and mitigation. *J. Power Sources* **165**, 739–756. (doi:10.1016/j.jpowsour.2006.12.012)

171. Zhang J, Wang H, Wilkinson DP, Song D, Shen J, Liu Z-S. 2005 Model for the contamination of fuel cell anode catalyst in the presence of fuel stream impurities. *J. Power Sources* **147**, 58–71. (doi:10.1016/j.jpowsour.2005.01.013)

172. Mohtadi R, Lee W -k., Van Zee JW. 2004 Assessing durability of cathodes exposed to common air impurities. *J. Power Sources* **138**, 216–225. (doi:10.1016/j.jpowsour.2004.06.036)

173. Schmidt TJ, Paulus UA, Gasteiger HA, Behm RJ. 2001 The oxygen reduction reaction on a Pt/carbon fuel cell catalyst in the presence of chloride anions. *J. Electroanal. Chem.* **508**, 41–47. (doi:10.1016/S0022-0728(01)00499-5)

174. Papageorgopoulos DC, Keijzer M, Veldhuis JBJ, Bruijn FA de. 2002 CO Tolerance of Pd-Rich Platinum Palladium Carbon-Supported Electrocatalysts : Proton Exchange Membrane Fuel Cell Applications. *J. Electrochem. Soc.* **149**, A1400. (doi:10.1149/1.1510131)

175. Sishtla C, Koncar G, Platon R, Gamburzev S, Appleby AJ, Velev OA. 1998 Performance and endurance of a PEMFC operated with synthetic reformate fuel feed. *J. Power Sources* **71**, 249–255. (doi:10.1016/S0378-7753(97)02719-5)

176. Yoda T, Uchida H, Watanabe M. 2007 Effects of operating potential and temperature on degradation of electrocatalyst layer for PEFCs. *Electrochimica Acta* **52**, 5997–6005. (doi:10.1016/j.electacta.2007.03.049)

177. Ferreira PJ, O' GJ la, Shao-Horn Y, Morgan D, Makharia R, Kocha S, Gasteiger HA. 2005 Instability of Pt/C Electrocatalysts in Proton Exchange Membrane Fuel Cells A Mechanistic Investigation. *J. Electrochem. Soc.* **152**, A2256–A2271. (doi:10.1149/1.2050347)

178. Guilminot E, Corcella A, Charlot F, Maillard F, Chatenet M. 2007 Detection of Pt z + Ions and Pt Nanoparticles Inside the Membrane of a Used PEMFC. *J. Electrochem. Soc.* **154**, B96–B105. (doi:10.1149/1.2388863)

179. Meier JC *et al.* 2014 Design criteria for stable Pt/C fuel cell catalysts. *Beilstein J. Nanotechnol.* **5**, 44–67. (doi:10.3762/bjnano.5.5)

180. Pourbaix M. 1974 *Atlas of Electrochemical Equilibria in Aqueous Solutions*. 2nd ed. Houston: NACE International.

181. Dam V a. T, Bruijn FA de. 2007 The Stability of PEMFC Electrodes: Platinum Dissolution vs Potential and Temperature Investigated by Quartz Crystal Microbalance. *J. Electrochem. Soc.* **154**, B494. (doi:10.1149/1.2714327)

182. Nikkuni FR, Ticianelli EA, Dubau L, Chatenet M. 2013 Identical-Location Transmission Electron Microscopy Study of Pt/C and Pt–Co/C Nanostructured Electrocatalyst Aging: Effects of Morphological and Compositional Changes on the Oxygen Reduction Reaction Activity. *Electrocatalysis* **4**, 104–116. (doi:10.1007/s12678-013-0126-5)

183. Shao Y, Yin G, Gao Y. 2007 Understanding and approaches for the durability issues of Pt-based catalysts for PEM fuel cell. *J. Power Sources* **171**, 558–566. (doi:10.1016/j.jpowsour.2007.07.004)

184. Wang X, Kumar R, Myers DJ. 2006 Effect of Voltage on Platinum Dissolution: Relevance to Polymer Electrolyte Fuel Cells. *Electrochem. Solid State Lett.* **9**, A225. (doi:10.1149/1.2180536)

185. Xie J, Wood DL, Wayne DM, Zawodzinski TA, Atanassov P, Borup RL. 2005 Durability of PEFCs at High Humidity Conditions. *J. Electrochem. Soc.* **152**, A104–A113. (doi:10.1149/1.1830355)

186. Cheng TTH, Rogers E, Young AP, Ye S, Colbow V, Wessel S. 2011 Effects of crossover hydrogen on platinum dissolution and agglomeration. *J. Power Sources* **196**, 7985–7988. (doi:10.1016/j.jpowsour.2011.05.034)

187. Zhang S, Yuan X, Wang H, Mérida W, Zhu H, Shen J, Wu S, Zhang J. 2009 A review of accelerated stress tests of MEA durability in PEM fuel cells. *Int. J. Hydrog. Energy* **34**, 388–404. (doi:10.1016/j.ijhydene.2008.10.012)

188. Chung CG, Kim L, Sung YW, Lee J, Chung JS. 2009 Degradation mechanism of electrocatalyst during long-term operation of PEMFC. *Int. J. Hydrog. Energy* **34**, 8974–8981. (doi:10.1016/j.ijhydene.2009.08.094)

189. Péron J, Nedellec Y, Jones DJ, Rozière J. 2008 The effect of dissolution, migration and precipitation of platinum in Nafion®-based membrane electrode assemblies during fuel cell operation at high potential. *J. Power Sources* **185**, 1209–1217. (doi:10.1016/j.jpowsour.2008.06.098)

190. Durst J *et al.* 2013 Degradation heterogeneities induced by repetitive start/stop events in proton exchange membrane fuel cell: Inlet vs. outlet and channel vs. land. *Appl. Catal. B-Environ.* **138**, 416–426. (doi:10.1016/j.apcatb.2013.03.021)

191. Zhang J, Litteer BA, Gu W, Liu H, Gasteiger HA. 2007 Effect of Hydrogen and Oxygen Partial Pressure on Pt Precipitation within the Membrane of PEMFCs. *J. Electrochem. Soc.* **154**, B1006. (doi:10.1149/1.2764240)

192. Bi W, Gray GE, Fuller TF. 2007 PEM Fuel Cell Pt/C Dissolution and Deposition in Nafion Electrolyte. *Electrochem. Solid State Lett.* **10**, B101. (doi:10.1149/1.2712796)

193. Kim L, Chung CG, Sung YW, Chung JS. 2008 Dissolution and migration of platinum after long-term operation of a polymer electrolyte fuel cell under various conditions. *J. Power Sources* **183**, 524–532. (doi:10.1016/j.jpowsour.2008.05.062)

194. Liu H, Gasteiger HA, Laconti A, Zhang J. 2006 Factors Impacting Chemical Degradation Of Perfluorinated Sulfonic Acid Ionomers. *ECS Trans.* **1**, 283–293. (doi:10.1149/1.2214561)

195. Macauley N, Ghassemzadeh L, Lim C, Watson M, Kolodziej J, Lauritzen M, Holdcroft S, Kjeang E. 2013 Pt Band Formation Enhances the Stability of Fuel Cell Membranes. *Ecs Electrochem. Lett.* **2**, F33–F35. (doi:10.1149/2.007304eel)

196. Maass S, Finsterwalder F, Frank G, Hartmann R, Merten C. 2008 Carbon support oxidation in PEM fuel cell cathodes. *J. Power Sources* **176**, 444–451. (doi:10.1016/j.jpowsour.2007.08.053)

197. Dubau L *et al.* 2014 Carbon corrosion induced by membrane failure: The weak link of PEMFC long-term performance. *Int. J. Hydrog. Energy* **39**, 21902–21914. (doi:10.1016/j.ijhydene.2014.07.099)

198. Macauley N, Papadias DD, Fairweather J, Spernjak D, Langlois D, Ahluwalia R, More KL, Mukundan R, Borup RL. 2018 Carbon Corrosion in PEM Fuel Cells and the Development of Accelerated Stress Tests. *J. Electrochem. Soc.* **165**, F3148–F3160. (doi:10.1149/2.0061806jes)

199. Reiser CA, Bregoli L, Patterson TW, Yi JS, Yang JD, Perry ML, Jarvi TD. 2005 A Reverse-Current Decay Mechanism for Fuel Cells. *Electrochem. Solid State Lett.* **8**, A273. (doi:10.1149/1.1896466)

200. Taniguchi A, Akita T, Yasuda K, Miyazaki Y. 2004 Analysis of electrocatalyst degradation in PEMFC caused by cell reversal during fuel starvation. *J. Power Sources* **130**, 42–49. (doi:10.1016/j.jpowsour.2003.12.035)

201. Roen LM, Paik CH, Jarvi TD. 2003 Electrocatalytic Corrosion of Carbon Support in PEMFC Cathodes. *Electrochem. Solid State Lett.* **7**, A19. (doi:10.1149/1.1630412)

202. Castanheira L, Dubau L, Mermoux M, Berthomé G, Caqué N, Rossinot E, Chatenet M, Maillard F. 2014 Carbon Corrosion in Proton-Exchange Membrane Fuel Cells: From Model Experiments to Real-Life Operation in Membrane Electrode Assemblies. *ACS Catal.* **4**, 2258–2267. (doi:10.1021/cs500449q)

203. Danerol AS, Bas C, Flandin L, Claude E, Alberola ND. 2011 Influence of ageing in fuel cell on membrane/electrodes interfaces. *J. Power Sources* **196**, 3479–3484. (doi:10.1016/j.jpowsour.2010.12.014)

204. El Kaddouri A, Flandin L, Bas C. 2018 Chemical degradation of PFSA ionomer binder in PEMFC's catalyst layer. *Int. J. Hydrog. Energy* **43**, 15386–15397. (doi:10.1016/j.ijhydene.2018.06.049)

205. Wang J, Yin G, Shao Y, Zhang S, Wang Z, Gao Y. 2007 Effect of carbon black support corrosion on the durability of Pt/C catalyst. *J. Power Sources* **171**, 331–339. (doi:10.1016/j.jpowsour.2007.06.084)

206. Zhang F-Y, Advani SG, Prasad AK, Boggs ME, Sullivan SP, Beebe TP. 2009 Quantitative characterization of catalyst layer degradation in PEM fuel cells by X-ray photoelectron spectroscopy. *Electrochimica Acta* **54**, 4025–4030. (doi:10.1016/j.electacta.2009.02.028)

207. Parry V, Berthomé G, Joud J-C, Lemaire O, Franco AA. 2011 XPS investigations of the proton exchange membrane fuel cell active layers aging: Characterization of the mitigating role of an anodic CO contamination on cathode degradation. *J. Power Sources* **196**, 2530–2538. (doi:10.1016/j.jpowsour.2010.11.027)

208. Silva RA, Hashimoto T, Thompson GE, Rangel CM. 2012 Characterization of MEA degradation for an open air cathode PEM fuel cell. *Int. J. Hydrog. Energy* **37**, 7299–7308. (doi:10.1016/j.ijhydene.2011.12.110)

209. Aoki M, Uchida H, Watanabe M. 2006 Decomposition mechanism of perfluorosulfonic acid electrolyte in polymer electrolyte fuel cells. *Electrochem. Commun.* **8**, 1509–1513. (doi:10.1016/j.elecom.2006.07.017)

210. Morawietz T, Handl M, Oldani C, Friedrich KA, Hiesgen R. 2016 Quantitative in Situ Analysis of Ionomer Structure in Fuel Cell Catalytic Layers. *ACS Appl. Mater. Interfaces* **8**, 27044–27054. (doi:10.1021/acsami.6b07188)

211. Xie T, Hayden CA. 2007 A kinetic model for the chemical degradation of perfluorinated sulfonic acid ionomers: Weak end groups versus side chain cleavage. *Polymer* **48**, 5497–5506. (doi:10.1016/j.polymer.2007.07.043)

212. Chen C, Fuller TF. 2009 The effect of humidity on the degradation of Nafion® membrane. *Polym. Degrad. Stab.* **94**, 1436–1447. (doi:10.1016/j.polymdegradstab.2009.05.016)

213. Takasaki M, Nakagawa Y, Sakiyama Y, Tanabe K, Ookubo K, Sato N, Minamide T, Nakayama H, Hori M. 2013 Degradation Study of Perfluorosulfonic Acid Polymer Electrolytes: Approach from Decomposition Product Analysis. *J. Electrochem. Soc.* **160**, F413–F416. (doi:10.1149/2.076304jes)

214. Collier A, Wang H, Zi Yuan X, Zhang J, Wilkinson DP. 2006 Degradation of polymer electrolyte membranes. *Int. J. Hydrog. Energy* **31**, 1838–1854. (doi:10.1016/j.ijhydene.2006.05.006)

215. Rodgers MP, Bonville LJ, Kunz HR, Slattery DK, Fenton JM. 2012 Fuel Cell Perfluorinated Sulfonic Acid Membrane Degradation Correlating Accelerated Stress Testing and Lifetime. *Chem. Rev.* **112**, 6075–6103. (doi:10.1021/cr200424d)

216. Yoon W, Huang X. 2010 Acceleration of Chemical Degradation of Perfluorosulfonic Acid Ionomer Membrane by Mechanical Stress: Experimental Evidence. *ECS Trans.* **33**, 907–911. (doi:10.1149/1.3484584)

217. Kusoglu A, Calabrese M, Weber AZ. 2014 Effect of Mechanical Compression on Chemical Degradation of Nafion Membranes. *ECS Electrochem. Lett.* **3**, F33–F36. (doi:10.1149/2.008405eel)

218. Lim C, Ghassemzadeh L, Van Hove F, Lauritzen M, Kolodziej J, Wang GG, Holdcroft S, Kjeang E. 2014 Membrane degradation during combined chemical and mechanical accelerated stress testing of polymer electrolyte fuel cells. *J. Power Sources* **257**, 102–110. (doi:10.1016/j.jpowsour.2014.01.106)

219. Mukundan R, Baker AM, Kusoglu A, Beattie P, Knights S, Weber AZ, Borup RL. 2018 Membrane Accelerated Stress Test Development for Polymer Electrolyte Fuel Cell Durability Validated Using Field and Drive Cycle Testing. *J. Electrochem. Soc.* **165**, F3085–F3093. (doi:10.1149/2.0101806jes)

220. Nitta I, Karvonen S, Himanen O, Mikkola M. 2008 Modelling the Effect of Inhomogeneous Compression of GDL on Local Transport Phenomena in a PEM Fuel Cell. *Fuel Cells* **8**, 410–421. (doi:10.1002/fuce.200700058)

221. Gittleman CS, Coms FD, Lai Y-H. 2012 Chapter 2 - Membrane Durability: Physical and Chemical Degradation. In *Polymer Electrolyte Fuel Cell Degradation* (eds MM Mench, EC Kumbur, TN Veziroglu), pp. 15–88. Boston: Academic Press. (doi:10.1016/B978-0-12-386936-4.10002-8)

222. Kim S, Ahn BK, Mench MM. 2008 Physical degradation of membrane electrode assemblies undergoing freeze/thaw cycling: Diffusion media effects. *J. Power Sources* **179**, 140–146. (doi:10.1016/j.jpowsour.2007.12.114)

223. Kusoglu A, Weber AZ. 2014 A Mechanistic Model for Pinhole Growth in Fuel-Cell Membranes during Cyclic Loads. *J. Electrochem. Soc.* **161**, E3311–E3322. (doi:10.1149/2.036408jes)

224. Moor GD *et al.* 2012 Understanding Membrane Failure in PEMFC: Comparison of Diagnostic Tools at Different Observation Scales. *Fuel Cells* **12**, 356–364. (doi:10.1002/fuce.201100161)

225. Shi S *et al.* 2020 Fatigue crack propagation behavior of fuel cell membranes after chemical degradation. *Int. J. Hydrog. Energy* , S0360319920326884. (doi:10.1016/j.ijhydene.2020.07.113)

226. Khattra NS, Lu Z, Karlsson AM, Santare MH, Busby FC, Schmiedel T. 2013 Time-dependent mechanical response of a composite PFSA membrane. *J. Power Sources* **228**, 256–269. (doi:10.1016/j.jpowsour.2012.11.116)

227. Kusoglu A, Karlsson AM, Santare MH, Cleghorn S, Johnson WB. 2007 Mechanical behavior of fuel cell membranes under humidity cycles and effect of swelling anisotropy on the fatigue stresses. *J. Power Sources* **170**, 345–358. (doi:10.1016/j.jpowsour.2007.03.063)

228. De Moor G, Bas C, Charvin N, Dillet J, Maranzana G, Lottin O, Caque N, Rossinot E, Flandin L. 2016 Perfluorosulfonic acid membrane degradation in the hydrogen inlet region: A macroscopic approach. *Int. J. Hydrog. Energy* **41**, 483–496. (doi:10.1016/j.ijhydene.2015.10.066)

229. Healy J, Hayden C, Xie T, Olson K, Waldo R, Brundage A, Gasteiger H, Abbott J. 2005 Aspects of the chemical degradation of PFSA ionomers used in PEM fuel cells. *Fuel Cells* **5**, 302–308. (doi:10.1002/fuce.200400050)

230. Huang X, Solasi R, Zou Y, Feshler M, Reifsnider K, Condit D, Burlatsky S, Madden T. 2006 Mechanical endurance of polymer electrolyte membrane and PEM fuel cell durability. *J. Polym. Sci. Part B Polym. Phys.* **44**, 2346–2357. (doi:10.1002/polb.20863)

231. Moukheiber E, Bas C, Flandin L. 2014 Understanding the formation of pinholes in PFSA membranes with the essential work of fracture (EWF). *Int. J. Hydrog. Energy* **39**, 2717–2723. (doi:10.1016/j.ijhydene.2013.03.031)

232. Jia R, Dong S, Hasegawa T, Ye J, Dauskardt RH. 2012 Contamination and moisture absorption effects on the mechanical properties of catalyst coated membranes in PEM fuel cells. *Int. J. Hydrog. Energy* **37**, 6790–6797. (doi:10.1016/j.ijhydene.2012.01.063)

233. Tang HL, Pan M, Wang F. 2008 A mechanical durability comparison of various perfluocarbon proton exchange membranes. *J. Appl. Polym. Sci.* **109**, 2671–2678. (doi:10.1002/app.28343)

234. Kusoglu A, Santare MH, Karlsson AM, Cleghorn S, Johnson WB. 2010 Numerical Investigation of Mechanical Durability in Polymer Electrolyte Membrane Fuel Cells. *J. Electrochem. Soc.* **157**, B705. (doi:10.1149/1.3328496)

235. Zhang Z, Shi S, Lin Q, Wang L, Liu Z, Li P, Chen X. 2018 Exploring the role of reinforcement in controlling fatigue crack propagation behavior of perfluorosulfonic-acid membranes. *Int. J. Hydrog. Energy* **43**, 6379–6389. (doi:10.1016/j.ijhydene.2018.02.034)

236. Qiu D, Peng L, Lai X, Ni M, Lehnert W. 2019 Mechanical failure and mitigation strategies for the membrane in a proton exchange membrane fuel cell. *Renew. Sustain. Energy Rev.* **113**, 109289. (doi:10.1016/j.rser.2019.109289)

237. Zatoń M, Rozière J, Jones DJ. 2017 Current understanding of chemical degradation mechanisms of perfluorosulfonic acid membranes and their mitigation strategies: a review. *Sustain. Energy Fuels* **1**, 409–438. (doi:10.1039/C7SE00038C)

238. LaConti AB, Hamdan M, McDonald RC. 2010 Mechanisms of membrane degradation. In *Handbook of Fuel Cells*, Hoboken, NJ (USA): John Wiley & Sons, Ltd. (doi:10.1002/9780470974001.f303055)

239. Danilczuk M, Coms FD, Schlick S. 2009 Visualizing Chemical Reactions and Crossover Processes in a Fuel Cell Inserted in the ESR Resonator: Detection by Spin Trapping of Oxygen Radicals, Nafion-Derived Fragments, and Hydrogen and Deuterium Atoms. *J. Phys. Chem. B* **113**, 8031–8042. (doi:10.1021/jp901597f)

240. Liu W, Zuckerbrod D. 2005 In Situ Detection of Hydrogen Peroxide in PEM Fuel Cells. *J. Electrochem. Soc.* **152**, A1165. (doi:10.1149/1.1904988)

241. Chen C, Fuller T. 2007 H2O2 Formation under Fuel-Cell Conditions. *ECS Trans.* **11**, 1127. (doi:10.1149/1.2781025)

242. Teranishi K, Tsushima S, Hirai S. 2006 Analysis of Water Transport in PEFCs by Magnetic Resonance Imaging Measurement. *J. Electrochem. Soc.* **153**, A664–A668. (doi:10.1149/1.2167954)

243. Inaba M, Kinumoto T, Kiriake M, Umebayashi R, Tasaka A, Ogumi Z. 2006 Gas crossover and membrane degradation in polymer electrolyte fuel cells. *Electrochimica Acta* **51**, 5746–5753. (doi:10.1016/j.electacta.2006.03.008)

244. Mittal V, Kunz R, Fenton J. 2006 H2O2 Formation Mechanism in PEMFC. *ECS Trans.* **1**, 295–301. (doi:10.1149/1.2214562)

245. Okada T. 2010 Effect of ionic contaminants. In *Handbook of Fuel Cells*, Hoboken, NJ (USA): John Wiley & Sons, Ltd. (doi:10.1002/9780470974001.f303054)

246. Ghassemzadeh L, Kreuer K-D, Maier J, Mueller K. 2010 Chemical Degradation of Nation Membranes under Mimic Fuel Cell Conditions as Investigated by Solid-State NMR Spectroscopy. *J. Phys. Chem. C* **114**, 14635–14645. (doi:10.1021/jp102533v)

247. Mittal VO, Kunz HR, Fenton JM. 2007 Membrane Degradation Mechanisms in PEMFCs. *J. Electrochem. Soc.* **154**, B652–B656. (doi:10.1149/1.2734869)

248. Panchenko A, Dilger H, Kerres J, Hein M, Ullrich A, Kaz T, Roduner E. 2004 In-situ spin trap electron paramagnetic resonance study of fuel cell processes. *Phys. Chem. Chem. Phys.* **6**, 2891–2894. (doi:10.1039/b404253k)

249. Lin L, Danilczuk M, Schlick S. 2013 Electron spin resonance study of chemical reactions and crossover processes in a fuel cell: Effect of membrane thickness. *J. Power Sources* **233**, 98–103. (doi:10.1016/j.jpowsour.2013.01.117)

250. Mittal VO, Kunz HR, Fenton JM. 2006 Effect of Catalyst Properties on Membrane Degradation Rate and the Underlying Degradation Mechanism in PEMFCs. *J. Electrochem. Soc.* **153**, A1755. (doi:10.1149/1.2219708)

251. Sethuraman VA, Weidner JW, Haug AT, Protsailo LV. 2008 Durability of Perfluorosulfonic Acid and Hydrocarbon Membranes: Effect of Humidity and Temperature. *J. Electrochem. Soc.* **155**, B119–B124. (doi:10.1149/1.2806798)

252. Zhao M *et al.* 2015 Influence of Membrane Thickness on Membrane Degradation and Platinum Agglomeration under Long-term Open Circuit Voltage Conditions. *Electrochimica Acta* **153**, 254–262. (doi:10.1016/j.electacta.2014.12.024)

253. Kinumoto T, Inaba M, Nakayama Y, Ogata K, Umebayashi R, Tasaka A, Iriyama Y, Abe T, Ogumi Z. 2006 Durability of perfluorinated ionomer membrane against hydrogen peroxide. *J. Power Sources* **158**, 1222–1228. (doi:10.1016/j.jpowsour.2005.10.043)

254. Holber M, Carlsson AH, Johansson P, Jörissen L, Jacobsson P. 2009 Raman Investigation of Degradation and Ageing Effects in Fuel Cell Membranes. *ECS Trans.* **25**, 807–811. (doi:10.1149/1.3210633)

255. Bas C, Flandin L, Danero A-S, Claude E, Rossinot E, Alberola ND. 2010 Changes in the Chemical Structure and Properties of a Perfluorosulfonated Acid Membrane Induced by Fuel-Cell Operation. *J. Appl. Polym. Sci.* **117**, 2121–2132. (doi:10.1002/app.31386)

256. Luo Z, Li D, Tang HL, Pan M, Ruan R. 2006 Degradation behavior of membrane-electrode-assembly materials in 10-cell PEMFC stack. *Int. J. Hydrog. Energy* **31**, 1831–1837. (doi:10.1016/j.ijhydene.2006.02.029)

257. Endoh E, Hommura S, Terazono S, Widjaja H, Anzai J. 2007 Degradation Mechanism of the PFSA Membrane and Influence of Deposited Pt in the Membrane. *ECS Trans.* **11**, 1083–1091. (doi:10.1149/1.2781021)

258. Danilczuk M, Lancucki L, Schlick S, Hamrock SJ, Haugen GM. 2012 In-Depth Profiling of Degradation Processes in a Fuel Cell: 2D Spectral-Spatial FTIR Spectra of Nafion Membranes. *ACS Macro Lett.* **1**, 280–285. (doi:10.1021/mz200100s)

259. Ohma A, Yamamoto S, Shinohara K. 2007 Analysis of Membrane Degradation Behavior During OCV Hold Test. *ECS Trans.* **11**, 1181–1192. (doi:10.1149/1.2781032)

260. Zhao D, Yi BL, Zhang HM, Liu M. 2010 The effect of platinum in a Nafion membrane on the durability of the membrane under fuel cell conditions. *J. Power Sources* **195**, 4606–4612. (doi:10.1016/j.jpowsour.2010.02.043)

261. Macauley N, Wong KH, Watson M, Kjeang E. 2015 Favorable effect of in-situ generated platinum in the membrane on fuel cell membrane durability. *J. Power Sources* **299**, 139–148. (doi:10.1016/j.jpowsour.2015.08.096)

262. Gummalla M, Atrazhev VV, Condit D, Cipollini N, Madden T, Kuzminyh NY, Weiss D, Burlatsky SF. 2010 Degradation of Polymer-Electrolyte Membranes in Fuel Cells: II. Theoretical model. *J. Electrochem. Soc.* **157**, B1542. (doi:10.1149/1.3481450)

263. Peron J, Jones D, Roziere J. 2007 Migration of Platinum Under Open Cell Voltage: Effect of the Type of Ionomer Membrane. *ECS Trans.* **11**, 1313. (doi:10.1149/1.2781044)

264. Kadirov MK, Bosnjakovic A, Schlick S. 2005 Membrane-derived fluorinated radicals detected by electron spin resonance in UV-irradiated nafion and dow ionomers: Effect of counterions and H2O2. *J. Phys. Chem. B* **109**, 7664–7670. (doi:10.1021/jp044987t)

265. Uegaki R, Akiyama Y, Tojo S, Honda Y, Nishijima S. 2011 Radical-induced degradation mechanism of perfluorinated polymer electrolyte membrane. *J. Power Sources* **196**, 9856–9861. (doi:10.1016/j.jpowsour.2011.08.006)

266. Ghassemzadeh L, Peckham TJ, Weissbach T, Luo X, Holdcroft S. 2013 Selective Formation of Hydrogen and Hydroxyl Radicals by Electron Beam Irradiation and Their Reactivity with Perfluorosulfonated Acid Ionomer. *J. Am. Chem. Soc.* **135**, 15923–15932. (doi:10.1021/ja408032p)

267. Hommura S, Kawahara K, Shimohira T, Teraoka Y. 2008 Development of a Method for Clarifying the Perfluorosulfonated Membrane Degradation Mechanism in a Fuel Cell Environment. *J. Electrochem. Soc.* **155**, A29–A33. (doi:10.1149/1.2800171)

268. Carlsson AH, Joerissen L. 2009 Accelerated Degradation of Perfluorinated Sulfonic Acid Membranes. *ECS Trans.* **25**, 725–732. (doi:10.1149/1.3210624)

269. Delaney WE, Liu W. 2007 Use of FTIR to Analyze Ex-Situ and In-Situ Degradation of Perfluorinated Fuel Cell Ionomers. *ECS Trans.* **11**, 1093–1104. (doi:10.1149/1.2781022)

270. Tang H, Peikang S, Jiang SP, Wang F, Pan M. 2007 A degradation study of Nafion proton exchange membrane of PEM fuel cells. *J. Power Sources* **170**, 85–92. (doi:10.1016/j.jpowsour.2007.03.061)

271. Wang F, Tang H, Pan M, Li D. 2008 Ex situ investigation of the proton exchange membrane chemical decomposition. *Int. J. Hydrog. Energy* **33**, 2283–2288. (doi:10.1016/j.ijhydene.2008.01.052)

272. Ghassemzadeh L, Kreuer KD, Maier J, Mueller K. 2011 Evaluating chemical degradation of proton conducting perfluorosulfonic acid ionomers in a Fenton test by solid-state F-19 NMR spectroscopy. *J. Power Sources* **196**, 2490–2497. (doi:10.1016/j.jpowsour.2010.11.053)

273. Mu S, Xu C, Yuan Q, Gao Y, Xu F, Zhao P. 2013 Degradation behaviors of perfluorosulfonic acid polymer electrolyte membranes for polymer electrolyte membrane fuel cells under varied acceleration conditions. *J. Appl. Polym. Sci.* **129**, 1586–1592. (doi:10.1002/app.38785)

274. Kundu S, Simon LC, Fowler MW. 2008 Comparison of two accelerated Nafion™ degradation experiments. *Polym. Degrad. Stab.* **93**, 214–224. (doi:10.1016/j.polymdegradstab.2007.10.001)

275. Chen C, Levitin G, Hess DW, Fuller TF. 2007 XPS investigation of Nafion® membrane degradation. *J. Power Sources* **169**, 288–295. (doi:10.1016/j.jpowsour.2007.03.037)

276. Zhou C, Guerra MA, Qiu Z-M, Zawodzinski Thomas A, Schiraldi DA. 2007 Chemical Durability Studies of Perfluorinated Sulfonic Acid Polymers and Model Compounds under Mimic Fuel Cell Conditions. *Macromolecules* **40**, 8695–8707. (doi:10.1021/ma071603z)

277. Qiao JL, Saito M, Hayamizu K, Okada T. 2006 Degradation of perfluorinated ionomer membranes for PEM fuel cells during processing with H2O2. *J. Electrochem. Soc.* **153**, A967–A974. (doi:10.1149/1.2186768)

278. Fernandes AC, Ticianelli EA. 2009 A performance and degradation study of Nafion 212 membrane for proton exchange membrane fuel cells. *J. Power Sources* **193**, 547–554. (doi:10.1016/j.jpowsour.2009.04.038)

279. Luo X, Ghassemzadeh L, Holdcroft S. 2015 Effect of free radical-induced degradation on water permeation through PFSA ionomer membranes. *Int. J. Hydrog. Energy* **40**, 16714–16723. (doi:10.1016/j.ijhydene.2015.07.118)

280. Hongsirikarn K, Mo X, Goodwin JG, Creager S. 2011 Effect of H2O2 on Nafion® properties and conductivity at fuel cell conditions. *J. Power Sources* **196**, 3060–3072. (doi:10.1016/j.jpowsour.2010.11.133)

281. Sun X, Shi S, Fu Y, Chen J, Lin Q, Hu J, Li C, Li J, Chen X. 2020 Embrittlement induced fracture behavior and mechanisms of perfluorosulfonic-acid membranes after chemical degradation. *J. Power Sources* **453**, 227893. (doi:10.1016/j.jpowsour.2020.227893)

282. Gubler L, Kuhn H, Schmidt TJ, Scherer GG, Brack H-P, Simbeck K. 2004 Performance and Durability of Membrane Electrode Assemblies Based on Radiation-Grafted FEP-g-Polystyrene Membranes. *Fuel Cells* **4**, 196–207. (doi:10.1002/fuce.200400019)

283. Cipollini NE. 2007 Chemical Aspects of Membrane Degradation. *ECS Trans.* **11**, 1071. (doi:10.1149/1.2781020)

284. Coms FD. 2008 The Chemistry of Fuel Cell Membrane Chemical Degradation. *ECS Trans.* **16**, 235–255. (doi:10.1149/1.2981859)

285. Bosnjakovic A, Kadirov MK, Schlick S. 2007 Using ESR spectroscopy to study radical intermediates in proton-exchange membranes exposed to oxygen radicals. *Res. Chem. Intermed.* **33**, 677–687. (doi:10.1163/156856707782169372)

286. Dreizler AM, Roduner E. 2012 Reaction Kinetics of Hydroxyl Radicals with Model Compounds of Fuel Cell Polymer Membranes. *Fuel Cells* **12**, 132–140. (doi:10.1002/fuce.201100157)

287. Ghassemzadeh L, Holdcroft S. 2013 Quantifying the Structural Changes of Perfluorosulfonated Acid Ionomer upon Reaction with Hydroxyl Radicals. *J. Am. Chem. Soc.* **135**, 8181–8184. (doi:10.1021/ja4037466)

288. Danilczuk M, Perkowski AJ, Schlick S. 2010 Ranking the Stability of Perfluorinated Membranes Used in Fuel Cells to Attack by Hydroxyl Radicals and the Effect of Ce(III): A Competitive Kinetics Approach Based on Spin Trapping ESR. *Macromolecules* **43**, 3352–3358. (doi:10.1021/ma1001386)

289. Gubler L, Dockheer SM, Koppenol WH. 2011 Radical (HO•, H• and HOO•) Formation and Ionomer Degradation in Polymer Electrolyte Fuel Cells. *J. Electrochem. Soc.* **158**, B755–B769. (doi:10.1149/1.3581040)

290. Coms FD, Liu H, Owejan JE. 2008 Mitigation of Perfluorosulfonic Acid Membrane Chemical Degradation Using Cerium and Manganese Ions. *ECS Trans.* **16**, 1735–1747. (doi:10.1149/1.2982015)

291. Endoh E. 2010 Highly durable PFSA membranes. In *Handbook of Fuel Cells*, Hoboken, NJ (USA): John Wiley & Sons, Ltd. (doi:10.1002/9780470974001.f500026)

292. Trogadas P, Parrondo J, Ramani V. 2008 Degradation Mitigation in Polymer Electrolyte Membranes Using Cerium Oxide as a Regenerative Free-Radical Scavenger. *Electrochem. Solid State Lett.* **11**, B113. (doi:10.1149/1.2916443)

293. Pearman BP, Mohajeri N, Brooker RP, Rodgers MP, Slattery DK, Hampton MD, Cullen DA, Seal S. 2013 The degradation mitigation effect of cerium oxide in polymer electrolyte membranes in extended fuel cell durability tests. *J. Power Sources* **225**, 75–83. (doi:10.1016/j.jpowsour.2012.10.015)

294. Lim C, Alavijeh AS, Lauritzen M, Kolodziej J, Knights S, Kjeang E. 2015 Fuel Cell Durability Enhancement with Cerium Oxide under Combined Chemical and Mechanical Membrane Degradation. *ECS Electrochem. Lett.* **4**, F29–F31. (doi:10.1149/2.0081504eel)

295. Zhao D, Yi BL, Zhang HM, Yu HM. 2010 MnO2/SiO2–SO3H nanocomposite as hydrogen peroxide scavenger for durability improvement in proton exchange membranes. *J. Membr. Sci.* **346**, 143–151. (doi:10.1016/j.memsci.2009.09.031)

296. D'Urso C, Oldani C, Baglio V, Merlo L, Aricò AS. 2014 Towards fuel cell membranes with improved lifetime: Aquivion® Perfluorosulfonic Acid membranes containing immobilized radical scavengers. *J. Power Sources* **272**, 753–758. (doi:10.1016/j.jpowsour.2014.09.045)

297. Schlick S. 2017 *The Chemistry of Membranes Used in Fuel Cells: Degradation and Stabilization*. First. Hoboken, NJ (USA): John Wiley & Sons.

298. Wong KH, Kjeang E. 2017 In-Situ Modeling of Chemical Membrane Degradation and Mitigation in Ceria-Supported Fuel Cells. *J. Electrochem. Soc.* **164**, F1179. (doi:10.1149/2.1201712jes)

299. D'Urso C, Oldani C, Baglio V, Merlo L, Aricò AS. 2016 Immobilized transition metal-based radical scavengers and their effect on durability of Aquivion® perfluorosulfonic acid membranes. *J. Power Sources* **301**, 317–325. (doi:10.1016/j.jpowsour.2015.10.019)

300. D'Urso C, Oldani C, Baglio V, Merlo L, Aricò AS. 2017 Fuel cell performance and durability investigation of bimetallic radical scavengers in Aquivion® perfluorosulfonic acid membranes. *Int. J. Hydrog. Energy* **42**, 27987–27994. (doi:10.1016/j.ijhydene.2017.07.111)

301. Trogadas P, Parrondo J, Mijangos F, Ramani V. 2011 Degradation mitigation in PEM fuel cells using metal nanoparticle additives. *J. Mater. Chem.* **21**, 19381–19388. (doi:10.1039/C1JM14077A)

302. Trogadas P, Parrondo J, Ramani V. 2011 Platinum supported on CeO2 effectively scavenges free radicals within the electrolyte of an operating fuel cell. *Chem. Commun.* **47**, 11549–11551. (doi:10.1039/C1CC15155J)

303. Venkatesan S velan, Lim C, Holdcroft S, Kjeang E. 2016 Progression in the Morphology of Fuel Cell Membranes upon Conjoint Chemical and Mechanical Degradation. *J. Electrochem. Soc.* **163**, F637–F643. (doi:10.1149/2.0671607jes)

304. Ehlinger VM, Kusoglu A, Weber AZ. 2019 Modeling Coupled Durability and Performance in Polymer-Electrolyte Fuel Cells: Membrane Effects. *J. Electrochem. Soc.* **166**, F3255–F3267. (doi:10.1149/2.0281907jes)

305. Kusoglu A, Weber AZ. 2015 Electrochemical/Mechanical Coupling in Ion-Conducting Soft Matter. *J. Phys. Chem. Lett.* **6**, 4547–4552. (doi:10.1021/acs.jpclett.5b01639)

306. Kundu S, Fowler MW, Simon LC, Grot S. 2006 Morphological features (defects) in fuel cell membrane electrode assemblies. *J. Power Sources* **157**, 650–656. (doi:10.1016/j.jpowsour.2005.12.027)

307. Alavijeh AS, Goulet M-A, Khorasany RMH, Ghataurah J, Lim C, Lauritzen M, Kjeang E, Wang GG, Rajapakse RKND. 2015 Decay in Mechanical Properties of Catalyst Coated Membranes Subjected to Combined Chemical and Mechanical Membrane Degradation. *Fuel Cells* **15**, 204–213. (doi:10.1002/fuce.201400040)

Chapter II

Experimental techniques

Table of contents

This chapter aims at describing the experimental techniques employed in this work to characterize the impact of the degradation on the structure and the functional properties of Nafion™ membranes. The commercial Nafion™ membranes studied in this work and their main features as well as the pretreatment and cleaning protocols are fully described in chapter III.

1. Chemical and electrochemical characterizations

1.1.Fluoride emissions measurement *via* ion-selective electrode (ISE)

The fluoride ions concentration of the solutions was estimated by using a fluoride ion-selective half-cell electrode (DX219, Mettler Toledo) associated to a reference electrode (InLab Reference, Mettler Toledo) and a pH/millivolt meter (SevenCompact S220, Mettler Toledo). The measurement consists in studying the potential variation of the ion-selective electrode as a function of the ionic activity of the measured species. In addition to ensuring a good repeatability, the main benefit of the potentiometric method is the possibility to analyze complex solutions that are unclear, cloudy, colored or fluorescent and/or contain various chemical elements. In the case of fluorine ions, the ion-selective electrode is a crystalline membrane electrode made of a single lanthanum trifluoride (LaF_3) crystal doped with europium. The potential of the LaF_3 crystalline membrane electrode E is given by the following relation [1]:

$$E = E^0 - 2{,}3\frac{RT}{F}\log_{10} a_F \qquad \textbf{Eq. 2.1}$$

With E^0 the standard potential (V), R the ideal gas constant equal to 8.314 $J.K^{-1}.mol^{-1}$, T the temperature (K), F the Faraday constant equal to 96 485 $C.mol^{-1}$ and a_F the fluoride ion activity.

After the experiments, the remaining Fenton solutions constitute a complex solution containing residual hydrogen peroxide, ferrous and ferric ions that have not reacted, and – if degradation occurs – dissolved hydrofluoric acid (HF) or fluoride ions as well as other degradation products coming from PFSA decomposition. In addition, fluoride ions having a great affinity for silica-based materials, all the solutions collected after the *ex-situ* aging tests were preferentially stored in polyethylene vessels rather than glass vessels. Prior to the analysis of the solutions *via* the ion-selective electrode, the residual hydrogen peroxide has to be deactivated in order to avoid detrimental material damages. For that purpose, a small piece of platinum was added to the solution which was then stored until complete H_2O_2 disproportionation. Moreover, it is important to note that the solutions containing a solid fraction of precipitate were filtered using syringe filters composed of a polypropylene membrane with a pore size of 0.2 µm before being analyzed.

In the case of complex solutions such as Fenton solutions, it is necessary to stabilize the ionic force of the analyzed species to obtain a linear response of the electrode in the whole range of concentration. It also requires to stabilize the pH of the solution within the measuring range of the electrode and to suppress the interferences caused by other ionic species. In our case, the only ionic specie which could interfere is the hydroxide ion and the pH range of our fluoride selective electrode extends from 4 to 10. Therefore, in order to control at the same time the ionic force, the pH and interfering ions, a Total Ionic Strength Adjustment Buffer (TISAB) was added to the solution to analyze. The commercial TISAB II solution is a buffer solution containing sodium acetate, sodium chloride, acetic acid, cyclohexanediaminetetraacetic acid (CDTA) able to stabilize the pH between 5 and 6, to enhance the ionic force of the fluoride ions and to complex cations such as Fe^{3+} to avoid interferences. In our case, 25 mL of TISAB II were systematically added to 25 mL of the Fenton solutions to sufficiently stabilize the solution without diluting it too much.

The electrode has to be calibrated prior to each measurement campaign. Before calibration, the selective electrode was conditioned through immersion in a 1000 ppm ISE fluoride standard solution for at least one hour and was then thoroughly rinsed with distilled water. For the electrode calibration, several solutions of known concentration were prepared by successive dilutions of the 1000 ppm ISE standard solution to cover a broad range of fluoride concentrations (from 0.057 ppm to 19 ppm). A TISAB II solution was added to each calibration solutions with a volume ratio of 1:1 to replicate the same conditions as those used for the analyzed solution. It is important to note here that even though the dilution was carried out using glass container, the resulting solutions were rapidly transferred into polyethylene vessels to avoid an eventual migration of fluoride ions in the glassware. We considered that the preparation duration was short enough to ensure perfectly reliable fluoride concentrations. The calibration curve was established beginning with the most diluted solutions to avoid saturation of the electrode and its slope had to be close to -0.057 V/10 ppm with a tolerance of 5 %.

According to the supplier, the detection limit of the fluoride ion-selective electrode is about 0.01 ppm. However, in the case of membrane electrode, the electrode response deviates from the calibration curve when the concentration of the calibration solutions is very low and two areas can be distinguished: a linear area corresponding to a Nernstian response and a non-linear area corresponding to the non-Nernstian response for very low concentrations (typically below to 0.1 ppm), as can be seen in Figure 2.1. In the non-linear area, the response time of the

electrode ranged between thirty minutes and one hour before the potential value could be considered stable.

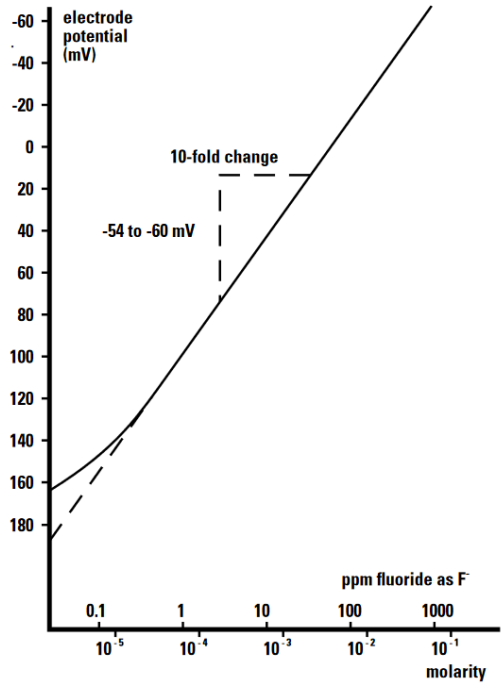

Figure 2.1 – Typical calibration curve of fluoride ion-selective electrode [2]

The fluoride concentration was determined using the standard addition method, which allows to consider complex matrices and more particularly the presence of possible other ions interfering with the electrode. To perform the measurement, we first determined the initial potential E_i of the solution and then the final potential E_f of the solution after the addition of a calibration solution (5 mL) with the closest upper potential to E_i. For each solution, E_i and E_f were measured allowing sufficient equilibration time for complete stabilization of the potential.

Thanks to equation 2.1, the initial potential E_i measured before the addition of the calibration solution is given by:

$$E_i = E^0 - 2{,}3\frac{RT}{F}\log_{10} a_F = E^0 - s \times \log_{10}[F^-] = E^0 - s \times \log_{10}\left(\frac{C_x^{tot} \times V_x}{V_x + V_{t1}}\right) \quad \textbf{Eq. 2.2}$$

Where C_x^{tot} is the fluoride concentration in the probed solution (mol.L^{-1}), V_x its volume, V_{t1} the volume of added TISAB II and s the slope of the calibration curve established before each measurement campaign. Parameter s is expected to be equal to $2{,}3\frac{RT}{F} \approx 0.057\ V/10\ ppm$ at room temperature (25 °C) according to the supplier data.

In the same manner, the final potential E_f measured after the addition of the calibration solution is given by:

$$E_f = E^0 - s \times \log_{10}[F^-] = E^0 - s \times \log_{10}\left(\frac{C_x^{tot} \times V_x + C_e \times V_e}{V_x + V_{t1} + V_e}\right) \quad \textbf{Eq. 2.3}$$

Where C_e is the fluoride concentration in the added calibration solution (mol.L^{-1}) and V_e its volume.

Therefore, the fluoride concentration in the probed solution C_x^{tot} was obtained by combining equations 2.2 and 2.3:

$$C_x^{tot} = \frac{C_e}{\left(\frac{V_x}{v_e}\right)\left(\times 10^{\frac{-(E_f - E_i)}{s}} \times \frac{(V_x + V_{t1} + V_e)}{(V_x + V_{t1})} - 1\right)} = C_e \times Q \quad \textbf{Eq. 2.4}$$

To systematize the measurement and avoid calculation errors, the parameter Q, which takes into account all the fixed solution volumes involved in the system and therefore only depends on the potential difference $E_f - E_i$ and the slope of the calibration curve, is introduced in equation 2.4. Furthermore, it is important to note that Q considers the fluorine concentration in the whole probed solution volume, *i.e.* the dilution of the solution to analyze generated by adding TISAB II solution is not taken into account.

Thus, the concentration of fluoride ions in the solution to analyze C_x^{ini} is expressed as a function of the concentration C_e of the added calibration solution, the dilution factor f (equal to 2 in this study) and Q, as followed:

$$C_x^{tot} = C_x^{ini} \times f = C_e \times Q \times f \quad \textbf{Eq. 2.5}$$

As mentioned earlier, parameter Q only allows to calculate the concentration in the whole volume of probed solution (50 mL) and does not consider the addition of TISAB II into the solution to be analyzed (25 mL). In that respect, it was necessary to introduce the dilution factor f in the final equation to determine the concentration of fluoride ions present in solution of interest.

The error on fluoride ion concentration was estimated to be on the order of 5 %, the main source of error being the preparation and dilution of calibration solutions. The total amount of

fluoride released during the degradation experiments was determined from the measured fluoride concentration and the volume of solution collected after the degradation experiments.

1.2.ATR-FTIR spectroscopy

Fourier-Transform InfraRed spectroscopy (FTIR) is a commonly used technique to characterize the chemical structure of organic materials. The FTIR spectroscopy is a vibrational spectroscopy based on the absorption of an infrared radiation. In each molecule, the chemical bonds vibrate with a specific frequency depending on the nature of the atoms involved in the bond and chemical environment of the bonding. These vibrations can be of different kind: asymmetric/symmetric stretching, bending, rocking, twisting, or wagging. The frequency at which the chemical bonds vibrate as well as the shape of vibration bands of a spectrum are characteristic of the functional groups. Therefore, each compound will have its own IR absorption spectral signature.

In the context of this work, FTIR spectroscopy was used to characterize the evolution of the ionomer chemical structure as a function of the chemical degradation induced to the Nafion™ membranes. As both reinforced and non-reinforced Nafion™ membranes were studied, all measurements were performed with an attenuated total reflectance (ATR) accessory in order to analyze exclusively the membrane surface and thus exclude the microporous polytetrafluoroethylene (PTFE) layer of reinforced XL membranes. Infrared spectra were obtained using a FTIR spectrometer (Vertex 80v, Bruker) equipped with a DTGS detector, a KBr beam splitter and a single reflection diamond ATR accessory. The spectra were recorded at room temperature with accumulation of 16 scans and a wavenumber resolution of 1 cm^{-1} from 400 to 6000 cm^{-1} in absorption mode.

Commercial Nafion™ membranes were systematically dried at 60 °C for 24 h prior to any degradation protocol. Numerous works have highlighted that IR spectra of a Nafion™ membrane are greatly influenced by its water content [3–10]. Consequently, a drying protocol were elaborated to dry the membrane samples and perform analysis in the same conditions for all measurements and samples. In that respect, the membrane samples were first dried at least overnight in an oven at 60°C before being placed on ATR accessory and then exposed to a dry nitrogen flow (99.9999 % of purity) with a 1 NL/min flow rate for 10 minutes just before the measurement. More details on the establishment of the membrane drying protocol for ATR-FTIR measurements can be found in § 1 of Appendix A. Figure 2.2 illustrates ATR-FTIR

spectra of a Nafion™ XL membrane exposed to the ambient air and exposed to the nitrogen flow under the conditions described above.

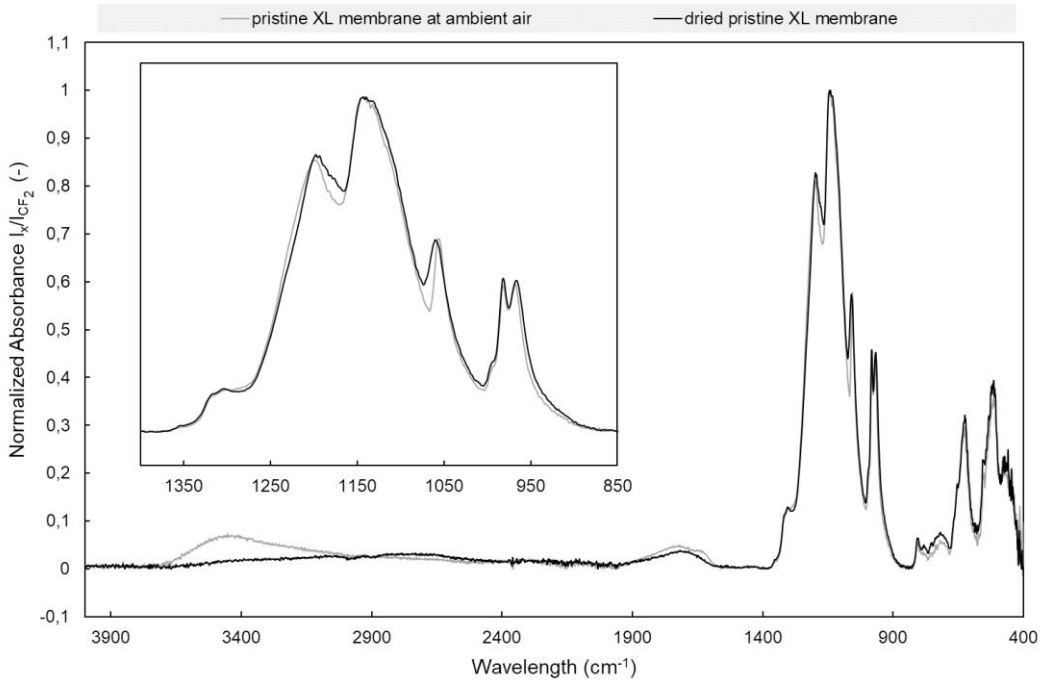

Figure 2.2 – ATR-FTIR spectra of Nafion™ XL membrane before and after the drying protocol. The inset illustrates the IR spectra focused on PFSA absorption bands.

The measurements were performed at various locations on the surface of the membrane samples and on both sides to check the homogeneity of the chemical structure for pristine membranes and to investigate aging heterogeneities for aged samples.

In ATR mode, the penetration depth of infrared radiation, d_p, into the sample primarily depends on three parameters according to the following equation:

$$d_p = \frac{\lambda}{2\pi n_c \sqrt{\sin^2\theta - \left(\frac{n_s}{n_c}\right)^2}} \qquad \textbf{Eq. 2.6}$$

where λ is the laser wavelength, n_c the refractive index of ATR crystal and n_s the refractive index of the sample. In our case, ATR crystal is a diamond with a refractive index of 2.41 and an angle of incidence θ of about 45°. The refractive index of Nafion™ membranes is 1.35 in the dry state [11]. Therefore, the penetration depth ranges from 0.17 to 2.58 µm for our wavelength range.

1.3.NMR spectroscopy

Nuclear Magnetic Resonance (NMR) spectroscopy is a characterization technique based on the nuclear magnetic moment of atomic nuclei. When exposed to an external magnetic field, the nuclear magnetic moments of the analyzed sample align with the external magnetic field (*i.e.* that of the NMR spectrometer). Atomic nuclei are then excited by applying a radio-frequency pulse perpendicular to the external magnetic field at a specific frequency, the Larmor frequency, in order to collect information about the chemical environment of each atomic nucleus contained in the sample. The resulting NMR spectrum presents various resonance peaks at different frequencies characteristics of the chemical environment surrounding each atomic nucleus. Consequently, the difference from the resonance frequency defines the chemical shift. For instance, the frequency of an atomic nucleus depends on the nature and the number of neighboring atoms as well as on the chemical bond involved between the nuclei. Any change in the chemical shift, width or intensity of the resonance peaks in the spectra is representative of chemical modification in the sample. Consequently, NMR spectroscopy is a powerful technique to characterize chemical structures.

In this work, two atomic nuclei were studied: fluorine and proton. ^{19}F-NMR spectroscopy in solid phase allowed us to investigate the evolution of PFSA chemical structure in Nafion™ membranes while the liquid-state ^{19}F-NMR spectroscopy was used to identify and quantify degradation products in the solutions collected after degradation tests. On the other hand, analyzes performed by liquid-state ^{1}H-NMR spectroscopy aimed at studying the diffusion of water molecules absorbed in the polymer structure of Nafion™ membranes. This latter technique and the associated experimental protocol will be described in § 2.1.

1.3.1. Solid-state ^{19}F-NMR

In liquids, anisotropic interactions between molecules are averaged and are negligible since Brownian motions generate extremely fast molecules reorientations. In solids, however, anisotropic interactions exist and the molecular motions are not fully averaged. These anisotropic interactions can be intense and thus have to be minimized. In that respect, solid-state NMR spectra are acquired by rotating the sample around a tilted axis of 54.7° with respect to the magnetic field in order to isotropically average the interactions. This angle is called “magic angle” and the associated method is commonly called “magic angle spinning” (MAS).

In this work, solid-state ^{19}F-NMR experiments were performed thanks to a collaboration with the Membrane Biophysics and NMR team in the Chemical Institute of Strasbourg. A Bruker Avance 500 wide-bore spectrometer operating at the Larmor frequency of 470.5 MHz and

equipped with a H/F/X magic-angle spinning (MAS) probe was used. The samples were rolled and loaded into 2.5 mm zirconia thin walls rotors with Vespel bottom and drive caps. All spectra were measured with a Hahn-echo pulse sequence at 24 °C under MAS conditions with a spinning frequency of 25 kHz. Each experiment was performed with the following parameters: a 90° pulse width of 1.25 µs, a recycle delay of 10 s, a dwell time of 2.5 µs and a number of accumulations of 64 scans. Figure 2.3 illustrates the characteristic ^{19}F-NMR spectra of a Nafion™ NR211 membrane as well as the resonance peaks attribution and peak areas prediction according to Chen and Schmidt-Rohr [12].

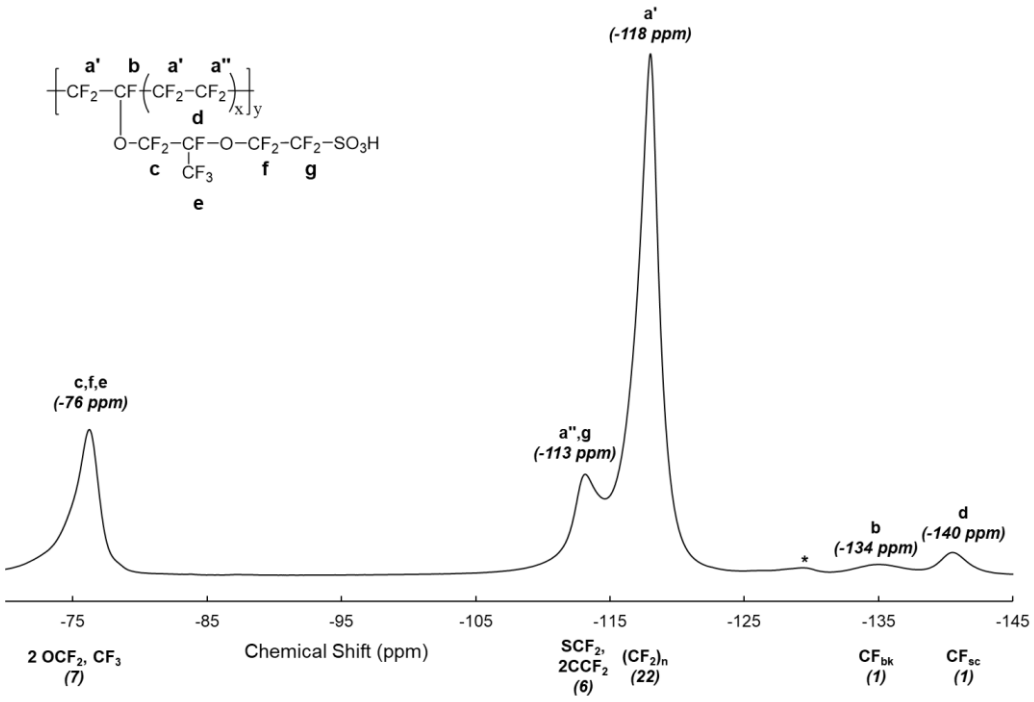

Figure 2.3 – solid-state ^{19}F-NMR spectra attribution for Nafion™ NR211 membrane and the corresponding peak areas predicted by Chen and Schmidt-Rohr [12]. The resonance peak with an asterisk designates a spinning sideband.

It is important to notice that in the case of Nafion™ XL membrane, which contains a PTFE-rich reinforcement layer, the resonance peak at -118 ppm corresponds at the same time to CF_2 groups of PFSA backbone and CF_2 groups of PTFE layer.

1.3.2. Liquid-state ^{19}F-NMR

The analysis of the solutions collected after degradation tests by ^{19}F-NMR spectroscopy is based on a three-step process [13]: **1)** the detection/identification of degradation products, **2)** the estimation of the orders of magnitude of the degradation products concentration, **3)** accurate quantification of the degradation products concentration.

In order to decrease the acquisition time per experiment as well as to enhance the NMR signal quality, the resulting solutions in which Nafion™ membranes have been exposed were concentrated prior to NMR analysis by evaporating the maximum amount of water thanks to a rotary evaporator (Rotavapor R-100, Büchi). Concentrated Fenton solution samples were then put into 5 mm NMR tubes and mixed with deuterium oxide (D_2O) for a final D_2O/H_2O ratio of 20:80 to provide a lock solvent and to prevent an eventual drift of the magnetic field.

Liquid-state ^{19}F-NMR experiments were conducted at the NMR plaform of Jean Barriol Institute (IJB) in Nancy on a Bruker Avance III 400 spectrometer operating at the Larmor frequency of 376.5 MHz and using a 5 mm BBFO probe. Both qualitative and quantitative NMR experiments were performed in this study. Qualitative experiments were carried out at room temperature with the following parameters: a 90° pulse width of 13.5 µs, a spectral width of 200 ppm, a recycle delay of 1 s and an acquisition time of 0.87 s. The ^{19}F-NMR spectra were obtained thanks to conventional single pulse experiments with a number of accumulations between 2048 and 30720 for qualitative measurements.

Quantification by ^{19}F-NMR was based on a protocol recently established by El Kaddouri *et al.* [13]. Their work consisted in investigating PFSA aqueous solutions to propose a new and efficient two-step ^{19}F-NMR quantification protocol to measure the fluorinated molecules concentration of unknown solutions. The first step consists in estimating the order of magnitude of fluorine concentration using the signal to noise ratio, which is conventionally defined as the ratio between a resonance peak height and the noise amplitude. The second step consists in using an external reference with a concentration inthe order of magnitude determined in the first step to evaluate more precisely the fluorine concentration. This two-step method was essential for our study due to the low concentration of decomposition products in the Fenton solutions in order to avoid time-consuming measurements. Following the same quantification protocol as described by El Kaddouri *et al.* [13], the concentration of decomposition products in Fenton solutions was first estimated by measuring the (S/N) ratio with the "SINO function" integrated into the TopSpin 3.5 software. The use of an external reference of trifluorotoluene (TFT) solution with an appropriate concentration permitted then to determine more accurately the fluorine concentration. The TFT solution was placed in a coaxial insert inside the 5 mm NMR tube. The choice of TFT as the external reference was motivated by its liquid state at room temperature, facilitating the practicability of the experiments, and its chemical shift not overlapping that of assumed degradation products present in the solution. This two-step method was systematically carried out in the same conditions for each Fenton solution sample. The

experiments were performed at room temperature with a 90° pulse width of 13.5 µs, a spectral width of 200 ppm, and between 12000 and 16384 accumulations. For accurate quantitative NMR experiments, the recycle delay should be at least five times higher than the relaxation time T_1 of the target molecule. The relaxation time of Nafion™ ionomer solutions was determined by Yuan *et al.* [14] to be 0.92 ± 0.05 s and that of TFT was determined by El Kaddouri *et al.* [13] to be 1.5 ± 0.1 s. Consequently, the recycle delay was fixed to 8 s for all quantitative NMR experiments.

2. Characterization of membrane functional properties

2.1.Liquid-state ^{1}H-NMR

The liquid-state ^{1}H-NMR experiments were performed on a Bruker Avance III 600 WB spectrometer with a Larmor frequency of 600.13 MHz and equipped with a 5 mm Diff30 probe capable of delivering a gradient intensity up to 1800 G/cm. The spectra were recorded at room temperature by accumulating 256 scans with the following parameters: a recycle delay of 3 s and a dwell time of 25 µs. An optimization of the proton 90° pulse width was carried out for each sample before recording the ^{1}H-NMR spectra to have suitable spin-echo during the measurement. Figure 2.4 illustrates the typical ^{1}H-NMR spectrum of water molecules contained in a pristine Nafion™ XL membrane at high hydration level (~23.5 wt.%). Two resonance peaks are visible in the spectrum corresponding to two different water populations, *i.e.* water molecules with different chemical environments.

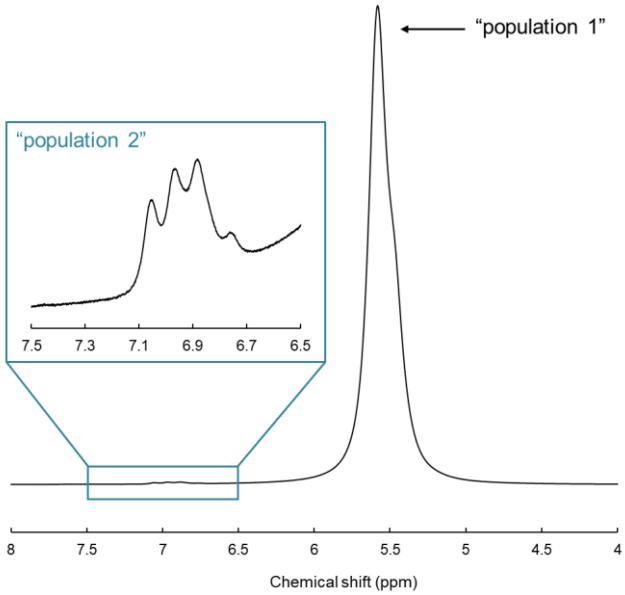

Figure 2.4 – ^{1}H NMR spectrum of the water populations present in a pristine Nafion™ XL membrane.

The existence of two water populations has been already put forward thanks to NMR experiments performed on reinforced Nafion™ XL and Gore-800s membranes [15,16]. It has been suggested that a first water population can be attributed to water molecules strongly bonded to sulfonic groups close to the ionomer pores. The second water population, for its part, could be assigned either to a small amount of water molecules which are tightly bonded at the interface between the ionomer phase and the PTFE-rich reinforcement layer or to water molecules present in void spaces of the PTFE matrix that have not be completely filled with ionomer phase during the manufacturing process. However, these two water populations are present in both reinforced (Nafion™ XL, Gore-800S) and non-reinforced (NR211) membranes which raises questions about the assumptions made to date [17]. More recently, Han *et al.* observed the appearance of a triplet – similar to that shown in Figure 2.4 – on ^{1}H-NMR spectrum and proposed that it could be related to hydronium ions (H_3O^+) [17]. In the case of this thesis work, the second water population was observed both for XL and NR211 membranes, whether membranes are degraded or not. Additionally, as it can be seen in Figure 2.4, the resonance peak associated to the "population 1" is very intense and well resolved while the other ("population 2") has a very low intensity and is partly overlapped with the main peak. It is important to note that these second resonance peak can be largely overlapped with the main peak in certain hydration conditions, making it difficult to follow the evolution of the small resonance peak. For this reason, only the evolution of the main peak will be considered all along this manuscript.

In addition to the acquisition of ^{1}H-NMR spectra, a Pulsed-Gradient Stimulated spin-Echo (PGSTE) sequence with unipolar gradients was used to measure the self-diffusion coefficients of water populations. Pulsed Field Gradient (PFG) and its derivate (PGSTE) NMR techniques are indeed common and accurate methods to directly measure the diffusion coefficients of water in Nafion™ membranes [18]. A PGSTE sequence is composed of a magnetic field gradient pulse sequence within a stimulated spin echo sequence (Figure 2.5). It is necessary to work with this sequence in porous media because additional relaxation mechanisms to those present in liquid phase occur during the measurement. As a consequence, the transverse relaxation time T_2 and the longitudinal relaxation time T_1 are strongly shortened, the relaxation time T_2 being always shorter or equal to the relaxation time T_1 for any system.

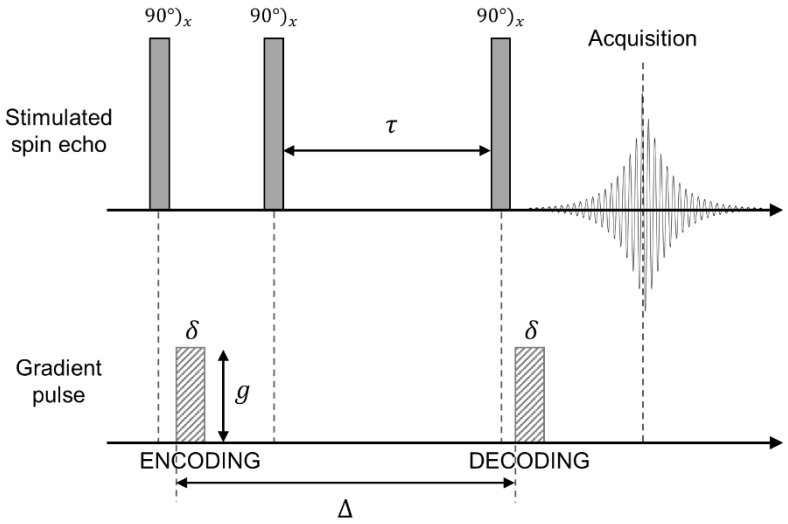

Figure 2.5 – Schematic representation of the PGSTE sequence.

The stimulated spin echo is based on the application of a 90° pulse to flip the magnetic moments in the transverse plane and a 90° pulse to flip the magnetic moments in the longitudinal direction to avoid the effects of T_2. They will then evolve during an evolution time τ before being refocused with a last 90° pulse (Figure 2.5). The gradient pulse sequence consists in applying a second spatially and temporally variable magnetic field superimposed to the static magnetic field. The gradient pulse sequence aims at voluntarily creating an inhomogeneity of the magnetic field allowing the "encoding" of the nuclear magnetic moments of the water molecules and consequently of their position in space. If the molecules diffuse during the diffusion delay Δ, refocusing of the spins does not fully take place and the consequence is an attenuation of the signal intensity as a function of the gradient strength g. This attenuation of the signal intensity thus gives us access to the diffusion coefficient. However, if the molecules have a coherent movement or have no motion, the signal intensity is only decreased due to the transversal relaxation phenomenon.

In this study, the measurements were performed with the following parameters: a gradient pulse duration δ = 0.66 – 1.50 ms, a diffusion delay Δ = 6.78 – 10.0 ms and a gradient strength g = 40 – 1 000 G/cm. The water self-diffusion coefficient D_s was then calculated by fitting the observed signal attenuation against the magnitude of the applied gradient strength g with the Stejskal – Tanner equation [19]:

$$I = I_0 * \exp\left[-(\gamma_H g \delta)^2 \left(\Delta - \frac{\delta}{3}\right) D_s\right] \qquad \textbf{Eq. 2.7}$$

with I the signal intensity of the sample in the presence of gradient pulse, I_0 the signal intensity of the sample in the absence of gradient pulse and γ_H the gyromagnetic ratio of the proton (equals to 26752.219 rad.s^{-1}.T^{-1}). Figure 2.6 illustrates experimental data of area peak fitted by Stejskal-Tanner equation (equation 2.7) in the case of a pristine XL membrane at 23.5 wt%:

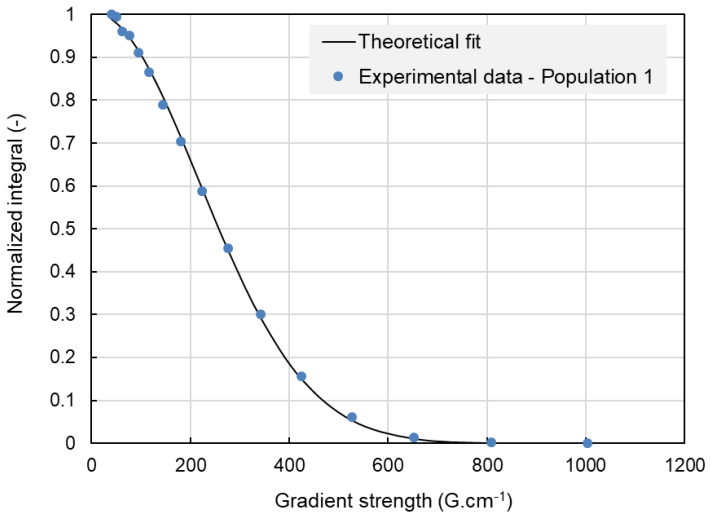

Figure 2.6 – Experimental NMR signal decay and theoretical fit of the main peak in a pristine XL membrane as a function of the gradient strength.

Water self-diffusion coefficient of pristine and aged membrane samples were here measured as a function of the water uptake. A few samples were fully immersed in distilled water at room temperature for several hours while some others were directly analyzed in the dry state, depending on the measurements campaign. In the case of immersed membranes, once out of the water, the hydrated samples were quickly pressed between two layers of absorbent paper to remove residual water droplets from the surface before being rolled and packed into 5 mm airtight NMR tubes. On the other hand, the dry samples were directly rolled and packed into 5 mm airtight NMR tubes. In both cases, the samples were equilibrated at least overnight before being weighed and analyzed. The sample size was approximately 1 x 5 cm² for both pristine and aged membranes. The hydration level of each sample was then adjusted by exposing the membrane samples to a water-saturated environment or to the ambient atmosphere in order to increase or decrease the membrane water content, respectively. It is important to note that no discrepancy has been observed in water self-diffusion coefficient evolution as a function of the membrane water content between the two operating modes (*i.e.* whether membrane samples are first hydrated and then dehydrated or the other way).

2.2.Water uptake measurements

Water sorption in Nafion™ membranes is commonly measured using gravimetric methods. They consist in measuring the mass change of a sample kept in an environment that is controlled in humidity at a constant temperature. More particularly, dynamic vapor sorption (DVS) analysis is a highly sensitive technique allowing to measure the water content of a membrane as a function of water vapor concentration in the climatic chamber containing the sample. The result is expressed under the form of a water sorption isotherm by plotting the membrane mass change as a function of the water activity or relative humidity.

In this work, the water sorption isotherms were measured using an IGASorp (Hidden Isochema, UK) DVS analyzer with a mass resolution of about ± 0.2 µg. The samples were first dried five hours under dry nitrogen at a temperature of 60 °C to attain nearly 0 % RH and thus set the reference dry mass. However, some residual water molecules strongly bonded to sulfonic groups still remains in the membrane even after intense drying protocols [3,4], which prevents easy access to the dry mass of membranes. Maldonado *et al.* [20] evaluated by NMR spectroscopy the quantity of residual water to $\lambda = 1.5 \pm 0.5$, which corresponded to 2.65 wt.% of water molecules, for N115 membrane dried at moderate temperature (60°C < T_{dry} < 100°C). The water isotherms were then recorded at 30 ± 0.1 °C for a water activity varying between 0.05 and 0.95, with an increment of 0.05. The relative humidity was obtained by mixing appropriate quantity of wet and dry gas streams automatically determined by an electronic gas flow controller. It is worth noting that water activities higher than 0.95 are not reachable due to possible water condensation inside the climatic chamber. At each water activity, the equilibrium threshold was fixed to 99 % and the equilibration time ranged between 3 and 10 hours. Furthermore, five measurements of pristine XL membrane samples were first performed in order to check the reproducibility of the pretreatment process as well as the repeatability of the measurement. The water sorption isotherms which will be presented all along this manuscript are nevertheless not corrected by the residual water quantity previously determined by Maldonado *et al.* [20] since all measurements were carried out with the same experimental protocol.

The sigmoidal shape of the sorption isotherm (Figure 2.7) is a result of the specific two-phase separated morphology of the membrane in which hydrophilic sulfonic sites, hydrophobic phase and water molecules coexist. Water sorption isotherm of a Nafion™ membrane can be decomposed into three components, each describing a specific mechanism of water molecules adsorption into PFSA polymer matrix. More details on the water sorption isotherm decomposition will be provided in § 5.1 of chapter IV.

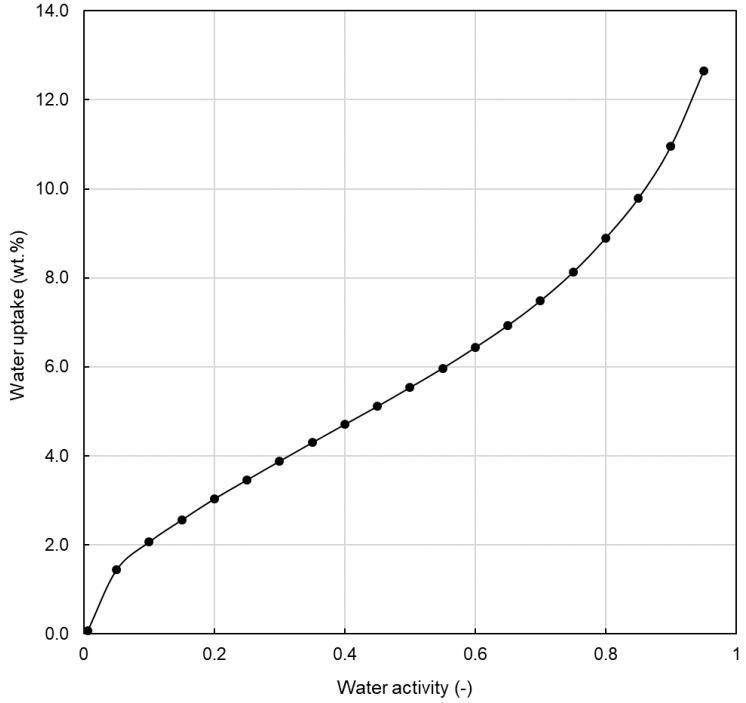

Figure 2.7 – Water sorption isotherm (30°C) of a pristine Nafion™ XL membrane.

Additionally, the maximal water sorption capacity of membrane samples was also evaluated. In this purpose, membrane samples were immersed in liquid water at room temperature for 24 hours and the total amount of water absorbed by the membranes was determined by weighing after the wet samples were quickly surface-dried using absorbent paper.

References

1. Durand G. 2010 Potentiométrie - Mesure du pH ou d'une concentration [en ligne]. *Tech. Ing.*

2. 2011 Fluoride Ion Selective Electrode - User Guide (Thermo Fischer). See http://tools.thermofisher.com/content/sfs/manuals/D15872~.pdf.

3. Korzeniewski C, Snow DE, Basnayake R. 2006 Transmission infrared spectroscopy as a probe of Nafion film structure: analysis of spectral regions fundamental to understanding hydration effects. *Appl. Spectrosc.* **60**, 599–604. (doi:10.1366/000370206777670620)

4. Ludvigsson M, Lindgren J, Tegenfeldt J. 2000 FTIR study of water in cast Nafion films. *Electrochimica Acta* **45**, 2267–2271. (doi:10.1016/S0013-4686(99)00438-7)

5. Laporta M, Pegoraro M, Zanderighi L. 1999 Perfluorosulfonated membrane (Nafion): FT-IR study of the state of water with increasing humidity. *Phys. Chem. Chem. Phys.* **1**, 4619–4628. (doi:10.1039/A904460D)

6. Gruger A, Régis A, Schmatko T, Colomban P. 2001 Nanostructure of Nafion® membranes at different states of hydration: An IR and Raman study. *Vib. Spectrosc.* **26**, 215–225. (doi:10.1016/S0924-2031(01)00116-3)

7. Liang Z, Chen W, Liu J, Wang S, Zhou Z, Li W, Sun G, Xin Q. 2004 FT-IR study of the microstructure of Nafion® membrane. *J. Membr. Sci.* **233**, 39–44. (doi:10.1016/j.memsci.2003.12.008)

8. Ostrovskii D, Paronen M, Sundholm F, Torell LM. 1999 State of water in sulfonated poly(vinyl fluoride) membranes: an FTIR study. *Solid State Ion.* **116**, 301–310. (doi:10.1016/S0167-2738(98)00357-9)

9. Falk M. 1980 An infrared study of water in perfluorosulfonate (Nafion) membranes. *Can. J. Chem.* **58**, 1495–1501. (doi:10.1139/v80-237)

10. Quezado S, Kwak J, Falk M. 1984 An Infrared Study of Water-Ion Interactions in Perfluorosulfonate (nafion) Membranes. *Can. J. Chem.-Rev. Can. Chim.* **62**, 958–966. (doi:10.1139/v84-158)

11. Leis AP, Schlicher S, Franke H, Strathmann M. 2005 Optically Transparent Porous Medium for Nondestructive Studies of Microbial Biofilm Architecture and Transport Dynamics. *Appl. Environ. Microbiol.* **71**, 4801–4808. (doi:10.1128/AEM.71.8.4801-4808.2005)

12. Chen Q, Schmidt-Rohr K. 2004 F-19 and C-13 NMR signal assignment and analysis in a perfluorinated ionomer (Nafion) by two-dimensional solid-state NMR. *Macromolecules* **37**, 5995–6003. (doi:10.1021/ma049759b)

13. Kaddouri AE, Perrin L, Jean B, Flandin L, Bas C. 2016 Investigation of perfluorosulfonic acid ionomer solutions by 19f NMR and DLS: Establishment of an accurate quantification protocol. *J. Polym. Sci. Part B Polym. Phys.* **54**, 2210–2222. (doi:10.1002/polb.24130)

14. Yuan T, Zhang H, Zou Z, Khatun S, Akins D, Adam Y, Suarez S. 2012 A Study of the Effect of Heat-Treatment on the Morphology of Nafion Ionomer Dispersion for Use in the Passive Direct Methanol Fuel Cell (DMFC). *Membranes* **2**, 841–854. (doi:10.3390/membranes2040841)

15. Robert M, El Kaddouri A, Perrin J-C, Leclerc S, Lottin O. 2018 Towards a NMR-Based Method for Characterizing the Degradation of Nafion XL Membranes for PEMFC. *J. Electrochem. Soc.* **165**, F3209–F3216. (doi:10.1149/2.0231806jes)

16. Ma Z, Jiang R, Myers ME, Thompson EL, Gittleman CS. 2011 NMR studies of proton transport in fuel cell membranes at sub-freezing conditions. *J. Mater. Chem.* **21**, 9302–9311. (doi:10.1039/c1jm10097a)

17. Han JH, Lee KW, Lee CE. 2017 1H nuclear magnetic resonance study of low-temperature water dynamics in a water-soaked perfluorosulfonic acid ionomer Nafion film. *Solid State Commun.* **250**, 28–30. (doi:10.1016/j.ssc.2016.11.005)

18. Yan L, Hu Y, Zhang X, Yue B. 2016 Chapter Three - Applications of NMR Techniques in the Development and Operation of Proton Exchange Membrane Fuel Cells. In *Annual Reports on NMR Spectroscopy* (ed GA Webb), pp. 149–213. Academic Press. (doi:10.1016/bs.arnmr.2015.11.003)

19. Stejskal EO, Tanner JE. 1965 Spin Diffusion Measurements: Spin Echoes in the Presence of a Time-Dependent Field Gradient. *J. Chem. Phys.* **42**, 288–292. (doi:10.1063/1.1695690)

20. Maldonado L, Perrin J-C, Dillet J, Lottin O. 2012 Characterization of polymer electrolyte Nafion membranes: Influence of temperature, heat treatment and drying protocol on sorption and transport properties. *J. Membr. Sci.* **389**, 43–56. (doi:10.1016/j.memsci.2011.10.014)

Chapter III

Accelerated chemical degradation of PFSA membranes: Fenton's reaction protocol

Table of contents

1. State of the art: chemical degradation of PFSA membranes induced by Fenton's reaction

As described in § 3.3.2 of chapter I, the chemical degradation of PFSA membranes results from the formation of hydrogen peroxide, permitted by the crossover of reactant gases, which decomposes to form highly reactive oxygen species (ROS): the hydroxyl ($HO^{\bullet}$), hydroperoxyl ($HOO^{\bullet}$) and hydrogen ($H^{\bullet}$) radicals [1–3]. These oxygen species attack the most vulnerable bonds of the PFSA structure, located both in the fluorocarbon backbone (carboxylic acid end groups and tertiary CF bond) [4–6] and the perfluorinated side chains (C-S bond, tertiary CF bond and ether linkages) [3,5–9], leading to a loss of membrane integrity and consequently to its thinning [10,11].

In order to study the chemical degradation and its impact on structure and properties of PFSA membranes, specific accelerated stress tests (AST) mimicking chemical and/or mechanical stresses encountered during fuel cell operation have been developed with both *in-situ* and *ex-situ* approaches (see § 3.3.2 of chapter I) [12–14]. Fenton's reaction is by far the most used *ex-situ* method to study the chemical degradation of PFSA membranes. This reaction consists in the simultaneous presence of hydrogen peroxide with iron ions to reproduce the aggressive and oxidizing environment of a fuel cell by generating $HO^{\bullet}$ and $HOO^{\bullet}$ radicals (equations 3.1–3.3) [1,3,15]:

$$H_2O_2 + Fe^{2+} \rightarrow Fe^{3+} + HO^{\bullet} + HO^{-} \quad \textbf{Eq. 3.1}$$

$$H_2O_2 + HO^{\bullet} \rightarrow HOO^{\bullet} + H_2O \quad \textbf{Eq. 3.2}$$

$$HOO^{\bullet} + Fe^{3+} \rightarrow Fe^{2+} + H^{+} + O_2 \quad \textbf{Eq. 3.3}$$

The effectiveness of the Fenton's reaction to reproduce the degradation occurring during fuel cell operation have been proven using ^{19}F-NMR and mass spectroscopy as similar degradation products of Nafion™ were detected in both *in-situ* (fuel cell operation) and *ex-situ* (Fenton's reaction) experiments (Healy *et al.* [11]). Although widely used in the literature as an accelerated aging protocol of PFSA membranes, the exact mechanisms involved by the Fenton's reaction are not yet fully understood [16].

Furthermore, depending on Fenton's reagents concentration and on the way the catalyst is introduced – in the H_2O_2 solution (solution method) or preliminary fixed into the membrane (exchange method) –, the impact on the chemical structure, morphology and properties of the

membrane can differ significantly. For example, Kundu *et al.* [17] investigated the differences between two accelerated degradation protocols of Nafion™ membranes: a first method named solution method and a second one named exchange method. The solution method consists in immersing the membrane in a solution of hydrogen peroxide and ferrous ions while the exchange method relies on the exchange of protons contained in the membrane by ferrous ions before immersing the membrane in a hydrogen peroxide solution. The authors analyzed the remaining Fenton solutions for both methods to evaluate the chemical degradation rate *via* fluoride ion emissions as well as the degraded membranes to characterize chemical, morphological and mechanical changes after chemical degradation. Their comparative study particularly demonstrated that both led to a significant chemical degradation of Nafion™ membranes: the authors observed similar (and significant) weight loss over the testing period and similar evolution of the average molecular weight regardless of the degradation method. Although the analysis of the chemical structure did not permit them to distinguish between the two methods, they nevertheless detected considerable differences in the morphological changes of the samples. Indeed, degradation *via* the solution method led to the formation of many defects, both on the surface and in thickness, to the point of splitting the membrane in two. On the other hand, the membrane degraded *via* exchange method remained unbroken with only the formation of minor defects. Moreover, N_2 crossover measurements also revealed that this difference led to distinct cell performances. For instance, a significant crossover rate was measured for membranes degraded by the solution method, due to the presence of large holes penetrating to the center of the membrane, while only a negligible crossover rate was observed in the case of the exchange method.

Both solution and exchange methods of the Fenton's reaction are widely applied in literature as accelerated *ex-situ* aging protocols but the protocols and/or operating conditions are not always precisely described, which can make difficult the comparison between the different studies [4,9,11,17–27]. In addition, a large variety of Fenton's reagents combinations is used – hydrogen peroxide (3 – 30 %) and catalyst concentrations (3 – 6000 ppm) – which shows different effects on PFSA membranes and makes difficult to choose the optimal concentrations to be used. Fortunately, the recent work of Frensch *et al.* [28] provided a better understanding of the effect of Fenton's reagent concentrations on chemical degradation of first generation Nafion™ 115 membranes. Firstly, they highlighted the high dependence of fluoride emissions on iron and hydrogen peroxide concentrations (Figure 3.1).

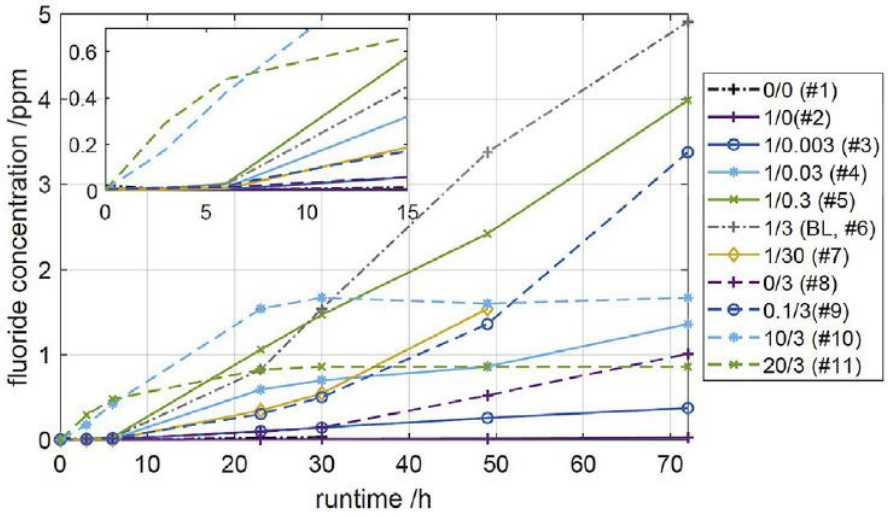

Figure 3.1– Fluoride concentration over time for all experiments performed by Frensch *et al* [28]. The legend refers to the initial concentrations as $[Fe^{2+}]/[H_2O_2]$, where BL = baseline test.

More precisely, they showed the existence of various trends depending on the initial concentrations of hydrogen peroxide and ferrous ions:

- The fluoride emissions were negligible when the membrane was exposed to a diluted solution containing only ferrous ions (1 ppm),
- The membrane exposure to only hydrogen peroxide solution (3 wt.%) led to significant fluoride emissions,
- The addition of a small amount of ferrous ions to hydrogen peroxide solution induced a considerable increase of fluoride emissions.

The authors thus confirmed that hydrogen peroxide acts as a necessary precursor to form free radicals and that iron ions only play the role of catalyst in the reaction. This conclusion has already been drawn by Hommura *et al.* [29] who demonstrated that membrane degradation can occur with a gaseous hydrogen peroxide exposure alone and thus that ferrous ions are not necessary to initiate the degradation. Additionally, Figure 3.1 shows that for a runtime of 48 hours, for example, the gradual increase of H_2O_2 concentration at a fixed Fe^{2+} concentration induces a gradual increase of fluoride emissions with the exception of a 30 wt.% H_2O_2 concentration for which fluoride emissions decrease. When the Fe^{2+} concentration is gradually increased from 0 to 10 ppm while H_2O_2 concentration is kept constant, fluoride emissions regularly increase before declining for the high Fe^{2+} concentration of 20 ppm.

Following the work undertaken by Frensch *et al.*, we performed a similar study targeting the second generation membranes Nafion™ XL and NR211. In that respect, an *ex-situ* aging

protocol based on the Fenton's reaction was developed and optimized in order to investigate the effects of Fenton's reagent concentrations on the degradation. This approach aims at determining the concentration of Fenton's reagents leading to the maximum fluoride emissions – and thus membrane degradation – without inducing extreme morphological changes such as delamination and/or formation of bubbles as observed by several authors [17,18,25,30,31]. Indeed, these phenomena have not been observed on membrane – or at least reported – during or after fuel cell operation.

2. Description of the aging and cleaning protocols

This experimental study was carried out on two commercial PFSA membranes purchased from Ion Power in the protonated form (H^+): Nafion™ XL and Nafion™ NR211. Both membranes are based on chemically stabilized copolymer of tetrafluoroethylene (TFE) and perfluoro(4-methyl-3,6-dioxa-7-octene-1-sulfonyl fluoride) [32], have similar ion exchange capacities (IEC) – 0.92 meq.g^{-1} for XL and 0.98 meq.g^{-1} for NR211 – and similar nominal thickness – 27.5 µm versus 25.4 µm. Nafion™ NR211 is unreinforced while Nafion™ XL contains an additional microporous PTFE-rich layer. Moreover, the Nafion™ XL membrane also contains radical scavengers able to mitigate radical attacks of the polymer [33–36]. As explained in chapter I (§ 3.3.2.5), radical scavengers – also called hydrogen peroxide decomposition catalyst (HPDC) or chemical stabilizers – aim at deactivating highly reactive oxygen species such as free radicals (HO$^\bullet$, HOO$^\bullet$) before they react with the polymer chains. Moreover, Stewart *et al.* analyzed commercial Nafion™ XL membrane using X-ray fluorescence spectroscopy and estimated its cerium content at 6.92 ± 0.16 µg/cm² [35].

2.1.Sample pretreatment

Prior to each utilization, the commercial membrane samples were pretreated according to a protocol close to the one established by Xu *et al.* [37]. The samples were first boiled one hour in a 3 wt.% hydrogen peroxide solution and rinsed thoroughly with distilled water to eliminate any organic impurities. They were then soaked 30 minutes at room temperature in nitric acid (10 mol.L^{-1}), rinsed again with distilled water and boiled one hour in deionized water. To ensure a complete substitution of the ionomer active sites, the samples were boiled one hour in sulfuric acid (1 mol.L^{-1}) and one hour again in distilled water. Finally, they were dried 24 hours in an oven at 60 °C.

2.2.Aging protocol based on Fenton's reaction and operating conditions

When PFSA membranes are immersed in an aqueous solution, they are deformed and can roll up on themselves, which can lead to an inhomogeneous surface exposition to the solution. To keep the membrane as flat as possible while soaked in the solution, a specific polycarbonate frame similar to that developed by Ghassemzadeh *et al.* [38] was designed. Holes were made in each corner of the samples before inserting them between both symmetrical parts of the frame. These half-frames were then held together with nylon screws. In this way, the membrane surface was kept flat and accessible during the whole duration of the experiment. Nylon and polycarbonate parts are not severely degraded by hydrogen peroxide and will not interfere with the chemical degradation of PFSA. The membrane dimensions were conditioned by those of the polycarbonate frame and were thus cut into 6 x 4 cm² samples before being fixed to the frame. These dimensions also correspond to those of the single cell utilized to carry out performance tests of the degraded membranes. The single cell and test protocols will be fully described in § 2.3 of chapter V dedicated to the effects of conjoint chemical and mechanical stress on PFSA membranes. The setup for the *ex-situ* aging protocol based on the Fenton's reaction and a photograph of the polycarbonate frame are shown in Figure 3.2.

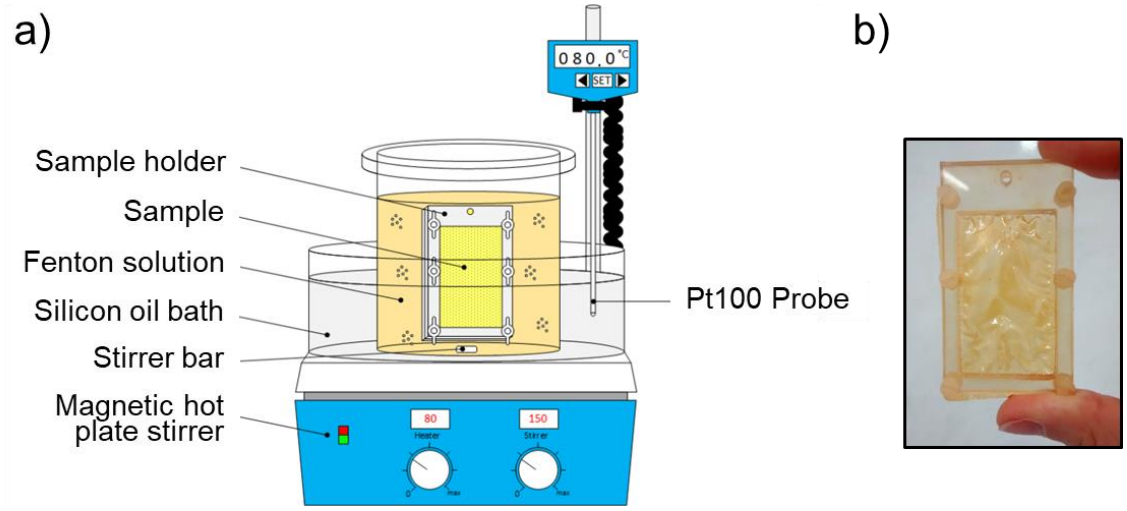

Figure 3.2 – (a) schematic representation of the ex-situ chemical degradation setup and (b) photograph of the polycarbonate frame holding a membrane sample.

A 50 mg.L^{-1} stock solution of ferrous ions was first prepared from iron (II) sulfate heptahydrate salt ($FeSO_4.7H_2O$) and a few drops of concentrated nitric acid were added to lower the pH below 3 before the addition of hydrogen peroxide. Indeed, ferrous ions are not stable in solution but naturally and rapidly oxidized to ferric ions Fe^{3+} with oxygen in the air. Various Fenton solutions were prepared from this acidified ferrous ion stock solution and the appropriate volume of a 30 vol.% hydrogen peroxide solution. The Fenton solution was added

to a beaker and heated to 80 °C thanks to a silicon oil bath kept at a constant temperature during the whole duration of the experiment. Finally, the polycarbonate frame containing the membrane was immersed into the Fenton solution. A watch glass was put at the top of the beaker to limit the evaporation of water. Each experiment was performed under magnetic stirring and for an exposure time to free radicals of approximately 24 hours. It is important to notice here that the experiment #3 (Table 3.1) with high concentrations of both ferrous ions and hydrogen peroxide lasted for only 3 minutes instead of 24 hours because of difficulty in setting up the experiment. As Fenton's reaction is exothermic, the reagents mixing led to significant bubbling of the solution that became unstoppable when the temperature exceeded 40 °C. When the polycarbonate frame containing the membrane was immersed into the solution, the bubbling was such that it provoked its partially overflow.

As mentioned earlier, Frensch *et al.* [28] recently investigated the effect of Fenton's reagents concentration on chemical degradation of first generation Nafion™ N115 membranes. The present study being focused on second generation Nafion™ membranes, it was necessary to conduct a similar approach on both NR211 and XL membranes by varying Fenton's reagents concentrations as reported in the Table 3.1.

Table 3.1 – Experimental matrix for the ex-situ degradation tests based on Fenton's reaction

Experiment #	Fe^{2+} concentration (ppm)	H_2O_2 concentration (vol.%)
1	44	0.2
2	44	3
3	44	20
4	1	0.2
5	1	3
6	4	20

Experiments #1, #2 and #3 corresponded to a high concentration of ferrous ions (44 ppm) and varying hydrogen peroxide concentrations (0.2, 3 and 20 vol.%). This high iron concentration was based on the assumption that an important amount of catalyst will allowed to generate high quantity of free radicals in order to reach high chemical degradations. In the case of experiments #4, #5 and #6, only traces of ferrous ions (1 or 4 ppm) were used and the hydrogen peroxide concentrations were varied in the same proportions than with experiments #1, #2 and #3. The experiment #5 – with 1 ppm Fe^{2+} and 3 vol.% H_2O_2 – corresponded to the optimal conditions leading to the highest fluoride emission rate determined by Frensch *et al.* [28].

2.3.Cleaning of aged samples

As seen earlier (§ 2.2), the Fenton's reaction implies the presence of metallic cations (Fe^{2+} and Fe^{3+}) able to interact with the membrane. During the degradation protocols, some membrane samples, initially translucent and colorless, became opaque and orange, probably because of the adsorption of iron cations. These impurities can lead to chemical structure changes through crosslinking effect and to the alteration of water sorption and diffusion properties. Indeed, ferrous and ferric ions have a greater affinity for sulfonate ions than protons [39]. Moreover, for high ferrous ion concentrations, the appearance of brick red precipitate was observed. The formation of this precipitate may be explained by the reactions involved in the aging protocol: Fenton's reaction leads to the formation of ferric ion Fe^{3+} that can precipitate as ferric hydroxide $Fe(OH)_3$. As the pH was not monitored during the experiments, it was possible that the addition of hydrogen peroxide caused the basification of the Fenton solution and thus provoked the ferric hydroxide formation. The orange color of degraded membranes might be explained by the deposition of ferric hydroxide on the surface or even within the membrane. That is the reason why the aged membranes had to be systematically depolluted prior to any analysis.

The cleanin protocol consists in two stages: depollution and re-acidification.

- The depollution step is close to that described by MacMillan *et al.* [40]. It consists in soaking the aged membranes in a 0.01 $mol.L^{-1}$ EDTA-Na_2 solution at room temperature overnight and thoroughly rinsing them with distilled water.
- The re-acidification step is close to the protocol established by Xu *et al.* [41]: the aged membranes were boiled two hours in a 1 $mol.L^{-1}$ nitric acid (HNO_3) solution at 80 °C for complete re-acidification before being washed in distilled water at 80 °C during two hours to remove all excess of nitric acid and residual contaminants.

Finally, the aged samples were dried six hours in an oven at 60 °C. More details on the cleaning protocol and the identification of the cationic contamination in aged Nafion™ membranes are given in § 2 of appendix A.

3. Effect of Fenton's reagent concentrations on the chemical degradation of PFSA membranes

The effects of Fenton's reagent concentrations on the degradation of XL and NR-211 membranes were analyzed following two steps: the degraded membranes were first examined at a macroscopic scale to detect potential changes in the morphology while the remaining

Fenton solutions were analyzed thanks to a fluoride ion-selective electrode to evaluate the chemical degradation.

3.1.Macroscopic morphology evolution of aged membranes

After the experiment and after the cleaning protocol described in § 2.3, the analysis of the degraded membranes to the naked eye permitted to give a first assessment on the impact of Fenton's reagent concentrations on the PFSA membrane morphology.

The morphology of PFSA membranes can be strongly affected by Fenton's reagents concentration and more particularly by high hydrogen peroxide concentration (around 20-30 vol.%) [17,18]. For instance, Mu *et al.* [18] showed that a high concentration of H_2O_2 – with and without ferrous ions – entails the appearance of numerous cracks and holes. In our case, the naked eye examination of aged membranes confirms these morphological evolutions: many bubbles appear on the whole surface with both XL and NR211 membranes when the H_2O_2 concentrations is the highest (20 vol.%). Figure 3.3 shows pictures of pristine and aged XL and NR211 membranes for various Fenton's reagents concentration.

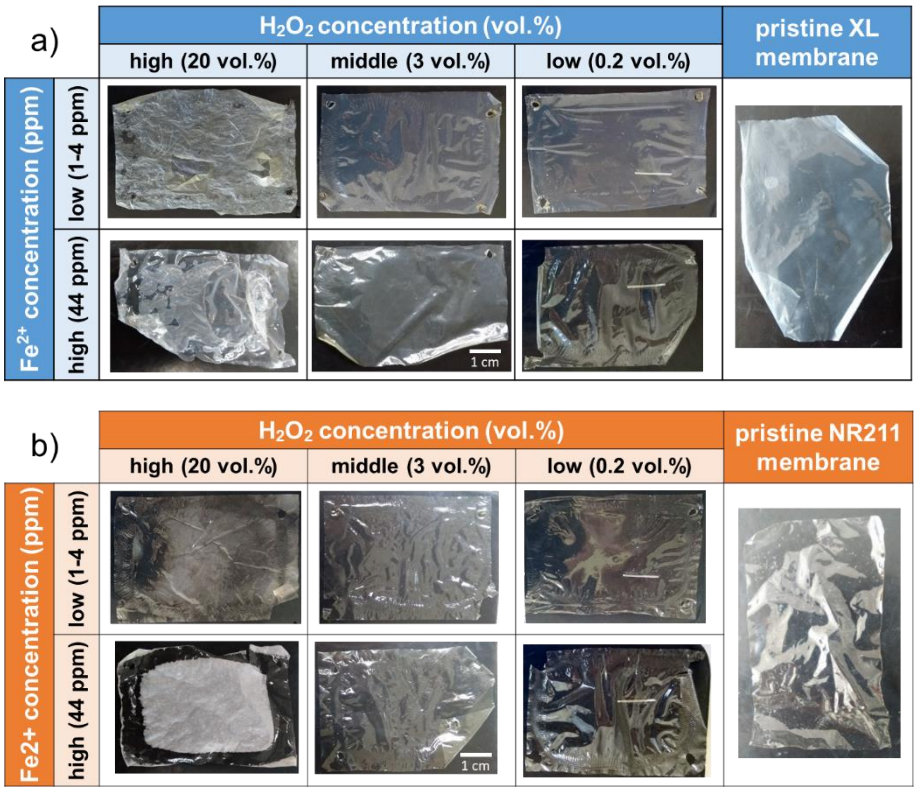

Figure 3.3 – Comparison of (a) XL and (b) NR211 macroscopic morphologies after exposure to the different Fenton's reagent concentrations.

In the case of experiment #6 (i.e. low Fe^{2+} and high H_2O_2 concentrations), morphology evolutions differ significantly between the two membranes: bubbles with various diameters

ranging from micrometers to millimeters appear on the Nafion™ XL surface while only tiny bubbles in the micrometer range locally appear on NR211. The analysis of the two aged samples is compared to pristine membrane in Figure 3.4.

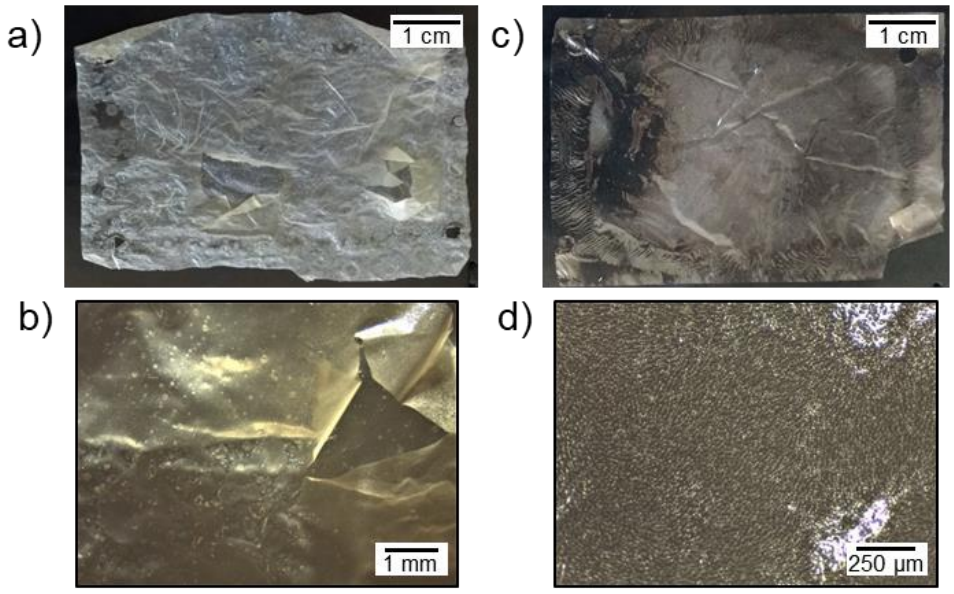

Figure 3.4 – Macroscopic changes after experiment #6 conducted with a high H_2O_2 concentration (20 vol.%) and low Fe^{2+} concentration (4 ppm) for Nafion™ XL, (a) without magnification and (b) with 8x magnification, as well as with Nafion™ NR211, (c) without magnification and (d) with 35x magnification.

Many publications report morphological changes at the surface and in the thickness of the membrane when exposed to Fenton solution with high H_2O_2 concentration [17–19,25,30,31,42]. More particularly, SEM images of the surface and cross-section of unreinforced Nafion™ membranes revealed the presence of severe damages after Fenton's reagents treatment with the appearance of many bubbles, bumps and tears evolving into cracks and pinholes, up to the rupture of the membrane into two pieces or more. More recently, Shi and his coworkers performed *ex-situ* chemical degradation (*i.e.* Fenton's reaction) tests on Nafion™ XL and NR212 membranes and observed the appearance of many bubbles at the surface and in the cross-section of chemically-degraded NR211 membrane while bubbles are formed only in the outer ionomer layers in the case of degraded XL membrane [42,43]. The Fenton's reagent concentrations were of about 22.5 % of H_2O_2 and 14 ppm of ferrous ions. In conclusion, Fenton's reaction involving high H_2O_2 concentration entails an important chemical degradation of PFSA membranes but also significant morphological changes of both reinforced and non-reinforced membranes. Nevertheless, it is important to note that to the best of our knowledge, such morphological changes have not been observed − or at least reported − in fuel cells. Indeed, the consequences of membrane degradation during fuel cell operation are

described as a membrane thinning resulting from chemical attacks of the polymer, as well as pinholes/cracks formation and propagation due to the mechanical constraints exerted by the flow field plates [10,11,44,45]. Furthermore, the H_2O_2 concentration in a fuel cell is estimated to be between 0.1 and 1.6 mmol.L^{-1}, depending on the membrane thickness and on the side where it is formed (anode or cathode) [46–48]. The concentration used here – and in similar studies – to accelerate the degradation rate (*i.e.* 6.5 mol.L^{-1} or 20 vol.%) is therefore 3 to 4 orders of magnitude higher. And it must be kept in mind that the morphological changes observed in this case could imply different degradation mechanisms or pathways than those involved during fuel cell operation. In these regards, high H_2O_2 concentrations cannot be considered as the most adapted or representative.

We have seen here that significant morphology evolutions can occurred when the hydrogen peroxide concentration is high, regardless of the ferrous ion concentration. The Fenton solutions are then analyzed to estimate the PFSA decomposition by determining the fluoride emission rate and the impact of Fenton's reagent concentrations on the PFSA membrane degradation.

3.2.Fenton solutions analysis: quantification of the chemical degradation

The water produced during fuel cell operation as well as the Fenton solutions are usually analyzed to evaluate the concentration of the degradation products and the impact of chemical degradation on PFSA membranes [1,11]. Fluoride ions, coming from the production of hydrofluoric acid (HF) during the PFSA decomposition, are the best known degradation products and the most commonly monitored [17,18,20–22,24]. Fluoride emission rates (FER) is believed to be a good indicator of the chemical degradation rate of the PFSA membrane and can be quickly and precisely determined using an ion-selective electrode (ISE).

Figure 3.5 summarizes the fluoride emission rate determined for the different experiments as a function of the ferrous ion and the hydrogen peroxide (Fenton's reagents) concentration. It is expressed as the total amount of fluoride ions released by the membrane sample with respect to its dry weight.

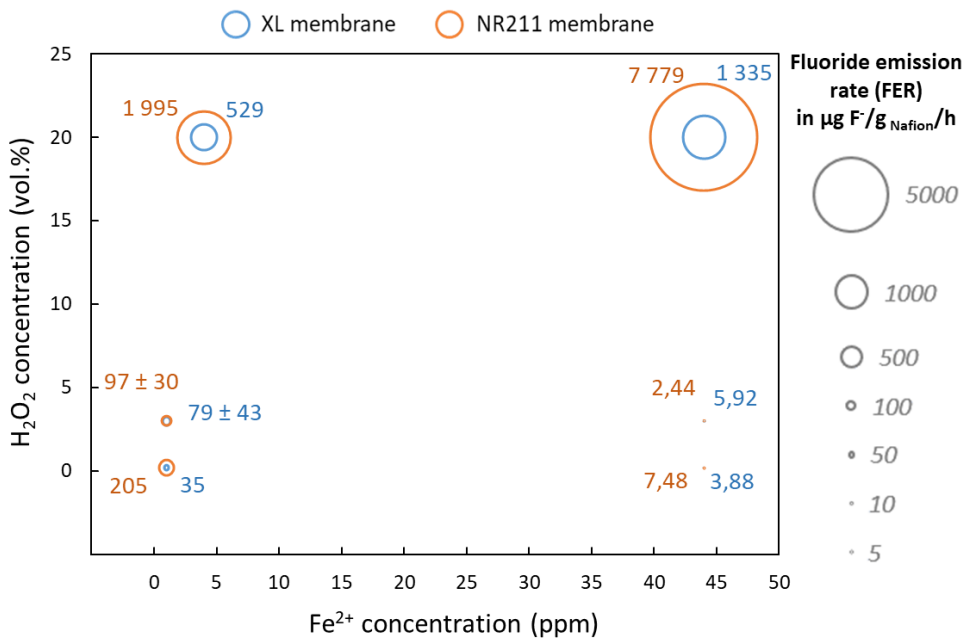

Figure 3.5 – Fluoride emission rate for Nafion™ XL (in blue circle) and NR211 (in orange circle) membrane samples as a function of Fenton's reagents concentration. Reproducibility tests have been performed in the baseline conditions determined by Frensch *et al.*[28]: 1 ppm Fe^{2+} and 3 vol.% H_2O_2.

As a first step, NR211 and XL membranes are soaked in a 3 vol.% hydrogen peroxide solution to establish a reference of degradation rate in the absence of iron ions. A non-negligible fluoride emission rate of 11 $\mu g/g_{Nafion}/h$ for both membranes is measured. In the case of Fenton's solution, as observed by Frensch *et al.* [28], the FER reveals a high dependence on reagents concentration as it significantly increases with the hydrogen peroxide concentration, regardless of ferrous ion concentration. Indeed, the fluoride emission rate is divided by 27 in the case of NR211 and divided by 9 in the case of XL when the ferrous ion concentration is increased from 1 ppm to 44 ppm, while keeping the H_2O_2 concentration constant at 0.2 vol.%. However, increasing the ferrous ion concentration leads to a higher FER with the 20 vol.% H_2O_2 solution only. It is important to remind here that experiment #3 lasted only 3 minutes instead of 24 hours in all the other cases and was not performed at 80 °C due to the excessive bubbling of the solution that occurred when the membrane was immersed and which became impossible to control for a temperature exceeding 40 °C. Interestingly, NR211 membranes always seemed to be more affected than XL membranes, with a FER 2 to 8 times higher.

A high amount of ferrous ions in the solution does not increase the efficiency of the Fenton's reaction [49,50], probably because of parasitic reactions such as the oxidation of iron (II) by the hydroxyl radical ($HO^{\bullet}$):

$$Fe^{2+} + HO^{\bullet} \rightarrow Fe^{3+} + HO^{-} \quad (3.4)$$

In addition to the consumption of hydroxyl radicals by such reactions, the low reaction rate of iron (II) regeneration limits the oxidizing power of the Fenton's reaction and consequently the membrane degradation.

The stability of Nafion™ membranes against hydrogen peroxide and Fenton's reagents has already been discussed in the literature by Kinumoto *et al.* [27]. Their work demonstrated that the presence of ferrous ion as counter ions enhanced significantly the decomposition rate of Nafion™ membranes in comparison with protonated ones. These results support the assumption already presented in the literature that H_2O_2 acts as a necessary precursor to induce chemical degradation while iron ions act as a catalyst [28,29].

Based on these results, Fenton's reaction seems to be more efficient at low iron concentration and high hydrogen peroxide concentration (20 vol.%) as performed in experiment #6. Indeed, the fluoride emissions are the highest for both membranes in these conditions. However, as seen in §3.1, the membrane morphology is strongly affected by the concentration of Fenton's reagents. In the case of experiments #6, the appearance of many bubbles for both XL and NR211 membranes correlates well with the high fluoride emissions measured. Furthermore, the fluoride emissions are also significant for experiment #5, corresponding to an iron concentration of 1 ppm and a hydrogen peroxide concentration of 3 vol.%, but degraded membranes presented no morphological evolution to the naked eye. Consequently, reproducibility tests have been performed in these "optimal" conditions, experiment #5 (Table 3.1) being repeated three times, to confirm the initial observation.

4. Conclusions

The results highlight a high dependence of the membrane degradation on the Fenton's reagents concentration, both from a chemical and a morphological points of view. Analysis of the degraded PFSA membranes to the naked eye permitted to rapidly evaluate the impact of Fenton's reagents concentration on the morphology. It is observed that a high hydrogen peroxide concentration generates severe macroscopic morphology evolutions, regardless of the iron concentration, for both XL and NR211 membranes with the appearance of numerous bubbles. No significant morphology evolution was observed for lower H_2O_2 concentration (0.2 and 3 vol.%).

Fluoride emission rate measurements thanks to an ion-selective electrode permitted to estimate more accurately the impact of Fenton's reagents concentration on PFSA membranes. First, the results confirm that the use of a small amount of Fe^{2+} is required to catalyze efficiently the decomposition reaction of H_2O_2 into free radicals and to ensure a significant membrane degradation. A high concentration of Fe^{2+}, as shown in this work and as observed in the literature, does not induce higher degradation. On the other hand, H_2O_2 concentrations must also be kept rather low (i.e. 3 vol.% in our case) so that the condition can be considered as representative of those occurring during fuel cell operation. Indeed, the H_2O_2 concentration in a fuel cell is most probably several orders of magnitude lower than that used for Fenton's reaction. In that respect, it seems necessary to keep the H_2O_2 concentration sufficiently high to accelerate degradation mechanisms but not too high to avoid severe morphological changes of membranes that are not assumed to occur during fuel cell operation.

Consequently, the efficient chemical degradation of PFSA membranes without inducing significant morphological changes is obtained with Fenton's reagents concentrations of 1 ppm Fe^{2+} and 3 vol.% H_2O_2. Therefore, these conditions are the most appropriate and will be used for the following additional studies presented in this manuscript.

References

1. LaConti AB, Hamdan M, McDonald RC. 2003 Mechanisms of membrane degradation. In *Handbook of Fuel Cells*, John Wiley & Sons, Ltd. (doi:10.1002/9780470974001.f303055)

2. Zatoń M, Rozière J, Jones DJ. 2017 Current understanding of chemical degradation mechanisms of perfluorosulfonic acid membranes and their mitigation strategies: a review. *Sustain. Energy Fuels* **1**, 409–438. (doi:10.1039/C7SE00038C)

3. Danilczuk M, Coms FD, Schlick S. 2009 Visualizing Chemical Reactions and Crossover Processes in a Fuel Cell Inserted in the ESR Resonator: Detection by Spin Trapping of Oxygen Radicals, Nafion-Derived Fragments, and Hydrogen and Deuterium Atoms. *J. Phys. Chem. B* **113**, 8031–8042. (doi:10.1021/jp901597f)

4. Curtin DE, Lousenberg RD, Henry TJ, Tangeman PC, Tisack ME. 2004 Advanced materials for improved PEMFC performance and life. *J. Power Sources* **131**, 41–48. (doi:10.1016/j.jpowsour.2004.01.023)

5. Coms FD. 2008 The Chemistry of Fuel Cell Membrane Chemical Degradation. *ECS Trans.* **16**, 235–255. (doi:10.1149/1.2981859)

6. Danilczuk M, Lancucki L, Schlick S, Hamrock SJ, Haugen GM. 2012 In-Depth Profiling of Degradation Processes in a Fuel Cell: 2D Spectral-Spatial FTIR Spectra of Nafion Membranes. *ACS Macro Lett.* **1**, 280–285. (doi:10.1021/mz200100s)

7. Mittal VO, Kunz HR, Fenton JM. 2007 Membrane Degradation Mechanisms in PEMFCs. *J. Electrochem. Soc.* **154**, B652–B656. (doi:10.1149/1.2734869)

8. Ghassemzadeh L, Kreuer K-D, Maier J, Mueller K. 2010 Chemical Degradation of Nation Membranes under Mimic Fuel Cell Conditions as Investigated by Solid-State NMR Spectroscopy. *J. Phys. Chem. C* **114**, 14635–14645. (doi:10.1021/jp102533v)

9. Ghassemzadeh L, Peckham TJ, Weissbach T, Luo X, Holdcroft S. 2013 Selective Formation of Hydrogen and Hydroxyl Radicals by Electron Beam Irradiation and Their Reactivity with Perfluorosulfonated Acid Ionomer. *J. Am. Chem. Soc.* **135**, 15923–15932. (doi:10.1021/ja408032p)

10. Lee S-Y, Cho E, Lee J-H, Kim H-J, Lim T-H, Oh I-H, Won J. 2007 Effects of purging on the degradation of PEMFCs operating with repetitive on/off cycles. *J. Electrochem. Soc.* **154**, B194–B200. (doi:10.1149/1.2403083)

11. Healy J, Hayden C, Xie T, Olson K, Waldo R, Brundage A, Gasteiger H, Abbott J. 2005 Aspects of the chemical degradation of PFSA ionomers used in PEM fuel cells. *Fuel Cells* **5**, 302–308. (doi:10.1002/fuce.200400050)

12. Mukundan R, Baker AM, Kusoglu A, Beattie P, Knights S, Weber AZ, Borup RL. 2018 Membrane Accelerated Stress Test Development for Polymer Electrolyte Fuel Cell Durability Validated Using Field and Drive Cycle Testing. *J. Electrochem. Soc.* **165**, F3085–F3093. (doi:10.1149/2.0101806jes)

13. Zhang S, Yuan X, Wang H, Mérida W, Zhu H, Shen J, Wu S, Zhang J. 2009 A review of accelerated stress tests of MEA durability in PEM fuel cells. *Int. J. Hydrog. Energy* **34**, 388–404. (doi:10.1016/j.ijhydene.2008.10.012)

14. Rodgers MP *et al.* 2013 Perfluorinated Sulfonic Acid Membrane and Membrane Electrode Assembly Degradation Correlating Accelerated Stress Testing and Lifetime Testing. *ECS Trans.* **58**, 129–148. (doi:10.1149/05801.0129ecst)

15. Fenton HJH. 1894 LXXIII.—Oxidation of tartaric acid in presence of iron. *J. Chem. Soc. Trans.* **65**, 899–910. (doi:10.1039/CT8946500899)

16. Barbusiński K. 2009 Fenton reaction - controversy concerning the chemistry. *Ecol. Chem. Eng. S* , 347–358.

17. Kundu S, Simon LC, Fowler MW. 2008 Comparison of two accelerated Nafion™ degradation experiments. *Polym. Degrad. Stab.* **93**, 214–224. (doi:10.1016/j.polymdegradstab.2007.10.001)

18. Mu S, Xu C, Yuan Q, Gao Y, Xu F, Zhao P. 2013 Degradation behaviors of perfluorosulfonic acid polymer electrolyte membranes for polymer electrolyte membrane fuel cells under varied acceleration conditions. *J. Appl. Polym. Sci.* **129**, 1586–1592. (doi:10.1002/app.38785)

19. Tang H, Peikang S, Jiang SP, Wang F, Pan M. 2007 A degradation study of Nafion proton exchange membrane of PEM fuel cells. *J. Power Sources* **170**, 85–92. (doi:10.1016/j.jpowsour.2007.03.061)

20. Chen C, Levitin G, Hess DW, Fuller TF. 2007 XPS investigation of Nafion® membrane degradation. *J. Power Sources* **169**, 288–295. (doi:10.1016/j.jpowsour.2007.03.037)

21. Merlo L, Ghielmi A, Cirillo L, Gebert M, Arcella V. 2007 Resistance to peroxide degradation of Hyflon® Ion membranes. *J. Power Sources* **171**, 140–147. (doi:10.1016/j.jpowsour.2006.11.012)

22. Ghassemzadeh L, Kreuer KD, Maier J, Mueller K. 2011 Evaluating chemical degradation of proton conducting perfluorosulfonic acid ionomers in a Fenton test by solid-state F-19 NMR spectroscopy. *J. Power Sources* **196**, 2490–2497. (doi:10.1016/j.jpowsour.2010.11.053)

23. Luo X, Ghassemzadeh L, Holdcroft S. 2015 Effect of free radical-induced degradation on water permeation through PFSA ionomer membranes. *Int. J. Hydrog. Energy* **40**, 16714–16723. (doi:10.1016/j.ijhydene.2015.07.118)

24. Kusoglu A, Calabrese M, Weber AZ. 2014 Effect of Mechanical Compression on Chemical Degradation of Nafion Membranes. *ECS Electrochem. Lett.* **3**, F33–F36. (doi:10.1149/2.008405eel)

25. Fernandes AC, Ticianelli EA. 2009 A performance and degradation study of Nafion 212 membrane for proton exchange membrane fuel cells. *J. Power Sources* **193**, 547–554. (doi:10.1016/j.jpowsour.2009.04.038)

26. Sethuraman VA, Weidner JW, Haug AT, Protsailo LV. 2008 Durability of Perfluorosulfonic Acid and Hydrocarbon Membranes: Effect of Humidity and Temperature. *J. Electrochem. Soc.* **155**, B119–B124. (doi:10.1149/1.2806798)

27. Kinumoto T, Inaba M, Nakayama Y, Ogata K, Umebayashi R, Tasaka A, Iriyama Y, Abe T, Ogumi Z. 2006 Durability of perfluorinated ionomer membrane against hydrogen peroxide. *J. Power Sources* **158**, 1222–1228. (doi:10.1016/j.jpowsour.2005.10.043)

28. Frensch SH, Serre G, Fouda-Onana F, Jensen HC, Christensen ML, Araya SS, Kær SK. 2019 Impact of iron and hydrogen peroxide on membrane degradation for polymer electrolyte membrane water electrolysis: Computational and experimental investigation on fluoride emission. *J. Power Sources* **420**, 54–62. (doi:10.1016/j.jpowsour.2019.02.076)

29. Hommura S, Kawahara K, Shimohira T, Teraoka Y. 2008 Development of a Method for Clarifying the Perfluorosulfonated Membrane Degradation Mechanism in a Fuel Cell Environment. *J. Electrochem. Soc.* **155**, A29–A33. (doi:10.1149/1.2800171)

30. Wang F, Tang H, Pan M, Li D. 2008 Ex situ investigation of the proton exchange membrane chemical decomposition. *Int. J. Hydrog. Energy* **33**, 2283–2288. (doi:10.1016/j.ijhydene.2008.01.052)

31. Hongsirikarn K, Mo X, Goodwin JG, Creager S. 2011 Effect of H2O2 on Nafion® properties and conductivity at fuel cell conditions. *J. Power Sources* **196**, 3060–3072. (doi:10.1016/j.jpowsour.2010.11.133)

32. Grot W. 2011 9 - Experimental Methods. In *Fluorinated Ionomers (Second Edition)*, pp. 211–233. William Andrew Publishing. (doi:10.1016/B978-1-4377-4457-6.10009-3)

33. Baker AM, Mukundan R, Spernjak D, Judge EJ, Advani SG, Prasad AK, Borup RL. 2016 Cerium Migration during PEM Fuel Cell Accelerated Stress Testing. *J. Electrochem. Soc.* **163**, F1023–F1031. (doi:10.1149/2.0181609jes)

34. Prabhakaran V, Arges CG, Ramani V. 2012 Investigation of polymer electrolyte membrane chemical degradation and degradation mitigation using in situ fluorescence spectroscopy. *Proc. Natl. Acad. Sci. U. S. A.* **109**, 1029–1034. (doi:10.1073/pnas.1114672109)

35. Stewart SM, Spernjak D, Borup R, Datye A, Garzon F. 2014 Cerium Migration through Hydrogen Fuel Cells during Accelerated Stress Testing. *Ecs Electrochem. Lett.* **3**, F19–F22. (doi:10.1149/2.008404eel)

36. Zatoń M, Prélot B, Donzel N, Rozière J, Jones DJ. 2018 Migration of Ce and Mn Ions in PEMFC and Its Impact on PFSA Membrane Degradation. *J. Electrochem. Soc.* **165**, F3281–F3289. (doi:10.1149/2.0311806jes)

37. Xu F, Innocent C, Bonnet B, Jones DJ, Roziere J. 2005 Chemical modification of perfluorosulfonated membranes with pyrrole for fuel cell application: Preparation, characterisation and methanol transport. *Fuel Cells* **5**, 398–405. (doi:10.1002/fuce.200400077)

38. Ghassemzadeh L. 2011 Polymer Electrolyte Membrane Degradation and Mobility in Fuel Cells: a Solid-state NMR Investigation. VDM Verlag, Saarbrücken, Germany.

39. Okada T, Satou H, Okuno M, Yuasa M. 2002 Ion and Water Transport Characteristics of Perfluorosulfonated Ionomer Membranes with H+ and Alkali Metal Cations. *J. Phys. Chem. B* **106**, 1267–1273. (doi:10.1021/jp013195l)

40. MacMillan B, Sharp AllanR, Armstrong RobinL. 1999 An n.m.r. investigation of the dynamical characteristics of water absorbed in Nafion. *Polymer* **40**, 2471–2480. (doi:10.1016/S0032-3861(98)00484-4)

41. Xu F, Leclerc S, Canet D. 2013 NMR Relaxometry Study of the Interaction of Water with a Nafion Membrane under Acid, Sodium, and Potassium Forms. Evidence of Two Types of Bound Water. *J. Phys. Chem. B* **117**, 6534–6540. (doi:10.1021/jp311062h)

42. Sun X, Shi S, Fu Y, Chen J, Lin Q, Hu J, Li C, Li J, Chen X. 2020 Embrittlement induced fracture behavior and mechanisms of perfluorosulfonic-acid membranes after chemical degradation. *J. Power Sources* **453**, 227893. (doi:10.1016/j.jpowsour.2020.227893)

43. Shi S *et al.* 2020 Fatigue crack propagation behavior of fuel cell membranes after chemical degradation. *Int. J. Hydrog. Energy* , S0360319920326884. (doi:10.1016/j.ijhydene.2020.07.113)

44. Gittleman CS, Coms FD, Lai Y-H. 2012 Chapter 2 - Membrane Durability: Physical and Chemical Degradation. In *Polymer Electrolyte Fuel Cell Degradation* (eds MM Mench, EC Kumbur, TN Veziroglu), pp. 15–88. Boston: Academic Press. (doi:10.1016/B978-0-12-386936-4.10002-8)

45. Moor GD *et al.* 2012 Understanding Membrane Failure in PEMFC: Comparison of Diagnostic Tools at Different Observation Scales. *Fuel Cells* **12**, 356–364. (doi:10.1002/fuce.201100161)

46. Liu W, Zuckerbrod D. 2005 In Situ Detection of Hydrogen Peroxide in PEM Fuel Cells. *J. Electrochem. Soc.* **152**, A1165. (doi:10.1149/1.1904988)

47. Chen C, Fuller T. 2007 H2O2 Formation under Fuel-Cell Conditions. *ECS Trans.* **11**, 1127. (doi:10.1149/1.2781025)

48. Shah AA, Ralph TR, Walsh FC. 2009 Modeling and Simulation of the Degradation of Perfluorinated Ion-Exchange Membranes in PEM Fuel Cells. *J. Electrochem. Soc.* **156**, B465. (doi:10.1149/1.3077573)

49. Stuglik Z, PawełZagórski Z. 1981 Pulse radiolysis of neutral iron(II) solutions: oxidation of ferrous ions by OH radicals. *Radiat. Phys. Chem. 1977* **17**, 229–233. (doi:10.1016/0146-5724(81)90336-8)

50. Brillas E, Sirés I, Oturan MA. 2009 Electro-Fenton Process and Related Electrochemical Technologies Based on Fenton's Reaction Chemistry. *Chem. Rev.* **109**, 6570–6631. (doi:10.1021/cr900136g)

Chapter IV

Time-resolved monitoring of PFSA membrane degradation induced by Fenton's reaction

Table of contents

1. Introduction

The previous work permitted to determine the most appropriate concentration of Fenton's reagents producing a degradation believed to be more representative to that occurring during fuel cell operation. It is now interesting to study the evolution of the *ex-situ* chemical degradation induced by Fenton's reaction over the time of exposure to Fenton's reagents and to understand the impact of the chemical degradation on the structure and the functional properties of Nafion™ membranes. In that respect, the chemical degradation of both XL and NR211 membranes was monitored as a function of the exposure time using several indicators such as fluoride emissions and chemical structure evolution, observed by ATR-FTIR spectroscopy. At the end of the degradation process, the impact of the chemical degradation on water sorption and transport properties was evaluated thanks to the DVS analyzer and the liquid-state ^{1}H-NMR spectroscopy. Furthermore, the comparison of results obtained for composite Nafion™ XL with those of the non-reinforced NR211 permitted to provide new understandings on the contribution of chemical and mechanical mitigation strategies against the chemical degradation. As mentioned in § 2 of chapter III, Nafion™ XL membrane contains radical scavengers based on cerium species as well as a mechanical reinforcement based on a microporous PTFE-based layer whereas NR211 one is neither chemically nor mechanically reinforced.

2. Establishment of the time-resolved monitoring of *ex-situ* chemical degradation

Membrane samples were pretreated according to the protocol detailed in § 2.1 of chapter III before being chemically-degraded by exposure to the optimal Fenton's reagents concentration previously determined, *i.e.* 1 ppm of ferrous ions and 3 vol.% of hydrogen peroxide. In that respect, identical setup than that described in § 2.2 of chapter III has been employed: membrane samples were fixed in the polycarbonate frame and fully immersed in the Fenton solution at 80°C and under magnetic stirring for several hours. The experiment lasted a total of 96 hours and the Fenton solution was renewed with fresh reagents at times 0, 24, 36, 48, 60 and 72 hours. Before each renewal, Fenton solutions were collected and further analyzed using the ion-selective electrode in order to evaluate the concentration of fluoride released by the membranes as well as using liquid-state ^{19}F-NMR spectroscopy to identify and quantify other degradation products. The membrane sample was then treated according to the cleaning protocol (more details in § 2.3 of chapter III and § 2 of Appendix A) in order to eliminate any cationic contaminant due to iron ions before being analyzed by FTIR spectroscopy. In addition,

membrane sample was weighed just after the drying step of cleaning protocol and before the FTIR spectroscopy analysis to assess the percent weight loss after chemical degradation. After that, membrane was put back into a fresh Fenton solution to pursue the chemical degradation except for the ending time, *i.e.* after 96 hours, where the membrane was cleaned before being analyzed to evaluate the impact of degradation on membrane functional properties through the measurement of water sorption capacity and water self-diffusion coefficient.

3. Chemical structure evolution after exposure to Fenton's reagents

3.1. ATR-FTIR spectroscopy

FTIR spectroscopy was performed with an ATR accessory to probe only a few micrometers close to the surface of the XL membranes and thus exclude its PTFE-based reinforcement layer from the analysis. Figure 4.1a and 4.1b illustrates the infrared spectra of XL and NR211 membranes, respectively, as a function of the exposure time to the Fenton solution. The spectra are focused in the range 1400 – 850 cm^{-1}, where the characteristic vibration modes of the PFSA are visible. The vibration bands in this range have been assigned in the literature [1–5] and five characteristic vibration bands have been outlined as illustrated in Figure 4.1a (the spectra are normalized to the most intense band at 1144 cm^{-1} associated to the asymmetric -CF_2 stretching mode). As described in § 1.2 of chapter II, the homogeneity of the chemical structure over the surface was verified by systematically performing at least three local measurements on both sides of the samples (pristine or aged with different exposure time). In Figure 4.1a and 4.1b, only one of these local measurements is represented – all the probed areas having a very similar evolution – and the results shows that the IR spectra did not evolve with the exposure time for both XL and NR211 membranes. In order to simplify the reading, the relative intensities of the PFSA side chain stretching bands were averaged over the all range of probed areas as a function of exposure time to Fenton solution (Figure 4.1c). The average relative intensity of the C–O–C and the S–O stretching bands do not vary significantly regardless of the type of membrane, which confirms the absence of IR spectra evolution.

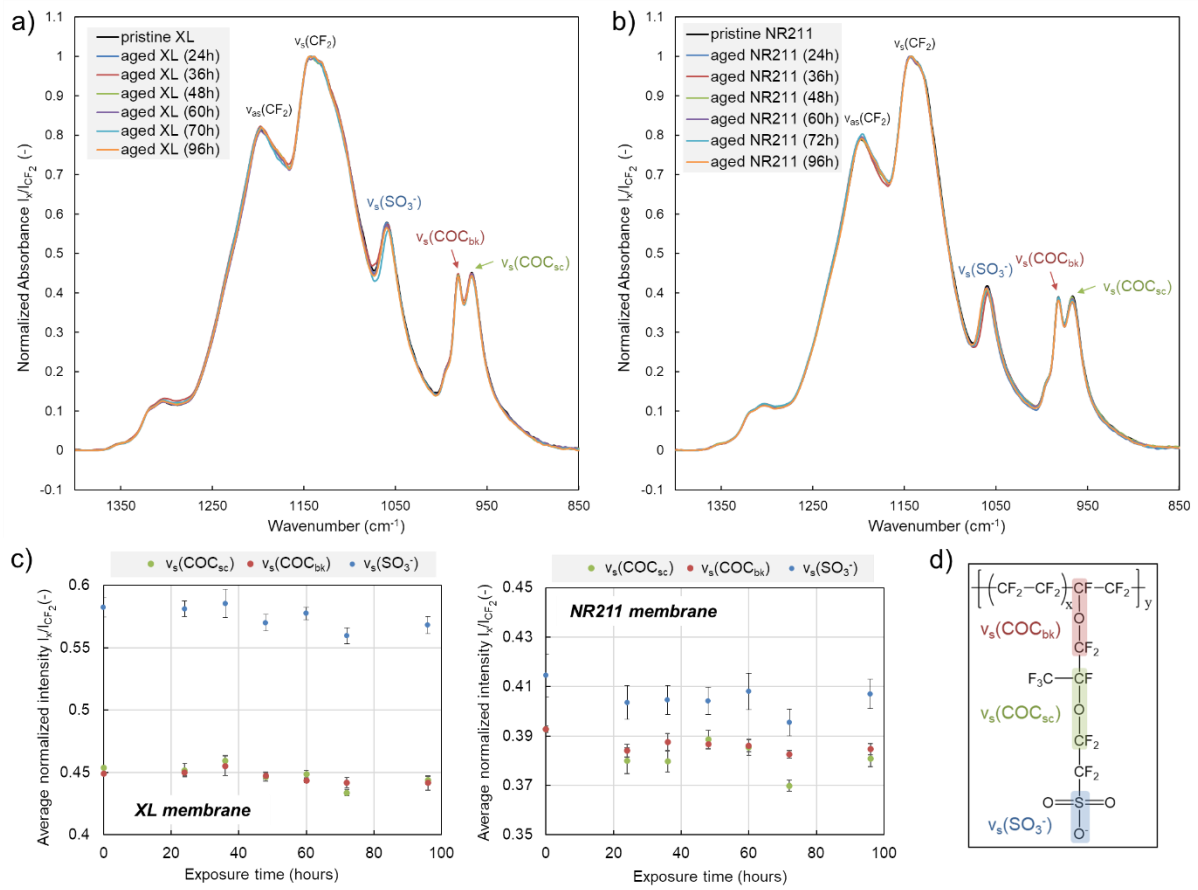

Figure 4.1 – IR spectra (a) of XL and (b) NR211 membranes as a function of the exposure time to Fenton solution and focused on PFSA absorption bands, (c) evolution of average relative intensity of the bands associated to the PFSA side chain over exposure time for XL and NR211 membranes, (d) structure of the PFSA repeat unit and attribution of PFSA side-chain vibration bands [1–5].

The constant intensity ratio between the side chain and the -CF_2 (predominantly in the main chain) vibration bands may result from two distinct behaviors: either there is no significant chemical degradation occurring or the chemical degradation induces both side and main chains decomposition in similar proportion: in this last case, the normalized intensity ratios I_x/I_{CF_2} may not change drastically. It has been shown in the literature that chemical degradation – in both *in-situ* and *ex-situ* conditions – can follow this trend, with possibly an evolution of the chemical structure of Nafion™ membranes that remains non-detectable with FTIR or solid NMR measurements [6–8]. For example, Kundu *et al.* reported no apparent change in chemical structure by FTIR as well as no change in IEC after chemical degradation by Fenton's reaction [6]. Nevertheless, they measured significant fluoride ion emissions and weight losses as well as important morphology evolutions, with the appearance of numerous cracks and bubbles at the membrane surface, evidencing the presence of significant chemical degradation. Furthermore, the constant intensity ratio between -SO_3^- (side chain fragment) and -CF_2 (mostly

main chain fragment) vibration bands also suggests that the IEC does not evolve after exposure to Fenton's reagents, as confirmed by ^{19}F-NMR spectroscopy in the following.

3.2.Solid-state ^{19}F-NMR spectroscopy

Although ATR-FTIR spectroscopy only permits to analyze the ionomer surface (on a few µm depth), it is believed to be quite representative of the overall PFSA structure since the membrane thickness is in the range 25–30 µm and degradations are expected to be homogeneous. Nevertheless, to confirm observations made by ATR-FTIR and to quantify the IEC, the overall chemical structure of degraded XL and NR211 membranes has been analyzed by solid-state ^{19}F-NMR spectroscopy.

Figure 4.2 illustrates the spectra of pristine and degraded Nafion™ membranes as well as the experimental IEC determined from these spectra. The resonance peaks of Nafion™ have been identified and attributed thanks to the work of Chen and Schmidt-Rohr [9]. CF_2 groups of the Nafion™ backbone is attributed to the resonance at -118 ppm by analogy with the NMR signal of PTFE while the CF group located at the junction between the backbone and the side chain gives rise to a peak at -135 ppm. The side chains signals appear at -76 ppm for the CF_3 and CF_2 groups close to ether linkages, at -140 ppm and around -113 ppm for the CF and CF_2 groups close to the sulfonic sites, respectively.

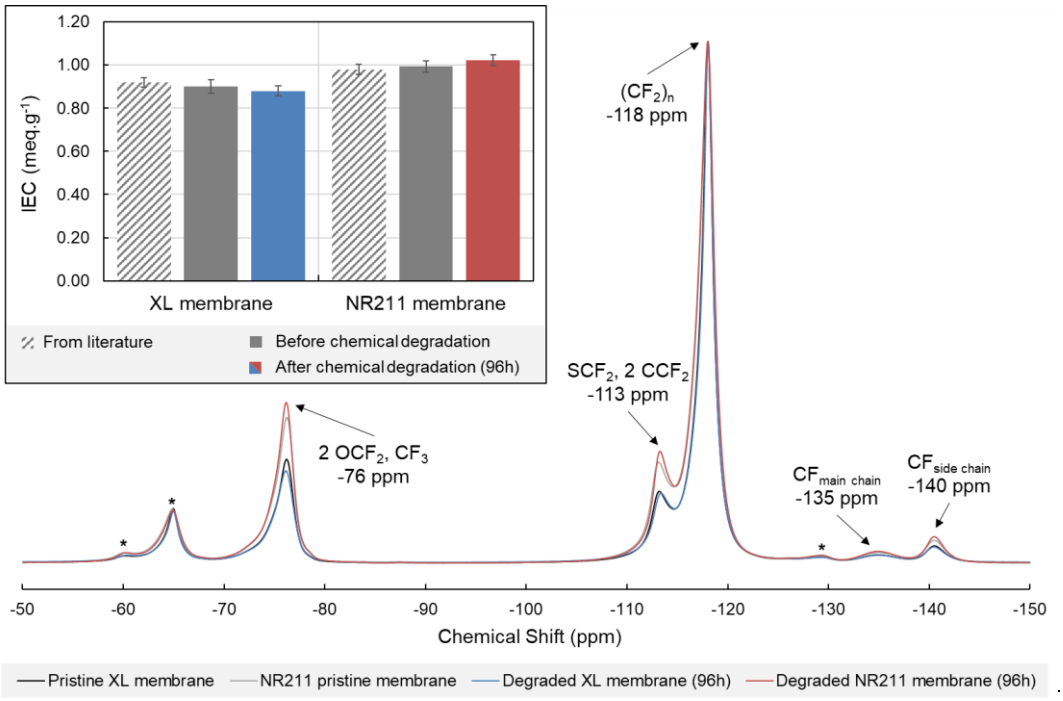

Figure 4.2 – ^{19}F MAS NMR spectra and resonance peak assignment of Nafion™ XL and NR211 membranes before and after chemical degradation. The resonance peaks with an asterisk designate spinning sidebands. The inset illustrates experimental IEC deduced from spectra in comparison with literature values [10,11].

As shown in Figure 4.2, the intensity of side chain resonance peaks does not significantly vary after 96 hours of Fenton's reagents exposure for both membranes, which supports the observations made by ATR-FTIR.

Furthermore, the integral of each resonance peak – associated to a specific fluorinated fragment of the polymer structure – is proportional to the number of fluorine atoms in this fragment. This makes it possible to evaluate the IEC through a theoretical relationship between the IEC and the ratio of the signal integral at -76 ppm ($I_{-76\ ppm}$), to those at -114 and -118 ppm ($I_{-114\ and-118\ ppm}$). The IEC is related to this ratio through n, the number of moles of tetrafluoroethylene (TFE) per moles of comonomer unit, according to the following equation:

$$IEC = \frac{1000}{EW} = \frac{1000}{100n + M} = \frac{1000}{100 \times \left(\frac{7}{4} \times \frac{I_{-114\ and-118\ ppm}}{I_{-76\ ppm}} - 1\right) + M} \quad (4.1)$$

where M designates the molecular weight of vinyl ether monomer, equals to 444 g.mol^{-1}. These peaks were chosen because they are the most intense and best resolved, and the relationship has been validated by previous studies investigating the IEC evolution of Nafion™ membranes by solid-state ^{19}F-NMR spectroscopy [11,12].

For reinforced XL membrane, the IEC determined from the ^{19}F-NMR spectra is impacted by the presence of the PTFE microporous layer. In that respect, this value is denoted as "global IEC" (IEC_g) to distinguish from the value measured in the case of unreinforced PFSA membranes. Although ^{19}F-NMR does not permit to assess directly the IEC of only the PFSA part of composite membranes, the evolution of IEC_g is sufficient to evaluate the effect of chemical degradation since the PTFE microporous layer is believed to have a good chemical stability against radical attacks.

In this work, the IEC of the NR211 and the IEC_g of XL membranes measured before degradation are in good agreement with the supplier datasheet and literature values [10,11]. After 96 hours of exposure, neither the IEC_g of the XL membrane nor the IEC of the NR211 membrane seemed to have changed significantly. This is consistent with the trend observed by ATR-FTIR spectroscopy stating that the main and side chains of Nafion™ membranes decompose in equal proportion. Other indicators are thus needed to confirm the degradation of both membranes.

4. Quantification of the chemical degradation

4.1.Weight loss and fluoride emissions

Weight loss is often considered as one of the primary indicators of PFSA chemical decomposition. Figure 4.3 shows the weight loss of both membranes as a function of time. The loss is significant and seems more pronounced for NR211: after 96 hours of Fenton's reagents exposure, the weight loss is of about 2 % of the initial dry weight for XL membranes and around 10 % for NR211. The presence of a PTFE reinforcement layer in the XL membrane probably helped to mitigate the weight loss thanks to a better mechanical strength [13,14]. Indeed, NR211 appeared more fragile than XL during the visual inspections carried out before each renewal of the solutions. Finally, it must be noted that an unquantifiable fraction of the weight loss may be due to the numerous disassembly and reassembly of the polycarbonate frames containing the membranes during the post-treatment process. Nonetheless, both membranes being subjected to the same protocol, this is not the only cause of their different behavior.

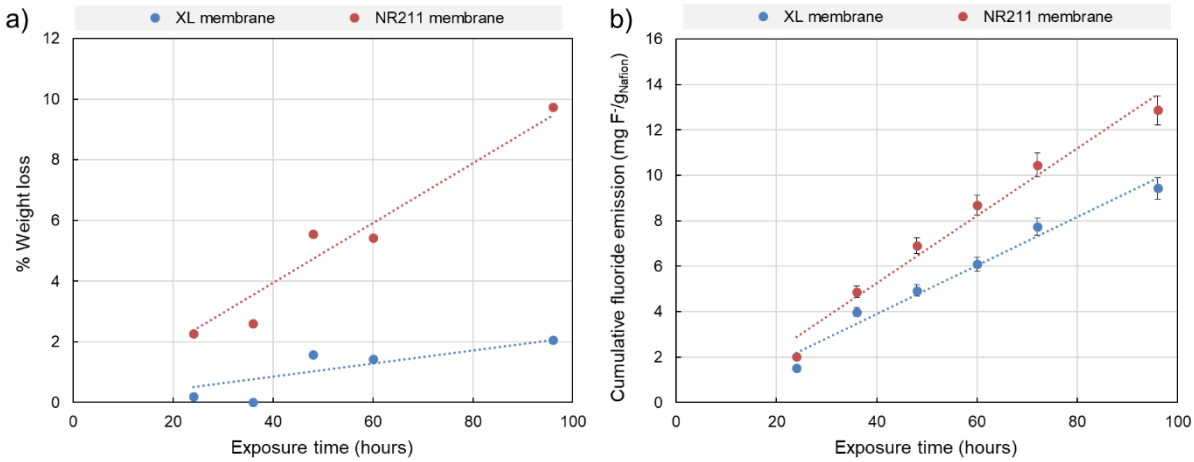

Figure 4.3 – Evolution of (a) percent weight loss and (b) cumulative fluoride emissions of NR211 and XL membranes as a function of exposure time.

Analysis of Fenton solutions after degradation, as well as the water produced during fuel cell operation, is an efficient way to evaluate the membrane degradation through the detection of degradation products. Among them, fluoride ions, related to the production of hydrofluoric acid (HF) due to radical attacks of the polymer, are believed to be a reliable and ease-to-measure indicator of PFSA decomposition [6,15–20]. Figure 4.3 shows significant and regular fluoride emission rates of about 143.7 µg/g_{Nafion}/h for NR211 and 102.4 µg/g_{Nafion}/h for XL (*i.e.* after 96 hours: 12.5 mg F^-/g_{Nafion} for NR211 and 9.1 mg F^-/g_{Nafion} for Nafion™ XL). Such a tendency of the emissions to remain quite constant with time has already been highlighted by several authors [6,15,18]. These results clearly demonstrate the effectiveness of the degradation process by Fenton's reaction, even though no chemical structure evolution of the membranes has been put

forward. Furthermore, the degraded NR211 membrane seems more impacted than the XL. It is also important to notice that the presence of other molecules in the solution cannot be excluded, as it will be seen in the next section.

4.2.Liquid-state ^{19}F NMR spectroscopy

To pursue the identification and monitoring of the degradation products released by the membranes over exposure time, a deeper investigation of the Fenton solutions was carried out using liquid-state ^{19}F-NMR spectroscopy. Figure 4.4 shows the spectra of the Fenton solutions collected between 0 and 24 hours (solution #1), between 24 and 36 hours (solution #2), between 72 and 96 hours (solution #6). They present various sharp resonance peaks corresponding to several fluorinated species. For example, three compounds can be identified in the solution #1 after 24 hours of Fenton's reagents exposure (Figure 4.4):

- The peak at -75.5 ppm is identified as the trifluoroacetic acid (TFA) molecule [21,22],
- The peak at -161 ppm can be attributed to fluoride ions, for which the chemical shift is known to depend on the concentration and/or the counter-ion [23–25],
- A set of resonance peaks, at -80.0 ppm, -80.4 ppm, -82.3 ppm, -82.9 ppm, -83.3 ppm, -118.0 ppm and -126.3 ppm, has been assigned in the literature to the perfluoro(3-oxapentane)-1-sulfonic-4-carboxylic diacid [16,26].

For clarity, the perfluoro(3-oxapentane)-1-sulfonic-4-carboxylic diacid will be thereafter denominated as "product A". It is important to note that some resonance peaks, denoted in Figure 4.4 by the symbol (*), are not yet attributed to specific fluorinated compounds. Some unidentified degradation products are therefore present in solution.

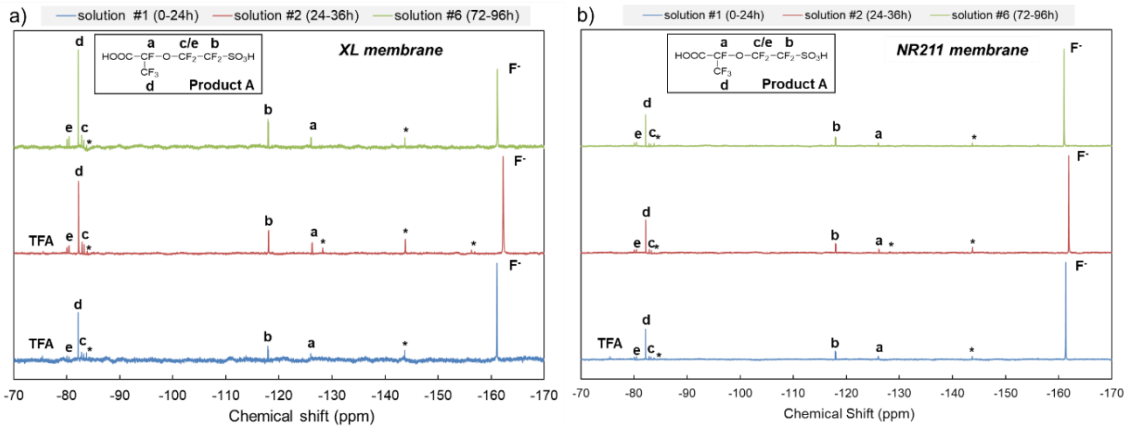

Figure 4.4 – ^{19}F-NMR spectra of Fenton solutions collected after 24, 36 and 96 hours of (a) XL membrane and (b) NR211 membrane exposure to Fenton's reagents. The inset illustrates the chemical structure of product A and the attribution of its resonance peaks. The resonance peaks with an asterisk designate unidentified molecules.

In the literature, analyses of water effluents during fuel cell operation as well as Fenton solutions after *ex-situ* degradation permitted to clearly identify the product A [16,26–28] and the trifluoroacetic acid (TFA) [28,29] as degradation products of PFSA membranes. More particularly, product A has a chemical structure deriving from that of the PFSA side-chain. This compound has also been identified as the main degradation product of PFSA membranes in both *in-situ* (fuel cell operation) and *ex-situ* (Fenton's reaction) aging experiments, demonstrating that the *ex-situ* degradation *via* the Fenton's reaction replicates at least some of the mechanisms involved in fuel cell operation [16]. Furthermore, product A is released by both XL and NR211 membranes all along the degradation process which suggests that the degradation mechanism is similar whether the membrane is reinforced or not and that the mechanism seems to remain unchanged throughout the testing period.

Similarly to fluoride ions, the emissions of product A and TFA have been monitored over time thanks to quantitative NMR measurements. The concentrations of product A and TFA were measured after each solution renewal and compared to that of fluoride ions in Figure 4.5. Although the quantification of fluoride emissions is also possible by ^{19}F-NMR spectroscopy, measurements *via* the ion-selective electrode is more accurate since NMR measurements required the evaporation of water solvent in Fenton solutions, a step during which molecules having a boiling temperature as low as hydrofluoric acid (19.5 °C) may easily evaporate too. Indeed, the analysis of Fenton solutions before and after the evaporation step have been carried out and confirmed that fluoride ions concentrations determined by quantitative NMR are significantly lower than those measured *via* the ion-selective electrode.

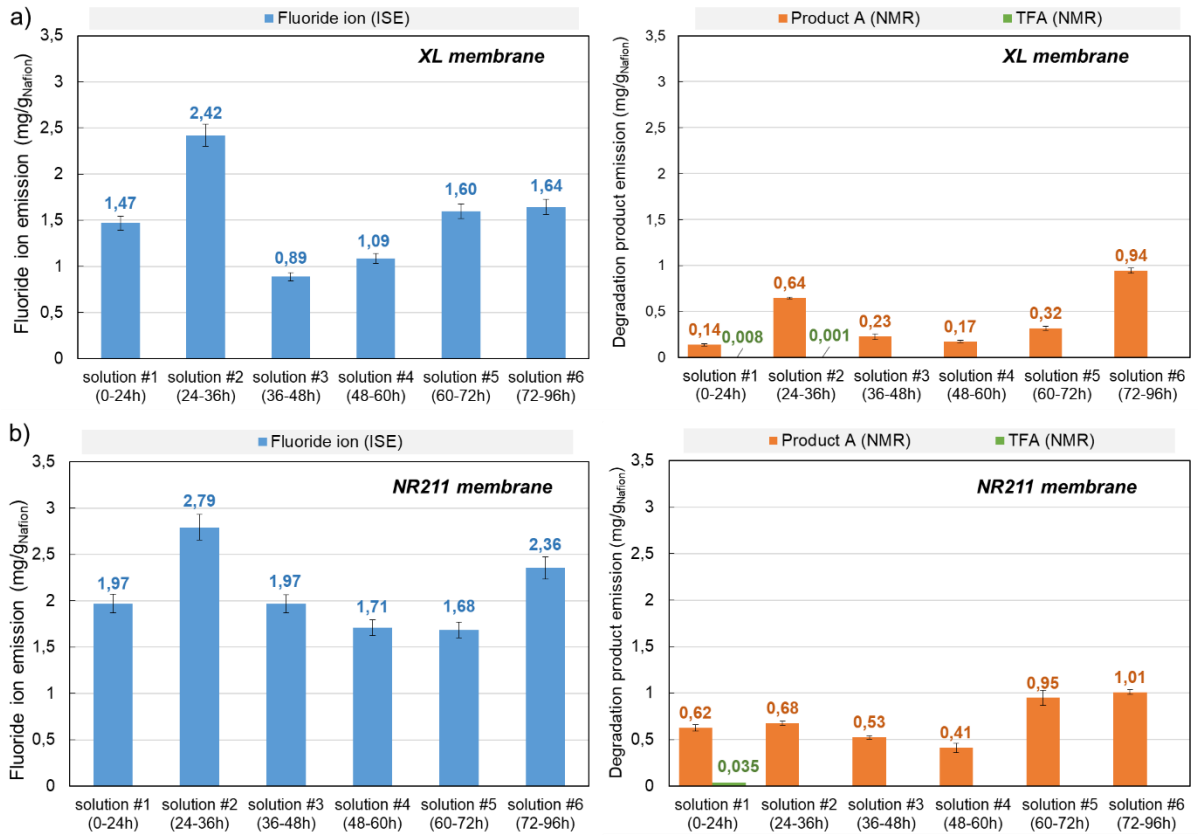

Figure 4.5 – Evolution of the emissions of the degradation products as a function of exposure time for (a) XL and (b) NR211 membranes. The fluoride emissions were evaluated thanks to the ion-selective electrode while the emissions of Product A and TFA were estimated by NMR.

Although the emissions of both fluoride and product A vary during the whole testing period, degradation products are released in the same order of magnitude for both membranes. It can be also noted that degradation product emissions seem slightly higher for NR211 than XL membrane.

4.3.Correlation between weight loss and emissions of degradation products

Table 4.1 summarizes the total amounts of degradation products emitted in solution in comparison with the weight loss. In the case of the XL membrane, the sum of the emissions reveals that 11.89 mg of degradation products per gram of dry Nafion™ have been released during the process. This accounts for about 56% of the global 20.6 mg/g$_{Nafion}$ weight loss. In the case of NR211, a total amount of 17.11 mg of degradation products per gram of dry Nafion™ have been detected, which only represents 15 wt.% of the total weight loss. As mentioned earlier, an unknown but significant fraction of the weight loss may be due to the multiple disassembly/reassemblies involved in the degradation protocol, more specifically in the case of the unreinforced NR211 membrane.

Table 4.1 – Weight loss analysis of PFSA membranes after 96 hours of chemical degradation.

	Material loss (mg/g_{Nafion})	Fluoride ion (mg/g_{Nafion})	Product A (mg/g_{Nafion})	TFA (mg/g_{Nafion})
XL membrane	20.60	9.10	2.44	0.01
NR211 membrane	108.30	12.48	4.20	0.04

Moreover, some degradation products were not identified (see § 4.2 and Figure 4.4) and/or may have evaporated during the degradation process, the system being not perfectly sealed. One must note that fluoride ions, which are present as hydrofluoric acid in acidic media, as well as other small molecules like TFA (its boiling temperature being 72°C) could evaporate upon degradation process taking place at 80°C. Finally, non-fluorinated molecules such as sulfate SO_4^{2-} or hydrogen sulfate HSO_4^- ions can also be released by the membranes in solution during the degradation process [16,28–31].

5. Impact of the degradation on PFSA membranes functional properties

5.1.Water sorption capacity in aged membranes

The water sorption property of PFSA membranes is strongly related to their microstructure and ion-exchange capacity (IEC). The sigmoidal shape of the sorption isotherm is a result of the specific two-phase separated morphology of the membrane in which hydrophilic sulfonic sites, hydrophobic phase and water molecules coexist. Water sorption in Nafion™ is generally associated to three distinct sorption mechanisms: the dissociation of the sulfonic groups at low water activity a_w, the adsorption of water molecules and the growth of hydrophilic domains for intermediate hydration levels and the aggregation of water molecules with a bulk-like behavior at high water activities. The first adsorption mechanism, described by the Langmuir adsorption model, characterizes the formation of the solvation shell where sulfonic groups form strong hydrogen bonds with water molecules. For intermediate hydration levels, the adsorbed water molecules are tightly bonded to the initial hydration shell and the mechanism is controlled by Henry's law: this step characterizes the solubility of water within the polymer phase. Finally, the weakly bonded water molecules aggregate when the water activity increases, which entails a macroscopic swelling of the membrane in accordance with its mechanical properties. This swelling conducts to the growth of the hydrophilic domains and their interconnection to form a percolated network of water. In this respect, contribution of Langmuir (C_L) and Henry's (C_H) sorption mechanisms were obtained by fitting experimental data for water activities a_w between 0 and 0.6 according to the following equation [32,33]:

$$\frac{\Delta m}{m} = C_L + C_H = \frac{A * B * a_w}{1 + B * a_w} + C * a_w \quad (4.2)$$

where $\frac{\Delta m}{m}$ designates the water uptake (wt.%), *A* and *B* are two parameters describing the Langmuir sorption mode and *C* is the Henry's solubility constant. The Cluster sorption contribution is then deduced by subtracting the Langmuir and Henry's contributions from the experimental data. The fitting parameters are listed in Table 4.2.

Table 4.2 – Fitting parameters of water sorption isotherm for $0 < a_{water} < 0.60$.

	Pristine XL membrane	Degraded XL membrane (96h)	Pristine NR211 membrane	Degraded NR211 membrane (96h)
Parameter A (-)	1.81 ± 0.16	1.27 ± 0.11	2.25 ± 0.13	1.50 ± 0.15
Parameter B (-)	21.40 ± 5.03	32.49 ± 9.52	25.65 ± 4.30	29.60 ± 8.50
Parameter C (-) (Henry's slope)	7.80 ± 0.25	7.22 ± 0.19	9.58 ± 0.21	8.49 ± 0.28

Figure 4.6 shows the evolution of the sorption isotherms after chemical degradation as well as their decomposition into the three mechanisms. The water content decreases slightly after degradation in both cases: for XL membrane, this evolution can be attributed to a decrease of the Langmuir component as well as a reduced Henry's slope (7.2 *vs.* 7.8 for the pristine XL membrane). This water-uptake is nevertheless compensated by a better aggregation of water molecules at high water activity. In the case of the NR211 membrane, similar trends are observed at low and intermediate water activities, with a decrease of the Henry's slope from 9.6 to 8.8, but no significant increase at high water activities.

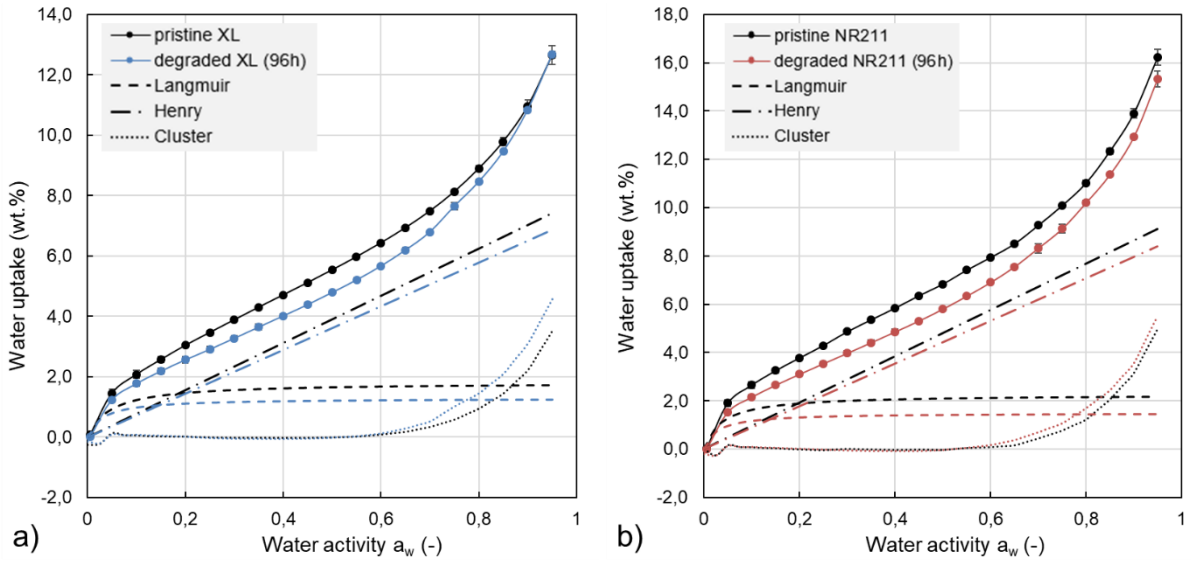

Figure 4.6 – Water sorption isotherms (30°C) decomposed into three adsorption mechanisms of (a) XL and (b) NR211 membranes after 96 hours of Fenton's reagents exposure in comparison with pristine membranes. Five measurements were performed on the pristine XL in order to control the repeatability of the measurements and of the pretreatment process. In the case of the degraded membranes, the initial samples were cut into two pieces and the results of the two measurements were averaged.

5.2.Water self-diffusion after chemical degradation

The water diffusion coefficient in PFSA membranes is commonly measured thanks to Pulsed-Field Gradient (PFG) NMR experiments. Before detailing these results, it is worth noting that our previous study has shown that the ^{1}H-NMR spectra of both pristine and aged membranes exhibit two resonance peaks corresponding to two different water populations, *i.e.* water molecules with different chemical environments [12]. Both these water populations have also been observed in the present study for both pristine and degraded membranes, whether reinforced or not. One of the two resonance peaks is very intense and well resolved while the other has a very low intensity and can be largely overlapped with the main peak in certain hydration conditions. This makes it difficult to follow the evolution of the small resonance peak. For this reason, only the water self-diffusion coefficient of the most intense peak is considered thereafter.

Figure 4.7 shows the evolution of the diffusion coefficient as a function of the water uptake for the pristine and degraded membranes. Firstly, there is a noticeable dispersion in the case of pristine membranes, which may highlight a consequential heterogeneity in pristine state. Furthermore, water self-diffusion coefficients of pristine XL and NR211 membranes are in agreement with those reported in the literature for first generation Nafion™ membranes [34–36].

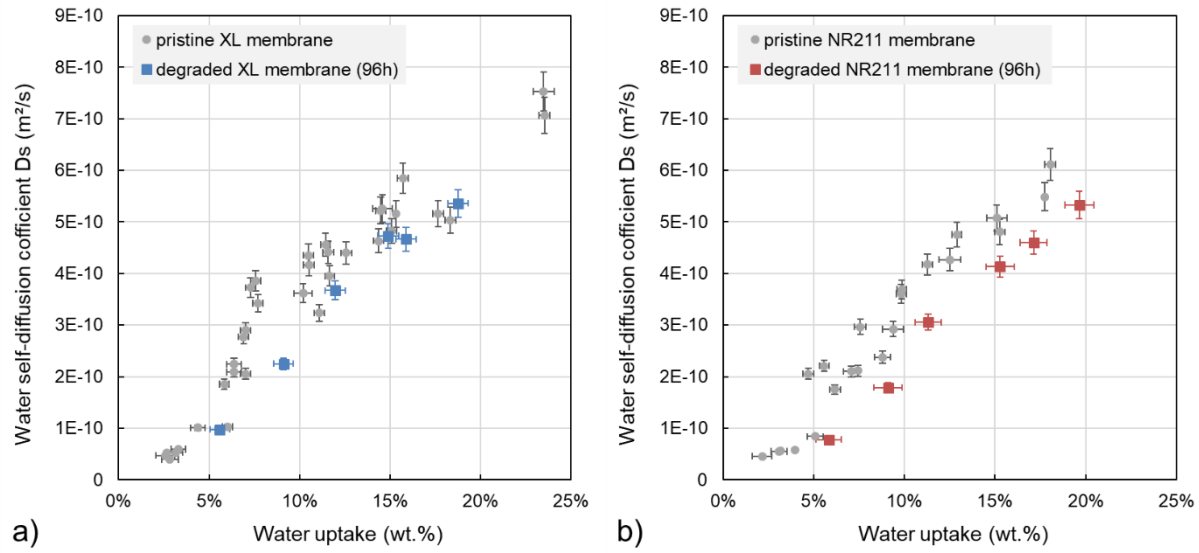

Figure 4.7 – Water self-diffusion coefficient evolution after 96 hours of Fenton's reagents exposure as a function of water uptake in (a) XL and (b) NR211 membranes (squared symbols) in comparison with pristine membranes (circles).

A 96 hours exposure to Fenton's reagents does not lead to significant modifications of the diffusion coefficient *vs.* water activity plots: in the case of degraded XL, the water self-diffusion coefficient is very close to the lower limit of values obtained for a pristine membrane. However, the water self-diffusion coefficient of degraded NR211 seems slightly lower than that of pristine state, regardless of the water uptake.

6. Discussions

6.1. Comparison of PFSA membrane degradation with literature

Our multi-techniques investigation demonstrates that both reinforced XL and unreinforced NR211 membranes experience non-negligible chemical decomposition with distinct degradation levels. Several complementary indicators, such as weight loss, fluoride and product A – perfluoro(3-oxapentane)-1-sulfonic-4-carboxylic diacid – emissions provided evidences of effective chemical degradation of membranes as a result of radical attacks. However, ATR-FTIR and solid-state ^{19}F-NMR analyses indicated that neither the chemical structure nor the IEC/IEC$_g$ varied. The PFSA membrane degradation mechanisms proposed in the literature involve either radical attacks on both the main and side chains or polymer decomposition starting from the side chains, propagating along the polymer structure, and possibly resulting into the severing of the main chains [37]. In the first case, the chemical degradation can occur without impacting the structure of the polymer repeating unit and thus, does not entail the evolution of the IR or ^{19}F-NMR spectra, as observed in this work. Furthermore, the PFSA

degradation mechanisms result from the attack of hydroxyl ($HO^{\bullet}$) and/or hydrogen ($H^{\bullet}$) radicals on vulnerable sites while Fenton's reaction only generates hydroxyl radicals [37]. In this regard, among the various degradation mechanisms implying the $HO^{\bullet}$ radical attack, the presence of product A in our solutions can only be explained by the unzipping reaction on PFSA backbone propagating up to the junction with a side chain and thus leading to its entire loss [29,38]. Although it has been demonstrated that chemically stabilized Nafion™ membranes present a reduced number of reactive end groups, they are nevertheless not completely free of vulnerable sites [15]. Moreover, it has been recently shown that although chemically stabilized Nafion™ membranes had lower fluoride emission rates than conventional ones, large fluorinated molecules were still emitted in equivalent or sometimes higher proportions [26,39]: chemical stabilization decreases the ionomer vulnerability against main chain radical attacks but does not inhibit its chemical decomposition *via* unzipping reaction. Additionally, TFA molecules have also been identified in Fenton solution and they can have two origins:

- *via* the radical attack of hydroxyl radical $HO^{\bullet}$ on the ether bond of PFSA side chain, thus leading to the formation of TFA and $HO\text{-}CF_2\text{-}CF_2\text{-}SO_3H$ molecules according to Chen and Fuller [29],
- or through the decomposition of product A into TFA and $HOOC\text{-}CF_2\text{-}SO_3H$ *via* unzipping mechanism, as suggested by Xie and Hayden [38].

Since we did not observe significant IEC evolution, the chemical decomposition of PFSA most probably occurred with proportional losses of backbone and side chain fragments in the polymer repeating unit, meaning that PFSA backbone unzipping reaction predominated and led to the entire loss of side chain and thus the formation of product A.

The evolutions of water sorption capacity and water self-diffusion coefficient showed that neither the water-uptake behavior nor the water mobility in XL and NR211 membranes were significantly altered after 96 hours of Fenton's reagents exposure. Although the chemical degradation of XL and NR211 membranes was clearly evidenced, it remained probably quite limited compared to what can occur after several thousand hours of operation in fuel cells: this can explain the moderate impact on membranes functional properties. A direct comparison with the literature is delicate because of the various operating conditions applied – the H_2O_2 concentration being comprised between 3 and 30 % and that of the Fe^{2+} catalyst between 3 and 6000 ppm –; however, the fluoride emission rates we measured were small but realistic [6,15,18]. Recently, Shi *et al.* studied the mechanical properties of Nafion™ XL and NR212

membranes after exposure to Fenton's reagents [40]. Their fluoride emission rates were larger than ours, with more variations between unreinforced NR212 and reinforced XL membranes. However, the authors performed their experiments in more severe conditions than ours: their Fenton's reagents concentration was of about 22.5 % for H_2O_2 and 14 ppm for ferrous ions whereas we have only 3 v% of H_2O_2 and 1 ppm of Fe^{2+}. Indeed, it has been recently demonstrated that the fluoride emission rate depends highly on Fenton's reagents concentration [41,42], with systematically lower emission for reinforced XL membranes than their unreinforced counterparts. Moreover, it has been shown that the use of high hydrogen peroxide concentration conducts to severe morphological changes which are – most probably – not representative of fuel cell operating conditions [41,42]. Therefore, in the present work, the moderate concentrations of Fenton's reagents chosen are believed to better replicate the chemical degradation occurring during fuel cell operation.

6.2. Contribution of reinforcement layer and radical scavengers against chemical degradation

The liquid-state ^{19}F-NMR analysis demonstrated that the chemical degradation mechanisms are similar for XL and NR211 membranes and that the emissions of degradation products are slightly lower for reinforced XL than unreinforced NR211 membrane all along the degradation process. When plotted as a function of the exposure time, the cumulative emissions of product A and fluoride ions increase quite linearly, showing rather constant emission rates (Figure 4.8).

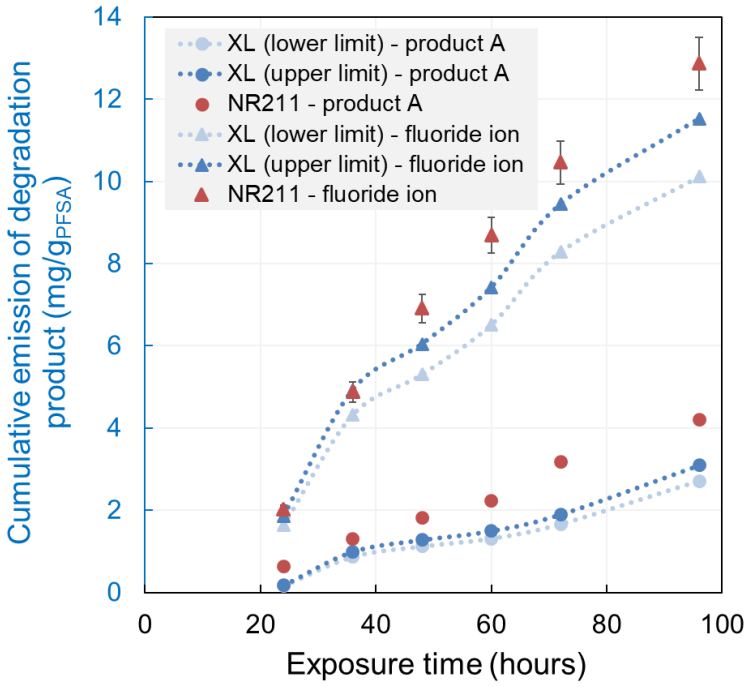

Figure 4.8 – Cumulative emissions of degradation products, expressed in mg/g_{PFSA}, *vs.* exposure time for XL (in blue) and NR211 (in red) membranes. Fluoride emissions (triangle symbols) were evaluated thanks to the ion-selective electrode while the emissions of Product A (circles) were estimated by quantitative NMR experiments. TFA emissions are not represented due to their low concentrations. Dotted lines designate the lower/upper limits of fluoride emissions when the PTFE-layer fraction in XL membrane is considered.

However, emissions of degradation products are expressed here in terms of Nafion™ dry weight and the presence of a reinforcement layer in XL membrane is thus not considered. PTFE being believed to have a greater chemical resistance against radical attacks than PFSA, it could be argued that fluoride emissions only result from the degradation of the PFSA ionomer. Moreover, PTFE containing only -CF_2 groups, it cannot release product A. Consequently, the fraction of PTFE-layer must be considered in order to properly compare the emissions of degradation products of XL and NR211 membranes. Thanks to wide-angle X-ray scattering (WAXS) measurements, the PTFE fraction in pristine XL membrane has been evaluated around 21 % [43,44]. On the other hand, Shi *et al.* [44] stated that Nafion™ XL membrane should contain 10 % of PTFE, 75 % to 90 % of PFSA/TFE copolymer and up to 5 % of proprietary additive compounds. Considering those two values as maximum and minimum limits, the lower and upper boundaries of the actual amount of degradation products emitted per gram of PFSA can be calculated and plotted in Figure 4.8. When expressed in mg/g_{PFSA}, we can observe that the emission of product A is consistently lower with XL membranes, indicating a lower degradation rate than its unreinforced counterpart. The same trend can be observed with fluorine emission, although the difference between XL and NR211 membranes is slightly less pronounced. Considering the evolution of the emissions of fluorine and product A, the PFSA

in reinforced XL membranes seems more chemically stable than in NR211 membrane. The better chemical durability of XL membrane could be assigned to the presence of the reinforcement layer and/or the presence of cerium-based radical scavengers into the membrane. Better mechanical properties of composite membranes have been indeed proven [35,37,38] and could explain, at least partially, the reinforcement contribution in protecting or slowing down the PFSA degradation by ensuring a better membrane integrity and thus preventing further chemical decomposition. On the other hand, the introduction of cerium-based radical scavengers limits the radicals concentration and thus the chemical degradation, as demonstrated by D'Urso *et al.* in the case of reinforced Aquivion® PFSA membranes [45]. The authors indeed showed that the introduction of SiO_2 supported cerium-based radical scavengers into reinforced Aquivion® membranes permitted to decrease by around 40 % the fluoride emission rate comparatively to a membrane free of radical scavenger. On another note, Shi *et al.* recently reported fluoride emission rates more than three times higher for NR212 than XL membranes and suggested that this discrepancy could be ascribed by the addition of radical scavengers [40]. To the best of our knowledge, no publication or commercial information have mentioned the presence of radical scavengers in NR211 or NR212 membranes. Consequently, the presence of radical scavengers in Nafion™ XL membrane could also explain its better resistance against chemical attacks.

Finally, we recently studied the chemical degradation of reinforced PFSA membranes after 12860 hours [42] of fuel cell operation. The significant intensity decrease of C–O–C and S–O stretching bands detected by ATR-FTIR spectroscopy indicated a partial loss of the PFSA side chains as well as a significant IEC reduction. Additionally, a decrease of water sorption capacity as well as a reduced water mobility have been observed and it has been suggested that this trend could be partly due to the partial loss of sulfonic groups by side chain cleavages. Such results are clearly different from those reported here following *ex-situ* chemical stress tests, since neither chemical structure evolution nor significant change of water uptake and water diffusion was observed. This may indicate that the polymer decomposition caused by radical attacks during short duration (*i.e.* 96 *vs.* > 12000 hours) – even though the Fenton process employed here is supposed to mimic an accelerated degradation – is not fully representative of the impact of membrane degradation on water sorption and transport properties. Degradation occurring during fuel cell operation is indeed believed to occur due to complex and interrelated mechanical and chemical degradation mechanisms. Future studies of the impact of conjoint chemical and mechanical *ex-situ* degradation modes on PFSA membrane structure and

properties will probably help to complement our understandings of PFSA degradation mechanisms and aging phenomena.

7. Conclusions

The impact of *ex-situ* chemical degradation induced by Fenton's reaction on the structure and the water sorption and transport properties of composite Nafion™ XL membrane was explored and compared to that of unreinforced Nafion™ NR211 membrane. Recent investigations have been only focused on the impact of chemical degradation or the contribution of reinforcement layer to the mechanical durability of XL membrane, but none of them have studied its chemical stability. This study aimed at providing some understandings on the chemical degradation of PFSA membranes and clarifying the contribution of the reinforcement layer and radical scavengers of XL membrane on polymer decomposition rate. The results permitted to highlight the following items:

- Reinforced XL membrane is chemically degraded by the exposure to Fenton's reagents, even though it contains an additional reinforcement layer and radical scavengers comparatively to its non-reinforced analogue, the NR211 membrane. In addition to important weight loss, fluoride concentration measurements using ion-selective electrode and liquid-state ^{19}F-NMR analysis highlighted significant emissions of fluoride ions and perfluoro(3-oxapentane)-1-sulfonic-4-carboxylic diacid (named product A in the paper for clarity), a fluorinated compound deriving from the PFSA side chains which has been already identified in the literature as one of the main PFSA degradation products. Moreover, the presence of identical degradation products for both membranes throughout the degradation process demonstrates that the degradation mechanisms are identical.
- In spite of significant chemical degradation, ATR-FTIR and solid-state ^{19}F-NMR analyses of degraded membranes highlighted no chemical structure evolution as well as no IEC/IEC_g variation, suggesting that degradation of the PFSA main and side chains takes place in equal proportions. Furthermore, the release of product A by the membranes while the IEC_g/IEC of XL and NR211 do not vary could imply that the polymer decomposition occurs *via* an unzipping reaction and leads to the loss of the side chains. Nevertheless, the water sorption and diffusion in degraded XL and NR211 membranes seem not to be significantly altered by the chemical degradation.

- Comparatively to NR211 membrane, when the emissions of degradation products are expressed in mg/g_{PFSA} to discriminate the presence of PTFE reinforcement layer in XL membrane and thus consider solely PFSA degradation, the composite XL membrane seems more enduring against radical attacks than its non-reinforced analogue. This difference may be explained by the presence of the additional PTFE layer, which could help to maintain the membrane mechanical integrity and thus avoid further chemical decomposition, and/or by the presence of cerium-based radical scavengers into the XL membrane which can mitigate the radical attacks on the polymer chains.

References

1. Mauritz KA, Moore RB. 2004 State of Understanding of Nafion. *Chem. Rev.* **104**, 4535–4586. (doi:10.1021/cr0207123)

2. Korzeniewski C, Snow DE, Basnayake R. 2006 Transmission infrared spectroscopy as a probe of Nafion film structure: analysis of spectral regions fundamental to understanding hydration effects. *Appl. Spectrosc.* **60**, 599–604. (doi:10.1366/000370206777670620)

3. Liang Z, Chen W, Liu J, Wang S, Zhou Z, Li W, Sun G, Xin Q. 2004 FT-IR study of the microstructure of Nafion® membrane. *J. Membr. Sci.* **233**, 39–44. (doi:10.1016/j.memsci.2003.12.008)

4. Laporta M, Pegoraro M, Zanderighi L. 1999 Perfluorosulfonated membrane (Nafion): FT-IR study of the state of water with increasing humidity. *Phys. Chem. Chem. Phys.* **1**, 4619–4628. (doi:10.1039/A904460D)

5. Cable KM, Mauritz KA, Moore RB. 1995 Effects of hydrophilic and hydrophobic counterions on the Coulombic interactions in perfluorosulfonate ionomers. *J. Polym. Sci. Part B Polym. Phys.* **33**, 1065–1072. (doi:10.1002/polb.1995.090330710)

6. Kundu S, Simon LC, Fowler MW. 2008 Comparison of two accelerated Nafion^{TM} degradation experiments. *Polym. Degrad. Stab.* **93**, 214–224. (doi:10.1016/j.polymdegradstab.2007.10.001)

7. Fernandes AC, Ticianelli EA. 2009 A performance and degradation study of Nafion 212 membrane for proton exchange membrane fuel cells. *J. Power Sources* **193**, 547–554. (doi:10.1016/j.jpowsour.2009.04.038)

8. Bas C, Flandin L, Danero A-S, Claude E, Rossinot E, Alberola ND. 2010 Changes in the Chemical Structure and Properties of a Perfluorosulfonated Acid Membrane Induced by Fuel-Cell Operation. *J. Appl. Polym. Sci.* **117**, 2121–2132. (doi:10.1002/app.31386)

9. Chen Q, Schmidt-Rohr K. 2004 F-19 and C-13 NMR signal assignment and analysis in a perfluorinated ionomer (Nafion) by two-dimensional solid-state NMR. *Macromolecules* **37**, 5995–6003. (doi:10.1021/ma049759b)

10. In press. DuPont Product Information: Nafion NR-211 and NR-212 PFSA membrane, 2008. See http://www.fuelcellsetc.com/store/DS/N211-N212-properties.pdf.

11. Moukheiber E, De Moor G, Flandin L, Bas C. 2012 Investigation of ionomer structure through its dependence on ion exchange capacity (IEC). *J. Membr. Sci.* **389**, 294–304. (doi:10.1016/j.memsci.2011.10.041)

12. Robert M, El Kaddouri A, Perrin J-C, Leclerc S, Lottin O. 2018 Towards a NMR-Based Method for Characterizing the Degradation of Nafion XL Membranes for PEMFC. *J. Electrochem. Soc.* **165**, F3209–F3216. (doi:10.1149/2.0231806jes)

13. Khattra NS, Lu Z, Karlsson AM, Santare MH, Busby FC, Schmiedel T. 2013 Time-dependent mechanical response of a composite PFSA membrane. *J. Power Sources* **228**, 256–269. (doi:10.1016/j.jpowsour.2012.11.116)

14. Tang Y, Kusoglu A, Karlsson AM, Santare MH, Cleghorn S, Johnson WB. 2008 Mechanical properties of a reinforced composite polymer electrolyte membrane and its simulated performance in PEM fuel cells. *J. Power Sources* **175**, 817–825. (doi:10.1016/j.jpowsour.2007.09.093)

15. Curtin DE, Lousenberg RD, Henry TJ, Tangeman PC, Tisack ME. 2004 Advanced materials for improved PEMFC performance and life. *J. Power Sources* **131**, 41–48. (doi:10.1016/j.jpowsour.2004.01.023)

16. Healy J, Hayden C, Xie T, Olson K, Waldo R, Brundage A, Gasteiger H, Abbott J. 2005 Aspects of the chemical degradation of PFSA ionomers used in PEM fuel cells. *Fuel Cells* **5**, 302–308. (doi:10.1002/fuce.200400050)

17. Tang H, Peikang S, Jiang SP, Wang F, Pan M. 2007 A degradation study of Nafion proton exchange membrane of PEM fuel cells. *J. Power Sources* **170**, 85–92. (doi:10.1016/j.jpowsour.2007.03.061)

18. Merlo L, Ghielmi A, Cirillo L, Gebert M, Arcella V. 2007 Resistance to peroxide degradation of Hyflon® Ion membranes. *J. Power Sources* **171**, 140–147. (doi:10.1016/j.jpowsour.2006.11.012)

19. Mu S, Xu C, Yuan Q, Gao Y, Xu F, Zhao P. 2013 Degradation behaviors of perfluorosulfonic acid polymer electrolyte membranes for polymer electrolyte membrane fuel cells under varied acceleration conditions. *J. Appl. Polym. Sci.* **129**, 1586–1592. (doi:10.1002/app.38785)

20. Kusoglu A, Calabrese M, Weber AZ. 2014 Effect of Mechanical Compression on Chemical Degradation of Nafion Membranes. *ECS Electrochem. Lett.* **3**, F33–F36. (doi:10.1149/2.008405eel)

21. Ellis DA, Martin JW, Muir DCG, Mabury SA. 2000 Development of an 19F NMR Method for the Analysis of Fluorinated Acids in Environmental Water Samples. *Anal. Chem.* **72**, 726–731. (doi:10.1021/ac9910280)

22. Pretsch E, Bühlmann P, Badertscher M. 2009 *Structure Determination of Organic Compounds: Tables of Spectral Data*. 4th edn. Berlin Heidelberg: Springer-Verlag. (doi:10.1007/978-3-540-93810-1)

23. Schaumburg K, Deverell C. 1968 Fluorine-19 nuclear magnetic resonance chemical shift of hydrofluoric acid in normal water and heavy water solutions. *J. Am. Chem. Soc.* **90**, 2495–2499. (doi:10.1021/ja01012a009)

24. Alzewel K. 1974 Relaxation-Time Measurements on Fluoride Ions in Aqueous-Solutions. *Z. Phys. Chem.-Leipz.* **255**, 193–198.

25. Hudlicky M. 1985 Chemical shifts of fluorine in hydrogen fluoride and fluoride ion. *J. Fluor. Chem.* **28**, 461–472. (doi:10.1016/S0022-1139(00)81136-7)

26. Takasaki M, Nakagawa Y, Sakiyama Y, Tanabe K, Ookubo K, Sato N, Minamide T, Nakayama H, Hori M. 2013 Degradation Study of Perfluorosulfonic Acid Polymer Electrolytes: Approach from Decomposition Product Analysis. *J. Electrochem. Soc.* **160**, F413–F416. (doi:10.1149/2.076304jes)

27. Zhou C, Guerra MA, Qiu Z-M, Zawodzinski Thomas A, Schiraldi DA. 2007 Chemical Durability Studies of Perfluorinated Sulfonic Acid Polymers and Model Compounds under Mimic Fuel Cell Conditions. *Macromolecules* **40**, 8695–8707. (doi:10.1021/ma071603z)

28. Carlsson AH, Joerissen L. 2009 Accelerated Degradation of Perfluorinated Sulfonic Acid Membranes. *ECS Trans.* **25**, 725–732. (doi:10.1149/1.3210624)

29. Chen C, Fuller TF. 2009 The effect of humidity on the degradation of Nafion® membrane. *Polym. Degrad. Stab.* **94**, 1436–1447. (doi:10.1016/j.polymdegradstab.2009.05.016)

30. Kinumoto T, Inaba M, Nakayama Y, Ogata K, Umebayashi R, Tasaka A, Iriyama Y, Abe T, Ogumi Z. 2006 Durability of perfluorinated ionomer membrane against hydrogen peroxide. *J. Power Sources* **158**, 1222–1228. (doi:10.1016/j.jpowsour.2005.10.043)

31. Wang F, Tang H, Pan M, Li D. 2008 Ex situ investigation of the proton exchange membrane chemical decomposition. *Int. J. Hydrog. Energy* **33**, 2283–2288. (doi:10.1016/j.ijhydene.2008.01.052)

32. Feng H. 2007 Modeling of vapor sorption in glassy polymers using a new dual mode sorption model based on multilayer sorption theory. *Polymer* **48**, 2988–3002. (doi:10.1016/j.polymer.2006.10.050)

33. Li Y, Nguyen QT, Buquet CL, Langevin D, Legras M, Marais S. 2013 Water sorption in Nafion (R) membranes analyzed with an improved dual-mode sorption model Structure/property relationships. *J. Membr. Sci.* **439**, 1–11. (doi:10.1016/j.memsci.2013.03.040)

34. Zawodzinski TA, Neeman M, Sillerud LO, Gottesfeld S. 1991 Determination of water diffusion coefficients in perfluorosulfonate ionomeric membranes. *J. Phys. Chem.* **95**, 6040–6044. (doi:10.1021/j100168a060)

35. Edmondson CA, Fontanella JJ, Chung SH, Greenbaum SG, Wnek GE. 2001 Complex impedance studies of S-SEBS block polymer proton-conducting membranes. *Electrochimica Acta* **46**, 1623–1628. (doi:10.1016/S0013-4686(00)00762-3)

36. Ma S, Chen Q, Jøgensen FH, Stein PC, Skou EM. 2007 19F NMR studies of Nafion^{TM} ionomer adsorption on PEMFC catalysts and supporting carbons. *Solid State Ion.* **178**, 1568–1575. (doi:10.1016/j.ssi.2007.10.007)

37. Zatoń M, Rozière J, Jones DJ. 2017 Current understanding of chemical degradation mechanisms of perfluorosulfonic acid membranes and their mitigation strategies: a review. *Sustain. Energy Fuels* **1**, 409–438. (doi:10.1039/C7SE00038C)

38. Xie T, Hayden CA. 2007 A kinetic model for the chemical degradation of perfluorinated sulfonic acid ionomers: Weak end groups versus side chain cleavage. *Polymer* **48**, 5497–5506. (doi:10.1016/j.polymer.2007.07.043)

39. Schlick S. 2017 *The Chemistry of Membranes Used in Fuel Cells: Degradation and Stabilization*. First. Hoboken, NJ (USA): John Wiley & Sons.

40. Shi S *et al.* 2020 Fatigue crack propagation behavior of fuel cell membranes after chemical degradation. *Int. J. Hydrog. Energy* , S0360319920326884. (doi:10.1016/j.ijhydene.2020.07.113)

41. Frensch SH, Serre G, Fouda-Onana F, Jensen HC, Christensen ML, Araya SS, Kær SK. 2019 Impact of iron and hydrogen peroxide on membrane degradation for polymer electrolyte membrane water electrolysis: Computational and experimental investigation on fluoride emission. *J. Power Sources* **420**, 54–62. (doi:10.1016/j.jpowsour.2019.02.076)

42. Robert M, El Kaddouri A, Perrin J-C, Mozet K, Daoudi M, Dillet J, Morel J-Y, André S, Lottin O. 2020 Effects of conjoint mechanical and chemical stress on perfluorosulfonic-acid membranes for fuel cells. *J. Power Sources* **476**, 228662. (doi:10.1016/j.jpowsour.2020.228662)

43. Mukundan R, Baker AM, Kusoglu A, Beattie P, Knights S, Weber AZ, Borup RL. 2018 Membrane Accelerated Stress Test Development for Polymer Electrolyte Fuel Cell Durability Validated Using Field and Drive Cycle Testing. *J. Electrochem. Soc.* **165**, F3085–F3093. (doi:10.1149/2.0101806jes)

44. Shi S, Weber AZ, Kusoglu A. 2016 Structure/property relationship of Nafion XL composite membranes. *J. Membr. Sci.* **516**, 123–134. (doi:10.1016/j.memsci.2016.06.004)

45. D'Urso C, Oldani C, Baglio V, Merlo L, Aricò AS. 2014 Towards fuel cell membranes with improved lifetime: Aquivion® Perfluorosulfonic Acid membranes containing immobilized radical scavengers. *J. Power Sources* **272**, 753–758. (doi:10.1016/j.jpowsour.2014.09.045)

Chapter V

Effects of conjoint chemical and mechanical stress on PFSA membranes

Table of contents

1. Introduction

As mentioned in chapter IV, no significant evolution of water sorption and diffusion properties has been observed after *ex-situ* chemical degradation (*i.e.* Fenton's reaction) of Nafion™ membranes. This is noticeably different from the decreased water sorption capacity and water mobility we measured – in a previous work – after long-time fuel cell operation [1]. In this latter case, however, membranes are additionally exposed to a mechanical fatigue so that it can be argued that usual Fenton aging protocols are not fully representative of such conditions. For this reason, it is necessary to also assess the impact of mechanical and chemical stresses when they occur simultaneously. Only few recent works [2–8] were related to the effect of the coupled mechanical and chemical degradation on PFSA membranes, and their results deserve to be discussed. Recently, Kusoglu *et al.* analyzed the effect of compressive stress on the chemical degradation of Nafion™ membrane through an *ex-situ* approach. The authors demonstrated that polymer decomposition increases in a non-linear way with the compression level, suggesting a synergistic nature of chemical and mechanical stresses but without providing quantitative information. In addition, membranes were exposed only to a static mechanical pressure, which is not the kind of solicitation mostly encountered during fuel cell operation. The works of Kusoglu *et al.* also showed by SAXS measurement that under compression, the chemical degradation led to a significant modification of PFSA microstructure with an increase of the spacing between water domains in the membrane. On another note, Yoon and Huang had previously examined the effect of mechanical tensile stress on the chemical degradation of Nafion™ membranes thanks to a modified gas-phase Fenton test. However, these conditions differ significantly from the approach taken in this study. Finally, other authors have developed accelerated stress tests (AST) to study the impact of coupled mechanical and chemical stress on PFSA membranes but only through *in-situ* approaches. A more detailed description of these works can be found in § 3.3.3 of chapter I.

In this work, a device was developed to better mimic the operating conditions of the fuel cell and thus provide some understandings on the consequences of conjoint mechanical and chemical stress on Nafion™ membranes. This device aims at exposing the membrane simultaneously to a free radical environment, through the circulation of a continuous flow of hydrogen peroxide or Fenton solutions, and a cyclic compression to reproduce the swelling/shrinkage sequences entailed by the membrane water-uptake during transient fuel cell operation.

2. Experimental device and protocols

2.1.Description of the aging device

To simulate *ex-situ* mechanical and chemical stresses occurring in fuel cell, two symmetric half-cells or flow field plates were machined in 316L stainless steel, with single serpentine channels. These plates, similar to those used in fuel cells, ensure the distribution of the solution on each side of the membrane. The land and channels are 1 mm wide and 0.7 mm deep (a schematic representation of the lower half-cell can be seen in Figure 5.1b). 316L stainless steel was chosen because of its great corrosion resistance and its chemical inertness against diluted hydrogen peroxide solution. In addition, its mechanical properties are excellent. The system can accommodate 40 to 45 mm wide and 60 to 70 mm long membrane samples and the area exposed to both the solution and the compressive stress is 19.5 x 39.5 mm² per half-cell. Figure 5.1a illustrates a schematic representation of the experimental setup.

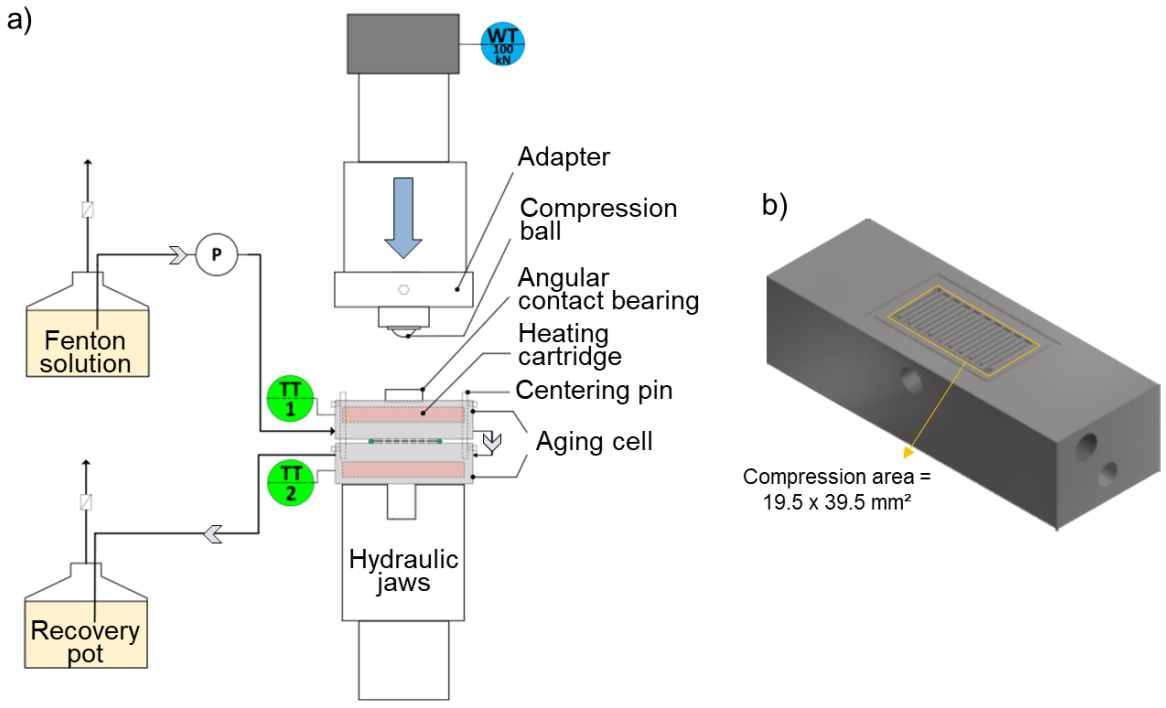

Figure 5.1 – Schematic representations of (a) the coupled mechanical and chemical degradations device and (b) the lower part of the stress cell designed for this study. The compression area is equal to the area of the channel ribs. They were made slightly protruding so that no mechanical pressure was exerted elsewhere.

To induce the chemical stress, a solution (*i.e.* water – as a reference –, H_2O_2, or Fenton solutions) is circulated at a continuous flow rate of 3.02 mL.min^{-1} through the two half-cells, ensuring a residence time of about 10 seconds per half-cell. This value was chosen for three main reasons:

- to guarantee a sufficient pre-heating of the solution in the cell before it meets the membrane samples.
- from a practical point of view, to be able to store enough solution in the upstream and downstream containers (5 L each) so that the degradation protocols could be performed during 8 hours without human intervention.
- finally, to guarantee a fast renewal of the solution in contact with the membrane: the solution flowing successively through one and the other flow-field plates, it was thus renewed every two cycles, *i.e.* every 20 seconds.

The mechanical force was induced through the channel ribs by applying static or sinusoidal constraints during several hours. In the case of cyclic solicitation, the frequency of 0.1 Hz was chosen in order to be significantly higher than the characteristic diffusion time of water through the membrane, which is in the order of 1.0-1.2 seconds by considering a water self-diffusion coefficient of about 6.10^{-10} $m^2.s^{-1}$ when membranes are fully hydrated. It must be noted that such cyclic mechanical stress can probably be considered as quite severe: indeed, 0.1 Hz, during 8 to 20 hours is roughly equivalent to 8 to 20 years of daily operation assuming a fuel cell startup and shutdown per day.

The mechanical force exerted on the membrane during fuel cell operation induce a significant increase of local compressive stresses, which could reach up to 10 MPa according to the modelling work of Khattra *et al.* [9]. On the other hand, Kusoglu *et al.* [4] showed that a 5 MPa pressure was sufficient to considerably enhance the chemical decomposition of Nafion™ membranes in the case of a static mechanical stress. Consequently, we chose to apply a pressure close to 5 or 10 MPa. In practice, the mechanical force was set to 3610 N and 7220 N, which correspond to 4.75 and 9.5 MPa for a compression area of about 19.5 x 39.5 mm^2. For the sake of simplicity, aging tests will be referenced at 5 MPa and 10 MPa thereafter. In addition, since only the channel ribs are in contact with the membrane – their effective area being of the order of 400 mm^2 –, the actual pressure applied to the polymer in the absence of gas diffusion layer is rather close to 9 MPa or 18 MPa. The compression area is only used here as a reference (see § 3.5) as it is commonly done with fuel cell active area.

An EPDM (Ethylene Propylene Diene Monomer) O-ring gasket was used to ensure perfect sealing. EPDM was chosen for its great compatibility with diluted hydrogen peroxide solution. Cartridge heaters and thermocouples were inserted into each half-cell as close as possible to the membrane to maintain the desired temperature (80 °C). The half-cells were inserted between

the clamps of an electromechanical universal testing machine (MTS load frame model 312.21). A preliminary test was carried out to determine the minimal pressure required to compress the gasket and thus ensure an optimum sealing. This minimal pressure was assumed to correspond to the 0 MPa reference seen by the membrane. In addition, a pressure measurement film (Prescale Super Low Pressure sheet, Fujifilm) was used to check the homogeneous distribution of the pressure on the compression area.

2.2. *Ex-situ* coupled mechanical and chemical stress tests

Various *ex-situ* stress tests were carried out with this device to investigate the impact of conjoint chemical and mechanical stress on both XL and NR211 membranes. This section aims at describing the operating conditions of the aging protocols. The parameters that remained constant for all tests were the flow rate (3.02 $mL.min^{-1}$) and the temperature (80 °C). As a first step, preliminary experiments were carried out as reference tests:

- to get a first idea of the membranes endurance under mechanical stress only (***mechanical aging tests***): NR211 and XL samples were compressed at 5 MPa and 0.1 Hz while the compression cell was fed with a continuous flow of distilled water for 20 hours. A similar test was also carried out with both XL and NR211 membranes in the same conditions but for 8 hours only.
- to assess the contribution of mechanical fatigue on chemical degradation: reference tests consisted in applying the 0 MPa reference pressure – the minimal pressure required to guarantee the optimum sealing of the aging cell – while circulating a 3 vol.% H_2O_2 solution (***control aging test #1***) or a Fenton solution containing the optimal reagents concentration determined in chapter III (***control aging test #2***), *i.e.* 3 vol.% of H_2O_2 and 1 ppm of ferrous ions Fe^{2+}.

Note that all the aging tests consisting in the circulation of Fenton solution were carried out with these concentrations (see § 3.2 of chapter III for the determination of these values). The second step consisted in applying a cyclic compressive stress of 5 MPa combined with the circulation of degrading solutions for 8 hours:

- the first experiment (***short-term aging test #1***) was performed with only hydrogen peroxide to simulate moderately aggressive conditions.
- another test was then performed in more aggressive conditions with a Fenton solution (***short-term aging test #2***).

Additionally, an aging test similar to ***short-term aging test #2*** was performed for 20 hours in order to study the effect of exposure time on combined chemical and mechanical stresses. This aging test will be referred to as ***long-term aging test #2*** all along this chapter. Complementary tests were carried out by coupling the circulation of Fenton solution and the application of a static 2.5 MPa compressive stress on the one hand (***static aging test***) and a 10 MPa cyclic compressive stress on the other hand (***high pressure aging test***). These tests were believed to provide some information on the effect of cyclic compression and of high pressure which can be locally experienced by the membrane during fuel cell operation.

Finally, aging tests were performed on membranes sandwiched between two gas diffusion layers (GDL) to get closer to the operating conditions of a PEM fuel cell. In that respect, Sigracet® SGL 24AA GDL (22 x 44 mm²) – with a thickness of 190 µm – were used since they contain no microporous layer (MPL) and no PTFE hydrophobized substrate which could interfere with fluoride emission measurements and restrain the diffusion of the solutions toward the membrane. The test consisted in applying a cyclic compressive stress of 5 MPa to the membrane + GDL assembly while a Fenton solution was circulated through the cell. Note that this value is calculated with reference to the channel ribs area, although the use of GDL will to some extent reduce the effective pressure endured by the membranes and increase the area submitted to the compressive stress.

Table 5.1 summarizes the main operating conditions used for the various coupled stress tests discussed in this chapter:

Table 5.1 – Summary of the operating conditions of the *ex-situ* tests coupling mechanical and chemical stresses

Name of the experiment	Mechanical strength	Chemical conditions	Duration	Number of tests
Mechanical aging test	Cyclic 5 MPa	Distilled water	8/20 hours	1/1
Control aging test #1	Static 0 MPa	H_2O_2 solution	8 hours	1
Control aging test #2	Static 0 MPa	Fenton solution	8 hours	2
Short-term aging test #1	5 MPa cycling	H_2O_2 solution	8 hours	2
Short-term aging test #2	5 MPa cycling	Fenton solution	8 hours	3
Long-term aging test	5 MPa cycling	Fenton solution	20 hours	1
Static aging test	Static 2.5 MPa	Fenton solution	8 hours	1
High pressure aging test	10 MPa cycling	Fenton solution	8 hours	1
Aging test with GDL	5 MPa cycling	Fenton solution	8 hours	2

After the tests, the samples were systematically extracted from the cell, immersed in distilled water before being treated with the same cleaning protocol than that of *ex-situ* chemical degradation tests (see § 2.3 of chapter III and § 2 of Appendix A) – with the exception of the membranes from the mechanical aging test who lasted for 20 hours –. The membrane samples were finally dried in an oven during 20 hours at 60 °C before being analyzed:

- macroscopic morphological evolution, to the naked eye and with a stereo microscope (Leica EZ4 HD),
- chemical structure evolution, by ATR-FTIR spectroscopy and solid-state ^{19}F-NMR,
- water transport and sorption properties thanks to Dynamic Vapor Sorption (DVS) analyzer and liquid-state ^{1}H-NMR spectroscopy,
- fuel cell performances were measured according to the protocol described in the next section.

It is also important to note that when characterizing the chemical structure and the functional properties of Nafion™, only the compression area (Figure 5.1b) was scrutinized, *i.e.* the parts located below the channel ribs where the membranes were exposed to mechanical fatigue and aggressive solutions.

Furthermore, the solutions that circulated through the cell were collected and stored before being analyzed to determine the fluorine ion concentrations. As in previous chapters, they will be expressed as fluoride emission rates in mg of fluoride ions released per gram of dry membrane per hour ($mg/g_{Nafion}/h$) all along this chapter. Furthermore, some of the solutions were also analyzed by liquid-state ^{19}F-NMR spectroscopy in order to compare the degradations with those occurring during purely *ex-situ* chemical stress tests (see chapter IV).

2.3.Electrochemical tests in single cell

The membrane samples submitted to *ex-situ* aging tests were used to make Membrane Electrodes Assemblies (MEA) to assess their functional properties in fuel cell conditions. In this chapter, we will discuss the evolutions of the polarization curves, high-frequency resistances and permeation currents *vs*. MEA made with pristine membrane. All MEA were made according to the following protocol:

- the membranes were inserted between two 235 µm Gas Diffusion Electrodes (GDE) from Hyplat made from Sigracet® SGL 29BC gas diffusion layers with a micro-porous layer. The GDE dimensions were 19 x 38 mm² and their Pt loading was 0.3 $mg.cm^{-2}$

on a Vulcan carbon. The two GDE were carefully aligned on both sides of the membrane thanks to a set of aluminum plates containing a 100 µm PTFE frame to the GDE dimensions.

- the membrane and GDE were then slightly pressed with a very low force (~50 N) while being heated during 8 minutes to a temperature of 135 °C.
- after the heating stage, the membrane and GDE were hot pressed 3 minutes and 30 seconds at a pressure of 4.1 MPa (3000 N). The temperature of the plates was kept to 135 °C.

The MEA were tested in a single cell made of identical gold-coated brass plates on both the anode and cathode sides, with a single serpentine channel (19 passes) of 0.7 mm depth and 1 mm width. The width of the channel rib was 1 mm. The anode and cathode flow field plates were thus identical to those used with the compression device. They were assembled using four M6 bolts tightened to 5 Nm. These plates were then inserted between two metallic plates maintained at 70 °C thanks to a water circulation loop.

Before the performance test, the MEA were first subjected to a conditioning and break-in stage consisting in:

- a 40 minute-temperature rise from 40 °C to 70 °C (each of the 10 °C steps being held 10 minutes) at Open Circuit Voltage (OCV), the anode and the cathode being both fed with 10 slph of nitrogen. Hydrogen is then introduced in the anode compartment (10 slph, 10minutes) followed by air at the cathode (10 slph of air, 10 minutes).
- two hours of constant voltage operation according to the following sequence: 0.6 V (45 seconds), open circuit (30 seconds) and 0.3 V (60 seconds).
- one-hour operation at a constant current density of 0.5 A/cm².

The gas supply during the constant voltage and constant current operation stages was identical to that of the performance test, *i.e.* pure hydrogen and air, both at 60 % RH and atmospheric pressure, with stoichiometries equal to 1.5 and 4 at the anode and cathode, respectively.

The performance test consisted in repeating five times the following sequence:

- measurement of the impedance spectra at 0.5 A/cm², with a frequency ranging between 0.02 Hz and 10 kHz. We usually choose 0.5 A/cm² to perform characterization test

after accelerated stress test protocols because aged materials may not be able to operate properly at higher current density. In most of cases, 0.5 A/cm² is sufficient to monitor the evolution of the fuel cell main impedance parameters [10–12].

- measurement of the polarization curve. The fuel cell voltage was measured once by increasing the current density, then by decreasing the current density. The average voltage values were retained.
- then the cathode compartment was flushed with nitrogen and the hydrogen permeation current (at 0.5 V) was measured. The cathode ElectroChemical Surface Area (ECSA) was also assessed by cycling the potential between 0.1 and 0.7 V at a sweep rate of 50 mV/s.
- finally, the FC was operated two hours at a constant current density of 0.5 A/cm².

This sequence was repeated five times to detect any possible malfunction and only the fifth measurement was considered for the presented polarization curves. Regarding the repeatability of the results, 14 and 4 identical tests were initially carried out with pristine XL and NR211 membrane samples, respectively, to ensure the reliability of the MEA making process. The reference polarization curve of pristine XL membrane is presented in Figure 5.11 while the characterization parameters of its cell performances – hydrogen permeation current, high frequency resistance and Open Circuit Voltage (OCV) – are presented in the Table 5.3. In the case of aged membranes, tests were always repeated a second time after swapping the air and hydrogen flows, each electrode being used as an anode and a cathode and the results were averaged (the dispersion was always negligible).

3. Characterization of membrane degradation

3.1.Preliminary tests

A Preliminary test is performed to ensure that fully hydrated Nafion™ membranes can withstand important pressure (5 MPa) and quick cycling (0.1 Hz) for quite a long time (20 h). This test is made in order to calibrate the duration of the experiments (most of them lasted 8 hours) and to minimize the probability of damaging the cell – in case the membranes were significantly damaged – with the flow field plates coming in direct contact with each other. At the end of the 20 hours' preliminary test, naked eye observations show that XL and NR211 membranes seem to withstand rather well this protocol. Although plastic deformations occur –

the location of the channel ribs could easily be seen at the membranes surface (Figure 5.2) – no cracks or holes is visible. Moreover, satisfying cell performances are obtained with both membranes – compared to pristine membranes – and no significant increase of the hydrogen permeation current is observed, which confirm the absence of significant defects (see Figure 5.11 and Table 5.3 of § 4.3). Additionally, and as expected, no fluoride ions are detected in the solution, meaning that no chemical degradation occurred.

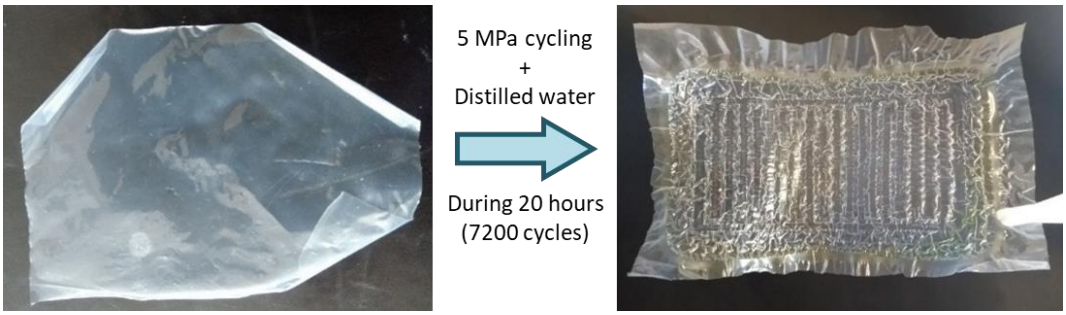

Figure 5.2 – Macroscopic morphology of XL membrane before and after mechanical aging test.

Then, ***control aging test #1*** and ***control aging test #2*** (Table 5.1) are carried out to set reference levels of fluoride emission rate (FER) – without mechanical pressure –. The trend is similar for both membranes, with FER 2.5 to 4 times higher when exposed to the Fenton solution than with hydrogen peroxide (Figure 5.3). This confirms the observations made in the case of *ex-situ* chemical degradation (see § 3.2 of chapter III): as a reminder, FER with membranes exposed to H_2O_2 solution were of about 11 µg/g_{Nafion}/h for both XL and NR211 membranes while they reached about 79 and 97 µg/g_{Nafion}/h with Fenton solution, respectively. Therefore, adding a cyclic compressive stress does not modify this feature. This time, curiously, FER are slightly lower with NR211 than with XL: 224 µg/g_{Nafion}/h *vs.* 249 µg/g_{Nafion}/h with the Fenton solution and 59 µg/g_{Nafion}/h *vs.* 107 µg/g_{Nafion}/h with H_2O_2. However, due to the height of the error bars – with Fenton – and the lack of reproducibility tests – with H_2O_2 –, this trend may not be significant.

3.2.Cyclic compression stress

As a second step, ***short-term aging test #1*** and ***short-term aging test #2*** are performed with a cyclic compression stress of 5 MPa. The trend observed with *ex-situ* chemical stress tests and control aging tests is once more confirmed, with FER at least twice higher with Fenton solution than with H_2O_2 (Figure 5.3). Interestingly, the FER of XL membranes under cycling of 5MPa are lower than without mechanical stress: by about 30% for ***control aging test #1*** (H_2O_2 solution) and by about 35% for ***control aging test #2*** (Fenton solution). On the contrary, no

significant variation of the FER can be observed with NR211, even though no definitive conclusion can be drawn due to the large error bars.

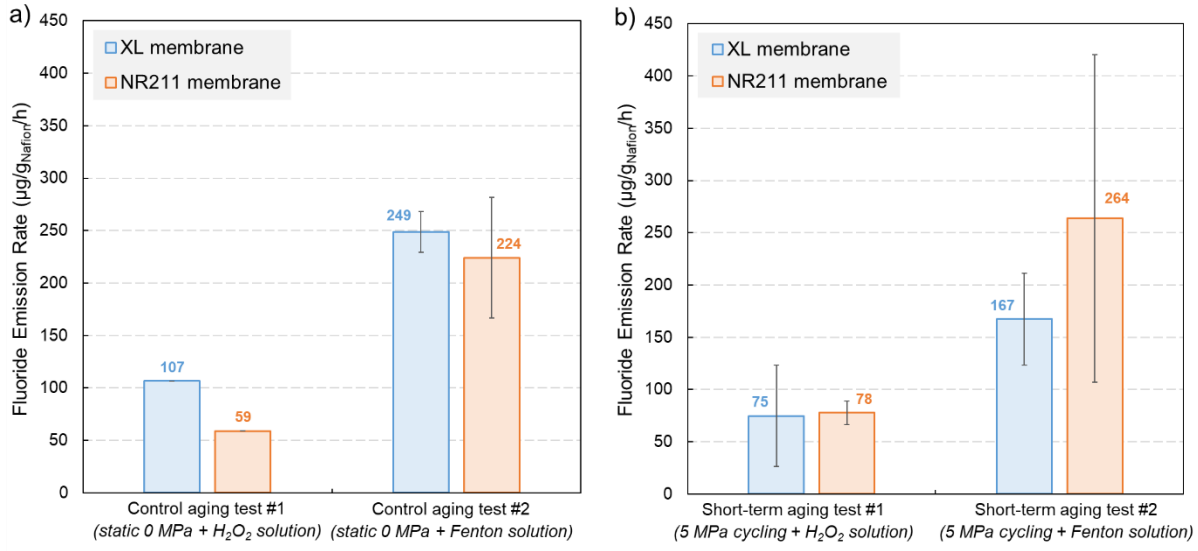

Figure 5.3 – Fluoride emission rates (FER) of Nafion™ XL and NR211 membranes under (a) static 0 MPa and (b) 5 MPa cycling compressive stress coupled to moderate (H_2O_2) and aggressive (Fenton) chemical stress.

In the case of XL membrane, ***short-term aging test #2*** and ***control aging test #2*** led to the appearance of tiny localized bubbles close to the membrane surface, and this mostly in the channels area: *i.e.* where the membranes were in direct contact with the Fenton solution but without mechanical stress (Figure 5.4). It is important to note that such defects are not observed with NR211, neither to the naked eye nor with a stereo microscope, regardless of the conditions.

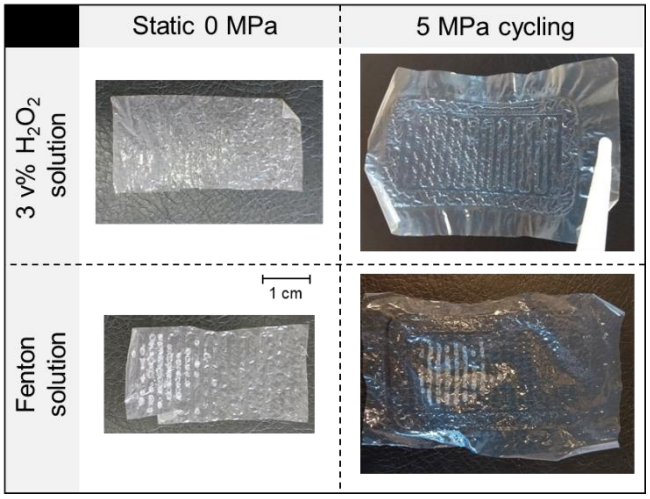

Figure 5.4 – Macroscopic changes of XL membranes under various chemical and mechanical degradation conditions. Photographs of membranes exposed to static 0 MPa mechanical stress correspond to the compression area mm² only (this area being cut for further analyses).

As a reminder, such defects have been observed in the case of pure chemical exposure to Fenton solutions (see § 3.1 of chapter III) but in harsher conditions (20 v% H_2O_2 *vs.* 3 v% H_2O_2

and same ferrous ions concentration) and with both reinforced and non-reinforced membranes. This may indicate that additional mechanical stress, whether the compression is static or cyclic, could induce more severe morphological changes than the exposure to Fenton solution only. Nevertheless, deeper investigations should be carried out to understand the relation between polymer decomposition and the appearance of bubbles, and in the worst-case blisters, at the membrane surface. In addition, we must keep in mind that the conditions in which the chemical stress is applied are not directly comparable: *i.e.* membranes immersed in a static solution in one case *vs*. a fresh and flowing solution in the other case.

3.3.Influence of the mechanical strength

The comparison of the various mechanical stress applied to a membrane (*i.e.* static 0 or 2.5 MPa, 5 or 10 MPa cycling) simultaneously exposed to a Fenton solution allow to detect two behaviors. Indeed, on the one hand, FER of NR211 membrane does not seem greatly affected, with values comprised between 224 and 268 $\mu g/g_{Nafion}/h$ (Figure 5.5). On the other hand, the behavior of XL membrane is different: doubling the mechanical strength (***high pressure aging test*** *vs.* ***short-term aging test #2***) leads to a significant increase of the FER, *i.e.* from 167 to 267 $\mu g/g_{Nafion}/h$. On another note, the FER observed when no or negligible mechanical pressure (*i.e.* 0 MPa) is applied to XL membranes is strikingly high and as important as with a cyclic 10 MPa pressure. This result cannot be simply explained in the view of our current results and deserves further investigations to shed light on this singular behavior.

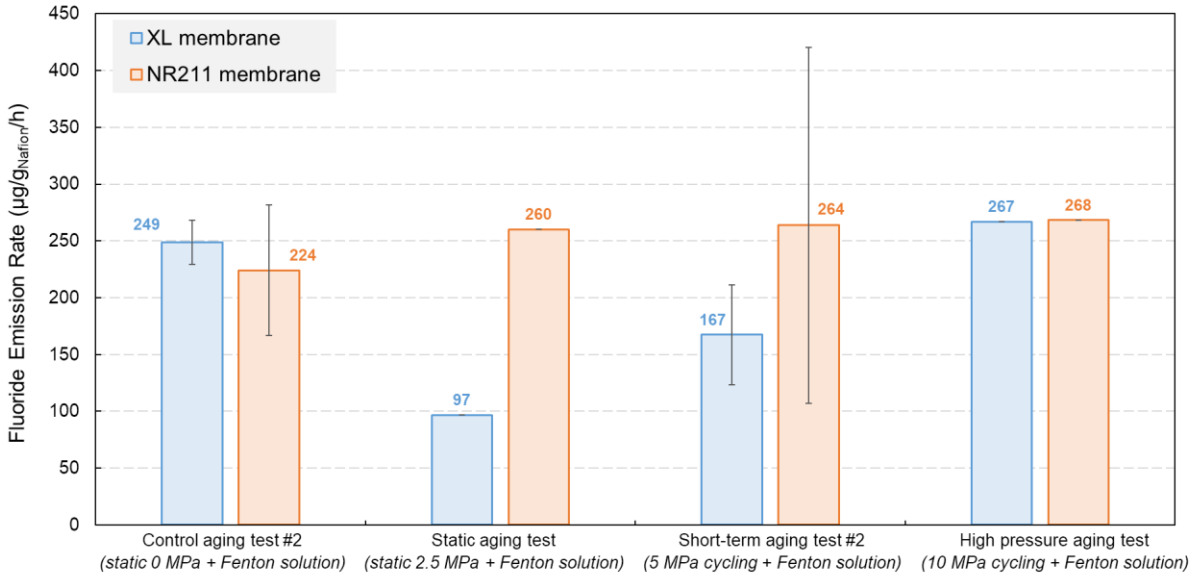

Figure 5.5 – Fluoride emission rates (FER) of Nafion™ XL and NR211 membranes under various mechanical stress coupled to the Fenton solution exposure.

The better behavior of XL membranes *vs.* NR211 – in terms of FER evolution – may be explained by the presence of the additional reinforcement layer [7,13]. The improved mechanical durability of XL membranes was already discussed in the literature and could be due to higher strength and toughness as well as a better resistance to creep and fatigue [14–18]. One can also imagine that when mechanical stress becomes too high, the reinforcement layer of XL membrane does no longer allow to impede polymer decomposition, so that FER reach the same orders of magnitude as those of non-reinforced NR211 membrane. On the other hand, it is important to remember that XL membrane also contains radical scavengers mitigating the chemical decomposition of the polymer which could contribute to prevent chemical degradation, and thus reduced FER, for some aging tests. In the view of our current results, it cannot be definitely concluded whether mechanical reinforcement protects membrane degradation better than radical scavengers or whether both are involved in preventing membrane from degradation.

3.4.Impact of aging test duration

Table 5.2 summarizes the evolution of fluoride emissions as a function of the exposure time for both XL and NR211 membranes in the case of aging test associating 5 MPa cyclic pressure and Fenton solution (***long term aging test*** *vs.* ***short-term aging test #2*** in Table 5.1). Fluoride emissions vary in non-linear way since much more ions are emitted between 8 and 20 hours than between 0 and 8 hours, and this with both membranes. This suggests an increase of the degradation rates throughout the testing period. It can also be observed that the FER of XL membranes during the 8-20h period approaches that of NR211, even though XL contains supplementary radical scavengers and mechanical reinforcement, while it was significantly lower for the 0-8h period. This is consistent with the comment made in the previous section: *i.e.*, that the reinforcement layer and/or radical scavengers of XL membrane does no longer allow to limit or slow down polymer degradation once a certain level of mechanical stress is reached.

Table 5.2 – Fluoride emissions of XL and NR211 membranes after short-term and long-term aging tests

	XL membrane		**NR211 membrane**	
	0-8h solution	**8-20h solution**	**0-8h solution**	**8-20h solution**
Fluoride emission (mg/g_{Nafion})	1.339 ± 0.351	7.5265	2.110 ± 1.254	7.6527

Again, the greater degradation of XL membrane after 20 hours of coupled degradations is consistent with the significant increase of bubbles close to the membrane surface (Figure 5.6).

Many bubbles and blisters with several diameter sizes ranging from micron to millimeter are present close to the XL membrane surface with an inhomogeneous distribution all along the channel area. Deeper investigations will be necessary to understand the appearance of these defects, such as analysis of the membrane by Scanning Electron Microscope (SEM).

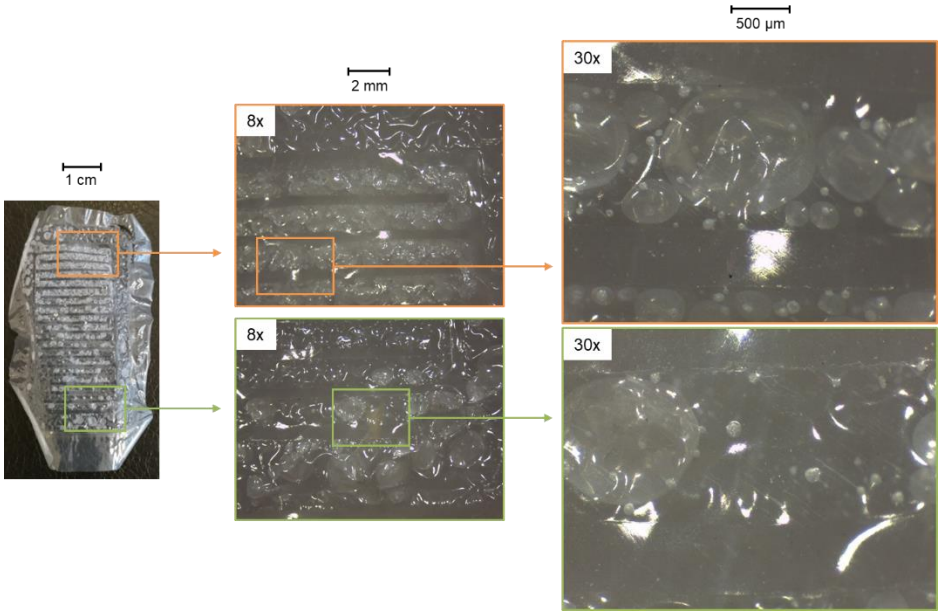

Figure 5.6 – Evolution of the macroscopic morphology of XL membrane after ***long-term aging test*** without magnification (*to the left*) and with 8x/30x magnifications (*in the middle and to the right*) for two different localizations at the membrane surface.

3.5.Impact of the presence of GDL

Finally, gas diffusion layers (GDL) were added between the membranes and the flow field plates, on the one hand to assess their ability to limit the mechanical stress induced by the direct contact with the channel ribs and on the other hand to get closer from fuel cell operating conditions. After the aging test (***aging test with GDL*** in Table 5.1), the apparent degradations of the membranes seem considerably diminished compared to those observed in the case of the aging tests performed on the membrane alone (Figure 5.7): the use of GDL limits FER by a factor of two for the XL membrane and by a factor of three for the NR211. This could indicate, that the GDL effectively protect the membrane since, as mentioned in § 2.2, the force applied was the same as for the other 5 MPa tests: the GDL increasing, at least to some extent, the area submitted to the compressive stress, the effective pressure endured by the membrane should thus be lower than with the test carried out without GDL.

However, three important points should also be taken into consideration:

- The examination of the membranes to the naked eye reveals a different behavior in comparison with all previous aging tests: many carbon residues are present at the membrane surface, and more particularly below the channel ribs. We show in section 4.3 that this contact of the membranes with the GDL carbon fibers has probably a negative impact regarding fuel cell operation.
- No bubbles appeared in the channels area in the case of XL membranes. Although this observation could be seen as the consequence of a lower mechanical stress, another point of view can also be considered: it could be explained by a less efficient renewal of the solution over the membrane surface because of the presence of the GDL. The solution would essentially flow within the channels, its velocity being significantly lower within the GDL. As a result, membranes exposure to the Fenton solution would differ from that occurring during aging tests carried out without GDL. It is worth mentioning here that a PTFE-based hydrophobic coating and a microporous layer (MPL) are generally used in GDL to improve water management in fuel cells. In this study, however, no MPL and no PTFE hydrophobic agent were used, thus facilitating the saturation of the pores.

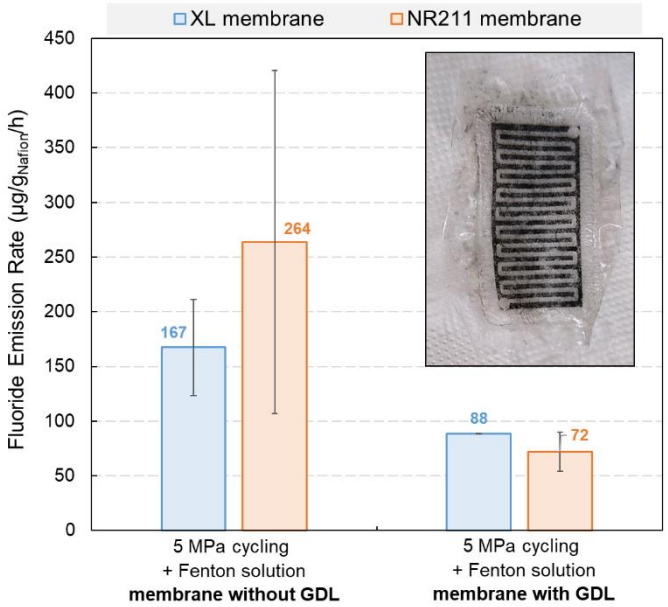

Figure 5.7 – Comparison of the fluoride emission rates (FER) of Nafion™ XL and NR211 membranes in the absence or in the presence of additional GDL. The inset corresponds to the photograph of XL membrane after the aging test with GDL.

Furthermore, XL and NR211 membranes have similar FER when additional GDL are introduced in the stress cell.

4. Impact of conjoint chemical and mechanical stress on the membrane structure and functional properties

4.1. Chemical structure evolution of membranes after conjoint stress

The chemical structure of aged XL and NR211 membranes is analyzed by solid-state ^{19}F-NMR spectroscopy. As seen in § 3.2 of chapter IV, this technique allows to determine the IEC of degraded membranes from the NMR spectra. Figure 5.8 illustrates the evolution of the spectra as well as the evolution of IEC in comparison with pristine membranes for ***short-term aging tests #1*** and ***#2***. Regardless of the degrading solutions (H_2O_2 or Fenton), neither significant evolution of the intensity of the side chain resonance peaks nor IEC evolution are observed for both membranes. This indicates that the global membrane degradation does not seem to affect the PFSA chemical structure. The observation is actually similar to those made after an *ex-situ* chemical stress induced by Fenton's reaction (see § 3.2 of chapter IV), with:

- a constant intensity ratio between the side chain and the CF_2 groups,
- no significant IEC change,
- but still significant fluoride emissions in the solution.

This leads us to the conclusion that the polymer decomposition occurs most probably in similar proportion for both main chains and side chains. Complementary arguments supporting this assumption are presented in § 5 with the comparison of degradations induced by coupling chemical-mechanical stress or chemical stress only.

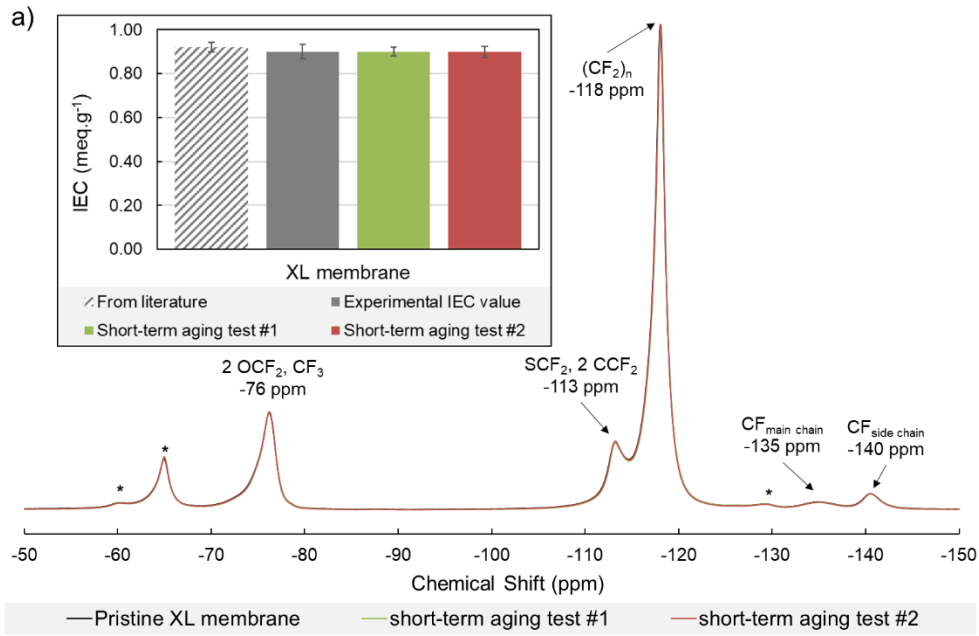

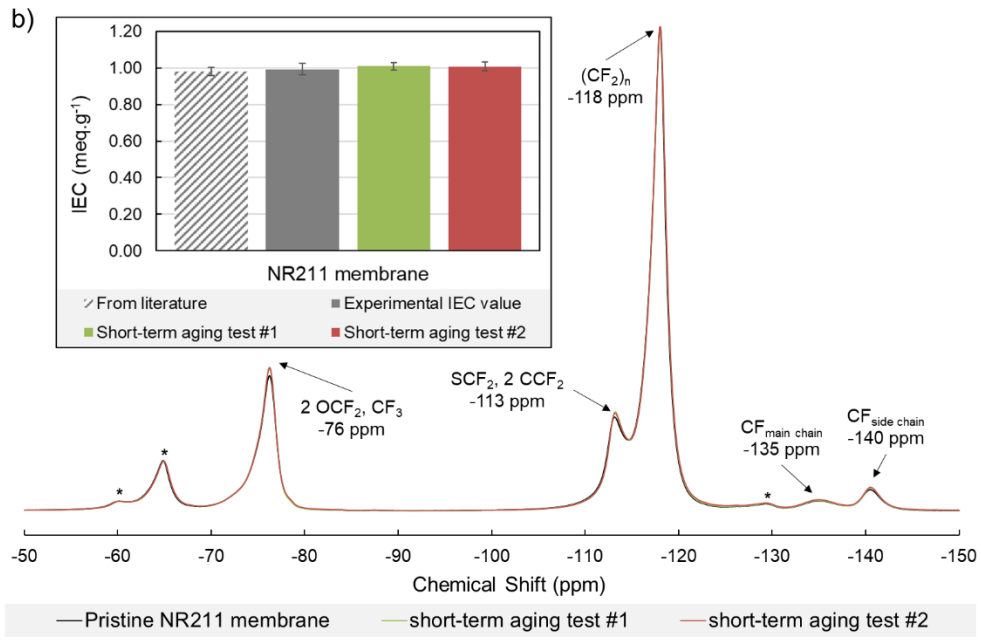

Figure 5.8 – ^{19}F MAS NMR spectra and resonance peak assignment of Nafion™ (a) XL and (b) NR211 membranes before and after cyclic compression aging tests. The resonance peaks with an asterisk designate spinning sidebands. The inset illustrates experimental IEC deduced from spectra in comparison with the literature values [19,20].

Since solid-state ^{19}F-NMR spectroscopy only permits to analyze the global chemical structure of aged membranes, ATR-FTIR spectroscopy was also employed to analyze the local evolution of PFSA chemical structure at the membranes surface, thus excluding the PTFE reinforcement of XL membrane. No significant variation of the relative intensity of side chain vibration bands are visible in the IR spectra for both membranes and regardless of the aging test performed. These results are consistent with those observed for *ex-situ* chemical degradation tests and confirm the conclusion made thanks to NMR measurement. Both techniques, ATR-FTIR and NMR spectroscopies, suggest that conjoint chemical and mechanical stresses do not significantly alter the chemical structure of repeat unit of Nafion™ membranes as observed for degradation induced by chemical stress only (§ 3 of chapter IV).

4.2.Evolution of water sorption and transport properties in aged membranes

For the sake of simplicity, only the results of aging tests coupling cyclic compression and H_2O_2 or Fenton solution exposure are presented, results obtained in the case of static compression are detailed in the appendix B. Figure 5.9 illustrates the evolution of the water sorption isotherms as well as the evolution of the different adsorption mechanisms of XL and NR211 membranes after three aging tests: ***short-term aging tests #1*** and ***#2, high pressure aging test*** (Table 5.1). More detailed explanations on sorption isotherms decomposition and

adsorption mechanisms can be found in § 4.1 of chapter IV. In the case of XL membranes, similar behaviors are observed for all three aging tests: the sorption isotherms differ from that of the pristine membrane only by a significant increase of the cluster contribution after degradation.

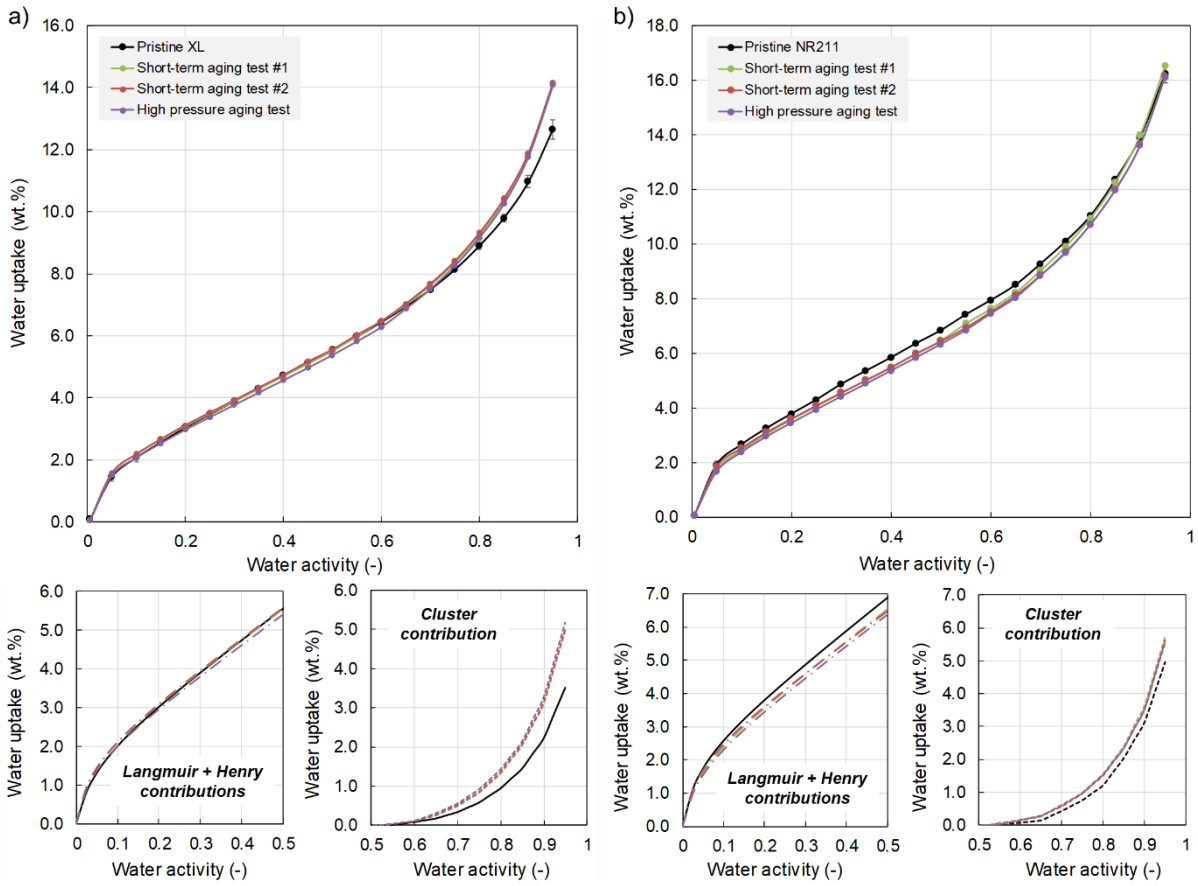

Figure 5.9 – Water sorption isotherms (30 °C) of (a) XL and (b) NR211 membranes after various aging tests in comparison with pristine membranes. The two plots at the bottom illustrate the evolution of the different adsorption mechanisms. Five measurements were performed on the pristine XL in order to control the repeatability of the measurements and of the pretreatment process.

As a reminder, the cluster contribution corresponds to the aggregation of water molecules at high water activities in the pores of the membrane, resulting in its macroscopic swelling. On the contrary, Langmuir + Henry contributions, describing the solvation and further hydration shells formed around sulfonic groups, do not seem to be affected by the degradation even though FER can be highly different from a compressive stress to another, *i.e.* between static 2.5 MPa and cyclic 10 MPa. In the case of NR211 membranes the sorption isotherms do not seem greatly impacted by the degradation. This is consistent with the absence of significant changes in the ^{19}F-NMR spectra or IEC discussed in § 4.1. Furthermore, these results are in agreement with those obtained in the case of purely chemical stress tests. This suggests that the severe mechanical stress experienced by the membranes probably has no significant impact on

the water sorption capacity of Nafion™ membranes. This assumption is supported by the evolution of the FER as a function of the mechanical force in the case of NR211 membrane since no FER evolution whether the membrane is exposed to a cyclic or static compressive stress of 0, 2.5, 5 or 10 MPa (see § 3.3). It is worth noting that the application of a static compression does not modify this trend (see appendix B).

On the other hand, the evolution of the water transport property in aged membranes is investigated by liquid-state ^{1}H-NMR spectroscopy. Again, only aging tests coupling cyclic compression and H_2O_2 or Fenton solution exposure are presented and the results obtained in the case of static compression are reported in Appendix B. Figure 5.10 illustrates the evolution of water self-diffusion coefficient measured in XL and NR211 membranes as a function of the water uptake for various aging tests in comparison with pristine membranes. After conjoint chemical and mechanical degradation, no significant variation of the water self-diffusion coefficient is observed on the all range of membrane water-uptake probed: for both aged XL and NR211 membranes, values are generally very close to the lower limit of those obtained for pristine membranes in the micron scale of NMR spectroscopy. Again, this trend has been already observed in the case of membranes submitted to only a chemical stress and it shows that the introduction of an additional mechanical stress does not affect the water diffusion behavior of membranes, reinforced or not.

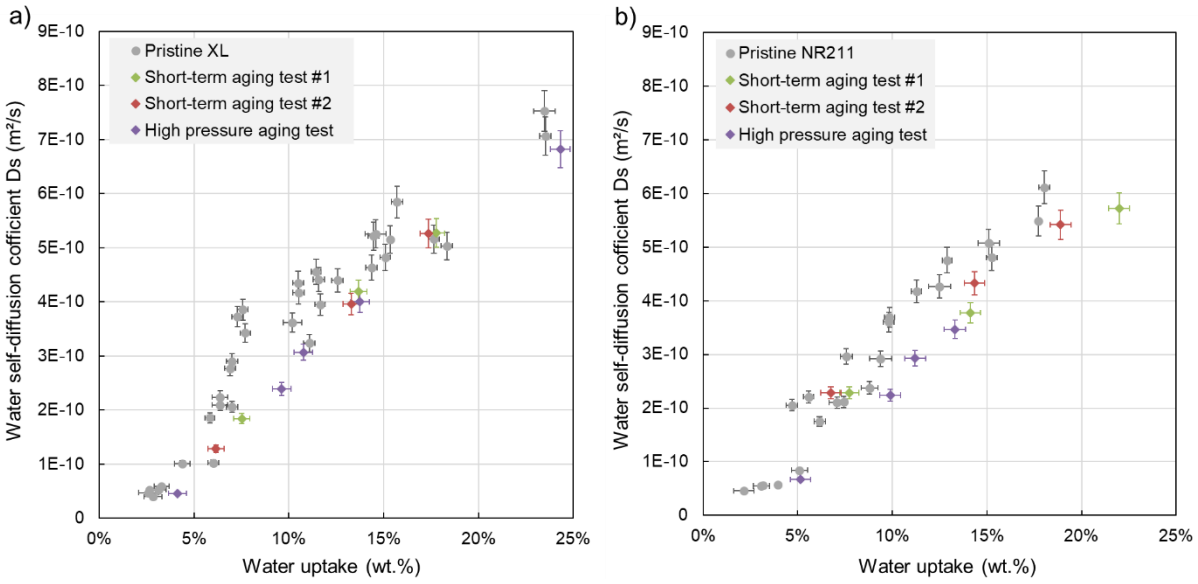

Figure 5.10 – Water self-diffusion coefficient evolution after various aging tests as a function of water uptake in (a) XL and (b) NR211 membranes (diamond symbols) in comparison with pristine membranes (circles).

More generally, in the light of these results, it can be concluded that the addition of a mechanical fatigue to a chemical degradation significantly increase FER emission but does not

alter further the Nafion™ membranes chemical structure (repeat unit, IEC) and functional properties (water sorption and self-diffusion). However, due to the presence of the flow field plates, the whole membrane surface has not been exposed to identical mechanical stress and might be exposed to the solution in different quantities over the whole experiment duration under the channel ribs and in the channels. It can thus be argued that the polymer decomposition could possibly be heterogeneous. To characterize the PFSA chemical structure and properties in these different regions, it would be necessary to perform localized analyses to study separately those two different areas.

4.3.Cell performances after conjoint mechanical and chemical stresses

To evaluate their functional properties and detect a possible increase of hydrogen permeation, aged membranes were used to make MEA and tested in a single cell. In the following section, we compare results obtained with membranes that were in direct contact with the flow field plates, *i.e*. without GDL.

4.3.1. Aging without GDL

The hydrogen crossover current was measured for both XL and NR211 membranes after the ***short-term aging tests #1*** and ***#2*** as well as ***long-term aging test*** to ensure that no cracks or pinholes appeared. Table 5.3 displays the permeation current, high frequency resistance and Open Circuit Voltage (OCV) measured for these degraded membranes in comparison with the values obtained for pristine and mechanically-aged membranes (5 MPa cyclic compressive stress with water for 8 hours). No significant permeation current is measured for XL membranes, indicating that they withstand rather well the combined aging in both cases and this despite the presence of defects in some cases (***short term-aging test #2*** and ***long-term aging test***). It may be possible that the MEA hot-pressing process led to the closing of some of the blisters close to the membrane surface. In any case, the low hydrogen permeation currents mean that none of the blisters led to a membrane failure. Conversely, NR211 membranes show no sign of degradation by macroscopic observations to the naked eye and using a stereo microscope, but a slight increase of the hydrogen permeation current is observed after both ***mechanical aging test*** and ***short-term aging test #1***. This may be the consequence of a membrane thinning or of micro-cracks that appeared through the membranes. Although the values we measured are not characteristic of critical membrane failure, they remain non-negligible. Wang *et al.* [21] for instance obtained a permeation current of 7.04 mA/cm² after 24 hours of Fenton's reagents exposure – with high H_2O_2 concentration (30 vol.%) – and

interpreted this as a degradation of the membrane (Nafion™ 111), possibly because of the appearance of bubbles through its thickness. Furthermore, our experience of hydrogen permeation current monitoring during fuel cell accelerated stress tests show that such trends are often a good indication of imminent membrane failure.

Table 5.3 – Characterization parameters of cell performances for Nafion™ XL and NR211 membranes exposed to various conjoint degradation protocol in comparison with pristine and mechanically-aged membranes. For both pristine and aged membranes, the parameters were averaged over the all measurements performed. The resulting dispersion corresponds to the standard deviation.

	Pristine membrane		**Mechanical aging test**		**Short-term aging test #1**		**Short-term aging test #2**		**Long-term aging test**	
	XL	**NR211**	**XL**	**NR211**	**XL**	**NR211**	**XL**	**NR211**	**XL**	**NR211**
Permeation current ($mA.cm^{-2}$)	1.80 ± 1.11	1.94 ± 0.75	1.36 ± 0.06	3.62 ± 0.27	0.86 ± 0.17	4.49 ± 0.27	1.68 ± 0.26	2.54 ± 0.20	1.16 ± 0.05	1.29 ± 0.07
High Frequency Resistance ($m\Omega.cm^{-2}$)	78.69 ± 10.78	67.88 ± 2.70	103.21 ± 1.74	91.04 ± 7.09	107.96 ± 5.39	73.12 ± 7.84	107.05 ± 5.20	72.69 ± 5.74	113.42 ± 3.83	82.60 ± 2.32
Open Circuit Voltage (V)	0.917 ± 0.018	0.907 ± 0.017	0.914 ± 0.003	0.900 ± 0.002	0.922 ± 0.05	0.878 ± 0.003	0.906 ± 0.006	0.895 ± 0.004	0.922 ± 0.004	0.920 ± 0.005

Polarization curves were also measured in order to confirm that the samples remained functional and possibly assess the impact of aging on cell performances. They are shown in Figure 5.11. The fuel cell performances of aged XL membranes are lower than those obtained with the pristine one, with a slight increase of the resistive losses. Moreover, no significant variation of the polarization curve is observed when the exposure time is increased (***long-term aging test***). The polarization curves of aged NR211 membranes seem globally less impacted than those of XL membrane, which is consistent with a lower increase of the high frequency resistances (Table 5.3). However, it is important to keep in mind that the increase of the resistive losses and the evolution of polarization curves (Figure 5.11) can be to some extent linked to the plastic deformation of the membranes surface, which do not make it possible to assess properly their functional properties because of the poor quality of the interface with the electrodes. This seems particularly true with XL membranes, which could suggest that plastic deformation is more detrimental for reinforced XL membrane than for its non-reinforced counterpart (while NR211 membranes are more prone to hydrogen permeation after the aging tests). However, and in all cases, the shape of the polarization curves confirms the absence of critical membrane failure.

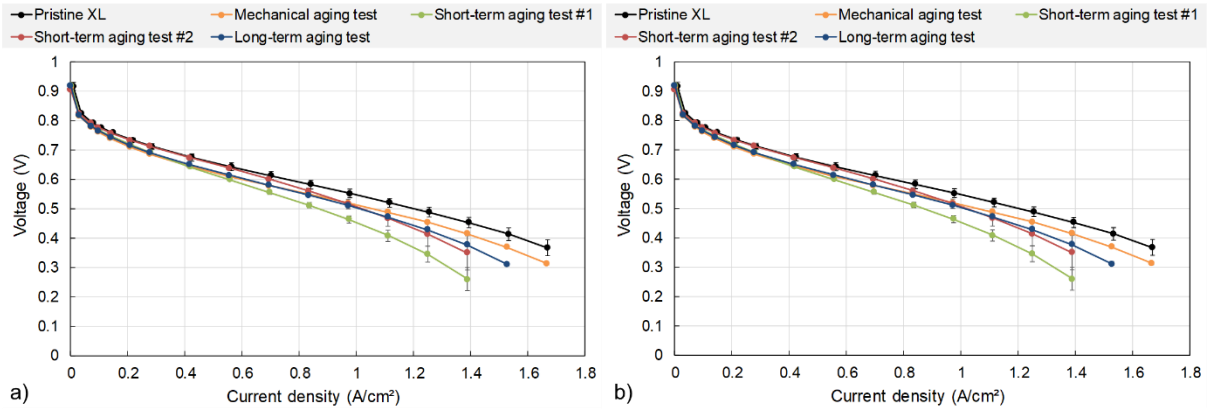

Figure 5.11 – Polarization curves in single cell with MEA made with Nafion™ (a) XL and (b) NR211 membranes for various aging tests. The cell was operated at 70°C and supplied with pure hydrogen and air, both at 60% RH and atmospheric pressure. The gas stoichiometries were equal to 1.5 and 4 at the anode and cathode, respectively.

In addition, fuel cell performances of membranes degraded by pure *ex-situ* chemical degradation induced by Fenton's reaction were also tested in single cell. These membranes were immersed during 24 hours in a Fenton solution with the optimal concentration of reagents and thus experienced no mechanical stress. No significant change of the polarization curves, no increase of high frequency resistance and no permeation currents are observed for both XL and NR211 membranes suggesting that, under these conditions, the *ex-situ* chemical degradation had no impact on the membrane integrity or on the performance of the fuel cell.

4.3.2. Aging with a GDL

In this section, we present results obtained with the membranes that were not in direct contact with the flow field plates thanks to the introduction of GDL. As a reminder, the visual aspects of these membranes seemed considerably better than that of membrane aged without GDL (Figure 5.7): many carbon residues can be seen on the membrane surface below channel ribs and no bubbles appeared in the channel area for both NR211 and XL membranes (§ 3.5). In addition, the use of GDL also reduces drastically the FER: the decrease was by about 50% for XL membrane and by about 33% for NR211. Permeation currents, high frequency resistances and OCV measured after identical aging tests performed with and without GDL are reported in Table 5.4. In the case of NR211 membrane, a considerable increase of the hydrogen permeation current associated to an important OCV drop (around 14%) is measured after the aging test performed with GDL. This reveals most probably the appearance of cracks through the membrane. This tendency is much less pronounced with Nafion™ XL but the OCV is nonetheless the lowest we measured with this membrane and the permeation current is the

highest. A possible explanation of this behavior is that some carbon fibers have locally punctured the membrane under the effect of mechanical constraint.

Table 5.4 – Comparison of permeation currents, high frequency resistances and Open Circuit Voltages (OCV) after 8 hours of 5 MPa cyclic compressive stress with a Fenton solution exposure, with and without GDL. For both pristine and aged membranes, the parameters were averaged over the all measurements performed. The resulting dispersion corresponds to the standard deviation.

	Pristine membrane		Aging test without GDL		Aging test with GDL	
	XL	NR211	XL	NR211	XL	NR211
Permeation current ($mA.cm^{-2}$)	1.80 ± 1.11	1.94 ± 0.75	1.68 ± 0.26	2.54 ± 0.20	3.11 ± 0.15	81.78 ± 4.91
High Frequency Resistance ($m\Omega.cm^{-2}$)	78.69 ± 10.78	67.88 ± 2.70	107.05 ± 5.20	72.69 ± 5.74	114.03 ± 2.51	79.18 ± 1.80
Open Circuit Voltage (V)	0.917 ± 0.018	0.907 ± 0.017	0.906 ± 0.006	0.895 ± 0.004	0.885 ± 0.003	0.782 ± 0.002

Despite of the high value of the hydrogen permeation current, one can see in Figure 5.12 that the polarization curve of NR211 membranes is not impacted by the presence of GDL, except for the lower OCV. However, this trend is commonly observed in such case, the hydrogen permeation current being an early indicator of membrane failure. With Nafion™ XL, the best polarization curve was obtained after the aging tests performed without GDL.

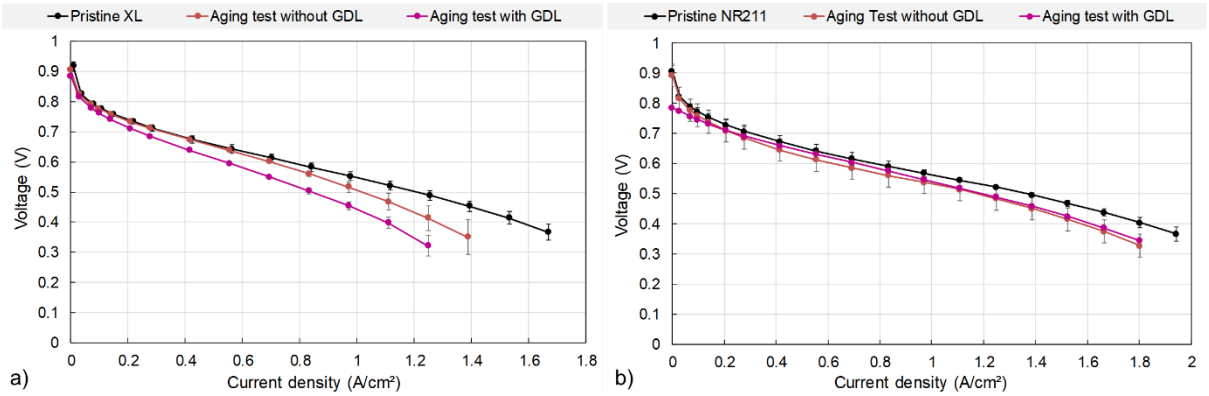

Figure 5.12 – Polarization curves in single cell with MEA made with Nafion™ (a) XL and (b) NR211 membranes for aging tests with and without additional GDL. For aged membranes, error bars refer to the average of the two faces.

The main and obvious conclusion from these results is that we observed absolutely no evidence of a possible positive impact of GDL. On the contrary, the tendency of Nafion™ XL to be more impacted by the mechanical stress than NR211 (in terms of fuel cell performance, see § 4.3.1) because of plastic deformations of its surface is confirmed. This can be explained by many cleavages of fibers evidenced by carbon depositions and by the lower Young modulus of GDL in the thickness direction, which is of the magnitude of 10 MPa when a compressive

stress is applied [22], compared to that of the membranes around 50-130 MPa in high humidity (90% RH or liquid water) and temperature (80-85°C) conditions [14,23]. Additionally, Yi *et al.* showed that strong compressive stress application (more than 2 MPa) led to the collapse of GDL structure, which can further damage the membrane [24]. Consequently, it can be argued that these broken fibers probably led to membrane punctures so that, on the whole, using GDL has a rather negative impact in the conditions of our study.

Although interesting, this result nevertheless deserves to be confirmed by reproducibility tests. Furthermore, it will be necessary to check that it can be generalized to other types of GDL, particularly those with MPL.

5. Contribution of the mechanical stress on membrane properties: comparison with pure chemical stress tests

First, by comparing the fluoride emissions obtained in the case of coupled chemical and mechanical stress tests with those of only chemical stress tests, one can observe that they are comparable: 7.53 mg/g_{Nafion} *vs.* 9.10 mg/g_{Nafion} for XL and 7.65 mg/g_{Nafion} *vs.* 12.48 mg/g_{Nafion} for NR211. Nevertheless, the duration of the aging tests were significantly different but so were the chemical conditions (96 hours in a static solution *vs.* 20 hours in a flowing solution) so that eventually, the amount of fluoride released by the membranes could be of the same order of magnitude. To go one step further and compare the degradation mechanisms occurring in coupled chemical-mechanical stress and chemical stress only, Fenton solutions were collected after conjoint stress tests of XL and NR211 membranes and analyzed by liquid-state ^{19}F-NMR spectroscopy (Figure 5.13). In that respect, we chose to analyze the Fenton solutions which have been circulated between the 8th and 20th hours of the ***long-term aging test*** because of their high fluoride ion concentrations measured with the ion-selective electrode. Degradation occurring during pure *ex-situ* chemical stress test (Fenton's reaction) involves degradation mechanism by main chain unzipping and thus the loss of entire side chains (see § 4.2 of chapter IV). This hypothesis has been advanced thanks, among other, to ^{19}F-NMR analysis of solutions through the identification of three main degradation products: fluoride ions, trifluoroacetic acid (TFA) and the perfluoro(3-oxapentane)-1-sulfonic-4-carboxylic diacid, referred to as "product A" for simplicity.

As illustrated on Figure 5.13, those same degradation products are found in Fenton solutions after mechanical and chemical stress tests, indicating that the addition of a mechanical constraint seems not to affect the mechanism that govern the polymer decomposition.

Moreover, these degradation products, and therefore the degradation mechanism, are similar whether the membrane is reinforced or not.

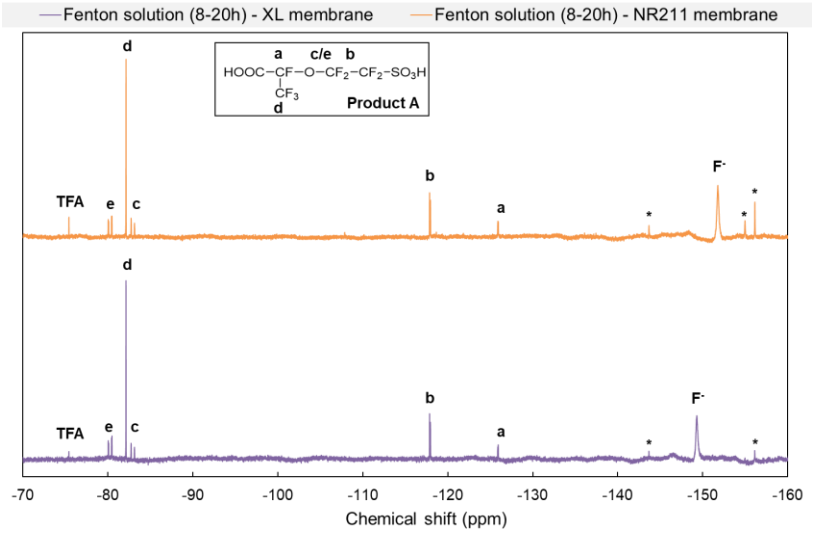

Figure 5.13 – ^{19}F-NMR spectra of the circulating Fenton solutions collected after the ***long-term aging test*** of XL and NR211 membranes. The inset illustrates the chemical structure of product A and the attribution of its resonance peaks. The resonance peaks with an asterisk designate unidentified molecules. The solutions were mixed with D_2O (with a D_2O/H_2O ratio of 20:80) and the spectra were recorded at room temperature.

Similarly, the evolution of water sorption property of composite Nafion™ XL membrane after coupled mechanical and chemical stress tests is compared to that of a purely *ex-situ* chemical stress test (Figure 5.14). The trend is similar for both since no significant change can be observed with the exception of cluster contribution which increases slightly in both cases in comparison with pristine XL membrane. This water sorption behavior of aged XL membranes is not easily understandable and explainable as, to the best of our knowledge, no studies have been carried out on the water sorption property of composite XL membranes in the literature. In addition, it must be kept in mind that the cyclic compression that was added to Fenton exposure in this chapter can – most probably – be considered as a rather severe solicitation (equivalent to several years of FC daily operation - see § 2.1) and we can only notice – as seen in § 4.1 and 4.2 – that it has a mild impact on the degradation.

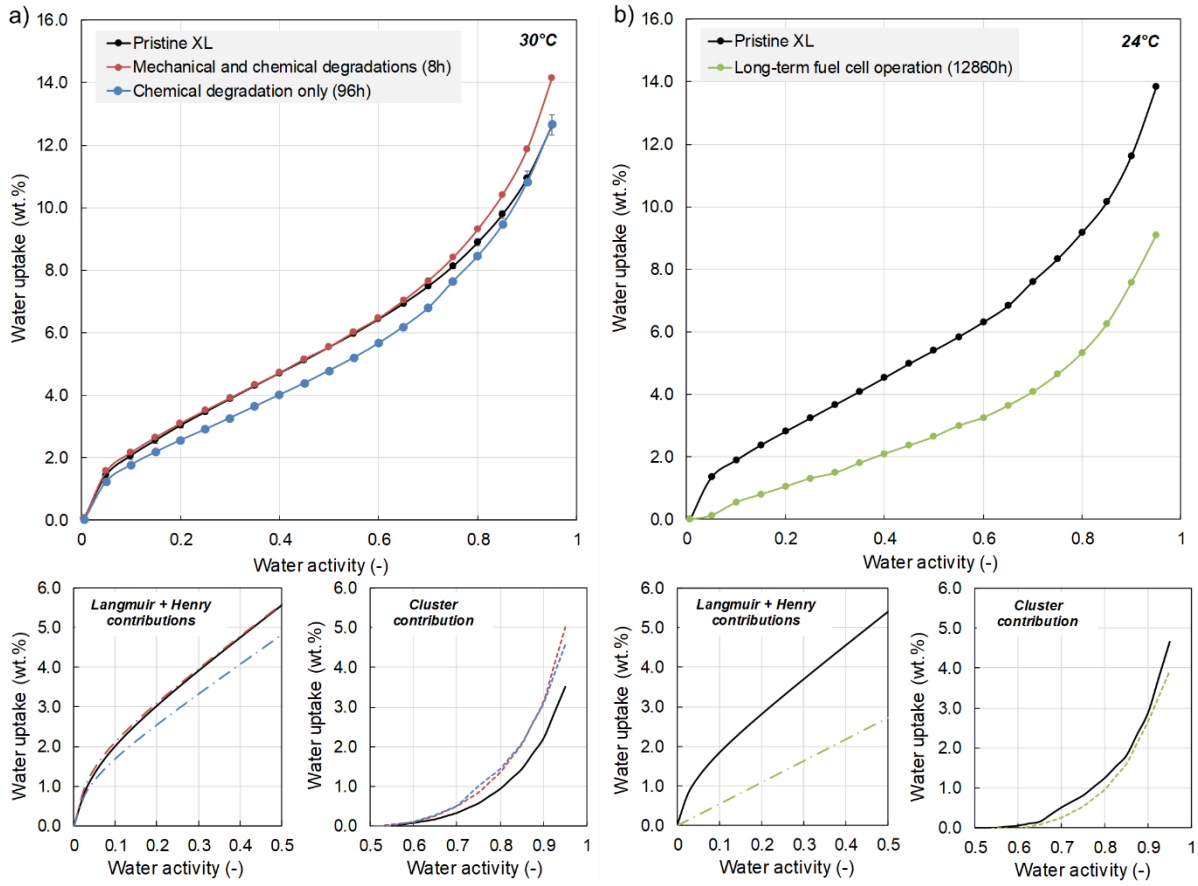

Figure 5.14 – Evolution of water sorption isotherms in XL membranes (a) after *ex-situ* conjoint degradation (***short-term aging test #2***) and after *ex-situ* chemical degradation only (Fenton solution exposure) in comparison with the evolution (b) after long-time fuel cell operation [1].

To this point, it may be worth comparing the evolutions of water sorption isotherms after *ex-situ* stress tests with those we measured after long-time fuel cell operation (Figure 5.14), for similar reinforced membrane, in a previous work [1].One can notice that the behaviors are clearly different in both cases: the cluster contribution was not impacted while the Langmuir contribution was strongly reduced after long-time fuel cell operation. This trend was attributed to a partial loss of sulfonic groups by side chain cleavages since a significant reduction IEC was observed.

In the previous chapter (§ 5.2 of chapter IV), we suggested that the addition of mechanical fatigue to chemical stress would lead to solicitations and degradation mechanisms closer to the aging phenomena occurring during fuel cell operation. In the light of these last results, it might be thought that this hypothesis is clearly not verified. However, it is difficult to conclude with certainty about the impact of conjoint stress on Nafion™ membranes since the measurement performed on membrane after long-time fuel cell operation was focused on a specific area extremely degraded – inlet/outlet of reactant gases – known to be exposed to severe conditions

(higher hydrogen crossover [25,26], low relative humidity of gases [27,28], air starvation [29]) during fuel cell operation. On the contrary, it seems that adding a rather important mechanical compressive stress to a chemical stress does not significantly alter Nafion™ degradation mechanisms, nor the functional properties (water sorption capacity and self-diffusion coefficient). This conclusion is supported by some of the results of this chapter (*e.g.* increasing from 0 MPa to 5 or 10 MPa the cyclic pressure applied to NR211 membrane during 8 to 20 hours has no impact on fluoride emissions) as well as by the comparison with the results of the previous chapter.

In this regard, the most probable explanation for the discrepancy between the degradation of XL membranes observed after long-time fuel cell operation [1] and those we observe in this work lies mostly in the nature of the chemical stress, with possibly:

- either experiment durations of the *ex-situ* stress tests carried out up to now were too short,
- and/or chemical conditions were not aggressive enough to have significant impacts on Nafion™ membrane functional properties, despite the clear chemical degradation evidenced in the previous chapter.

Moreover, the aging heterogeneities induced by the fuel cell operating conditions, and more particularly the severe degradation experienced by the MEA in the inlet/outlet regions, cannot be neglected [20,30]. It might be argued that regions less prone to a severe degradation could have a behavior similar to that observed in the present study. Of course, it is conceivable that our *ex-situ* stress tests (chemical or mechanical + chemical) do not faithfully replicate the more complex conditions encountered by the membranes in actual use.

Our observations are also not consistent with the recent results of Kusoglu *et al.* [4], who observed an increase of polymer degradation when applying a static pressure to the membrane. However, it must be kept in mind that on the one hand the authors provided only few quantitative information and, on the other hand, their work was carried out in conditions significantly different from ours:

- they used a much thicker Nafion™ 117 membrane (178 µm) previously exchanged with ferrous ions and a 6 vol.% H_2O_2 solution *vs.* 3 vol.% H_2O_2 concentration with or without the addition of 1 ppm of Fe^{2+} (Fenton solution) in our case,

- contrary to the present work, the stress cell designed by Kusoglu *et al.* did not contain single serpentine flow channel, implying a homogenous exposure of the mechanical force in their case.

Despite of these *a priori* more aggressive conditions, they observed much lower degradation rates than ours (*i.e.* more than 50 times lower![1]) so that their results and ours are probably not comparable.

6. Conclusions

This study aimed at investigating the impact of coupled mechanical and chemical stress on PFSA membranes through an *ex-situ* approach. In that respect, a custom-made device able to reproduce conditions close to that experienced by the membranes during fuel cell operation was developed. The initial results show that fully hydrated membranes seem to withstand severe sinusoidal constraints as no crack formed. Numerous aging tests were performed to provide new understandings on the influence of mechanical constraints, whether they were static or cyclic with negligible or high pressure level, on the chemical degradation of Nafion™ membranes, and its impact on their chemical structure and functional properties. In addition, the effect of the presence of additional GDL into the stress cell was also investigated. The results permitted to highlight the following items:

- The severe mechanical stress that was applied in this work does not overcome or dominate chemical degradations, with a response of the samples to chemical stress that does not seem to differ, at least qualitatively: the degradation rates remain more significant when the membranes are exposed to Fenton's reagents instead of hydrogen peroxide only. However, although Fenton's reagent concentrations were low in order to be as close as possible to real fuel cell operating conditions – *i.e.* without inducing dramatic morphological changes –, the combination of mechanical constraint and Fenton solution exposure led to the appearance of bubbles and blisters in the case of aged XL membranes. Conversely, no such morphological changes were observed for NR211 membranes.

[1] According to the figure 2 of reference [4], the exposure of a Fe^{2+}-Nafion™ 117 membrane to a 5 MPa static compression and 6 vol.% H_2O_2 solution during 24 hours conducts to a fluoride release by about 1.65 µmol, which corresponds to a FER of 0.069 µmol/h. In this study, the ***long-term aging test*** (5 MPa cyclic compression + Fenton solution for 20 hours) performed with XL and NR211 membranes led to a fluoride release around 71-75 µmol, corresponding to a FER of 3.55-3.76 µmol/h.

- Higher fluoride emission rates were generally obtained with NR211 than with Nafion™ XL. The better behavior of XL membranes *vs.* NR211 can be explained by the presence of the additional reinforcement layer which provides better mechanical strength and dimensional stability [7,13]. In this work, the higher resistance of XL was confirmed by the absence of significant increase in the hydrogen permeation current after combined mechanical and chemical accelerated stress tests, contrary to NR211 membranes. In addition, the mechanical strength had no significant impact on NR211 membrane chemical degradation while an important increase of FER with the cyclic compression level was observed in the case of XL membrane.
- In the case of XL membranes, even though plastic deformations were observed on the membrane surface after the experiments, the samples remain fully functional when tested in fuel cells with only a slight decrease of the performances that can be attributed to the degradation of the membrane-electrodes interface. This is most probably linked to the plastic deformation of the membrane samples, which were in direct contact with the channel ribs in the compression cell.
- Although a significant polymer decomposition is observed after conjoint stress tests, no change in the chemical structure on in the water sorption and transport properties of the Nafion™ membranes has been noticed. These behaviors are clearly different from those observed after long-time fuel cell operation (in a previous work [1]), suggesting that either experiment durations of the *ex-situ* stress tests were too short or chemical conditions were not aggressive enough to get closer to fuel cell operating conditions. Nevertheless, it is important to keep in mind that the membrane degradation during long-time fuel cell operation is heterogeneous since particular regions are exposed to more severe conditions (for instance, the hydrogen inlet region).
- The introduction of GDL between the membrane and the flow field plates permitted consequently to decrease the membrane apparent degradation rate since no bubbles appeared at the surface of XL membranes and the FER was at least reduced by about 33% for both membranes. Although this drastic diminution could be at first sight attributed to a reduced effective mechanical pressure experienced by the membrane because of the presence of GDL, we must also consider a less efficient exposure of the membrane to the Fenton solution that would flow mostly in the channels, and not – or less – through the GDL. In addition, significantly lower fuel cell performances were obtained for XL while an important increase of hydrogen permeation current was

observed for NR211 membrane: these behaviors could suggest that some broken carbon fibers have locally punctured the membrane under the effect of the mechanical constraint.

The development of accelerated tests combining chemical and mechanical stresses is a necessary step to quickly assess the durability of membranes [3,5,7] and gain a deeper understanding of their degradation mechanisms. Nevertheless, the device that was designed for this work opens up various perspectives and additional works will be required to optimize the conditions in which such accelerated tests are performed. On the other hand, further investigations and reproducibility tests are needed in order to understand the morphological changes experienced by the reinforced membranes and the influence of GDL, as well as to clarify the contribution of the mechanical stress on membrane chemical degradation and the impact of conjoint stress on the chemical structure and functional properties of Nafion™ membranes.

References

1. Robert M, El Kaddouri A, Perrin J-C, Leclerc S, Lottin O. 2018 Towards a NMR-Based Method for Characterizing the Degradation of Nafion XL Membranes for PEMFC. *J. Electrochem. Soc.* **165**, F3209–F3216. (doi:10.1149/2.0231806jes)

2. Yoon W, Huang X. 2010 Acceleration of Chemical Degradation of Perfluorosulfonic Acid Ionomer Membrane by Mechanical Stress: Experimental Evidence. *ECS Trans.* **33**, 907–911. (doi:10.1149/1.3484584)

3. Lim C, Ghassemzadeh L, Van Hove F, Lauritzen M, Kolodziej J, Wang GG, Holdcroft S, Kjeang E. 2014 Membrane degradation during combined chemical and mechanical accelerated stress testing of polymer electrolyte fuel cells. *J. Power Sources* **257**, 102–110. (doi:10.1016/j.jpowsour.2014.01.106)

4. Kusoglu A, Calabrese M, Weber AZ. 2014 Effect of Mechanical Compression on Chemical Degradation of Nafion Membranes. *ECS Electrochem. Lett.* **3**, F33–F36. (doi:10.1149/2.008405eel)

5. Alavijeh AS, Goulet M-A, Khorasany RMH, Ghataurah J, Lim C, Lauritzen M, Kjeang E, Wang GG, Rajapakse RKND. 2015 Decay in Mechanical Properties of Catalyst Coated Membranes Subjected to Combined Chemical and Mechanical Membrane Degradation. *Fuel Cells* **15**, 204–213. (doi:10.1002/fuce.201400040)

6. Venkatesan S velan, Lim C, Holdcroft S, Kjeang E. 2016 Progression in the Morphology of Fuel Cell Membranes upon Conjoint Chemical and Mechanical Degradation. *J. Electrochem. Soc.* **163**, F637–F643. (doi:10.1149/2.0671607jes)

7. Mukundan R, Baker AM, Kusoglu A, Beattie P, Knights S, Weber AZ, Borup RL. 2018 Membrane Accelerated Stress Test Development for Polymer Electrolyte Fuel Cell Durability Validated Using Field and Drive Cycle Testing. *J. Electrochem. Soc.* **165**, F3085–F3093. (doi:10.1149/2.0101806jes)

8. Ehlinger VM, Kusoglu A, Weber AZ. 2019 Modeling Coupled Durability and Performance in Polymer-Electrolyte Fuel Cells: Membrane Effects. *J. Electrochem. Soc.* **166**, F3255–F3267. (doi:10.1149/2.0281907jes)

9. Khattra NS, Karlsson AM, Santare MH, Walsh P, Busby FC. 2012 Effect of time-dependent material properties on the mechanical behavior of PFSA membranes subjected to humidity cycling. *J. Power Sources* **214**, 365–376. (doi:10.1016/j.jpowsour.2012.04.065)

10. Abbou S, Dillet J, Spernjak D, Mukundan R, Fairweather JD, Borup RL, Maranzana G, Didierjean S, Lottin O. 2013 Time Evolution of Local Potentials during PEM Fuel Cell Operation with Dead-Ended Anode. *ECS Trans.* **58**, 1631. (doi:10.1149/05801.1631ecst)

11. Abbou S, Dillet J, Spernjak D, Mukundan R, Borup RL, Maranzana G, Lottin O. 2015 High Potential Excursions during PEM Fuel Cell Operation with Dead-Ended Anode. *J. Electrochem. Soc.* **162**, F1212. (doi:10.1149/2.0511510jes)

12. Abbou S, Dillet J, Maranzana G, Didierjean S, Lottin O. 2017 Local potential evolutions during proton exchange membrane fuel cell operation with dead-ended anode – Part II: Aging mitigation strategies based on water management and nitrogen crossover. *J. Power Sources* **340**, 419–427. (doi:10.1016/j.jpowsour.2016.10.045)

13. Rodgers MP *et al.* 2013 Perfluorinated Sulfonic Acid Membrane and Membrane Electrode Assembly Degradation Correlating Accelerated Stress Testing and Lifetime Testing. *ECS Trans.* **58**, 129–148. (doi:10.1149/05801.0129ecst)

14. Tang Y, Kusoglu A, Karlsson AM, Santare MH, Cleghorn S, Johnson WB. 2008 Mechanical properties of a reinforced composite polymer electrolyte membrane and its simulated performance in PEM fuel cells. *J. Power Sources* **175**, 817–825. (doi:10.1016/j.jpowsour.2007.09.093)

15. Khattra NS, Lu Z, Karlsson AM, Santare MH, Busby FC, Schmiedel T. 2013 Time-dependent mechanical response of a composite PFSA membrane. *J. Power Sources* **228**, 256–269. (doi:10.1016/j.jpowsour.2012.11.116)

16. Moukheiber E, Bas C, Flandin L. 2014 Understanding the formation of pinholes in PFSA membranes with the essential work of fracture (EWF). *Int. J. Hydrog. Energy* **39**, 2717–2723. (doi:10.1016/j.ijhydene.2013.03.031)

17. Lin Q, Liu Z, Wang L, Chen X, Shi S. 2018 Fracture property of Nafion XL composite membrane determined by R-curve method. *J. Power Sources* **398**, 34–41. (doi:10.1016/j.jpowsour.2018.07.052)

18. Zhang Z, Shi S, Lin Q, Wang L, Liu Z, Li P, Chen X. 2018 Exploring the role of reinforcement in controlling fatigue crack propagation behavior of perfluorosulfonic-acid membranes. *Int. J. Hydrog. Energy* **43**, 6379–6389. (doi:10.1016/j.ijhydene.2018.02.034)

19. DuPont Product Information: Nafion NR-211 and NR-212 PFSA membrane, 2008. See http://www.fuelcellsetc.com/store/DS/N211-N212-properties.pdf.

20. Moukheiber E, De Moor G, Flandin L, Bas C. 2012 Investigation of ionomer structure through its dependence on ion exchange capacity (IEC). *J. Membr. Sci.* **389**, 294–304. (doi:10.1016/j.memsci.2011.10.041)

21. Wang F, Tang H, Pan M, Li D. 2008 Ex situ investigation of the proton exchange membrane chemical decomposition. *Int. J. Hydrog. Energy* **33**, 2283–2288. (doi:10.1016/j.ijhydene.2008.01.052)

22. García-Salaberri PA, Vera M, Zaera R. 2011 Nonlinear orthotropic model of the inhomogeneous assembly compression of PEM fuel cell gas diffusion layers. *Int. J. Hydrog. Energy* **36**, 11856–11870. (doi:10.1016/j.ijhydene.2011.05.152)

23. Lu Z, Lugo M, Santare MH, Karlsson AM, Busby FC, Walsh P. 2012 An experimental investigation of strain rate, temperature and humidity effects on the mechanical behavior of a perfluorosulfonic acid membrane. *J. Power Sources* **214**, 130–136. (doi:10.1016/j.jpowsour.2012.04.094)

24. Yi P, Peng L, Lai X, Ni J. 2011 A Numerical Model for Predicting Gas Diffusion Layer Failure in Proton Exchange Membrane Fuel Cells. *J. Fuel Cell Sci. Technol.* **8**. (doi:10.1115/1.4002312)

25. Baik KD, Hong BK, Kim MS. 2013 Effects of operating parameters on hydrogen crossover rate through Nafion® membranes in polymer electrolyte membrane fuel cells. *Renew. Energy* **57**, 234–239. (doi:10.1016/j.renene.2013.01.046)

26. Chippar P, Oh K, Kim W-G, Ju H. 2014 Numerical analysis of effects of gas crossover through membrane pinholes in high-temperature proton exchange membrane fuel cells. *Int. J. Hydrog. Energy* **39**, 2863–2871. (doi:10.1016/j.ijhydene.2013.05.117)

27. Matsuura T, Chen J, Siegel JB, Stefanopoulou AG. 2013 Degradation phenomena in PEM fuel cell with dead-ended anode. *Int. J. Hydrog. Energy* **38**, 11346–11356. (doi:10.1016/j.ijhydene.2013.06.096)

28. Hommura S, Kawahara K, Shimohira T, Teraoka Y. 2008 Development of a Method for Clarifying the Perfluorosulfonated Membrane Degradation Mechanism in a Fuel Cell Environment. *J. Electrochem. Soc.* **155**, A29–A33. (doi:10.1149/1.2800171)

29. Mousa G, DeVaal J, Golnaraghi F. 2014 Diagnosis of hydrogen crossover and emission in proton exchange membrane fuel cells. *Int. J. Hydrog. Energy* **39**, 20116–20126. (doi:10.1016/j.ijhydene.2014.09.116)

30. Durst J *et al.* 2013 Degradation heterogeneities induced by repetitive start/stop events in proton exchange membrane fuel cell: Inlet vs. outlet and channel vs. land. *Appl. Catal. B-Environ.* **138**, 416–426. (doi:10.1016/j.apcatb.2013.03.021)

Conclusions and Perspectives

The development of the hydrogen industry and of PEMFC are among the solutions considered to accelerate the energy transition. Although they offer clear advantages as safe and clean power sources to replace fossil fuels, PEMFC are still facing strong durability and performance issues limiting their lifetime and thus their widespread commercialization. This thesis work aimed at providing some clarifications on the aging phenomena of PFSA membranes and especially on the effects of chemical and mechanical stresses experienced by the membranes during fuel cell operation in terms of chemical structure, functional properties and fuel cell performances.

1. Influence of ex-situ chemical stress test on PFSA membrane degradation

First, it was necessary to understand the impact of pure *ex-situ* chemical degradation on PFSA membranes without the contribution of mechanical fatigue. As highlighted in the bibliographical study, Fenton's reaction is by far the most widely-used accelerated *ex-situ* aging protocol to study the chemical degradation of PFSA membranes. It permits to reproduce the harmful environment observed during fuel cell operation by generating hydroxyl $HO^{\bullet}$ and hydroperoxyl $HOO^{\bullet}$ radicals. However, a wide range of Fenton's reagents combinations can be found in the literature and can have different effect on PFSA membranes, which makes difficult to determine the most suitable *ex-situ* aging protocols. In that respect, a study was carried out to clarify the influence of Fenton's reagent concentrations on the chemical degradation of Nafion™ XL and NR211 membranes.

Our results highlighted a high dependence of the membrane degradation to the Fenton's reagent concentrations, both from chemical and morphological points of view. Moreover, they demonstrated that the use of a small amount of Fe^{2+} is required to catalyze efficiently the decomposition reaction of H_2O_2 into free radicals, thus ensuring a significant membrane degradation. On the other hand, high H_2O_2 concentrations can have detrimental effects on the macroscopic morphology of PFSA membranes and can generate defects that are not representative of those occurring during fuel cell operation. This preliminary study permitted to establish the most appropriate conditions required for this thesis work, *i.e.* the Fenton's reagent concentrations leading to the more efficient chemical degradation without inducing dramatical morphological changes of membranes: 1 ppm of ferrous ions (Fe^{2+}) and 3 vol.% of hydrogen peroxide (H_2O_2).

2. Evolution of the chemical degradation as a function of time and its impact on the structure and properties of PFSA membranes

On the basis of this first study, a time-resolved monitoring of *ex-situ* chemical degradation of PFSA membranes induced by Fenton's reaction was then performed. In this regard, the chemical degradation of both composite Nafion™ XL and non-reinforced NR211 membranes was systematically evaluated as a function of exposure time to Fenton's reagents thanks to several indicators such as the weight loss, fluoride ion emissions or chemical structure evolution.

Our results demonstrated that both XL and NR211 membranes are significantly chemically-degraded by the exposure to Fenton's reagents since the analysis of Fenton solutions revealed the presence of several degradation products in non-negligible quantities. More particularly, liquid-state ^{19}F-NMR permitted to highlight high emissions of perfluoro(3-oxapentane)-1-sulfonic-4-carboxylic diacid – named Product A for simplicity in the manuscript –, a fluorinated compound deriving from the PFSA side chain which has been already identified in the literature as one of the main PFSA degradation products. Nevertheless, no evolution of the chemical structure and no change in the IEC were observed, which suggest that the degradation of the PFSA main and side chains arises in equal proportions. This result indicates that the polymer decomposition probably occurs *via* an unzipping reaction, thus leading to the loss of the entire side chains. Furthermore, the characterization of water transport and sorption properties of PFSA membranes after 96 hours of Fenton's reagents exposure highlighted that the chemical degradation does not significantly alter these properties. These behaviors differ greatly from those detected after long-time fuel cell operation for which reduced water sorption capacity and water mobility have been observed. This discrepancy can be attributed either to the short duration of the degradation process (*i.e.* 96 *vs.* more than 12000 hours) or to an incomplete mimicking of the impact of the chemical degradation occurring during fuel cell operation on PFSA membranes.

More particularly, the innovation of this study is based on the analysis of the chemical stability of the composite Nafion™ XL membrane. Our results demonstrated that the chemical degradation of XL membrane is lower than that of unreinforced NR211 membrane, which can be explained by the presence of an additional PTFE-rich reinforcement, maintaining the membrane mechanical integrity and thus avoiding further chemical decomposition, and/or by

the presence of cerium-based radical scavengers which can mitigate the radical attacks on the polymer chains.

3. Impact of conjoint chemical and mechanical stress on PFSA membranes

Finally, the effects of combined mechanical and chemical stress on PFSA membranes were studied, again through an *ex-situ* approach, with a custom-made device. The objective was to mimic the aging conditions encountered by the membrane during fuel cell operation. Numerous aging tests were performed to provide new understandings on the influence of mechanical constraints, whether they were static or cyclic with negligible or high pressure level, on the chemical degradation of Nafion™ membranes, and its impact on the chemical structure and functional properties. The results demonstrated that the application of a mechanical constraint does not modify the chemical mechanisms since degradation products identical to those identify in the case of only chemical stress were detected. However, the response of the XL membrane to chemical stress seemed to slightly differ since the addition of a mechanical constraint led to the appearance of bubbles and blisters close to the membrane surface. These morphological changes were already observed with pure chemical stress tests performed with harsher conditions, indicating that an additional mechanical stress could accelerate the membrane degradation. To this day, further investigations are needed to understand the appearance of theses defects.

Furthermore, higher fluoride emission rates as well as higher hydrogen permeation currents were obtained with NR211 rather than XL in most cases which could be explained by the better mechanical strength provided by the additional reinforcement layer in the case of the XL membrane. However, this advantage seemed to vanish when the pressure level increased – from 5 to 10 MPa – since similar degradation rate were measured for both reinforced XL and non-reinforced NR211 membranes.

Moreover, although a significant polymer decomposition was observed after conjoint stress tests, neither the functional properties such as water sorption capacity and water mobility nor the fuel cell performances of the membrane were significantly impacted. These results can suggest that either the conditions implemented in our study were not sufficiently representative of the fuel cell operating conditions or the experiment duration was too short to have measurable effects. However, it is worth noting that the averaged membrane degradation was characterized while stresses are undoubtedly experienced in a different way by the membrane whether it is immobilized under the channel ribs or looser in the channel. Aging heterogeneities at the

membrane scale, and more generally within the MEA, have indeed already been observed and characterized after fuel cell operation.

On another note, aging test performed with GDL introduced between the membrane and the flow field plates showed that no clear benefit can be drawn with this configuration in our stress cell. The results suggested that the presence of GDL probably hinders the distribution of the solution to the membrane surface and that broken carbon fibers led to serious membrane damages which could then provoke the membrane failure.

4. Perspectives of this thesis work

The development of our custom-made device and the associated accelerated aging tests can be seen as the building blocks toward a better understanding on chemical and mechanical degradations phenomena of PFSA membranes and opens up a wide variety of perspectives.

In the first place, it will be necessary to perform several reproducibility tests to confirm the tendencies observed in chapter V. The large discrepancy measured for fluoride emission rate cannot allow us to clearly conclude for the moment. More particularly, the peculiar degradation behavior of XL membrane exposed to a negligible static compressive stress deserves further investigations. Then, additional aging tests can be considered to gain a deeper understanding of conjoint chemical and mechanical stresses on PFSA membranes degradation. For instance, one can imagine extending the experiment duration to several tens of hours to challenge the mechanical durability of the membranes.

As seen in chapter V, coupling mechanical constraint and Fenton solution exposure led to the formation of bubbles, and in the worst case of blisters, at the surface of composite Nafion™ XL membranes. Such morphological changes are not representative of the defects encountered during fuel cell operation and will require deeper investigations to understand their appearance as well as their eventual correlation with the chemical decomposition of the polymer. It would be interesting for example to perform further morphological and chemical analysis such as Scanning Electron Microscopy (SEM), Wide-Angle X-ray Scattering (WAXS), ATR-FTIR microscopy. On another note, these two techniques can also be considered to locally analyze and discriminate the membrane degradation behavior between the area under channels and that under the channel ribs.

The introduction of GDL between the flow field plates and the membrane in our stress cell aimed to better mimic the mechanical constraint encountered by membranes during fuel cell

operation. However, the results demonstrated that characterizing the membrane degradation in the presence of GDL, in the case of our experimental setup, is not straightforward and deserves a special attention. For example, it would be interesting to repeat the aging test with a GDL containing a microporous layer (MPL) to eventually modify the solution distribution at the surface of the membrane.

Finally, to get closer to the operating conditions of a fuel cell, one can imagine modifying the experimental cell in order to circulate humidified gases carrying the Fenton's reagents required to initiate the chemical degradation. This configuration could avoid flooding in the GDL pores and ensure a better distribution of the Fenton's reagents at the membrane surface.

Appendix A

Optimization of the experimental protocols

1. Establishment of a drying protocol for ATR-FTIR measurements

As mentioned in § 1.2 of chapter II, analysis using Fourier-Transform InfraRed (FTIR) spectroscopy was carried out with an Attenuated Total Reflectance (ATR) accessory in order to study chemical structure changes at the surface of PFSA membranes. The characteristic vibration bands of PFSA membranes are visible in the spectral range 1400 – 400 cm^{-1} while those of water molecules contained in the membrane are characterized by a wide band between 3900 and 2600 cm^{-1} and several bands in the range 1900 – 1500 cm^{-1}. The assignment of PFSA vibration bands, as illustrated in Table A.1 below, is fairly well established nowadays, although some absorption bands are still open to discussion.

Table A.1 – Assignment of IR vibration bands of polymer and water molecules of PFSA membranes based on the literature.

Wavenumber (cm^{-1})	Vibration mode assignment	References
3720	O-H stretching (free water CF···HOH···FC)	[1–4]
3450	O-H stretching (bulk water)	[1–4]
2900 – 2000	O-H stretching (H_3O^+)	[4–6]
1720	H-O-H asymmetric bending (H_3O^+)	[4,7]
1680	H-O-H bending ($H_3O^+.H_2O$)	[6]
1630	H-O-H bending (H_2O)	[1,4–10]
1420	S=O asymmetric stretching (SO_3H)	[5–8]
1302	C-C stretching	[11]
1200	C-F asymmetric stretching (CF_2 groups)	[11–15]
1200	S=O symmetric stretching (SO_3H)	[1,4,10,16]
1145	C-F symmetric stretching (CF_2 groups)	[1,4,6,9,13–15,17]
1130	S=O asymmetric stretching (SO_3^-)	[10]
1055 – 1060	S-O symmetric stretching (SO_3^-)	[10,11,13,15,17,18]
982	C-F stretching (CF_2-$CF(CF_3)$- group)	[11,12]
982/966	C-O stretching (ether linkages)	[4,7,8,10,13–15,17,19,20]
920	S-O symmetric stretching (SO_3H)	[4–8]
805	CS stretching	[4]

Most studies agree on the vibration bands assignment with the exception of the peak located at 980 cm^{-1} for which some authors attributed it to the stretching mode of C-O-C group [4,7,8,10,14,16,17] while others assigned it to CF stretching mode of the CF_2-$CF(CF_3)$- group [11,12]. More recently, Coms *et al.* suggested that the 3 characteristics peaks associated to PFSA side chain between 1080 and 950 cm^{-1} cannot be simply assigned to single functional groups since vibration modes associated to these bands are greatly connected [18]. Bands at 1060 and 966 cm^{-1} would be both linked to the symmetric stretching of SO_3^- groups and would entail the motions of many adjacent atoms within the PFSA side chains. On the other hand, band centered at 982 cm^{-1} would not be related to SO_3^- symmetric stretching. Their assumption is verified by the absence of bands located around 1060 and 966 cm^{-1} in IR spectrum of a dry Nafion™ membrane.

It is worth noting that many studies demonstrated that IR spectrum of a Nafion™ membrane is significantly influenced by the membrane water content [2–5,9–11,19,20]. In order to study the impact of the degradation on PFSA chemical structure, it is necessary to perform the measurement in identical conditions where the influence of water molecules on the IR spectrum is negligible, *i.e.* in a state close to the dry state. In that respect, several experiments were performed to optimize the drying protocol of Nafion™ membranes before the ATR-FTIR analysis. Figure A.1 illustrates the IR spectra of a fully hydrated pristine XL membrane during its dehydration at ambient air. The pristine XL membrane was initially immersed in distilled water at room temperature during 7 hours before being quickly wiped between two absorbent papers and analyzed by ATR-FTIR spectroscopy at different time intervals.

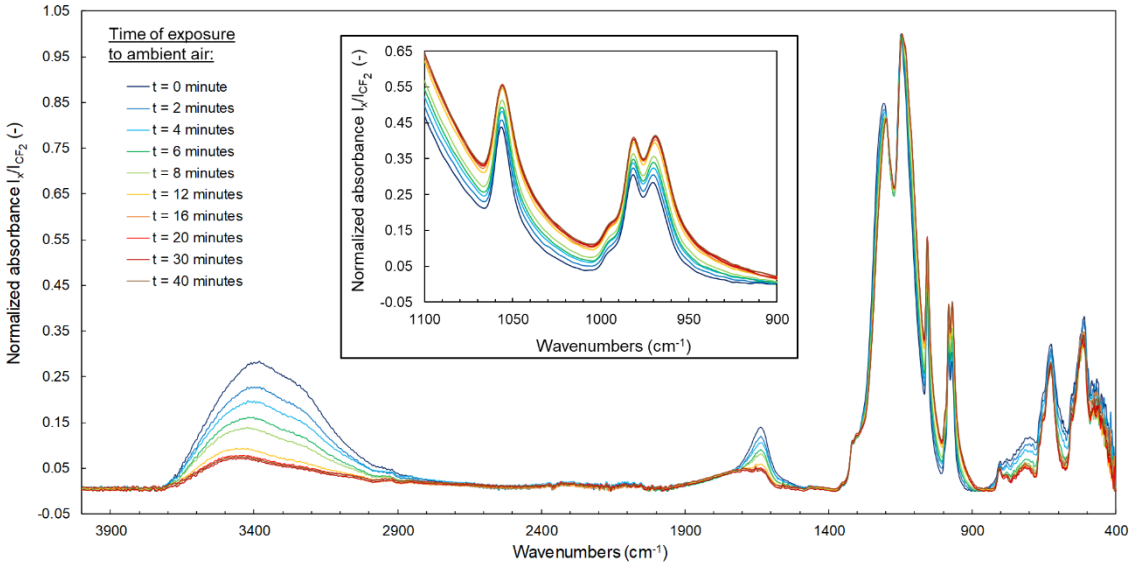

Figure A.1 – Change in ATR-FTIR spectrum of a pristine Nafion™ XL membrane during its dehydration at ambient air. The inset is a focus on vibration bands associated to PFSA side chains.

As expected, vibration bands associated to the water molecules around 3400 cm^{-1} and at 1630 cm^{-1} exhibit an important decrease of absorbance magnitude as a function of time, indicating the dehydration of the membrane. On the other hand, it can be seen that the characteristic vibration bands of PFSA are also greatly influenced by the membrane water content: as seen in the inset of Figure A.1, the absorbance magnitude of PFSA vibration bands significantly increase with time. As the normalized intensity ratio between the PFSA side chain and -CF_2 groups vibration bands varies significantly as a function of the membrane water content, it is thus essential to control the hydration level of the membrane to detect eventual chemical structure changes as a consequence of the degradation.

Consequently, as the membrane water content strongly influences the IR spectrum, it is necessary to perform analysis in the same conditions for all local measurements and for all membrane samples to properly compare aged and pristine membranes. To this end, a protocol measurement was established to analyze membrane samples after drying under inert gas. Measurements were performed in order to estimate the time needed to dry the membrane and attain an equilibrium state. In that respect, a membrane was exposed to a dry nitrogen flow (99.9999 % of purity) with a 2 NL/min flow rate during several minutes and the IR spectrum was measured at different time intervals during the drying protocol. Figure A.2 illustrates the IR spectrum evolution of a pristine XL membrane during the drying.

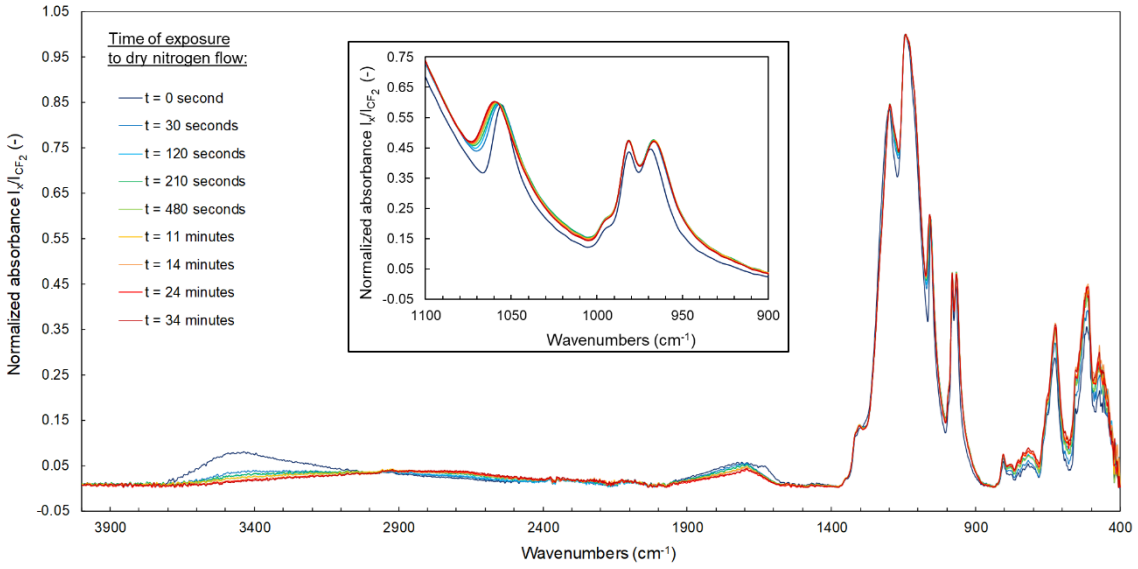

Figure A.2 – Change in ATR-FTIR spectrum of a pristine Nafion™ XL membrane during its exposure to a dry nitrogen flow. The inset is a focus on vibration bands associated to PFSA side chains.

It is important to note that the equilibrium state referred here is not the totally dry state of the membrane – some residual water molecules strongly bonded to sulfonate groups still being

present in the membrane even after drastic drying protocols – but only a state for which the membrane water content does no longer affect the absorbance magnitude of PFSA vibration bands. After only 30 seconds under a dry nitrogen flow, the water content of the membrane has drastically dropped since the absorbance magnitude of water molecules vibration bands is significantly diminishes. On the other hand, the absorbance magnitude of PFSA vibration bands increase and the symmetrical stretching band of the sulfonate group is shifted slowly to higher wavenumbers (from 1055 to 1060) cm^{-1} as the membrane water content diminishes until reaching a stationary state. It was therefore determined from these experiment that the exposure of the membrane to a dry nitrogen flow with a flow rate of 2 $NL.min^{-1}$ for 15 minutes permitted to reach an equilibrium state since the absorbance magnitude of PFSA vibration bands does no longer evolve.

Additionally, further ATR-FTIR analyses demonstrated that if the membrane is measured after a first drying overnight in an oven at 60°C – after pretreatment for example – the exposure time to inert atmosphere necessary to reach the equilibrium state is reduced to 10 minutes.

2. Cleaning protocol after *ex-situ* accelerated stress tests

In this thesis work, most of the *ex-situ* accelerated stress tests involved the exposure of the Nafion™ membranes to Fenton solution. As mentioned in § 2.3 of chapter III, after several hours of exposure to Fenton solution, some membrane samples – initially translucent and colorless – became opaque and orange, probably because of the adsorption of iron cations. Additionally, a brick red precipitate was formed when concentration of ferrous ions was high (44 ppm) and its deposition on the surface or even within the pores of the membrane might explain the orange color of degraded membranes (see Figure A.3):

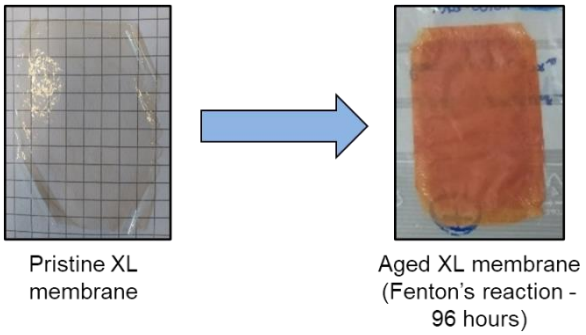

Figure A.3 – Evolution of the membrane color of 96 hours of exposure to Fenton solution during an *ex-situ* chemical stress test.

The presence of impurities into the membrane can provoke changes in chemical structure through crosslinking effect and can alter the properties of water sorption and transport. Indeed, the presence of paramagnetic cations within aged membranes have detrimental effects on NMR signal (large resonance peak) and relaxation phenomena (too short relaxation time), thus impacting the study of the chemical degradation impact on water self-diffusion coefficient into Nafion™ membranes. Additionally, the exchange of protons, counter-ions of Nafion™ sulfonate groups, with metallic cations is known to have an important impact on the water sorption capacity [21].

Therefore, in order to solve the cationic contamination of the membranes after *ex-situ* accelerated stress tests involving the exposure to Fenton solution, it was necessary to establish a cleaning protocol of aged membranes. The first step of this protocol was similar to that suggested by MacMillan *et al.* [22] and consisted in using the ethylenediaminetetraacetic acid (EDTA) as a strong chelating agent to complex ferrous and ferric ions within the aged membranes. More particularly, the use of EDTA in a salted form enables to exchange metallic counter-cations of PFSA sulfonate groups with cations from the soaking solution. Therefore, aged membranes were first soaked in EDTA-Na_2 solution at 0.01 mol.L^{-1} overnight at room temperature. Aged membranes were then thoroughly rinsed with distilled water at room temperature before being immersed in a nitric acid HNO_3 solution at 1 mol.L^{-1} at 80 °C during 2 hours for complete re-acidification, *i.e.* complete exchange of Na^+ ions with protons. Finally, they were washed in distilled water at 80 °C for two hours to remove all excess of nitric acid and residual contaminants and dried 6 to 20 hours in an oven at 60 °C. At the end of the cleaning protocol, the pronounced orange color of aged membranes was significantly attenuated as aged membranes became slightly yellow tinted (Figure A.4).

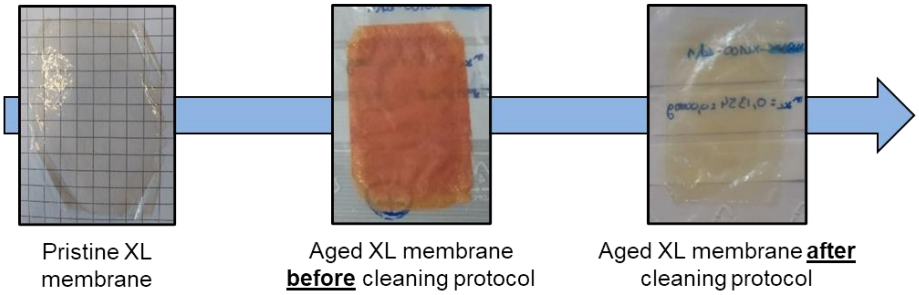

Figure A.4 – Evolution of the membrane color before and after cleaning protocol in comparison with a pristine membrane. The protocol was repeated three times to obtain adequate decontamination of the aged XL membrane.

To ensure the complete re-protonation of aged membranes, analysis of aged membranes was carried out by ATR-FTIR spectroscopy. Indeed, the use of ATR-FTIR spectroscopy as a tool for the identification of contaminants and microstructural changes in PFSA membranes has been already demonstrated [23]. Indeed, the work of E. Moukheiber permitted to identify the changes in FTIR spectra of Nafion™ membranes after the exchange of their proton counter-ions with metallic cations: the disappearance of the vibration band at 1730 cm^{-1}, which is associated to the H-O-H bending of hydronium ions H_3O^+, and the appearance of a vibration band around 870 cm^{-1}. The disappearance of the vibration band at 1730 cm^{-1} in IR spectra of Fe^{3+}-Nafion™ membranes confirms that H_3O^+ ions bonded to membrane sulfonates groups were exchanged with Fe^{3+} ions [24]. The vibration band around 870 cm^{-1} has already been observed in the literature for Nafion™ membranes degraded by Fenton's reaction and can be attributed to the formation of oxo-bonded Fe-O-Fe in Fe^{3+}-Nafion membranes [23–25]. Moreover, a shift in the C-O-C and S=O stretching bands was observed for exchanged XL membranes and can be explained by interactions of Fe^{3+} ions with the PFSA side chain moieties, as it has been suggested by the work of E. Moukheiber [23].

In the case of this thesis work, the same changes in ATR-FTIR spectrum have been observed for aged membranes after exposure to Fenton's reagents (Fe^{2+} and H_2O_2). Figure A.5 illustrates the ATR-FTIR spectra of a XL membrane aged by Fenton's reaction during 96 hours before and after the cleaning protocol in comparison with a pristine XL membrane.

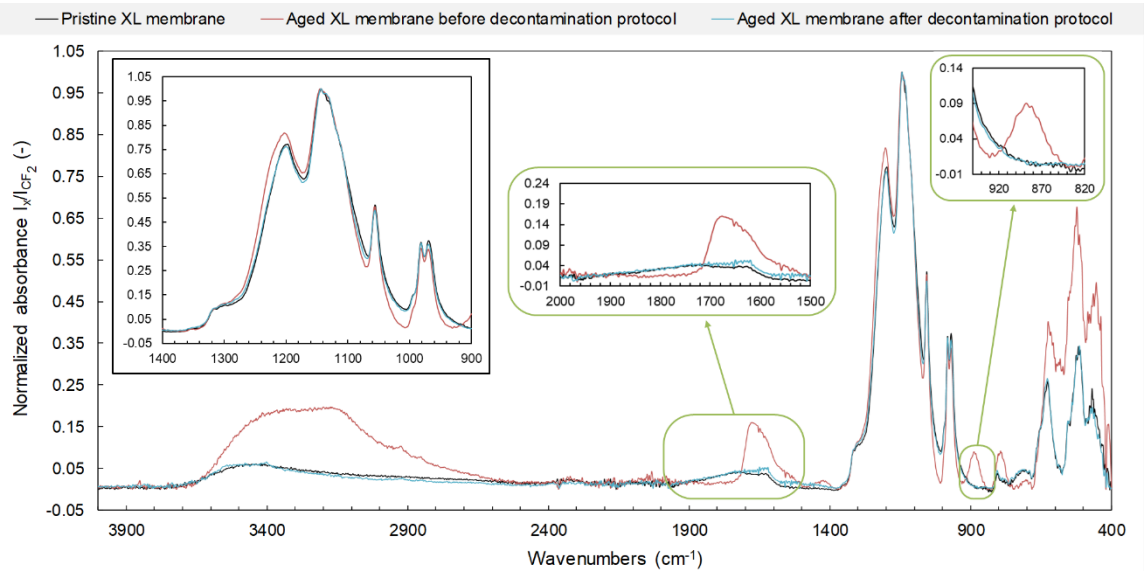

Figure A.5 – Impact of the cleaning protocol on the IR spectrum of an aged XL membrane (Fenton's reaction – 96 hours) in comparison with a pristine XL membrane. The inset to the left is a focus on characteristic PFSA vibration bands and the other insets are magnifications on evidence for cationic contaminants identification. IR spectra were measured at the ambient air.

It is important to note that aged XL membrane is considerably contamined (see Figure A.3) and thus made it difficult to have a convenient IR signal, which could explain the intensification of vibration bands associated to both water molecules and PFSA. After the cleaning protocol, vibration bands associated to the presence of Fe^{2+} and/or Fe^{3+} ions disappeared, suggesting that aged XL membrane was properly cleaned.

Since ATR-FTIR measurement only allows to probe membrane surface (0.17 to 2.58 micrometers) it is important to confirm the efficiency of the cleaning protocol with technique capable of analyzing the entire membrane. This is why, in addition to ATR-FTIR analysis, sorption measurements were performed first on a pristine XL membrane immersed in Fe^{2+} solution and then on the same membrane sample after the cleaning protocol. Figure A.6 illustrates the sorption isotherms of a pristine XL membrane in the protonated form compared to XL membrane completely exchanged with Fe^{2+} ions before and after the cleaning protocol. First of all, the results confirm that the presence of Fe^{2+} ions in membrane impacts water capacity sorption. After the cleaning protocol, it can be seen that sorption isotherm became identical to the non-exchanged membrane meaning that the water sorption capacity of XL membrane is restored. This thus confirmed that the cleaning protocol established in this thesis work permitted to efficiently eliminate cationic contaminants.

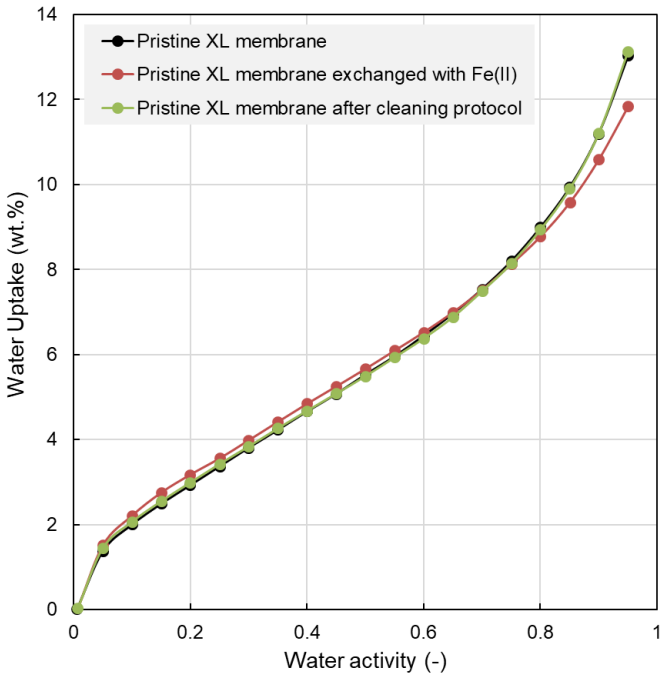

Figure A.6 – Water sorption isotherms of XL membranes as a function of the sulfonate group counter-ions

References

1. Wang Y, Kawano Y, Aubuchon SR, Palmer RA. 2003 TGA and Time-Dependent FTIR Study of Dehydrating Nafion−Na Membrane. *Macromolecules* **36**, 1138–1146. (doi:10.1021/ma020156e)

2. Quezado S, Kwak J, Falk M. 1984 An Infrared Study of Water-Ion Interactions in Perfluorosulfonate (nafion) Membranes. *Can. J. Chem.-Rev. Can. Chim.* **62**, 958–966. (doi:10.1139/v84-158)

3. Falk M. 1980 An infrared study of water in perfluorosulfonate (Nafion) membranes. *Can. J. Chem.* **58**, 1495–1501. (doi:10.1139/v80-237)

4. Laporta M, Pegoraro M, Zanderighi L. 1999 Perfluorosulfonated membrane (Nafion): FT-IR study of the state of water with increasing humidity. *Phys. Chem. Chem. Phys.* **1**, 4619–4628. (doi:10.1039/A904460D)

5. Ludvigsson M, Lindgren J, Tegenfeldt J. 2000 FTIR study of water in cast Nafion films. *Electrochimica Acta* **45**, 2267–2271. (doi:10.1016/S0013-4686(99)00438-7)

6. Buzzoni R, Bordiga S, Ricchiardi G, Spoto G, Zecchina A. 1995 Interaction of H2O, CH3OH, (CH3)2O, CH3CN, and Pyridine with the Superacid Perfluorosulfonic Membrane Nafion: An IR and Raman Study. *J. Phys. Chem.* **99**, 11937–11951. (doi:10.1021/j100031a023)

7. Ostrowska J, Narebska A. 1983 Infrared study of hydration and association of functional groups in a perfluorinated Nafion membrane, Part 1. *Colloid Polym. Sci.* **261**, 93–98. (doi:10.1007/BF01410686)

8. Blanchard RM, Nuzzo RG. 2000 An infrared study of the effects of hydration on cation-loaded nafion thin films. *J. Polym. Sci. Part B Polym. Phys.* **38**, 1512–1520. (doi:10.1002/(SICI)1099-0488(20000601)38:11<1512::AID-POLB110>3.0.CO;2-2)

9. Korzeniewski C, Snow DE, Basnayake R. 2006 Transmission infrared spectroscopy as a probe of Nafion film structure: analysis of spectral regions fundamental to understanding hydration effects. *Appl. Spectrosc.* **60**, 599–604. (doi:10.1366/000370206777670620)

10. Gruger A, Régis A, Schmatko T, Colomban P. 2001 Nanostructure of Nafion® membranes at different states of hydration: An IR and Raman study. *Vib. Spectrosc.* **26**, 215–225. (doi:10.1016/S0924-2031(01)00116-3)

11. Liang Z, Chen W, Liu J, Wang S, Zhou Z, Li W, Sun G, Xin Q. 2004 FT-IR study of the microstructure of Nafion® membrane. *J. Membr. Sci.* **233**, 39–44. (doi:10.1016/j.memsci.2003.12.008)

12. Y. Levy L, Jenard A, D. Hurwitz H. 1982 Hydration and ion-exchange process in carboxylic membranes. Part 1.—Infrared spectroscopic investigation of the acid membranes. *J. Chem. Soc. Faraday Trans. 1 Phys. Chem. Condens. Phases* **78**, 29–36. (doi:10.1039/F19827800029)

13. Negro E, Vittadello M, Vezzù K, Paddison SJ, Di Noto V. 2013 The influence of the cationic form and degree of hydration on the structure of Nafion^{TM}. *Solid State Ion.* **252**, 84–92. (doi:10.1016/j.ssi.2013.09.017)

14. Di Noto V, Piga M, Lavina S, Negro E, Yoshida K, Ito R, Furukawa T. 2010 Structure, properties and proton conductivity of Nafion/[(TiO2)·(WO3)0.148]ψTiO2 nanocomposite membranes. *Electrochimica Acta* **55**, 1431–1444. (doi:10.1016/j.electacta.2009.06.011)

15. Vittadello M, Negro E, Lavina S, Pace G, Safari A, Noto VD. 2008 Vibrational Studies and Properties of Hybrid Inorganic−Organic Proton Conducting Membranes Based on Nafion and Hafnium Oxide Nanoparticles. *J. Phys. Chem. B* **112**, 16590–16600. (doi:10.1021/jp804117w)

16. Basnayake R, Peterson GR, Casadonte DJ, Korzeniewski C. 2006 Hydration and Interfacial Water in Nafion Membrane Probed by Transmission Infrared Spectroscopy. *J. Phys. Chem. B* **110**, 23938–23943. (doi:10.1021/jp064121i)

17. Perusich SA. 2011 FTIR equivalent weight determination of perfluorosulfonate polymers. *J. Appl. Polym. Sci.* **120**, 165–183. (doi:10.1002/app.32871)

18. Mauritz KA, Moore RB. 2004 State of Understanding of Nafion. *Chem. Rev.* **104**, 4535–4586. (doi:10.1021/cr0207123)

19. Cable KM, Mauritz KA, Moore RB. 1995 Effects of hydrophilic and hydrophobic counterions on the Coulombic interactions in perfluorosulfonate ionomers. *J. Polym. Sci. Part B Polym. Phys.* **33**, 1065–1072. (doi:10.1002/polb.1995.090330710)

20. Heitner-Wirguin C. 1979 Infra-red spectra of perfluorinated cation-exchanged membranes. *Polymer* **20**, 371–374. (doi:10.1016/0032-3861(79)90103-4)

21. Coms FD, Fuller TJ, Schaffer CP. 2018 A Mechanistic Study of Perfluorosulfonic Acid Membrane Water Permeance Degradation in Air. *J. Electrochem. Soc.* **165**, F3104–F3110. (doi:10.1149/2.0141806jes)

22. Ostrovskii D, Paronen M, Sundholm F, Torell LM. 1999 State of water in sulfonated poly(vinyl fluoride) membranes: an FTIR study. *Solid State Ion.* **116**, 301–310. (doi:10.1016/S0167-2738(98)00357-9)

23. Kunimatsu K, Bae B, Miyatake K, Uchida H, Watanabe M. 2011 ATR-FTIR Study of Water in Nafion Membrane Combined with Proton Conductivity Measurements during Hydration/Dehydration Cycle. *J. Phys. Chem. B* **115**, 4315–4321. (doi:10.1021/jp112300c)

24. Xu F, Leclerc S, Lottin O, Canet D. 2011 Impact of chemical treatments on the behavior of water in Nafion® NRE-212 by 1H NMR: Self-diffusion measurements and proton quantization. *J. Membr. Sci.* **371**, 148–154. (doi:10.1016/j.memsci.2011.01.038)

25. MacMillan B, Sharp AllanR, Armstrong RobinL. 1999 An n.m.r. investigation of the dynamical characteristics of water absorbed in Nafion. *Polymer* **40**, 2471–2480. (doi:10.1016/S0032-3861(98)00484-4)

26. Moukheiber E. 2011 Compréhension par établissement de courbes d'étalonnage de la structure des membranes perfluorées sulfoniques pour pile à combustible. Grenoble.

27. Chen C, Levitin G, Hess DW, Fuller TF. 2007 XPS investigation of Nafion® membrane degradation. *J. Power Sources* **169**, 288–295. (doi:10.1016/j.jpowsour.2007.03.037)

28. Kiwi J *et al.* 2002 Catalytic Fe3+ Clusters and Complexes in Nafion Active in Photo-Fenton Processes. High-Resolution Electron Microscopy and Femtosecond Studies. *Langmuir* **18**, 9054–9066. (doi:10.1021/la020648k)

Appendix B

Impact of a static compressive stress on the functional properties of PFSA membranes

As mentioned in § 4.2 of chapter V, the evolution of the water sorption capacity was also investigated in the case of a static compressive stress. In this regard, Figure B.1 illustrates the water sorption isotherms and its decomposition into the three adsorption mechanisms of XL and NR211 membranes after different aging tests: ***control aging tests #1*** and ***#2, static aging test*** (mechanical and chemical stress conditions are given in Table 5.1 of chapter V).

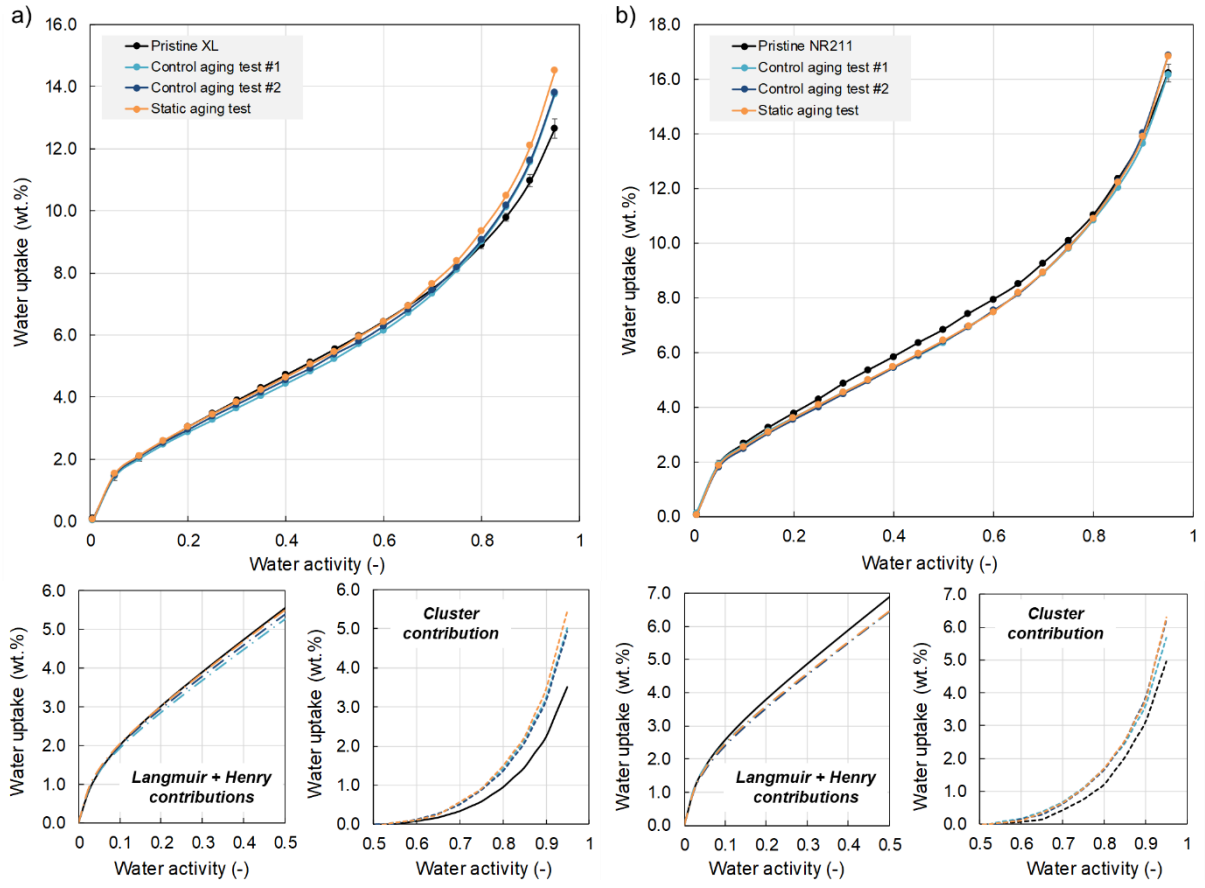

Figure B.1 – Water sorption isotherms (30 °C) of (a) XL and (b) NR211 membranes after various aging tests in comparison with pristine membranes. The plots at the bottom illustrate the evolution of the different adsorption mechanisms. Five measurements were performed on the pristine XL in order to control the repeatability of the measurements and of the pretreatment process.

The results are similar to those observed in the case of cyclic compressive stress: on the one hand, a significant increase of cluster contribution is observed for aged XL membranes while no clear evolution of Langmuir + Henry contributions is visible and no significant changes of

all the three contributions is observed in the case of aged NR211 membranes on the other hand. These evolutions confirm the assumption made in the case of cyclic compressive stress stating that the addition of a mechanical constraint does not alter the water sorption behavior.

The same conclusion can be drawn by studying the evolution of the water transport property in aged membranes (Figure B.2): no significant impact of the conjoint chemical and mechanical stress on the water self-diffusion coefficient is observed on the all range of membrane water-uptake probed for both NR211 and XL membranes.

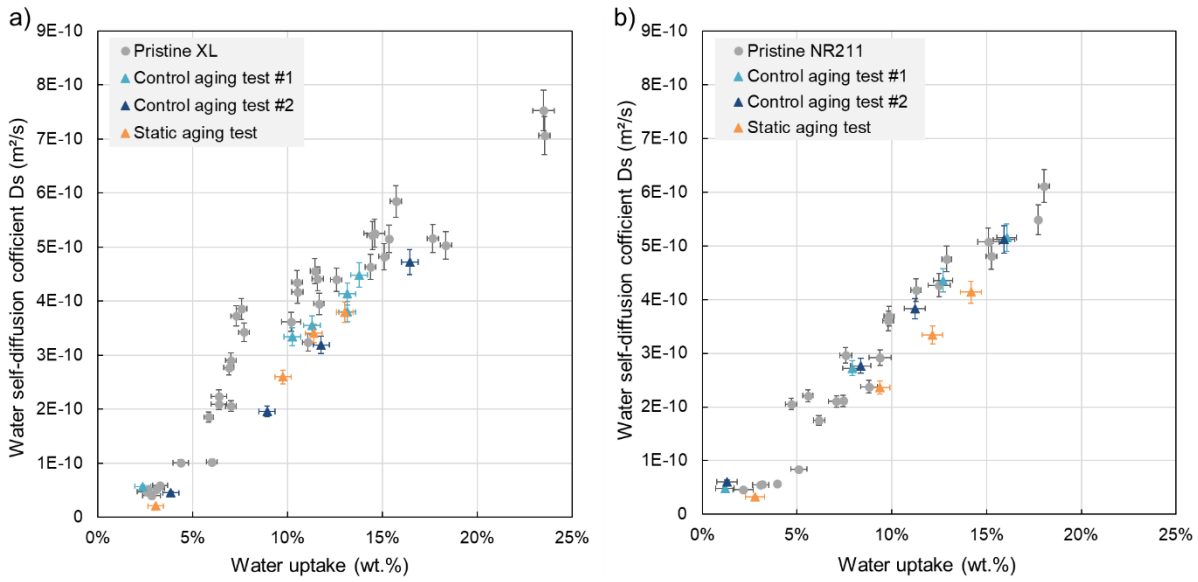

Figure B.2 – Water self-diffusion coefficient evolution after various aging tests as a function of water uptake in aged (a) XL and (b) NR211 membranes (triangle symbols) in comparison with pristine membranes (circles).

Impact des dégradations et du vieillissement sur les propriétés des membranes PFSA pour pile à combustible

Résumé

Bien que déjà présentées comme une technologie sûre et propre, les piles à combustible à membrane échangeuse de protons (PEMFC) restent confrontées à de solides verrous en termes de durabilité et de fiabilité, limitant leur commercialisation à large échelle. De nombreuses études ont déjà permis d'affiner la compréhension des phénomènes de vieillissement et ont permis de désigner la dégradation de la membrane comme l'un des principaux facteurs limitant la durée de vie des PEMFC.

Cette étude vise à apporter des éléments de compréhension sur les mécanismes de dégradations chimique et mécanique par l'intermédiaire de protocoles de vieillissement *ex-situ*, ainsi qu'à comprendre l'impact de ces dégradations sur la structure et les propriétés fonctionnelles des membranes.

Dans un premier temps, il a été nécessaire de clarifier l'influence de la réaction de Fenton, un protocole de vieillissement *ex-situ* largement reconnu dans la littérature, sur la dégradation chimique des membranes Nafion™. Les résultats ont confirmé que la concentration en réactifs de Fenton influençait significativement la décomposition chimique du polymère, à la fois d'un point de vue chimique et morphologique.

Par la suite, nous avons choisi de suivre l'évolution de la dégradation chimique des membranes Nafion™ en fonction du temps et d'étudier son impact sur la structure de la membrane, ses propriétés de sorption et de diffusion de l'eau ainsi que son fonctionnement en pile. À cet égard, différentes techniques de caractérisation telles que la spectroscopie RMN ^{19}F ou ^{1}H ainsi que la spectroscopie FTIR ont permis de corréler les propriétés physico-chimiques de la membrane à ses caractéristiques structurelles et de mettre ainsi en évidence plusieurs marqueurs de la dégradation chimique.

Enfin, un dispositif sur-mesure a été conçu afin d'étudier l'impact des contraintes mécanique et chimique conjointes sur les membranes Nafion™. L'objectif de ce dispositif était de reproduire des conditions de vieillissement proches de celles rencontrées lors du fonctionnement en pile.

Mots-clés : hydrogène, PEMFC, membranes Nafion™, durabilité, dégradation chimique, fatigue mécanique, réaction de Fenton.

Impact of degradation and aging on properties of fuel cell PFSA membranes

Abstract

Although proton-exchange membrane fuel cells (PEMFC) are nowadays considered as a safe and clean energy technology, they still suffer from durability and reliability issues restricting their widespread commercialization. Innumerable studies have already led to a better understanding of aging phenomena and highlighted membrane degradation as one of the main factors limiting PEMFC lifetime.

This study aims at bringing some clarifications on the chemical and mechanical degradation mechanisms of membranes through *ex-situ* aging protocols as well as understanding the impact of these degradations on the membrane structure and functional properties.

First, it was necessary to clarify the influence of Fenton's reaction, an *ex-situ* aging protocol widely recognized in the literature, on the chemical degradation of Nafion™ membranes. The results confirmed that Fenton's reagents concentration significantly influenced polymer chemical decomposition, both from a chemical and morphological point of view.

Subsequently, we chose to monitor the evolution of pure chemical degradation of Nafion™ membranes as a function of time and to study its impact on the membrane structure, water sorption and diffusion properties, as well as operability in fuel cells. In that respect, various characterization techniques such as ^{19}F or ^{1}H-NMR as well as FTIR spectroscopies allowed us to correlate physico-chemical properties of the membrane to its structural characteristics and to thus highlight several indicators of chemical degradation.

Finally, a custom-made device has been developed to study the impact of conjoint mechanical and chemical stress on Nafion™ membranes. The objective of this device was to replicate aging conditions close to those encountered during fuel cell operation.

Keywords: hydrogen, PEMFC, Nafion™ membranes, durability, chemical degradation, mechanical fatigue, Fenton's reaction.